

FIELD AND STABLE ISOTOPIC CHARACTERISTICS
OF CARBONATE ALTERATION ZONES,
TIMMINS AREA

FIELD AND STABLE ISOTOPIC CHARACTERISTICS
OF CARBONATE ALTERATION ZONES,
TIMMINS AREA

By

JOHN ANDREW FYON, B.Sc., M.Sc.

A Thesis

Submitted to the School of Graduate Studies
in Partial Fulfilment of the Requirements
for the Degree
Doctor of Philosophy

McMaster University

March, 1986

DOCTOR OF PHILOSOPHY (1986)
(Geology)

McMASTER UNIVERSITY
Hamilton, Ontario

TITLE: Field And Stable Isotopic Characteristics Of
Carbonate Alteration Zones, Timmins Area.

AUTHOR: John Andrew (Andy) Fyon, B.Sc. (Queen's University),
M.Sc. (McMaster University)

SUPERVISORS: Dr. J. H. Crocket
Dr. H. P. Schwarcz

NUMBER OF PAGES:xviii, 399

Abstract

Hydrothermal carbonate was introduced into igneous rock in the Timmins area during an early, sea water alteration event when calcite ($\delta^{13}\text{C} = 0$ to -3‰) filled the primary porosity of basalt flows and during a later hydrothermal event when mafic and ultramafic igneous rock were altered into a zoned sequence consisting of an inner zone of ferroan or magnesian carbonate flanked by calcite- and chlorite-rich assemblages. The younger intense carbonate alteration event predated or was synchronous with regional metamorphism and deformation and was focused along structurally induced, permeable zones. Gold was introduced during and after the intense carbonate alteration.

Away from carbonaceous sediments, $\delta^{13}\text{C}$ -values of the ferroan carbonate are very uniform (-3.5 to -5‰) regardless of stratigraphic position, size, or gold tenor of the alteration zone. As carbonaceous sediments are approached, ^{13}C of the ferroan carbonate becomes upto 4‰ heavier. The ^{13}C of the CO_2 and $\delta^{18}\text{O}$ and δD of the water components of the hydrothermal fluid are estimated to have been -3 to -6 , $+5$ to $+10$, and -40 to -60‰ respectively. The geological controls on the distribution of carbonate alteration, and the stable isotopic values of the hydrothermal components suggest that the $\text{H}_2\text{O}-\text{CO}_2$ hydrothermal fluid was of magmatic origin, a result of mantle degassing.

Acknowledgements

I express my appreciation to Dr. J.H. Crocket and Dr. H.P. Schwarcz for their insightful comments during the evolution of this thesis. Their tolerance of my frequent digressions is a tribute to their patience. Funding for the work was provided by an Ontario Geoscience Research Grant, Grant 49, to Drs. Crocket and Schwarcz.

Access to many mining properties in the Timmins area would not have been possible without the permission and co-operation of Pamour Porcupine Mines Ltd. and Gowganda Resources Ltd.

The assistance and advice offered by many individuals resident in the Department of Geology, McMaster University, is gratefully acknowledged. Mr. Jack Whorwood took and prepared most of the photographs incorporated in the text, under trying conditions and at short notice. Mr. Len Zwicker provided excellent thin sections, most prepared totally by hand. Mr. Abdul Kabir performed some of the activation analyses of material from the Carshaw and Malga properties. Mr. Ota Mudrock carefully explained the preparation and analytical methods for both the LECO CO₂ analyser and XRF. Dr. Doug Grundy described the idiosyncrasies of the older XRD equipment. Mr. John Ceker provided many services essential to my research.

Table Of Contents

	Page
CHAPTER 1 Introduction.....	1
1.1 Statement of The Problem.....	3
1.2 Methodology.....	4
1.2.1 Field mapping.....	4
1.2.2 Laboratory studies.....	6
1.3 Thesis.....	9
1.4 Geology.....	10
1.4.1 Marine dolomitic sediment.....	14
1.5 Geochronology.....	15
CHAPTER 2 Rock Alteration.....	16
2.1 Sea Water Alteration-Burial Metamorphism	18
2.2 Intense Carbonatization.....	22
2.2.1 Hydrous alteration facies.....	22
2.2.2 Transitional alteration facies.....	24
2.2.3 Intense carbonatization facies.....	24
2.3 Contact Metamorphism.....	28
2.4 Summary Of Carbonate Types In The Timmins Area.....	29
2.5 Alteration Chronology.....	30
CHAPTER 3 Carbonate Alteration Zones.....	37
3.1 General Distribution.....	37
3.2 Morphology and Localization of Carbonatization.....	38
3.2.1 Intraunit.....	38
3.2.2 Shear zones.....	41
3.2.3 Dykes.....	51
3.2.4 Unconformity.....	52
3.2.5 Bedding plane.....	52
3.2.6 Vein envelope.....	56
3.3 Summary Of Carbonatization Habits and Fluid Access.....	60
3.4 Relationship of Carbonate Alteration Zones To Stratigraphy.....	66
3.5 Volume of Carbonatized Rock.....	70
CHAPTER 4 Types of Gold Mineralization.....	75
4.1 Pyritic, Carbonaceous, Interflow Sediments.....	77

	Page
4.1.1 Pyrite habits and gold tenor of the carbonaceous sediments.....	80
4.1.2 Gold enrichment in the carbonaceous sediments.....	82
4.2 Pyritic, Carbonatized Tholeiitic Basalt..	87
4.2.1 Pyrite habits.....	88
4.2.2 Gold-pyrite association.....	89
4.2.3 Relative age of pyritic gold mineralization in the 55 vein zone.....	89
4.2.4 Other analogues.....	91
4.3 Iron Formation-Hosted Gold.....	92
4.3.1 Gold mineralization.....	94
4.3.2 Gold distribution.....	97
4.3.3 Relative age of gold mineralization....	99
4.3.4 Nature of auriferous fluids.....	101
4.4 Quartz Veins In Carbonatized Mafic and Ultramafic Flows.....	103
4.4.1 Intermineral textures within the veins.	104
4.4.1.1 Hollinger vein suite.....	106
4.4.1.1.1 Primary textures of open-space deposition.....	108
4.4.1.1.2 Replacement textures.....	109
4.4.1.1.3 Deformation textures.....	109
4.4.1.2 Paragenesis of Hollinger veins.....	118
4.4.2 Paragenetic sequences for other properties.....	125
4.4.3 Intramineral textures: implications for stable isotope geothermometry.....	125
4.5 Summary Of Gold Mineralization Features..	129
4.6 Gold/Silver Ratios Of The Mineralization.	130
4.6.1 Geological regimes.....	130
4.6.2 Metal zoning.....	134
4.6.3 Factors influencing the gold/silver ratio.....	134
4.6.3.1 Bulk rock composition.....	136
4.6.3.2 Magmatic centre.....	138
 CHAPTER 5 Characterization and Evolution of The Hydrothermal Fluid Responsible For The Carbonatization.....	 141
5.1 Fluid Inclusion Constraints.....	141
5.2 Constraints On The Fluid System Deduced From Altered Ultramafic Rock.....	144
5.2.1 pH.....	146
5.2.2 fO_2	148
5.2.3 Reaction temperature and CO_2/H_2O molar ratio of the hydrothermal fluid.....	150

	Page
5.2.4 Summary of fluid parameter variations deduced from altered ultramafic rock and fluid inclusions.....	152
5.3 Application of Model to Basalt System....	153
5.4 Miscible or Immiscible Hydrothermal Fluid	155
5.4.1 Implications for carbon and oxygen stable isotopic studies.....	158
5.5 Model Summary.....	159
CHAPTER 6 Stable Isotope Geochemistry.....	161
6.1 Isotope Notation.....	162
6.2 Analytical Methods.....	163
6.2.1 CO ₂ liberation from carbonate minerals.	163
6.2.1.1 Acid fractionation factor.....	164
6.2.2 Fluorination of silicate minerals.....	166
6.2.3 Fluid inclusion H ₂ O and CO ₂	166
6.2.4 Analytical standards.....	166
6.2.5 Analytical precision and accuracy.....	168
6.3 Equilibrium Isotope Fractionation Expressions.....	169
6.4 Error Analysis of Oxygen Isotope Fractionation Expressions.....	176
6.4.1 Experimentally derived isotope fractionation expressions.....	177
6.4.1.1 Error component related to laboratory analyses.....	184
6.4.4 Empirically-derived isotope fractionation expressions.....	186
6.4.2.1 Dolomite-water.....	186
6.4.2.2 Chlorite-water.....	188
6.4.3 Linearly combined isotope fractionation expressions.....	191
CHAPTER 7 Oxygen Isotopic Characteristics Of Quartz Vein Systems.....	193
7.1 Equilibrium Mineral Assemblages.....	194
7.1.1 Equilibrium Tests.....	195
7.1.1.1 Isotopic equilibrium assumed.....	196
7.1.1.2 Concordancy test.....	203
7.1.2 Discussion of equilibrium tests.....	207
7.2 Summary Statement.....	210
7.3 $\delta^{18}\text{O}$ of Vein Quartz and Stratigraphic Position.....	212

	Page
7.4 $\delta^{18}\text{O}$ and $\delta^{13}\text{C}$ of Vein and Wallrock Replacement Carbonate.....	216
7.4.1 Covariation of quartz vein gold tenor with $\delta^{13}\text{C}$ and $\delta^{18}\text{O}$ of vein carbonate..	217
7.5 δD and $\delta^{13}\text{C}$ of Fluid Inclusions From Vein Quartz.....	219
7.5.1 Discussion of the fluid inclusion isotopic results.....	225
7.6 Summary.....	232
CHAPTER 8 Isotope Geochemistry Of Replacement Carbonates From Volcanic Rock.....	235
8.1 Sedimentary Marine Carbonate.....	236
8.2 Hydrothermal Carbonate.....	239
8.2.1 Dispersed calcite.....	240
8.2.2 Replacement carbonate in intense carbonate alteration zones.....	247
8.2.2.1 Replacement calcite.....	248
8.2.2.2 Replacement dolomite and magnesite....	248
8.2.3 Explanation of the stable isotopic profiles.....	251
8.2.3.1 Change in carbonate mineralogy.....	255
8.2.3.2 Temperature.....	256
8.2.3.3 $\text{CO}_2/\text{H}_2\text{O}$ molar ratio.....	259
8.2.3.4 pH and $f\text{O}_2$	265
8.2.4 Summary.....	267
8.3 Regional Isotopic Variation of Hydrothermal Dolomite or Magnesite.....	269
8.3.1 Methane stabilization.....	269
8.3.2 $\delta^{18}\text{O}$ -rich hydrothermal dolomite and vein quartz.....	280
8.3.2.1 Temperature change.....	281
8.3.2.2 Two different fluids.....	282
8.3.2.3 Fluid immiscibility.....	283
8.3.3 Discussion.....	286
8.4 Enhanced Precipitation of Gold.....	288
8.5 Summary.....	288
CHAPTER 9 Source Of Hydrothermal Constituents.....	292
9.1 $\delta^{18}\text{O}$ Of The Water.....	292
9.2 δD Of The Water.....	293
9.3 $\delta^{13}\text{C}$ Of The CO_2	293

	Page
9.4 Reservoirs of H ₂ O and CO ₂ For The Hydrothermal Fluid.....	297
9.4.1 Metamorphic H ₂ O.....	300
9.4.2 Metamorphic CO ₂	302
9.4.3 Hydrospheric CO ₂	305
9.4.4 Magmatic carbon.....	306
9.4.5 Summary.....	309
9.5 Comparison With Other Carbonatized Systems	310
9.6 Geological Constraints On Fluid Origin....	310
CHAPTER 10 Genetic Link With Archean Granulitization....	313
10.1 Characteristics of Granulite Metamorphism	318
10.1.1 Metamorphic fluid constitution.....	318
10.1.1.1 Role of major, crustal structures....	320
10.1.2 Geochemistry of granulite-grade rocks..	321
10.1.3 Depletion mechanism.....	322
10.1.4 $\delta^{13}\text{C}$ of the fluid involved in granulite metamorphism.....	326
10.2 Model.....	329
10.2.1 Extension of the Model.....	330
10.2.1.1 Fluid evolution with progressive CO ₂ influx.....	330
10.2.1.2 Associated igneous K- and Na-rich intrusive suite.....	332
10.2.1.3 Sodic and potassic alteration.....	334
10.2.2 Summary.....	335
References.....	338
Appendix-1: Geochemical Data Base And Some Property Maps.....	362
Appendix-2: Textural Relationships Between And Paragenesis Of Carbonate And Silicate Phases In Quartz Veins.....	382
Appendix-3: Sample Preparation, Analytical Techniques And Model Calculations For Oxygen And Carbon Isotopic Measurements.....	388
Micro-fiche Containing Geochemical Data Base and Large Field Maps Contained In Back Folder	

List Of Figures

Figure	Page
1-1 Location of mining properties in the Timmins area.....	2
1-2 Location of Stewart Abate and Croesus properties..	5
1-3 Stratigraphic subdivision of the volcano-sedimentary units, Timmins area.....	11
1-4 General geology, Timmins area.....	12
2-1 Alteration chronology, Timmins area.....	17
2-2 Subdivision of carbonate alteration facies.....	23
2-3 [MgO/(MgO+CaO)] weight percent ratio as a function of loss on ignition for ultramafic rocks.....	26
3-1 Surface geological plan of the Davidson-Tisdale property, Tisdale Township.....	40
3-2 Surface geological plan of the Stewart Abate property, Beatty Township.....	42
3-3 Surface geological plan of the McEnaney property, Ogden Township.....	43
3-4 Surface geological plan of the Canusa property, Whitney Township.....	44
3-5 Surface geological plan of the Porcupine Triumph property, Deloro Township.....	45
3-6 Surface geological plan of the McLaren (Duval) Porcupine glory hole property, Deloro Township....	47
3-7 Large-scale fault controlled carbonate alteration in the McDonald Lake area, Deloro Township.....	49
3-8 Surface geological plan of the Faymar property, Deloro Township.....	50
3-9 Surface geological plan of the Carshaw iron formation property, Carmen Township.....	54
3-10 Surface geological plan of the McLaren (Duval) south vein property, Deloro Township.....	55
3-11 Surface geological plan of the Croesus property, #2 vein, Munro Township.....	57
3-12 Summary of carbonatization environments.....	61
3-13 Regional spatial association between major structures and gold mines and prospects in the Abitibi Greenstone Belt of northeastern Ontario...	63
3-14 Hierarchical fluid distribution scheme.....	65
3-15 Surface geological plan of the Armstrong-McGibbon property, Tisdale Township.....	69
3-16 Regional CO ₂ abundance in volcanic rock, Timmins area.....	71
4-1 Surface geological plan of the south half of the Hollinger Mine, Tisdale Township.....	84

Figure	Page
4-2 #92 vein system in carbonaceous sediment, Hollinger Mine.....	85
4-3 Surface geological plan of the Malga and Carshaw iron properties, Shaw/Carmen Townships.....	93
4-4 Paragenesis for quartz vein samples from the Hollinger Mine.....	119
4-5 Subdivision of Timmins area into five geological regimes.....	131
5-1 Alteration assemblages in ultramafic rocks.....	145
5-2 CO ₂ -H ₂ O fluid evolution as it interacts with ultramafic rocks.....	147
5-3 T-XCO ₂ for the system MgO-SiO ₂ -CO ₂	151
5-4 Isobaric equilibrium curves for the reaction: 1Talc + 3CO ₂ = 4Quartz + 3 Magnesite + 1H ₂ O at 1 and 2Kb fluid pressure.....	154
5-5 Empirical solvus for CO ₂ -H ₂ O with 2.6 wt % NaCl.....	157
6-1 Time studies for reaction of ferroan dolomite and magnesite with 100% phosphoric acid at 25°C.....	165
7-1 Quartz-sericite-chlorite oxygen isotope concordancy plot for samples from the Dome Mine and Yellowknife areas.....	204
7-2 Quartz-dolomite-chlorite oxygen isotope concordancy plot for data from the Carshaw Mine...	206
7-3 Quartz-calcite-chlorite oxygen isotope concordancy plot for data from the Faymar Mine....	208
7-4 Oxygen isotope values of vein quartz, gold tenor and stratigraphic position.....	215
7-5 Sample location on the 51 vein, Pamour #1 Mine....	218
7-6 Covariation of oxygen and carbon isotopic values of vein dolomite and gold tenor in the 51 vein, Pamour #1 Mine.....	220
7-7 D-values of fluid inclusion water, liberated from vein quartz.....	224
7-8 Quantitative model of D partitioning between H ₂ O, CH ₄ or H ₂ , resulting from the stabilization of CH ₄ or H ₂ at the expense of H ₂ O.....	227
7-9 Quantitative model of ¹³ C partitioning between CO ₂ and CH ₄	229

Figure	Page
7-10 Covariation between hydrogen and carbon isotopic values of water from fluid inclusions, liberated from vein quartz.....	230
8-1 $\delta^{13}\text{C}$ -values for different carbonate types in the Timmins area.....	241
8-2 $\delta^{18}\text{O}$ -values for different carbonate types in the Timmins area.....	242
8-3 Calculated $\delta^{18}\text{O}$ -value of a hydrothermal fluid which reacted with basalt as a function of varying water/rock ratios.....	245
8-4 $\delta^{13}\text{C}$ and $\delta^{18}\text{O}$ profiles of hydrothermal carbonate and whole rock CO_2 across the Beaumont alteration zone, Tisdale Township.....	250
8-5A Variation of $\delta^{13}\text{C}$ - and $\delta^{18}\text{O}$ -values of hydrothermal carbonate and whole rock CO_2 , Davidson Tisdale alteration zone.....	252
8-5B Variation of $\delta^{13}\text{C}$ - and $\delta^{18}\text{O}$ -values of hydrothermal carbonate and whole rock CO_2 , McEnaney alteration zone.....	253
8-6 Change in fractionation of carbon isotopes between dolomite-carbon dioxide and dolomite-water as a function of temperature.....	258
8-7 Effect of Rayleigh distillation on the $\delta^{13}\text{C}$ -value of the CO_2 component of a fluid as a function of temperature.....	264
8-8 pH-log $f\text{O}_2$ trajectory for a CO_2 -bearing, subcritical, aqueous, hydrothermal fluid which reacts with an ultramafic rock.....	266
8-9 Regional variation of $\delta^{13}\text{C}$ -values of hydrothermal vein and wallrock replacement dolomite and magnesite.....	270
8-10 Regional variation of $\delta^{18}\text{O}$ -values of hydrothermal vein and replacement dolomite and magnesite and vein quartz.....	271

Figure	Page
8-11 Regional variation of $\delta^{13}\text{C}$ -values of hydrothermal vein and wallrock replacement dolomite and magnesite in northern Whitney Township.....	273
8-12 $\delta^{13}\text{C}$ -values of hydrothermal dolomite and magnesite as a function of gold tenor of properties.....	275
8-13 Rayleigh distillation model of the change in $\delta^{18}\text{O}$ of water resulting from the separation of CO_2 from an initially miscible $\text{CO}_2\text{-H}_2\text{O}$ fluid.....	284
9-1 $\delta_{\text{D}}\text{-}\delta^{18}\text{O}$ fluid classification diagram.....	298
9-2 $\delta^{13}\text{C}$ of terrestrial carbon-bearing phases.....	299
9-3 $\delta^{13}\text{C}\text{-}\delta^{18}\text{O}$ fluid classification diagram.....	301
10-1 Distribution of host rock ages for lithologies which host gold mineralization.....	315
10-2 Geochemical, P-T, and constitutional characteristics of the fluids which are inferred to have induced granulite and amphibolite grade metamorphism.....	319
10-3 Schematic model.....	331

List Of Tables

Table	Page
1-1 Volcano-sedimentary stratigraphy in the Timmins area.....	7
3-1 Geological features which served to localize carbonate alteration.....	39
3-2 Present day masses of carbon in crustal reservoirs.....	74
4-1 Habits of gold mineralization.....	76
4-2 Gold concentrations in pyrite separated from carbonaceous sediments.....	83
4-3 Gold concentrations in pyrite separated from ore material and iron formation mesobands, Carshaw property.....	100
4-4 Properties from which quartz vein samples were sampled for examination in thin section.....	105
4-5 Intermineral textures and paragenesis of quartz vein samples from the Hollinger Mine.....	107
4-6 Paragenesis of other quartz vein systems.....	126
4-7 Gold/silver ratios of mineralization in each geological regime.....	132
4-8 Gold/silver production figures and ratios for gold mineralization in the Kirkland Lake and Larder Lake areas.....	137
5-1 Compilation of fluid inclusion data for Archean gold-quartz veins.....	143
6-1 Carbonate-acid oxygen isotope fractionation factors.....	167
6-2 Replicate isotopic analyses of GCS, the "inhouse" carbonate standard.....	170
6-3 Equilibrium mineral-water and mineral-mineral oxygen isotopic fractionation expressions.....	171
6-4 Equilibrium mineral-CO ₂ and gas-CO ₂ carbon isotopic fractionation expressions.....	175
6-5 Error analysis for quartz-water oxygen isotope fractionation expression.....	178
6-6 Cumulative error analysis of several oxygen isotope fractionation expressions.....	181
6-7 Temperature uncertainty for several mineral-mineral oxygen isotope geothermometers.....	192
7-1 Oxygen isotope data for vein minerals from various properties in the Timmins area.....	197
7-2 Oxygen isotope geothermometry for quartz veins in the Timmins and Yellowknife areas.....	200

Table	Page
7-3 Oxygen and carbon isotopic analyses of ferroan dolomite and magnesite for some gold properties....	213
7-4 Carbon and hydrogen isotopic analyses of fluid inclusion CO ₂ and H ₂ O respectively, liberated from vein quartz.....	223
8-1 Chemical analysis of sedimentary marine dolomite...	237
8-2 Criteria to distinguish dispersed calcite from the replacement calcite.....	249
9-1 $\delta^{13}\text{C}$ -values of hydrothermal dolomite and magnesite from the Timmins and Larder Lake areas...	296
9-2 $\delta^{13}\text{C}$ -values of hydrothermal carbonates from the Archean of Australia and the Phanerozoic Motherlode belt.....	311

List Of Photographic Plates

Photo	Page
2-1a Colloform textured, vesicle-filling quartz.....	20
2-1b Blocky, vesicle-filling quartz.....	20
2-1c Quartz and chlorite filling a vesicle.....	20
2-1d Blocky quartz and calcite filling vesicle.....	21
2-2 Carbonate alteration assemblage replacing pre-existing vesicle-filling assemblage.....	31
2-3 Carbonatized, ultramafic conglomerate, Pamour #1 Mine.....	33
2-4 Ultramafic and quartz-feldspar porphyry fragmental, Buffalo Ankerite Mine.....	33
3-1 Carbonatized, flow top breccia, Kinch property....	53
3-2 Secondary, ferroan carbonate replacing matrix of a flow top breccia.....	53
3-3 Flat quartz veins in carbonatized, ultramafic flow, Beaumont property, Tisdale Township.....	59
3-4 Highly strained pillows, ore zone of Buffalo Ankerite Mine, Deloro Township.....	68
4-1 Carbonaceous sediment, 68E vein zone, Hollinger Mine, Tisdale Township.....	79
4-2 Deformed, microbanded pyrite in carbonaceous sediment, 68E vein zone, Hollinger Mine.....	79
4-3a Fine grained, laminated pyrite from carbonaceous sediment, Hollinger Mine.....	81
4-3b Recrystallized pyrite domains within fine grained laminated pyrite.....	81
4-4 Disseminated pyrite from carbonatized basalt, 55 vein zone, Hollinger Mine.....	90
4-5 Shallow dipping quartz veins in 55 vein zone, Hollinger Mine.....	90
4-6 Secondary ferroan carbonate in magnetite mesoband Carshaw iron formation.....	95
4-7 Pyrite replacement envelope developed adjacent to a quartz vein, Carshaw iron formation.....	96
4-8 Stratiform pyrite in chlorite mesoband, Carshaw iron formation.....	98
4-9a Transmitted light photo of sulphidization of carbonate-bearing, magnetite mesoband, Carshaw iron formation.....	102
4-9b Reflected light photo of sulphidization of carbonate-bearing, magnetite mesoband, Carshaw iron formation.....	102
4-10a Quartz and later dolomite in quartz vein, 55 vein zone, Hollinger Mine.....	110
4-10b Chlorite fills vug and coats euhedral vein quartz crystal, Carshaw iron formation.....	110

Photo	Page
4-11a Dolomite replaces vein quartz.....	111
4-11b Dolomite cross-cuts vein quartz crystals.....	111
4-11c Rafted quartz by secondary white mica.....	112
4-12a Strained extinction in vein quartz.....	114
4-12b Subgrained vein quartz.....	114
4-12c Deformed, deformation twins in vein albite.....	115
4-12d Kinked white mica in quartz vein replaces dolomite, Duval south vein.....	116
4-12e Trains of secondary fluid inclusions cross-cut vein quartz crystals.....	116
4-12f Styolitic chlorite developed in vein quartz.....	117
4-13a Pyrite and chalcopyrite cross-cut vein quartz, Faymar Mine.....	121
4-13b Gold in cataclastic pyrite, Faymar mine.....	121
4-13c Gold, galena and gangue localized along an apparent growth plane in pyrite, Hollinger Mine..	122

List Of Field Maps

Map No.		Location
1	Aunor Mine surface.....	Appendix-1
2	Aunor Mine, 1000 foot level.....	Appendix-1
3	Beaumont property.....	Micro-fiche
4	Broulan Reef.....	Appendix-1
5	Buffalo Ankerite.....	Micro-fiche
6	Buffalo Ankerite, northwest.....	Appendix-1
7	Canusa Surface.....	Micro-fiche
8	Canusa glory hole.....	Appendix-1
9a	Carshaw Surface.....	Micro-fiche
9b	Malga Surface.....	Micro-fiche
10	Davidson-Tisdale, Armstrong-McGibbon, Crown Chartered.....	Appendix-1
10a	Davidson-Tisdale.....	Micro-fiche
11	Davidson-Tisdale glory hole.....	Appendix-1
12	Armstrong-McGibbon/Crown Chartered....	Micro-fiche
13	Delnite Mine Surface.....	Micro-fiche
14	Dobell Surface.....	Micro-fiche
15	Duval Surface Area.....	Appendix-1
16	Duval Glory Hole.....	Appendix-1
17	Duval South Vein.....	Appendix-1
18	Faymar Mine Surface.....	Appendix-1
19	Hugh Pam Mine Surface.....	Appendix-1
21	Northern Whitney Township.....	Micro-fiche
22	North Whitney property.....	Appendix-1
23	Hollinger Mine Surface Area.....	Appendix-1
24	Kinch property.....	Appendix-1
25	McEnaney property.....	Appendix-1
25b	McEnaney Trench Detail.....	Micro-fiche
26	Porcupine Triumph property.....	Appendix-1
27	Russel property.....	Micro-fiche
28	Stewart-Abate property.....	Micro-fiche
30	Tisdale Township, northeast.....	Micro-fiche
31	Whitney Township, northwest.....	Micro-fiche
32	Whitney Township, northeast.....	Micro-fiche
33	Deloro Township, northwest.....	Micro-fiche

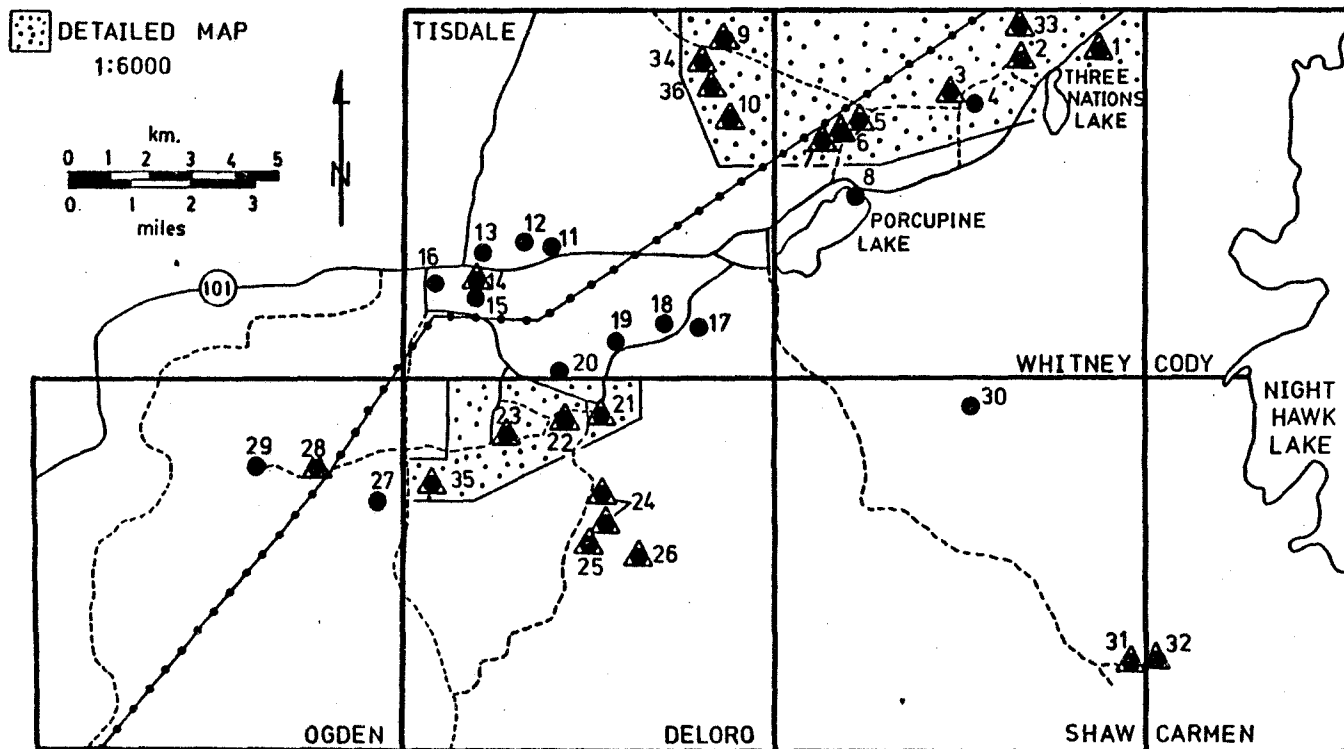
1. Introduction

The Porcupine Camp lies within the Early Precambrian Abitibi Greenstone Belt in northeastern Ontario. The city of Timmins, located approximately 700 Km north of Toronto and 700 Km northwest of Ottawa, Canada's capital, lies at the centre of the Porcupine Camp. To date (1985), approximately 1,600,000,000 g of gold (57 million troy ounces) have been won from 25 deposits (Fig. 1-1). With respect to production from other primary gold mining districts in Precambrian terranes, the Porcupine Camp ranks 4th behind the Witwatersrand, the Egypt-Sudan and Zimbabwe (Kavanagh, 1979). Of this total production, approximately 40% came from the former Hollinger Mine (Pamour Porcupine Mine Timmins Property), while the Dome Mine and McIntyre Mine (Pamour Porcupine Mine Schumacher Property) each contributed about 20% of the total production. Presently (spring 1985) only 3 mines are still in production; Dome Mine, Pamour #1 Mine and Pamour Schumacher Property (formerly McIntyre Mine). New discoveries in the area include the Owl Creek and Hoyle Pond deposits (Kidd Creek Mines), the Canamax Resources-Du Pont Hoyle property and the Asarco Aquarius deposit.

Fig. 1-1: Location of mining properties in the Timmins area which are referenced in this report

- | | |
|----------------------|-------------------------|
| 1. Hoyle | 19. Paymaster Porcupine |
| 2. Pamour #1 | 20. Edwards |
| 3. Hallnor | 21. Buffalo Ankerite |
| 4. Reef | 22. Aunor |
| 5. Broulan Reef | 23. Delnite |
| 6. Hugh Pam | 24. Duval |
| 7. Canusa | 25. Porcupine Triumph |
| 8. Porcupine Lake | 26. Faymar |
| 9. Beaumont | 27. Kenilworth |
| 10. Davidson Tisdale | 28. McEnaney |
| 11. Coniaurum | 29. Desantis |
| 12. McIntyre | 30. Goose Lake |
| 13. Gilles Lake | 31. Malga |
| 14. Hollinger | 32. Carshaw |
| 15. Vipond | 33. North Whitney |
| 16. Moneta | 34. Kinch |
| 17. Preston | 35. Russel |
| 18. Dome | 36. Dobell |

Triangular symbols illustrate properties where detailed mapping has been carried out for this study. The city centre of Timmins is located in the southwest corner of Tisdale Township. The older familiar names of properties have been used on this figure.



1.1. Statement of The Problem

It has long been recognized that gold mineralization in the Timmins area, and elsewhere in the Abitibi Belt, occurs within zones of carbonate alteration (Burrows, 1924; Hurst, 1935; Ferguson et al., 1968; Karvinen, 1976, 1978, 1981; Pyke, 1975, 1981, 1982). However, not all zones of carbonate alteration are associated with gold mineralization. Did the mineralized and unmineralized alteration zones form from different hydrothermal fluids? Perhaps the fluids which produced the carbonate alteration were genetically unrelated to the auriferous fluids, but the carbonatization provided a suitable ground preparation for the later deposition of gold.

The following questions have been addressed in this thesis: 1) what are the field, mineralogical and chemical characteristics of the carbonate alteration zones?; 2) what controlled the localization of the carbonate alteration?; 3) when did the carbonate alteration take place?; 4) what were the conditions (temperature, pH, fO_2) of carbonatization?; 5) from what reservoir or source(s) was the hydrothermal carbon derived?; 6) what genetic link, if any, existed between the carbonate alteration and gold mineralization? Unique solutions, although desirable, are not possible for all these questions because of uncertainty associated with some aspects of the geological and geochemical systems.

1.2. Methodology

1.2.1. Field mapping

Field mapping at scales of 1:6000, 1:2400 and 1:1200 was carried out in parts of Whitney, Tisdale, Deloro and Ogden Townships in the Porcupine Camp (Fig. 1-1) and in Beaty and Munro Townships, located east of the Porcupine Camp (Fig. 1-2), to characterize the mesoscopic features of the alteration systems, to establish the volcanic stratigraphy on a flow-by-flow basis, to establish the spatial relationship between the zones of carbonate alteration and the volcano-sedimentary stratigraphy, to identify the regional extent of carbonate alteration, and to acquire a regional sample data base. In general, detailed mapping (1:1200) was restricted to selected mining properties or prospects which had attracted past prospecting because carbonate alteration and/or quartz veining with or without gold mineralization was present. In total, 23 properties were examined in detail in the Timmins area (Fig. 1-1) and 2 were studied east of Matheson (Fig. 1-2).

Field maps are included in Appendix-1 and in the map pocket. Individual property geology must be considered in the context of the regional geological setting and excellent summaries by Burrows (1924), Carlson (1967), Ferguson et al. (1968), Davies (1977), Karvinen (1981), and Pyke (1982), should be consulted. The stratigraphic subdivision proposed

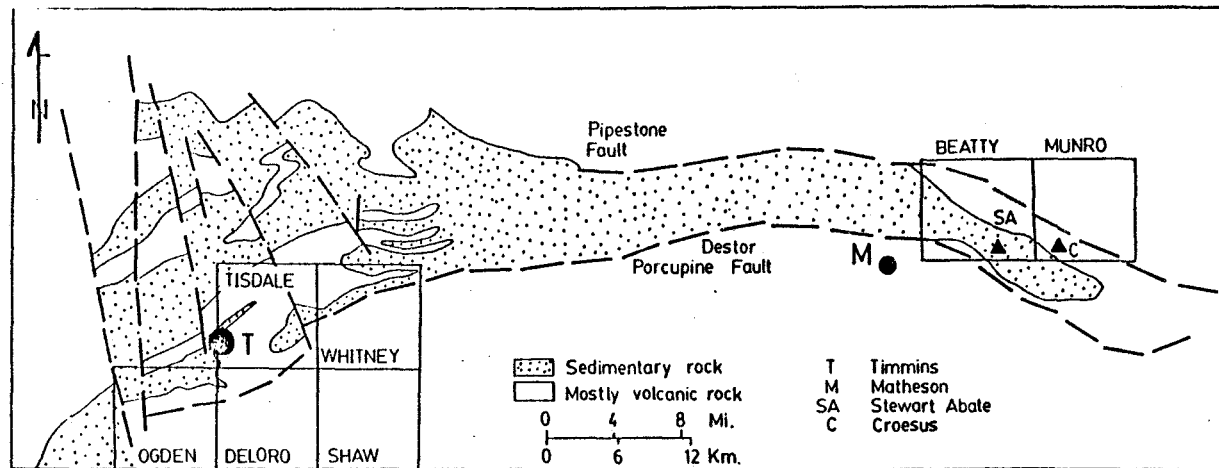


Figure 1-2: Location of the Stewart Abate and Croesus properties with respect to the Timmins area.

by Pyke (1982, 1975) will be followed here (Table 1-1) as are the volcanic rock classification schemes proposed by Jensen (1976) and Arndt and Nisbet (1982).

The field mapping is a necessary prerequisite to the follow-up laboratory studies as it defines a geological control for the samples in terms of their spatial relationship to each other and to important geological features. Further, the controls on the distribution of carbonate alteration, an important parameter to be ascertained for this thesis, can be deduced only from the detailed field geology. With this geological control, hypothetical models describing fluid access into and circulation within the supercrustal sequence, can be deduced. The comprehension of this system is a critical aspect of the hydrothermal event which culminated with the localized concentration of gold at levels 3 to 4 orders of magnitude above its Clarke value.

1.2.2. Laboratory studies

Selected samples were examined petrographically in both transmitted and reflected light mode to identify the mineralogy and textural relationships. The carbonate mineralogy was identified by X-ray diffraction (XRD) which distinguishes between calcite, siderite, magnesite and dolomite-ankerite, but does not allow a resolution of the dolomite-ankerite solid solution series. Carbonates

Table 1-1: Volcano-sedimentary stratigraphic subdivision of the Timmins area.

Dunbar (1948)	Ferguson <u>et al.</u> (1968)	Pyke (1975)	Pyke (1981)
Timiskaming	Timiskaming	Porcupine Group	Porcupine Group
	Keewatin	Upper Formation	Upper Formation
		Lower Formation	Lower Formation
Hoyle	Tisdale Group	Tisdale Group	Tisdale Group
	Gold Centre Subgroup	Krist Formation	Upper Formation
	Vipond Subgroup	Schmuacher Formation	Middle Formation
Tisdale Group	Central Subgroup	Goose Lake Formation	Lower Formation
	Northern Subgroup		
Deloro Group	Deloro Group	Deloro Group	Deloro Group
		Boomerang Formation	Upper Formation
		Redstone Formation	Middle Formation
		Donut Formation	Lower Formation

identified as dolomite-ankerite are referred to as ferroan dolomite in this thesis. This information forms the basis of the alteration assemblage description, the nature of the gold mineralization, and a chronological synthesis for major hydrothermal events. Some samples were analysed by X-ray fluorescence (XRF) or neutron activation for major and certain trace elements to allow a chemical rock classification and to permit a chemical characterization of the alteration process. This analytical data, including some from a M.Sc. thesis by the author (Fyon, 1980), are included in Appendix-1, where samples are filed on a property basis.

To deduce the thermal history of the alteration and mineralization processes and to identify possible source reservoirs for the hydrothermal fluid constituents, the following stable isotopic systems were examined: 1) oxygen isotope geochemistry of quartz, calcite, ferroan dolomite and chlorite from veins; 2) carbon isotope geochemistry of hydrothermal calcite, magnesite and ferroan dolomite from hydrothermally altered volcanic rock; 3) carbon and hydrogen isotope geochemistry of CO_2 and H_2O extracted from fluid inclusions in vein quartz.

This thesis should not be considered as an exhaustive treatise on the stable isotope characteristics of the carbonate alteration and related gold mineralization in the Timmins area. Rather, it is an attempt to assess the

application potential of stable isotopic studies to polyphase deformed mineralized systems of Archean age and to integrate the laboratory support tools into a geological framework from which a geologically reasonable and consistent model of alteration and mineralization is presented.

1.3. Thesis

By considering the field and geochemical data collectively, it will be argued that the CO₂-bearing hydrothermal fluid which carbonatized volcano-sedimentary, supercrustal rocks, was derived from the mantle. These juvenile CO₂-bearing fluids gained access to the supercrustal rocks by utilizing regionally extensive deformation zones, which probably penetrated to the lower levels of the crust. The fluids were dispersed through the supercrustal volcano-sedimentary sequences along less extensive subsidiary planar zones such as faults, shear zones and flow contacts.

1.4. Geology

The geology of the Timmins area has been reviewed by Dunbar (1948), Ferguson et al. (1968), Davies (1979), Pyke (1975, 1981), and Hodgson (1982). Two cycles of volcanic rock are recognized (Fig. 1-3, 1-4). The older Deloro Group consists of a poorly preserved lower division of komatiitic flows (Formation I), a largely calc alkaline basalt-andesite middle division (Formation II) and is capped by felsic calc alkaline extrusive volcanic rock, and abundant sulphide- and oxide-rich iron formation (Formation III). The overlying, younger Tisdale Group also consists of three volcanic formations. Ultramafic and basaltic komatiitic flows and magnesium tholeiitic basalt define the lowest division of the Tisdale Group (Formation IV). The middle and upper divisions consist of iron-rich tholeiitic basalt (Formation V) and felsic calc alkaline pyroclastic deposits (Formation VI) respectively. Quartz-albite feldspar porphyry (QFP) intrusive dykes and sills are concentrated in the immediate Timmins area and cut the volcanic rocks in Formations IV and V of the Tisdale Group. Iron formations are quite rare in the Tisdale Group, although carbonaceous interflow sedimentary rocks are common.

The Porcupine Group metasediments consist dominantly of turbidites, although a thin unit of fluvial deposits is developed at the top of the clastic sequence (Lorsong, 1975; Pyke, 1982). The lower portion of the Porcupine Group

Figure 1-3: Stratigraphic subdivision of the volcano-sedimentary stratigraphy in the Timmins area, simplified after Pyke (1981).

LEGEND



GRANITIC ROCKS



PORCUPINE GROUP



TISDALE GROUP

FORMATION 6



FORMATION 5



FORMATION 4



DELORO GROUP

FORMATION 3



FORMATION 2

GEOLOGICAL CONTACT

FAULT

ANTICLINE, SYNCLINE

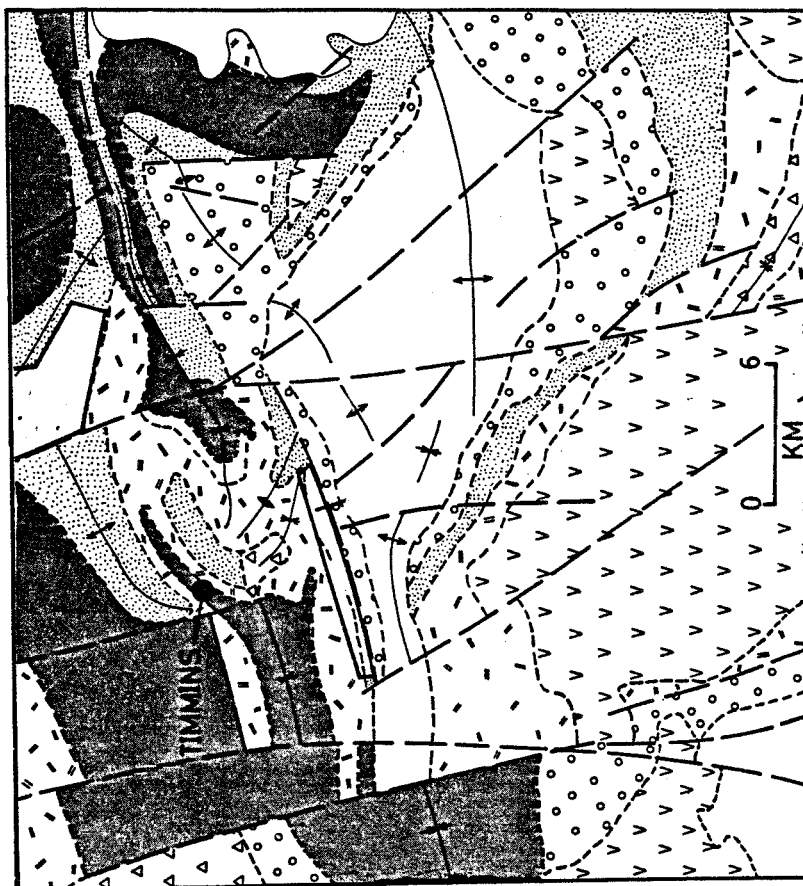
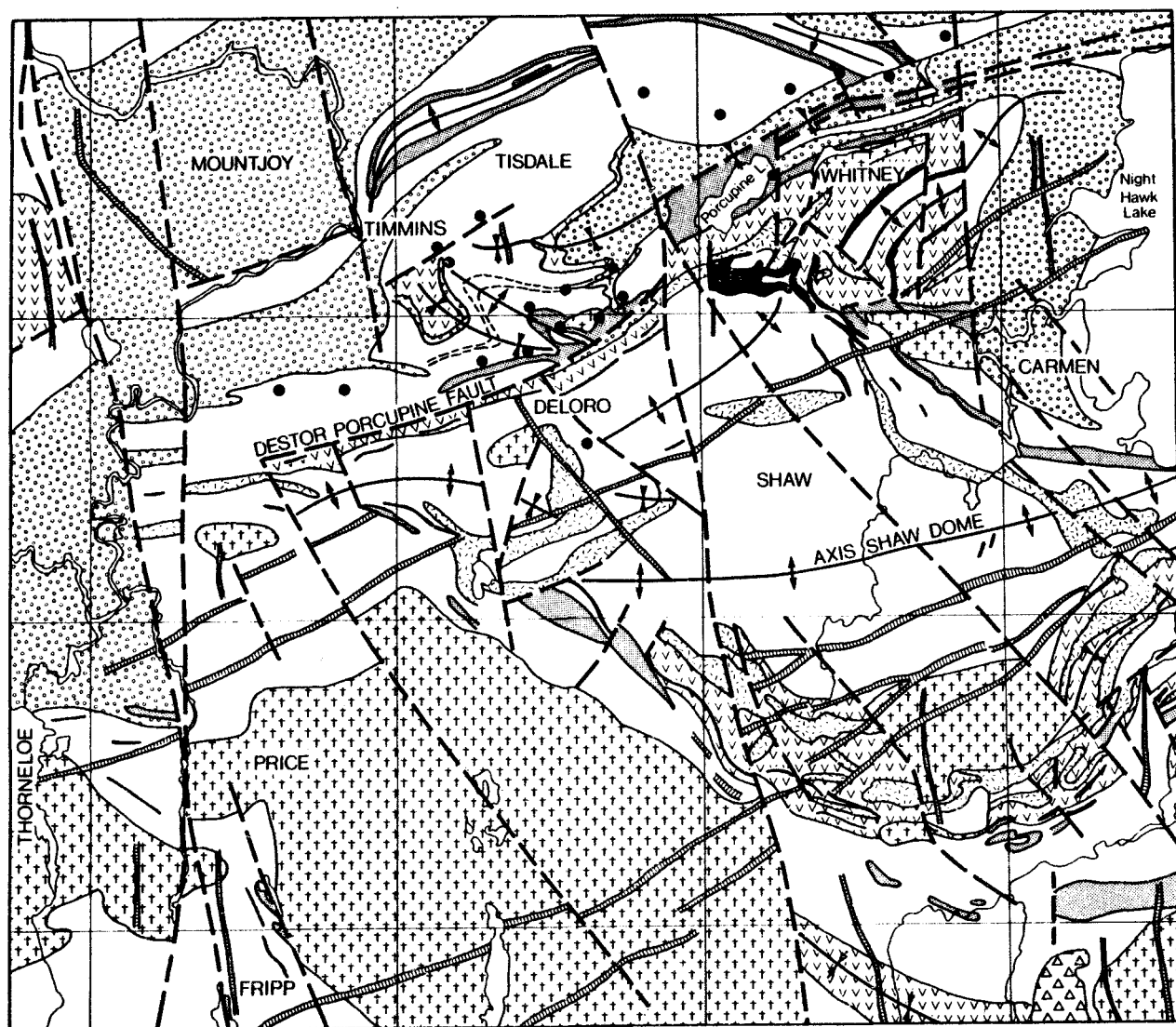



Figure 1-4: General geology of the Timmins area,
after Pyke (1981).


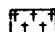
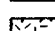



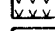




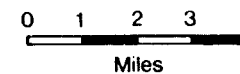
LEGEND

MIDDLE PRECAMBRIAN

-  Cobalt Formation
greywacke, arkose, argillite, conglomerate
unconformity

EARLY PRECAMBRIAN

-  Diabase *
-  Intrusive Contact
-  Granitic intrusive rocks
Intrusive Contact
-  Ultramafic intrusive rocks
Intrusive Contact
-  Sediments (dominantly turbidites)
-  Iron formation
-  Felsic to intermediate volcanics
-  Mafic volcanics
-  Ultramafic volcanics
- * Some diabase dikes are Middle to Late Precambrian age
- Location of gold mines (present and past producers)
- - - Fault
- - - Anticlinal axis
- - - Synclinal axis



(historically called Keewatin) is interpreted to be time equivalent with the top of the Deloro Group (Pyke, 1982). The upper portion of the Porcupine Group sediments, formerly called Temiskaming, is interpreted to be time equivalent to the top of the Deloro Group and to the entirety of the Tisdale Group (Pyke, 1980).

An important structural feature, the Destor-Porcupine Fault zone, transects the area. It is a structure of regional extent, having been traced for approximately 500 Km from the Kapuskasing structure in the west to the Grenville Front, east of the Noranda area in Quebec (Milne, 1972; Gelinas et al., 1977). This structure appears to have localized clastic sedimentation and some komatiitic volcanism and is interpreted to have been active during the early evolution of the Abitibi belt (Pyke, 1982; Dimroth et al., 1982).

In the immediate Timmins area, north of the Destor-Porcupine fault, two periods of folding are recognized. Original north-south fold axes appear to have been refolded about an east-west axis (Ferguson et al., 1968; Pyke, 1982). The Shaw Dome defines the main structural feature south of the Destor-Porcupine fault. Within the Tisdale Group, subsidiary faults, such as the Hollinger and Dome faults, trend subparallel to and merge with the Destor-Porcupine fault.

Hodgson (1983) suggests an alternative structural evolution. Following the Tisdale volcanism and deposition of the Lower Porcupine Group sediments, the strata were rotated into subvertical attitudes along listric normal faults. Erosion followed and the Upper Porcupine Group sediments were deposited. Following a prolonged history of strike-slip faulting, a penetrative foliation and strong east plunging lineation was imparted to the volcanic and sedimentary rocks, including the intrusive, quartz-feldspar porphyry bodies.

1.4.1. Marine dolomitic sediment

A carbonate-rich rock exposed on the former Buffalo Ankerite Mine property (northwest area Maps 5 and 6) has some features which suggest it is a marine sediment. Although some discussion is presented now and in later chapters, it is emphasized that this rock type is not abundant in the Timmins area. This buff-coloured, stratiform unit lies within pillowed, magnesium-rich tholeiitic basalts. It rarely exceeds 0.5 metre in thickness and is composed of dolomite and quartz. Some of the quartz in this unit occurs as vein material; however, finer grained (<1mm) polygonalized quartz is intimately mixed with the dolomite and resembles recrystallized chert. No banding is recognizable and so a bedded aspect appears to be absent. This unit is interpreted to be a marine, chert-

bearing, dolomitic precipitate. The carbon isotopic characteristics of this rock, discussed in Chapter 8, are also consistent with such an origin.

1.5. Geochronology

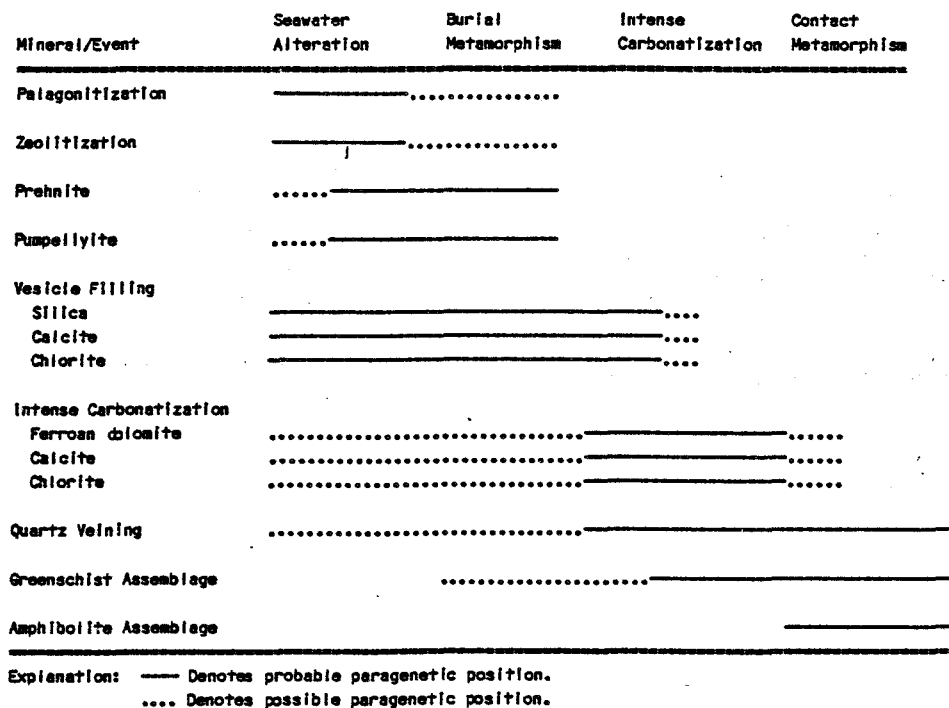
The felsic volcanic rocks which lie at the tops of the Deloro (Formation III) and Tisdale (Formation VI) Groups have ages of 2725 \pm and 2703 \pm 2 million years (m.y.) respectively (Nunes and Pyke, 1980; zircon age). The Pearl Lake and Preston intrusive quartz-feldspar porphyry bodies have zircon ages of 2685 \pm 3 m.y. (S. Marmont, geologist, Mineral Deposits Section, Ontario Geological Survey, pers. com., 1985). The absolute age of the gold mineralization is less well constrained. Preliminary ages, based on single step $^{39}\text{Ar}/^{40}\text{Ar}$ determinations using muscovite, yield an age of 2570 m.y. for the Hollinger mineralization (Kerrick et al., 1984). York et al. (1985) report an age of 2633 \pm 5 m.y. for mica from the Dome Mine and 2617 \pm 5 m.y. for green mica (fuchsite) from the former Hollinger Mine using a multiple step $^{39}\text{Ar}/^{40}\text{Ar}$ mica degassing procedure. Given that the gold-bearing quartz veins cut the intrusive quartz-feldspar porphyry bodies, and assuming that the Dome and Hollinger gold is pre- or syn-mica, then the age of the gold mineralization must lie between 2633 \pm 5 m.y. and 2685 \pm 3 m.y..

2. Rock Alteration

For many ore deposit types, there exists a fundamental relationship between the mineralization and the type of associated rock alteration. Hence the study of rock alteration can reveal much about the chemical characteristics of the hydrothermal fluid and can be a useful guide to economic mineralization.

In the Timmins area, and elsewhere in the Abitibi Greenstone Belt, at least four different rock alteration events can be documented empirically or by inference (Fig. 2-1): 1) low temperature ($< 300^{\circ}\text{C}$) sea water alteration yielding clay-zeolite assemblages (Beaty and Taylor, 1982; Dimroth and Lichtblau, 1979; ; Kerrich and Fryer, 1979); 2) burial metamorphism to prehnite-pumpellyite grade (Jolly, 1978, 1980) or lower greenschist, in part during sea water alteration (Beaty and Taylor, 1982; Dimroth and Lichtblau, 1979); 3) intense carbonatization (Fyon and Crocket, 1982; Karvinen, 1976); 4) contact metamorphism to greenschist and amphibolite facies (Jolly, 1978, 1980). The temporal relationships between the alteration types are not easily deciphered because of mineralogical recrystallization induced by contact metamorphism.

FIGURE 2-1: Idealized alteration chronology deduced to have affected basaltic volcanic rock in the Timmins area.



2.1. Sea Water Alteration - Burial Metamorphism

The earliest hydrothermal event to have affected the volcanic rocks in the Abitibi Belt resulted from lower temperature ($<300^{\circ}\text{C}$) sea water/rock interaction. Possible mineralogical evidence recording this event area in the Timmins area is the presence of calcite and quartz which fill vesicles in the basalt flows. Neither relict clay-zeolite nor prehnite-pumpellyite assemblages persist, although their former presence in the Kirkland Lake (Jolly, 1979, 1980) and Noranda (Dimroth and Lichtblau, 1979) areas of the Abitibi Belt has been documented. Elevated oxygen isotopic whole rock values (+6 to +15‰ SMOW; Beatty and Taylor, 1979, 1982; Kerrich and Fryer, 1979) for the basalt flows from the Timmins area also suggest that they underwent a low temperature, sea water alteration. Such elevated whole rock oxygen isotopic values are characteristic of recent, submarine basalts which have undergone low temperature weathering by sea water (Garlick and Dymond, 1970; Muehlenbachs, 1977). The conspicuous absence of the clay and zeolite mineral assemblages from rocks in the Timmins area can be attributed to the regional greenschist metamorphic overprint.

Jolly (1978, 1980) proposed that following their extrusion the lavas of the Abitibi greenstone belt underwent burial metamorphism to prehnite-pumpellyite grade by simple increase in the temperature with increasing burial depth.

Dimroth and Lichtblau (1979) assign the formation of prehnite and pumpellyite to the low temperature sea water alteration event.

Related to this earliest alteration of the volcanic rocks is the filling of primary porosity (such as vesicles) by quartz, calcite and chlorite. The observed succession of pore-space minerals from vesicle wall to core consists of: 1) quartz, chlorite; 2) quartz, calcite; 3) quartz, chlorite, quartz; 4) quartz. Of these sequences, quartz and quartz-chlorite are the most common, although several sequences may be seen in the same thin section. The vesicle-filling quartz is commonly equant or blocky, but rarely colloform and bladed textures are observed suggesting that this quartz may have had a chalcedony precursor.

The habits of these phases (Photo 2-1), their presence in rocks having elevated oxygen isotope whole-rock compositions (Beatty and Taylor, 1979, 1980; Kerrich and Fryer, 1979) and, as will be argued, the carbon isotope composition of calcite (0 to -3.0‰ PDB; Fyon et al., 1980, 1981) is consistent with their formation during the early, lower temperature ($<300\text{ }^{\circ}\text{C}$) sea water alteration. Although it is uncertain if the chlorite is authigenic or pseudomorphous after a clay precursor, the latter hypothesis is preferred in light of the $\delta^{18}\text{O}$ whole rock compositions. Throughout the balance of this text, the calcite which occurs as a vesicle-filling mineral is

Photo 2-1a: Colloform textured quartz which fills a vesicle in a basalt flow exposed on the Malga property.

Photo 2-1b: Block quartz fills a vesicle in a basalt flow.

Photo 2-1c: Vesicle filled by chlorite (Ch) in the core and quartz (Q) around the outer edge.

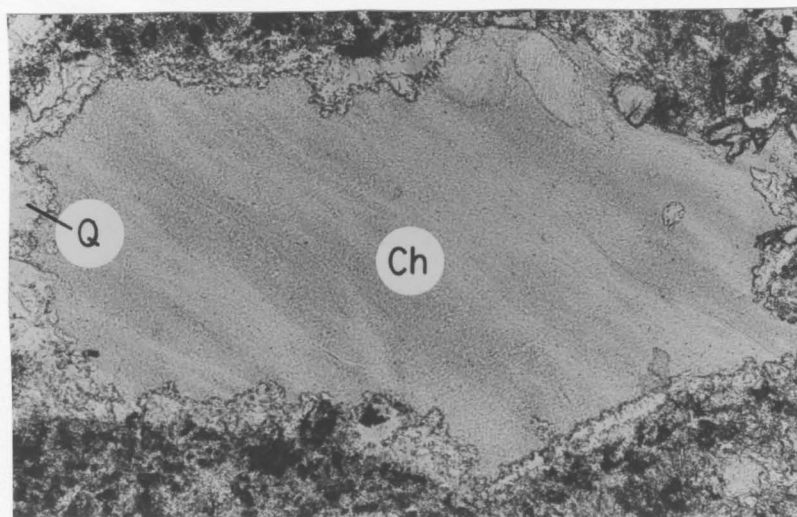
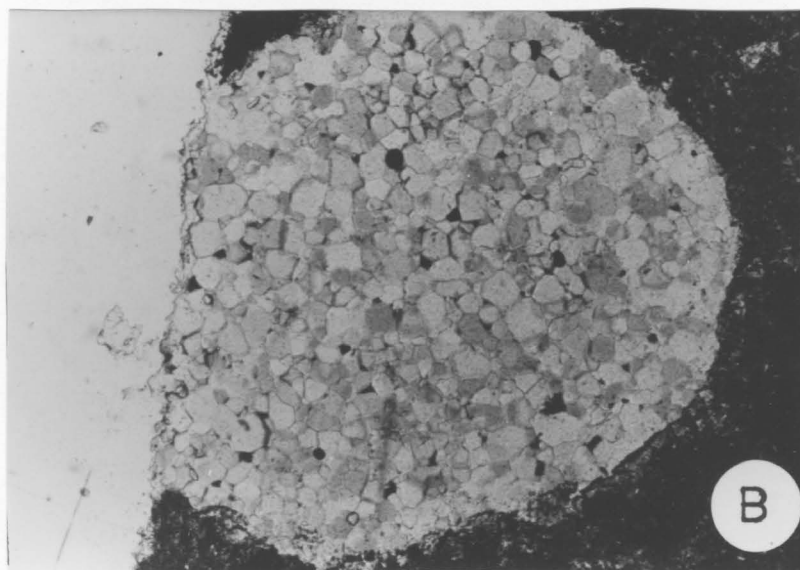
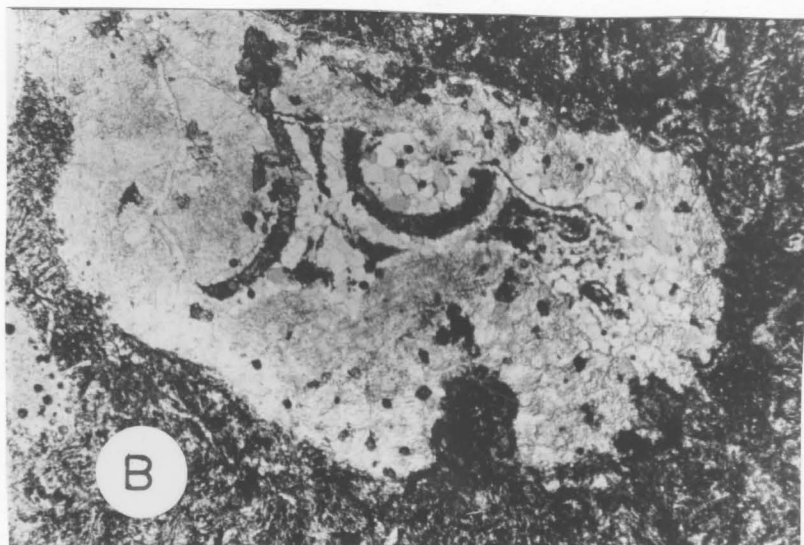
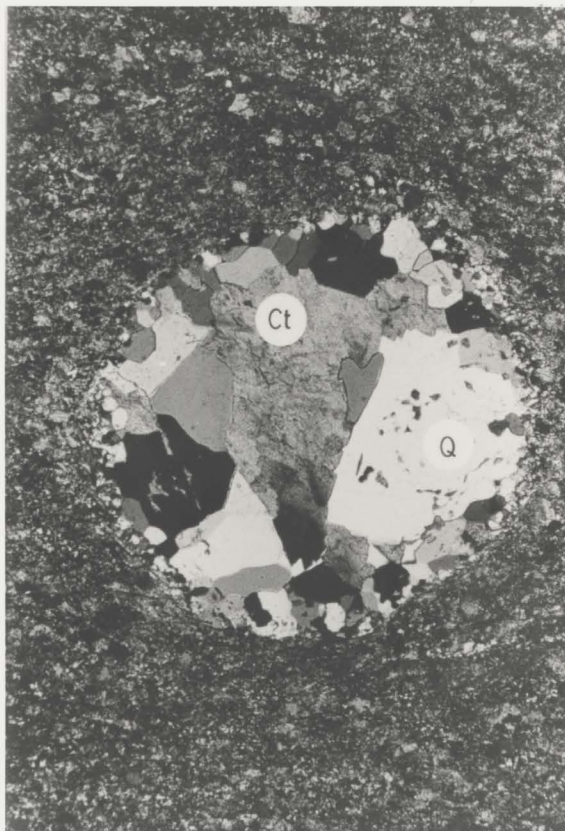


Photo 2-1d: Blocky quartz (Q) and calcite (Ct)
filling a vesicle in a basalt flow.



referred to as "dispersed calcite".

2.2. Intense Carbonatization

This type of alteration is characterized by the development of hydrous and carbonate-rich secondary assemblages (Fig. 2-2). The hydrous alteration assemblage envelopes an inner carbonate-rich assemblage. These two assemblages are separated by a thin transitional zone which consists of both hydrous and carbonate minerals (Bain, 1933; Fyon and Crocket, 1982). This mixed assemblage is called the Transitional Alteration Assemblage. The specific alteration mineralogy in each alteration facies is dependent on the bulk composition of the protolith (Fig. 2-2).

2.2.1. Hydrous alteration facies

Hydration of basaltic rock is marked by the formation of chlorite in veinlets and as a replacement of the rock matrix. Phenocrysts of feldspar (albite) and ferromagnesium minerals are chloritized in the advanced stages of this alteration. Some quartz is produced as a reaction product, although the proportion of free quartz in chloritized rock generally does not exceed 10 to 20 modal percent. In ultramafic rocks, serpentine, talc and tremolite predominate in the hydrous alteration facies (Fig. 2-2). Hydrated basaltic and ultramafic rocks are dark green

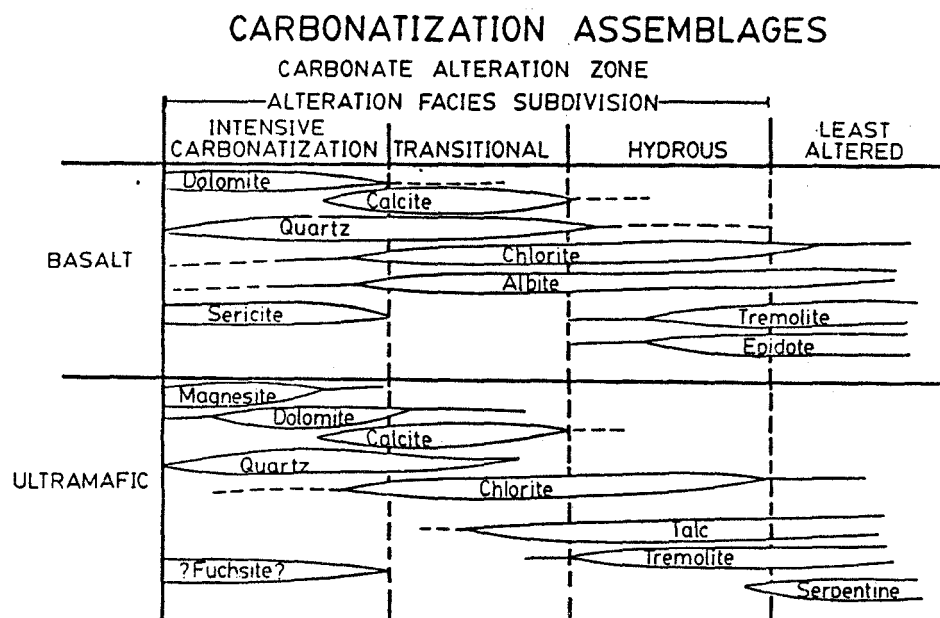


Figure 2-2: Subdivision of carbonate alteration facies in terms of mineral phases in basaltic and ultramafic igneous rock (modified after Fyon and Crocket, 1982).

on the fresh surface and the ultramafic varieties are highly magnetic due to the presence of discrete magnetite grains and veinlets.

2.2.2. Transitional alteration facies

The transitional alteration facies is characterized by the presence of discrete porphyroblastic calcite and/or ferroan dolomite grains present in a chloritic (basaltic rock) or talc-chlorite-tremolite (ultramafic rock) matrix. Grain size of the euhedral carbonate grains can range up to 3 mm. and gives the rock a spotted texture. The boundary between the transitional and the hydrous alteration facies is gradational and somewhat arbitrary. For basaltic rock, this boundary has been assigned at the first appearance of macroscopically visible ferroan dolomite and corresponds to the complete destruction of such calcium-aluminosilicates as epidote and tremolite (or their premetamorphic precursors). The appearance of white mica (sericite) marks the boundary between the transitional and intense carbonatization alteration facies (Fig. 2-2).

2.2.3. Intense carbonatization facies

During the intense carbonatization, all pre-existing Na-Mg-Ca-Fe silicate minerals are destroyed (Fig. 2-2) to produce an alteration assemblage consisting of carbonate,

quartz and sericite. However, the carbonate alteration facies is subdivided into two different assemblages distinguished on the basis of their carbonate mineralogy. An inner ferroan dolomite- or magnesite-bearing assemblage is enveloped by an outer calcite-bearing assemblage (Fyon and Crocket, 1982). Whether magnesite is stable in this alteration facies is dependent on the initial bulk rock composition. Altered komatiitic flows contain secondary calcite, ferroan dolomite or magnesite, depending on the alteration intensity and bulk rock composition (Fig. 2-3). Magnesite is present only in carbonatized ultramafic komatiitic flows (> 20 wt. % MgO) containing at least 18 wt. % loss on ignition (> 14 wt. % CO_2). Magnesite abundance increases with increasing loss on ignition and $MgO/(MgO + CaO)$ whole rock ratio (Fig. 2-3; Fyon et al., 1983b). Basaltic rocks stabilize ferroan dolomite (Fryer et al., 1979) or calcite, depending on alteration intensity (Fig. 2-3).

Rocks which have been intensely carbonatized are light grey (calcite-rich) or buff coloured (ferroan dolomite-rich) on fresh surface and weather rusty brown when the dominant carbonate is ferroan dolomite. The calcite-rich rocks have a weathered surface which is indistinguishable from carbonate-free protoliths.

White mica (sericite or fuchsite) also occurs as an accessory phase within the zone of intense carbonatization.

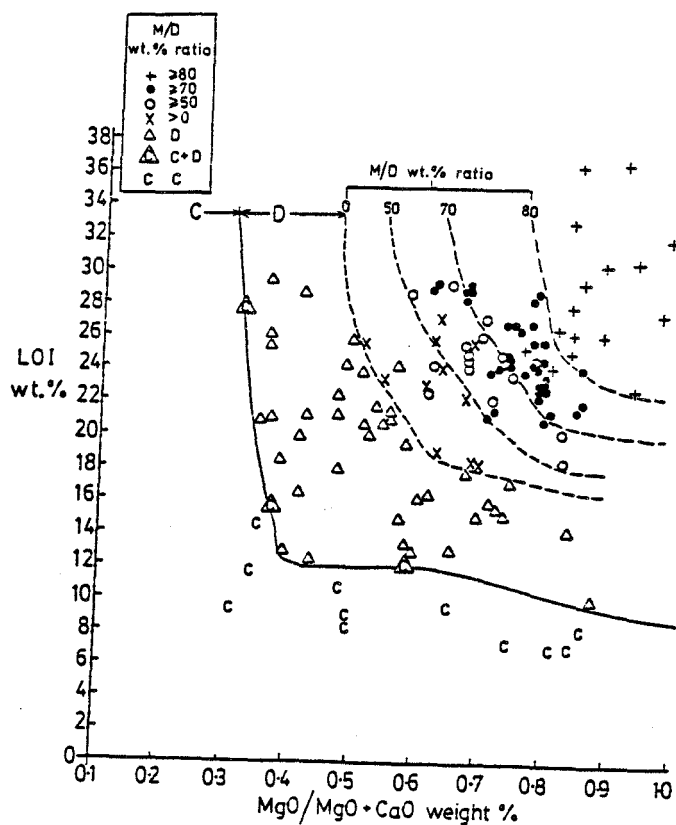


Figure 2-3: Whole-rock $\text{MgO}/(\text{MgO}+\text{CaO})$ weight percent ratio plotted against loss on ignition in weight percent (LOI wt. %) for carbonatized mafic and ultramafic komatiitic flows from the Timmins area. The dashed lines represent magnesite to dolomite weight ratio contours, as established by X-Ray diffraction patterns. The solid line separates the calcite- and dolomite-bearing sample fields. Symbols are as follows: M = magnesite; D = ferroan dolomite; C = calcite.

The restriction of this mica to the carbonate-bearing assemblages and the strong covariation between K_2O or Li whole rock concentration and white mica modal abundance as a function of increasing carbonatization intensity (Fyon, 1980), implies that the mica formed simultaneously with the intensive ferroan dolomite-bearing assemblage.

These observations regarding white mica distribution apply only to those carbonate alteration zones developed in volcanic rocks where quartz veining is not prominent. Downes (1979) demonstrated that fuchsite in the Kerr Addison "green carbonate" ore zone (Larder Lake area) formed after the intense carbonatization of ultramafic flows, adjacent to a late set of quartz veins. Prominent fuchsite-bearing zones in ultramafic rock are relatively rare on the properties examined in the Timmins area. They occur relatively frequently on the Russel, Kenilworth and Desantis properties and sparingly on the former Buffalo Ankerite, North Whitney, and Hollinger (west end of 400 pit) Mine properties. Because the timing of fuchsite deposition on these properties is uncertain, a question mark has been assigned to the fuchsite paragenetic position on Figure 2-2.

Reference will be made periodically to intense carbonatization. Unless otherwise stated, the presence of the hydrous, transitional and carbonate alteration facies is inferred.

2.3. Contact Metamorphism

Jolly (1978, 1980) concluded that the greenschist and amphibolite metamorphic assemblages observed in the Abitibi Greenstone Belt formed by contact metamorphism during the intrusion of Kenoran aged granitoid bodies. Jolly's maps (Jolly, 1978, 1980) clearly illustrate that the greenschist/amphibolite isograd in the metavolcanic rocks is located within 2 kilometres of the granitoid intrusive contact. The regional extent of the greenschist mineralogy is less as convincingly related to the distribution of the intrusive granitoid bodies.

The greenschist facies mineralogy of the least altered basaltic rocks in the Timmins area consists of chlorite, tremolite/actinolite, epidote, albite, quartz and trace calcite. Ultramafic komatiitic flows consist of serpentine with traces of talc, tremolite, chlorite and magnetite. No amphibolite-grade assemblages are developed in the thesis area.

Greenschist assemblages can and do form in modern, submarine basaltic rocks as a result of high temperature (>350°C) seawater/rock interaction (Aumento et al., 1976; Spooner and Fyfe, 1973). These rocks have depleted oxygen isotope whole rock values ($<5.5\text{‰}$, SMOW; Muehlenbachs, 1977), whereas basaltic rock reacted with sea water at low temperatures (<350°C) are replaced by clays, zeolites, prehnite and pumpellyite (Andrews, 1977; Aumento et al.,

1976; Honnorez, 1978; Scarfe and Smith, 1977) and have enriched oxygen isotopic whole rock values ($>5.5\text{‰}$ SMOW; Garlick and Dymond, 1970; Muehlenbachs and Clayton, 1977). The greenschist facies basalts in the Abitibi Belt, including those in the Timmins area, have enriched oxygen isotopic whole rock values ($>5.5\text{‰}$ SMOW; Beaty and Taylor, 1979, 1980; Kerrich and Fryer, 1979). These oxygen isotope data suggest that the greenschist metamorphic assemblage was superimposed upon a pre-existing, lower temperature ($<350^{\circ}\text{C}$) sea water alteration assemblage. This argument is consistent with the textural and mineralogical observations by Jolly (1978, 1980) and Dimroth and Lichtblau (1979) who concluded that the earliest diagenetic and burial metamorphic assemblages, consisted of clay-zeolite and prehnite-pumpellyite-actinolite assemblages respectively, which were subsequently replaced by the greenschist and ultimately amphibolite grade assemblages.

2.4. Summary of carbonate types in the Timmins area

Before addressing the relative temporal relationships between the alteration types, it is important to review the different carbonate habits that occur in the Timmins area:

- 1) a dolomitic sedimentary unit occurs on the former Buffalo Ankerite Mine property (Chapter 1);

2) calcite is widely distributed as a vesicle-filling (dispersed calcite) mineral which was introduced in large part during the early sea water alteration event (Section 2.1);

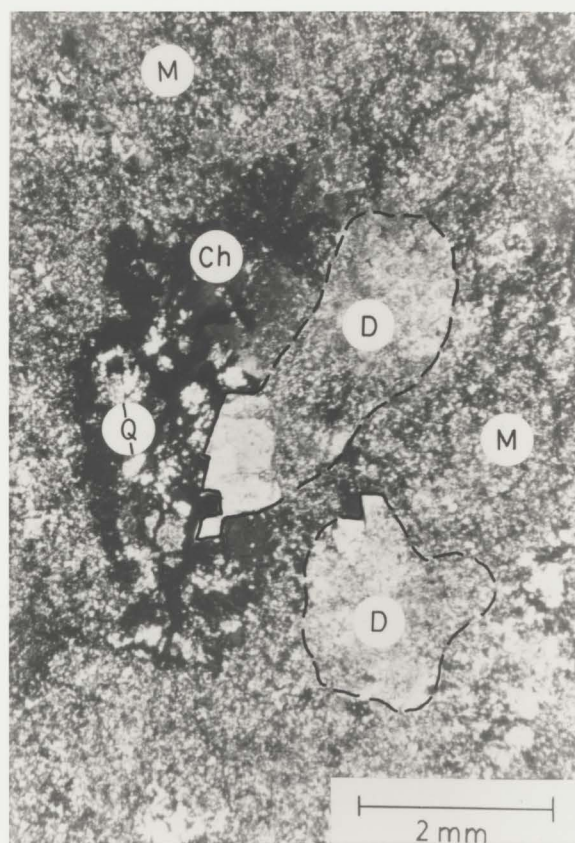
3) calcite and ferroan dolomite exist as replacement minerals in the intensely carbonatized zones and as accessory minerals in quartz veins which cut the carbonatized rocks.

2.5. Alteration Chronology

The following relative chronology describes the precipitation sequence of carbonate in the Timmins area. The precipitation of carbonate began with the accumulation of the subaqueous, dolomitic sediment. Similar, but controversial carbonate-rich sediments occur in the Dome and former Aunor Mines (Fryer and Hutchinson, 1976; Roberts et al ., 1978). On the basis of the very limited distribution of these sediments, this material represents a very small amount of the carbonate in the Timmins area.

The bulk of the carbonate in the Timmins area precipitated from hydrothermal fluids. The precipitation of hydrothermal calcite began with the filling of primary volcanic porosity as the volcanic sequence underwent low temperature sea water alteration. Ferroan dolomite-rich assemblages are superimposed upon the vesicle-filling quartz and calcite (Photo 2-2) which illustrates that the intense

Photo 2-2: Ferroan dolomite (D) replaces the matrix of a chloritized basalt (M) and is superimposed upon an earlier quartz (Q)-chlorite (Ch) vesicle-filling assemblage.



carbonatization event took place later in the alteration history of the volcanic rocks.

The temporal relationship between the intense carbonate alteration and the contact metamorphic greenschist/deformation event is less certain. Evidence favouring a relatively early age for the intense carbonatization includes:

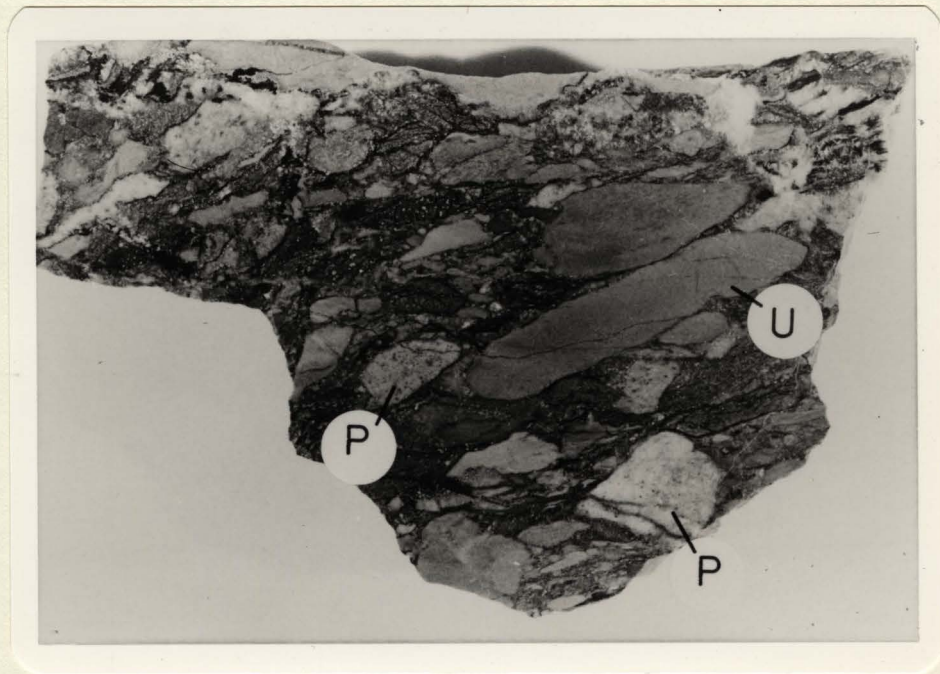
- 1) carbonate-rich clastic units (Photo 2-3) occur within parts of the Porcupine Group sediments which are interpreted by Pyke (1975, 1981) to be time equivalent with and derived from the Tisdale Group volcanic rock, suggesting that a carbonatized ultramafic source rock existed on the ocean floor from which the conglomeratic material was derived.

- 2) ultramafic clasts present in a fragmental unit, exposed on the former Buffalo Ankerite Mine property (Photo 2-4), show variable degrees of carbonatization, suggesting that this sedimentary rock was derived from a variably carbonatized ultramafic source rock exposed on the ocean floor;

- 3) carbonatized rock has been deformed and bears the same regional deformation fabrics as carbonate-free, least altered protoliths (Roberts et al., 1978; Roberts, 1981), indicating that the intense carbonatization event either predated or took place synchronously with the regional deformation and metamorphic event. For example, the

Photo 2-3: Carbonate-rich (carbonatized) ultramafic fragments sit in a carbonate-rich matrix of apparently ultramafic initial composition. This unit lies intermittently along the volcanic-sedimentary unconformity in northern Whitney Township. This outcrop is exposed to the west of the Pamour #1 Mine property.

Photo 2-4: Fragmental rock consisting of variably carbonatized ultramafic (U) and quartz-feldspar porphyry (P) fragments, exposed in the open pits on the Buffalo Ankerite Mine property, Deloro Township.



carbonatized rock exposed in the former Hollinger Mine (Pamour Timmins Property) bears the north 50° east foliation and the -45° plunge which was emprinted regionally in carbonate-bearing and carbonate-free lithologies (ultramafic and basaltic volcanics and the quartz-feldspar porphyries). The regional deformation was coincident with the greenschist metamorphism because it is chlorite which defines the penetrative foliations and extension lineations in the least altered volcanic rock.

It must be acknowledged that the argument in support of synvolcanic intense carbonatization is weak and still remains controversial. For example, the carbonate-rich ultramafic conglomerate exposed at the base of the Porcupine Group sediments near the Pamour #1 Mine (Photo 2-3) overlies a unit of intensely carbonatized ultramafic flows (Map 21). It is conceivable, perhaps probable, that the ultramafic debris deposit was carbonatized contemporaneously with the underlying flows by virtue of its favourable bulk composition (c.f. Downes, 1979). If this was the case, then the timing of the carbonatization event could have postdated the accumulation of the sediments. This would minimize the significance of carbonate-rich clastic sedimentary units. The presence of isolated carbonatized volcanic rock clasts sitting in a carbonate-free matrix would be stronger evidence in support of the existence of an early carbonatized, sea floor volcanic terrain, but no such

material has been observed by the author within the Porcupine Group sedimentary rocks.

The fragmental unit (Photo 2-4) exposed on the former Buffalo Ankerite Mine property (Maps 5, 6) which appears to consist of variably carbonatized clasts of ultramafic rock, might appear to offer more sound evidence in favour of synvolcanic intense carbonatization. Had this unit been carbonatized after burial (assuming the unit is in fact a sediment) it is difficult to reconcile why fragments of apparently similar dimension and bulk composition failed to react equally with the hydrothermal pore fluid. However, similar units in the Timmins area have been interpreted as intrusive breccias.

Arguments in favour of synvolcanic intense carbonate alteration, based on the presence of sedimentary carbonate in the Dome and former Aunor Mines, must also be viewed with caution as the sedimentary origin of this material is still debated (Hodgson, 1983). There is little question that multiple events did occur during which carbonate precipitated in the Archean supercrustal rocks possibly as a carbonate-rich sediment, a precipitate that filled primary porosity in basalt flows, and as a replacement of pre-existing lithologies; however, the possibility that there had been multiple intense carbonatization events exists without strong empirical supportive evidence.

Thus, the strongest empirical evidence which constrains the relative timing between the intense carbonatization and the regional greenschist metamorphism and deformation in the Timmins area, are the similar penetrative tectonic fabrics present in both the intensely carbonatized and least altered volcanic rocks. This indicates that the intense carbonatization event either predated or developed synchronously with the regional deformation and greenschist metamorphism.

3. Carbonate Alteration Zones

3.1. General Distribution

Zones of carbonate alteration occur throughout parts of Formations II and III of the Deloro Group and Formations IV and V of the Tisdale Group (Burrows, 1924; Carlson, 1967; Davies et al., 1980, 1982; Ferguson et al., 1968; Fyon and Karvinen, 1978; Fyon and Crocket, 1982; Hurst, 1935; Karvinen, 1976, 1978, 1981; Pyke, 1975, 1981; Roberts, 1981; Roberts and Spiteri, 1979; Roberts et al., 1978). In addition, carbonatized turbiditic wackes and conglomerates occur in the Whitney, Beaty and Dome formations of the Porcupine Group. Some carbonate also occurs locally as a minor (<5%) constituent in the crossbedded sandstones of the Three Nations Lake formation, the uppermost clastic sequence in the Porcupine Group. Illustrated on maps 30, 31, 32, and 33 is a generalized distribution of carbonatized Tisdale Group volcanic rock in northeastern Tisdale, northern Whitney and northwestern Deloro Townships.

In the Deloro Group, the following rock types have locally been carbonatized: ultramafic, komatiitic dykes; basaltic and andesitic massive and pillowed flows; andesitic, dacitic and rhyolitic tuffs and breccias; quartz feldspar porphyry dykes; and chert-hematite-magnetite-

chlorite iron formations. In the Tisdale Group, ultramafic to basaltic flows of komatiitic and tholeiitic affinity have been carbonatized locally. In addition, the quartz-feldspar porphyry bodies which occur in Formations IV and V, also contain carbonate. Carbonate alteration is not obvious in the felsic pyroclastic rocks of Formation VI.

3.2. Morphology and Localization of Carbonatization

Table 3-1 notes some commonly observed features which are spatially associated with and probably served to localize the carbonatization: 1) shear zones; 2) dyke contacts; 3) unconformities; 4) bedding planes; and 5) vein envelopes. Some alteration zones are not associated with any obvious planar feature and are termed "intraunit" zones.

3.2.1. Intraunit

These carbonatized zones developed in volcanic rock are characterized by equant morphologies in plan view and granular textures in thin section. These zones appear to bear neither the fabric nor shape (in plan view) of shear or fault controlled domains. Carbonatization may cross cut individual or several flow contacts.

Virtually all situations studied display this carbonatization morphology to some extent. It is best illustrated on the Davidson-Tisdale property (Fig. 3-1).

TABLE 3-1: Geological features which served to localize intense carbonatization.

Property	Intra- Unit	Fault Shear	Vein Envelope	Dyke Envelope	Bedding Contact	Unconformity
Armstrong-McGibbon	X	X	X?	-	-	-
Aunor	X	X	-	-	-	-
Beaumont	X	-	-	-	X?	-
Brouian Reef	X	-	-	-	-	-
Buffalo Ankerite	X	X	-	-	-	-
Canusa-North	X	X	X	-	-	-
-South	X	X	-	-	-	-
Carshaw	X	-	-	X	-	-
Croesus	-	-	X	-	-	-
Crown Chartered	X	-	-	-	-	-
Davidson Tisdale	X	-	-	-	-	-
Definite	X	X	-	-	-	-
Dobell-West	X	X?	-	-	-	-
-East	X	-	X	-	-	-
Duval- Glory hole	-	X?	-	X	-	-
- South vein	-	X?	X	X	-	-
Hallnor	X	-	X	-	-	X
Hollinger	X	X	X	X?	-	-
Hugh Pam	X	X	X?	-	-	-
Kenilworth	X	X	X?	-	-	-
Kinch	X	-	X	-	X	-
Meigs	X	-	X?	X	-	-
McEnaney	X	X	X?	-	-	-
North Whitney	X	-	X?	-	-	-
Pamour #1	X	-	X	-	-	X
Porcupine Triumph	X	X	-	X	-	-
Russell	X	X	-	X?	-	-
Stuart Abate	X	X	X?	-	-	-

Notes: X- Indicates that feature is present on the property in question.

?- Indicates that the feature may not be present on the property in question.

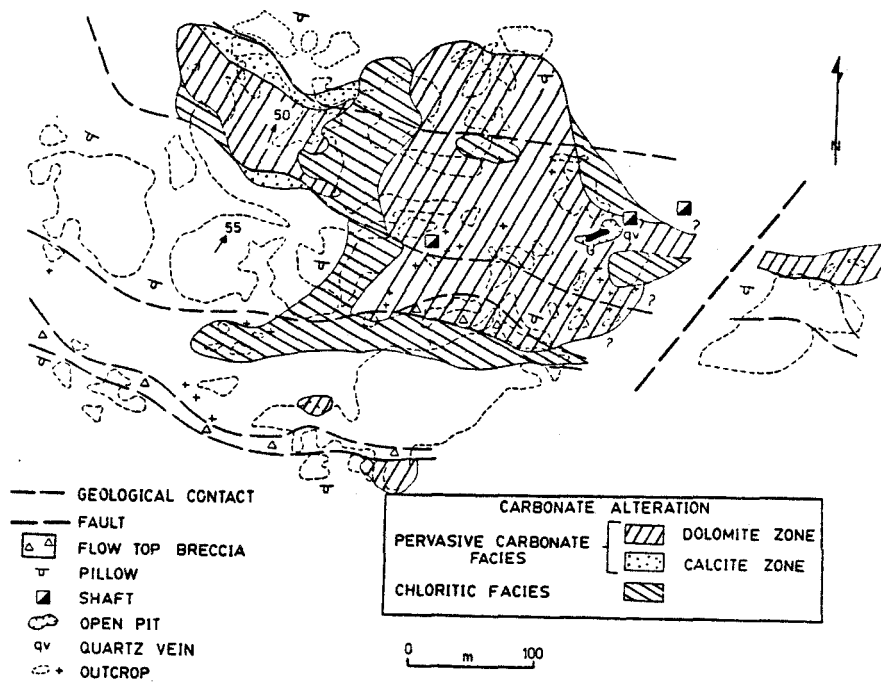


Figure 3-1: Surface geological plan of the Davidson-Tisdale property, Tisdale Township, illustrating the relationship between intraunit carbonate alteration and volcanic stratigraphy. Geology by Fyon (1980).

On most properties, this style of carbonatization can be traced laterally into a planar structure such as a shear zone or vein (this feature will be illustrated in the following subsections). This suggests that those intraunit carbonate alteration zones which lack zones of obvious planar fabric (eg. Davidson-Tisdale) may have developed off unexposed planar, permeable structures.

3.2.2. Shear zones

In approximately 60% of the situations examined, the locus of carbonatization can be assigned to a zone bearing an intensely developed planar fabric interpreted to be a shear zone. In many of these situations the orientation of the shear zone is subparallel to bedding so that unit displacement is not obvious; the displacement of a mafic dyke on the Stuart Abate property (Fig. 3-2) provides one example where faulting and carbonatization are coplanar. Some of the shear zones are wide (10's m.), for example on the McEnaney property (Fig. 3-3), while others are quite narrow (1 m.). For example, the shear (A) exposed south of the power line on the Canusa property (Fig. 3-4) or the shear exposed on the Armstrong-McGibbon property (map 12) are less than 1 metre in width.

The locus or focus mechanism for shearing is not always obvious. There appears to be no obvious explanation for the location of the shear zone on the McEnaney or Canusa

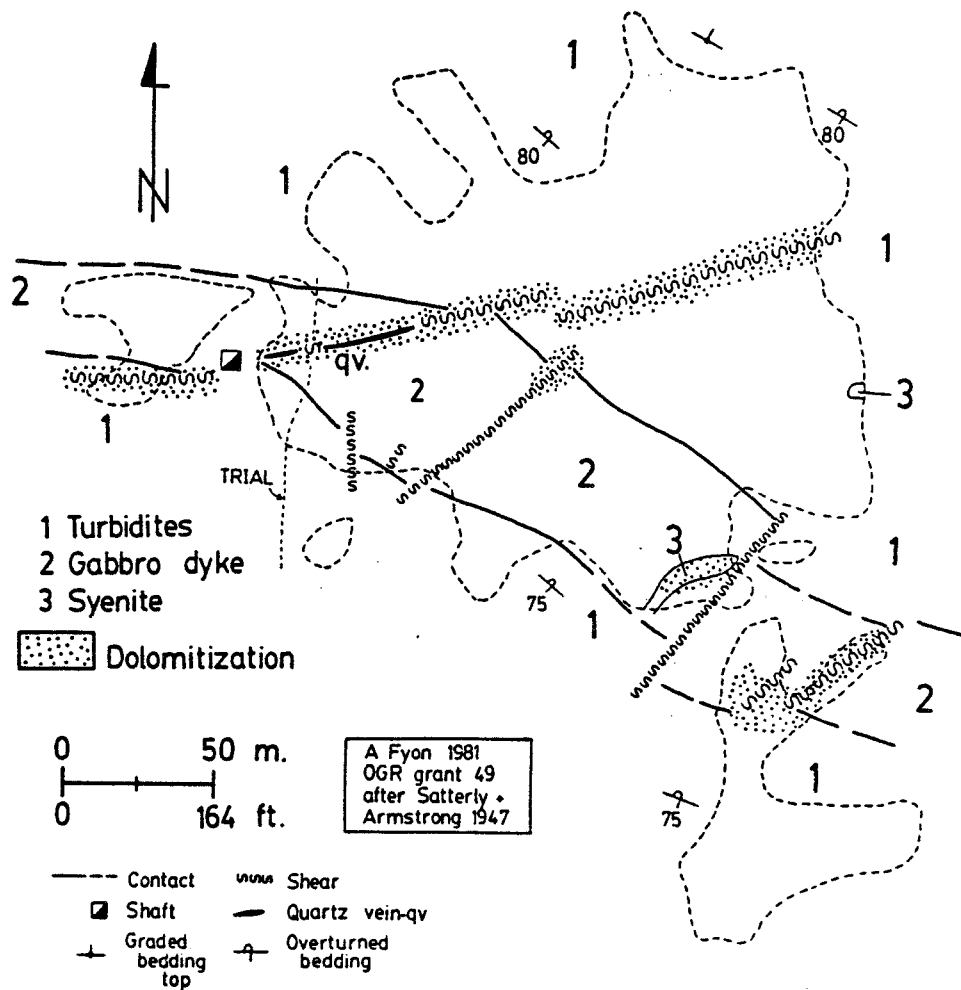


Figure 3-2: Simplified surface geological plan of the Stewart Abate property, Beatty Township, District of Timiskaming, illustrating fault localized carbonate alteration. See Map 29 in Appendix-1 for more detailed surface geological plan.

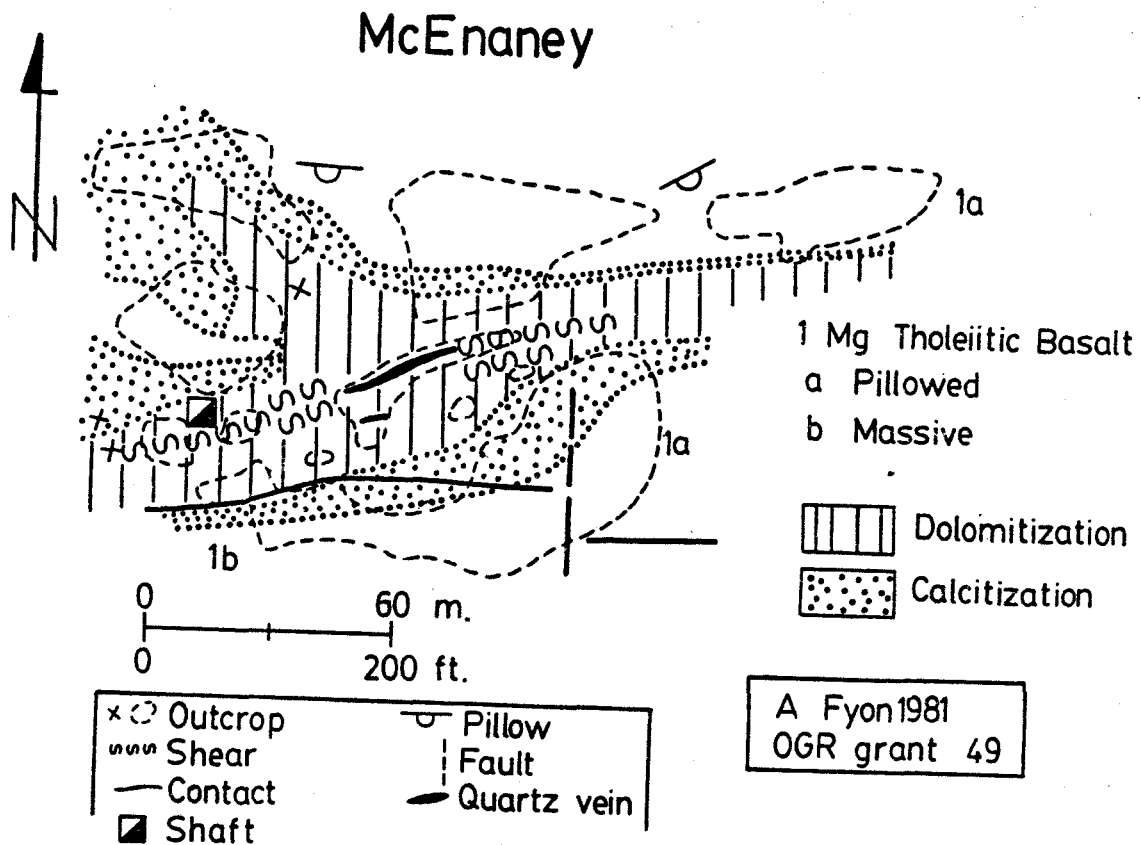
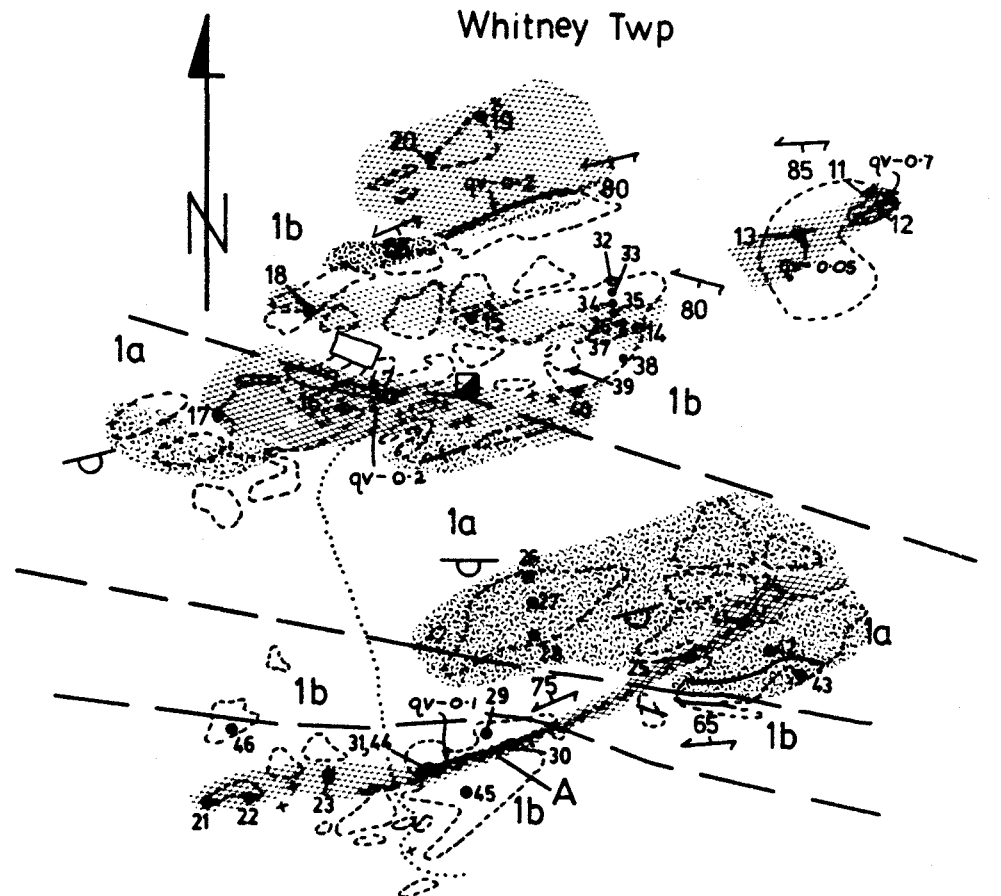


Figure 3-3: Surface geological plan of the McEnaney Property, Ogden Township, illustrating the localization of carbonate alteration along a shear zone.

Figure 3-4: Surface geological plan of the Canusa property. Those alteration zones associated with the northern cluster of outcrops appear to be of the intraunit and vein envelope types. Alteration zone 'A' is shear localized.

CANUSA MINE Whitney Twp



LEGEND - SYMBOLS

1 Magnesium Tholeiitic Basalt

a Pillowed

b Massive

○ x Outcrop

--- Contact

~~~~~ Shear

↗ Foliation

⌒ Pillow top

⊖ Pit

■ Shaft

⌒ Dump

□ Building

qv--2 Quartz vein-width(m)

..... Road

Can-1 • Sample

Carbonatization

▨ Dolomite zone

▨ Calcite zone

Geology: A Fyon-1977  
OGS project 76-37

properties. However, flow contacts or dyke contacts seem to have served as shear planes on some properties. For example, on both the Porcupine Triumph (Fig. 3-5) and Duval glory hole (Fig. 3-6) showings, the contact between an ultramafic dyke and basalt country rock has been sheared and carbonatized. Conversely, a shear developed on the Beaumont property (Map 3) cuts both carbonate-rich and carbonate-absent volcanic rocks. This shear is subparallel to a large quartz vein, but from the distribution of intensely carbonatized volcanic rock, it appears that the shear is later than and superimposed upon the carbonatized rock. An alternative interpretation would have the shear zone subject to periodic reactivation, the last event of which was not accompanied by fluids capable of carbonatizing the rocks.

Carbonatization is not just restricted to the shear zones, but often extends out into the adjacent unsheared wallrock where it resembles the intraunit carbonatization habit. This feature is illustrated on the McEnaney property (Fig. 3-3). No consistent relationship linking the width of the shear zone to the extent of wallrock carbonatization has been observed.

Although the scale of shear-related carbonatization zones exposed on the properties is one of meters or tens of meters, regional structures of kilometer extent also appear to be associated with carbonatization. For example, Davies et al., (1982) related the broad zone of carbonatization

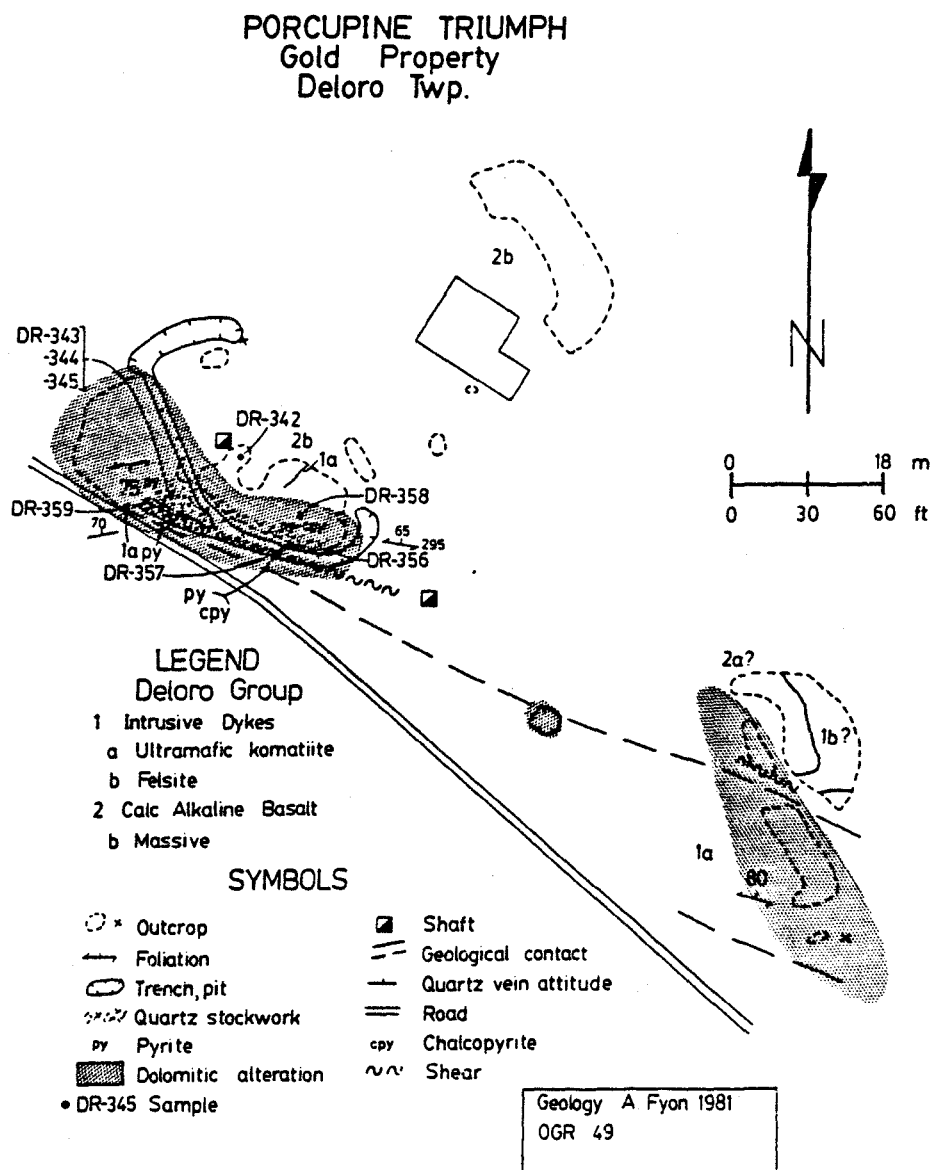


Figure 3-5: Surface geological plan of the Porcupine Triumph property, Deloro Township, where carbonatization is localized in and along the sheared contact between an ultramafic dyke and massive, calc alkaline basalt flows.

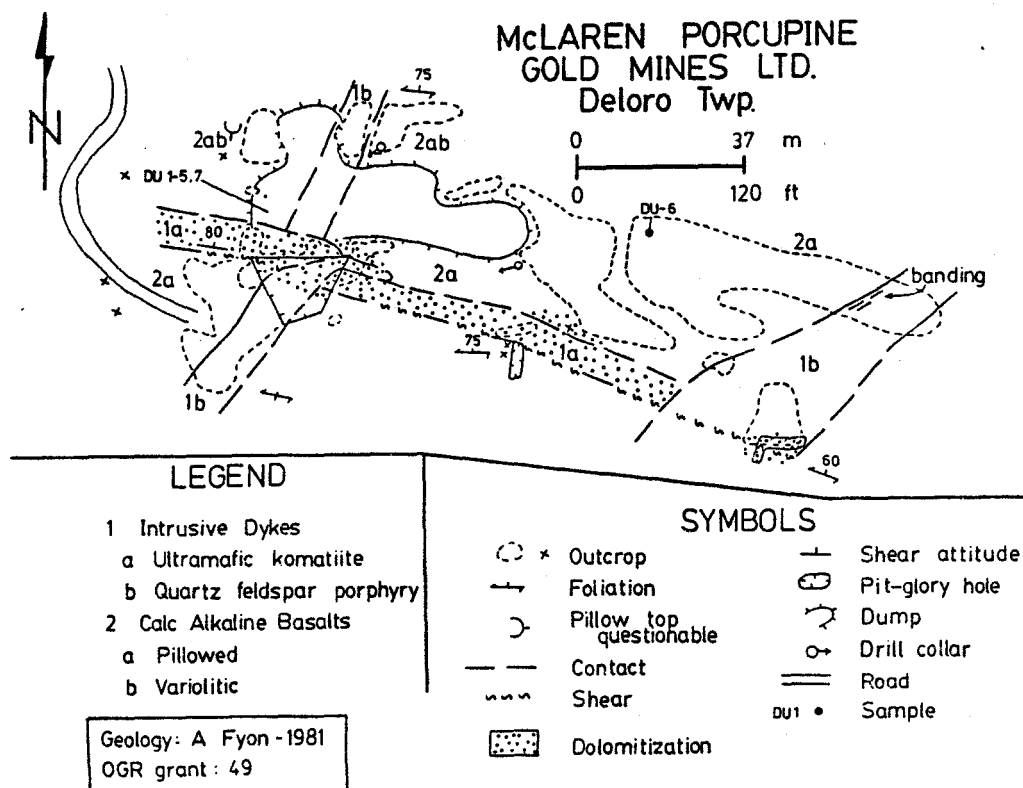


Figure 3-6: Surface geological plan of the McLaren Porcupine (Duval) glory hole area. An ultramafic dyke and the immediate country rock is intensely carbonatized. Approximately 6200 gm (200 oz) of gold were extracted from the glory hole.

centered on the Hollinger Mine, to the Hollinger main fault. A similar scale of carbonatization is associated with a shear zone trending southeast from McDonald Lake in Deloro Township (Fig. 3-7), which may represent slippage along the north limb of the Kayorum Syncline. The highly altered zone in the Dome Mine has been interpreted as a carbonatized shear zone (Holmes, in Ferguson et al., 1968; Davies, 1977; Hodgson, 1983). Over a greater scale, the surface trace of the Destor-Porcupine Fault in Whitney and Deloro Townships is associated with carbonatized ultramafic flows.

It must be emphasized that not all shear zones are marked by associated carbonatization. For example, the Faymar Mine surface ore-zone showing (Fig. 3-8) is characterized by lensey quartz-calcite-pyrite-chalcopyrite veins localized in east-west trending shear zones which lack intense carbonatization, although these vein systems yielded gold.

Most carbonatized shear zones also contain a single quartz vein or a vein array whose structural attitudes, as measured at the surface, can be similar to those of the shear fabric (eg. McEnaney, Fig. 3-3; shear A on the Canusa, Fig. 3-4; Armstrong-McGibbon shear, map 12). Deformation textures (reviewed in section 4) observed within the vein minerals indicate that some deformation postdated the vein formation; however, considering that many veins were introduced along zones of weakness, it should not be

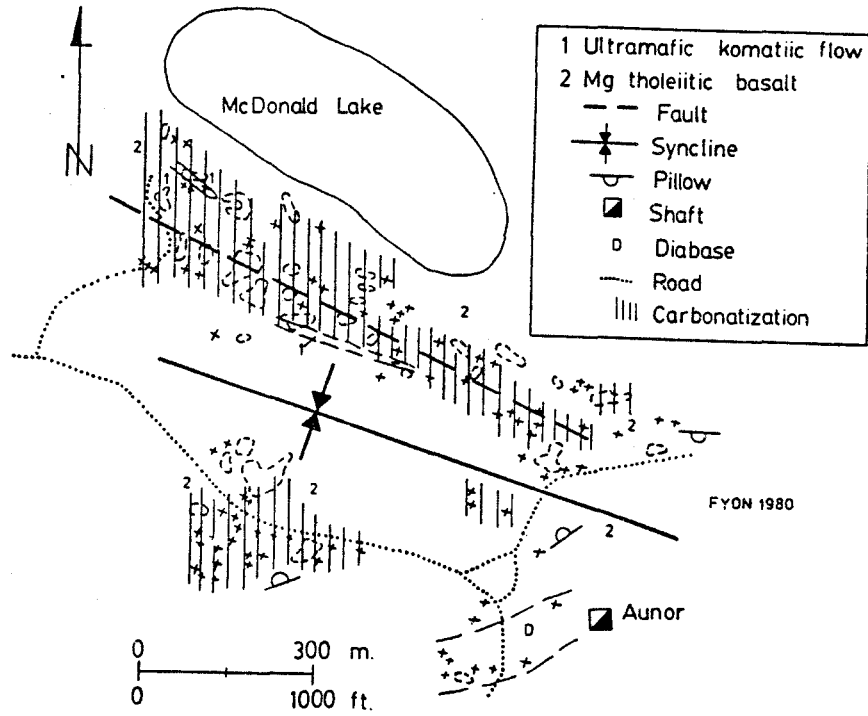


Figure 3-7: Large scale fault or shear controlled carbonatized habit, north-central Deloro Township.



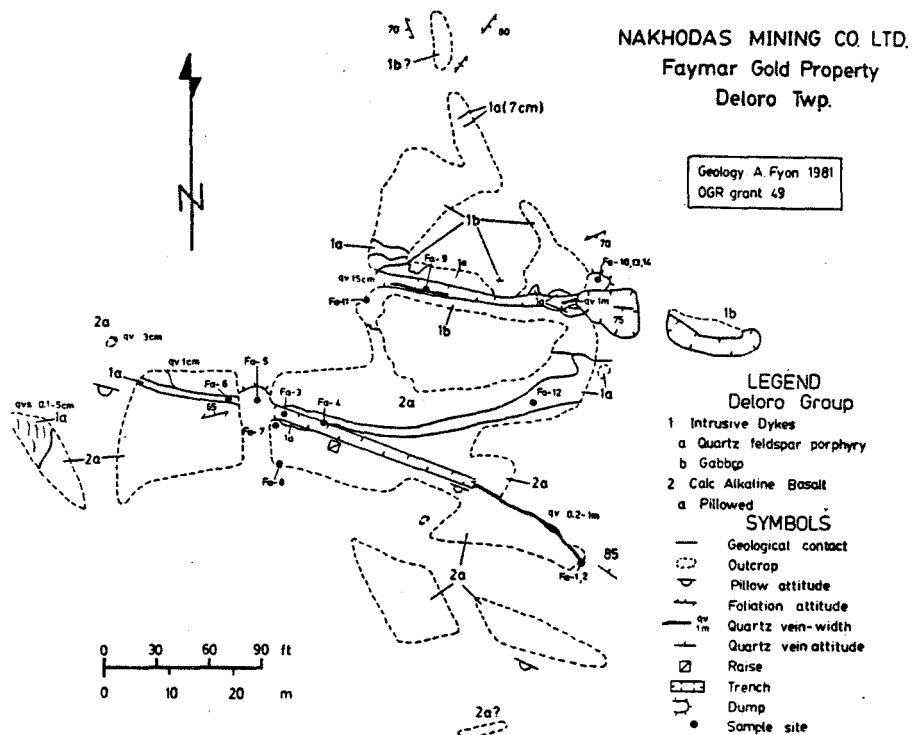


Figure 3-8: Surface geological plan of the Faymar Gold property, Deloro Township. Within two parallel, chloritized shear zones, quartz veins occur. Approximately  $2.2 \times 10^4$  g gold was produced from this property.

surprising to realize that these structures had undergone periodic reactivation.

### 3.2.3. Dykes

On nearly 40% of the properties studied, intrusive rocks crop out which are intensely carbonatized, and/or are enveloped (envelope-habit) by zones of carbonate alteration. The intrusives are generally less than 30 metres in width and may either be felsic or ultramafic in composition. In general, where envelope-habit carbonatization is best developed, the dyke is felsic in composition. Such a felsic dyke would generally contain less than 5 wt.%  $\text{CO}_2$  whereas the basalts adjacent to the dyke may contain as much as 15 wt.%  $\text{CO}_2$ . Conversely, ultramafic dykes tend to be intensely carbonatized (>15 wt.%  $\text{CO}_2$ ), whereas the adjacent basaltic wallrock may be relatively carbonate-free. These features reflect the control of bulk rock composition on carbonatization intensity, the ultramafic rock being much more susceptible to carbonatization.

Not all felsic dykes in a given area are associated with an envelope-type alteration. Neither are all ultramafic dykes carbonatized, although all ultramafic dykes have been hydrated to some degree (Muir, 1979). Where developed, the envelope habit of carbonatization does not extend along the entire exposed strike length of the dyke. Also, some zones of envelope-habit carbonatization extend

much further away from the dyke and are morphologically similar to the intraunit alteration habit. Examples of this alteration habit are found on the Carshaw property (Fig. 3-9), Porcupine Triumph property (Fig. 3-5) and the Duval south vein showing (Fig. 3-10).

#### 3.2.4. Unconformity

Carbonatized igneous and sedimentary rocks crop out in northern Whitney Township (map 21) in proximity to the Unconformity between the volcanic and sedimentary rocks. Karvinen (1981) considered the Unconformity to be an important structure which localized the carbonatization. It must be noted that surface outcrop is poor in northern Whitney Township and hence the control on the localization of carbonatization by the Unconformity is poorly constrained.

#### 3.2.5. Bedding plane

This type of alteration habit was emphasized by Fyon and Crocket (1982) and is manifest by the presence of carbonatization along flow contacts, notably flow top breccias (Map 24; Kinch Property). Photo 3-1 illustrates a carbonatized flow top breccia exposed on the Kinch property and Photo 3-2 illustrates the habit of this carbonate which occurs as a matrix replacement, interstitial to the breccia fragments.

Photo 3-1: Carbonatized flow top breccia exposed on the Kinch property, Tisdale Township. The pitted weathering reflects the preferential weathering of the carbonate-rich matrix material.

Photo 3-2: Ferroan dolomite preferentially replaces the matrix of a flow top breccia, developed on an iron-rich tholeiitic basalt flow. Outcrop is located southeasts of the community of Gold Centre, Tisdale Township.



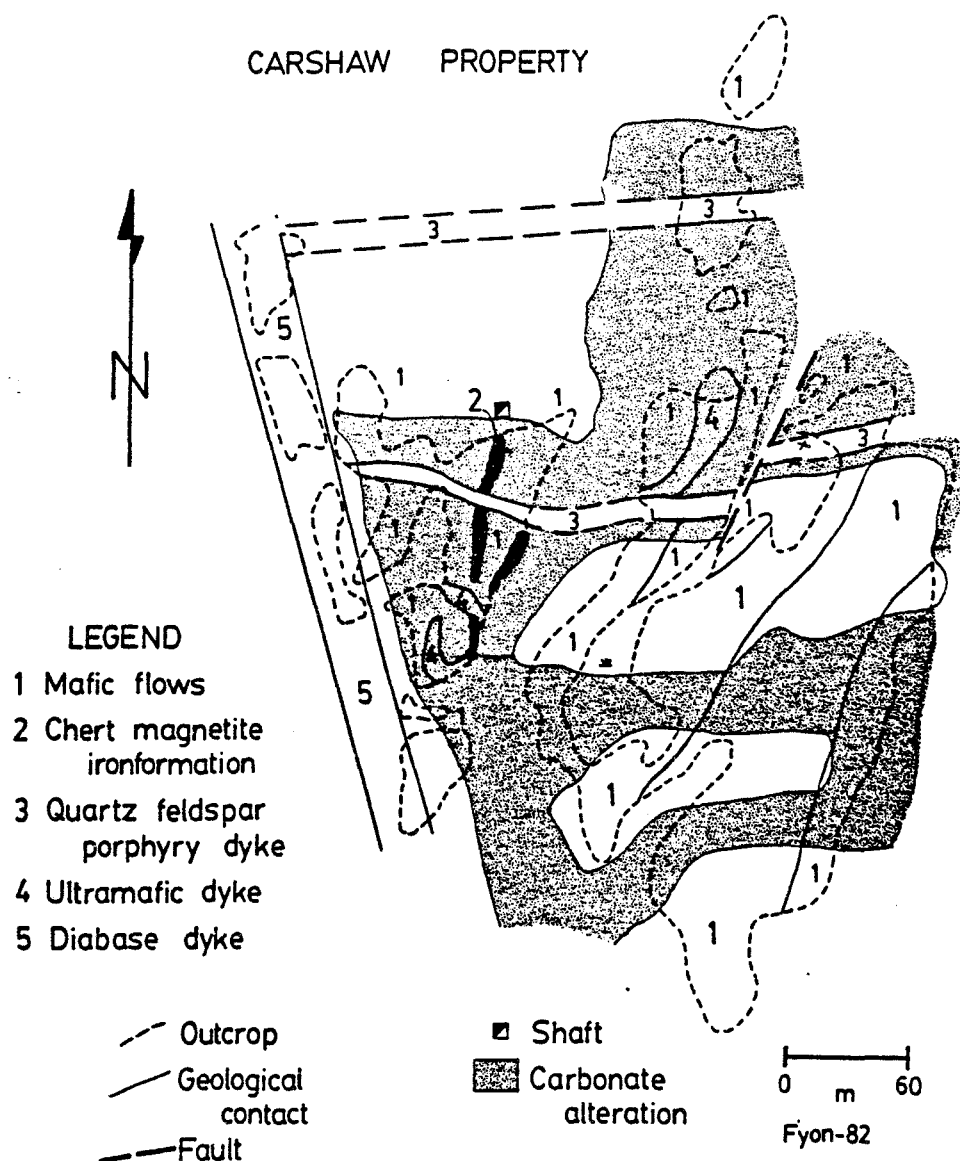


Figure 3-9: Simplified surface geological plan of the Carshaw property, Shaw/Carmen Townships, where gold occurs adjacent to quartz veins which cut oxide facies, banded iron formation. Intraflow and dyke-envelope type carbonate alteration is present. See Map 9 (Appendix-1) for a more detailed surface geological plan.

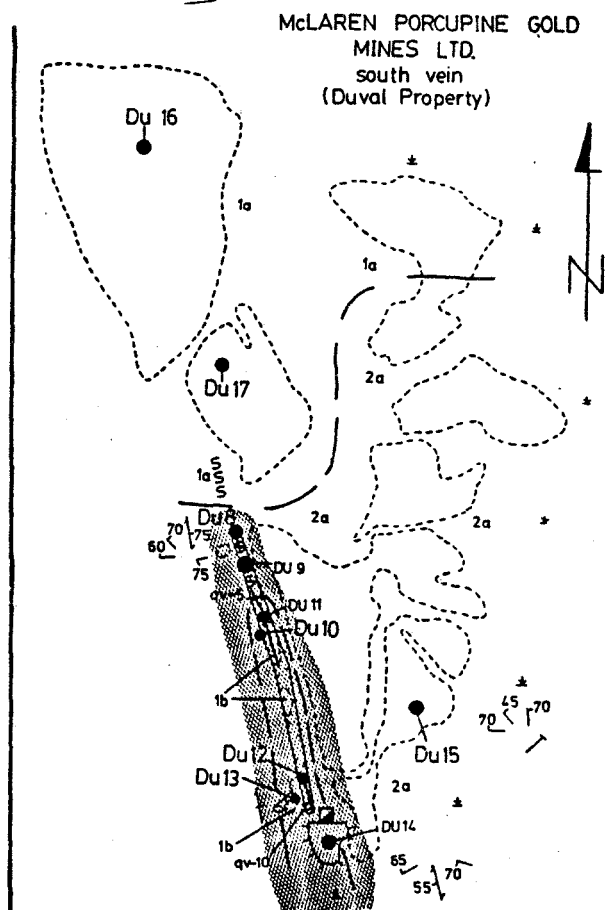
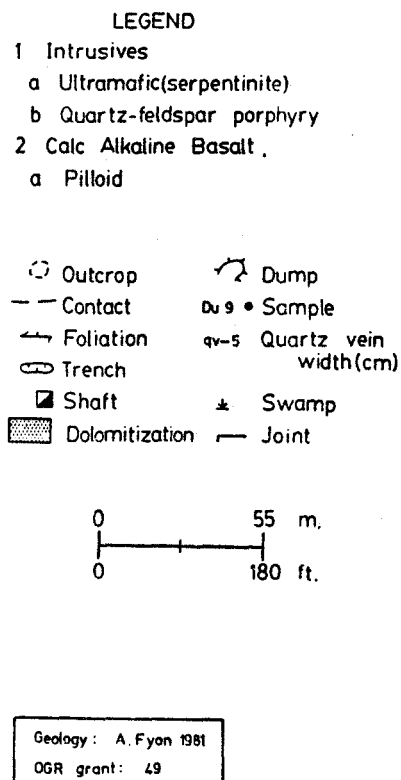


Figure 3-10: Surface geological plan of the Duval, south vein showing, Deloro Township, illustrating the dyke-envelope habit of carbonate alteration.

The locus of carbonatization need not be restricted to the actual flow contact or flow top breccia and the zone of intense carbonatization can shift into the adjacent pillowed or massive flow facies, but tends to remain subparallel to the flow contact.

In the context of this more regional study, the occurrence of this style of carbonatization is quite rare (Table 3-1). Fyon and Crocket (1982) overestimated the abundance and importance of this carbonatization habit because of the geographically restricted area involved in that study.

#### 3.2.6. Vein envelope

Most auriferous quartz veins in the mine areas cut or are spatially associated with dolomitized rock (Bain, 1933; Hurst, 1935). An excellent surface exposure of this vein envelope alteration habit exists at the #2 vein, Croesus property (Munro Township; Fig. 3-11). Similar, but less spectacular examples may be observed on the Canusa (Fig. 3-4), Hugh Pam (Map 19) and Kinch properties (Map 24). In this alteration environment, the quartz vein(s) appears to be the locus of intense carbonatization. Shearing may be the controlling structure in which some quartz veins occur (eg. McEnaney, Croesus, Canusa) while joint systems may be prominent in other cases (eg. Beaumont). Ferroan dolomite is an accessory phase in those quartz veins associated with



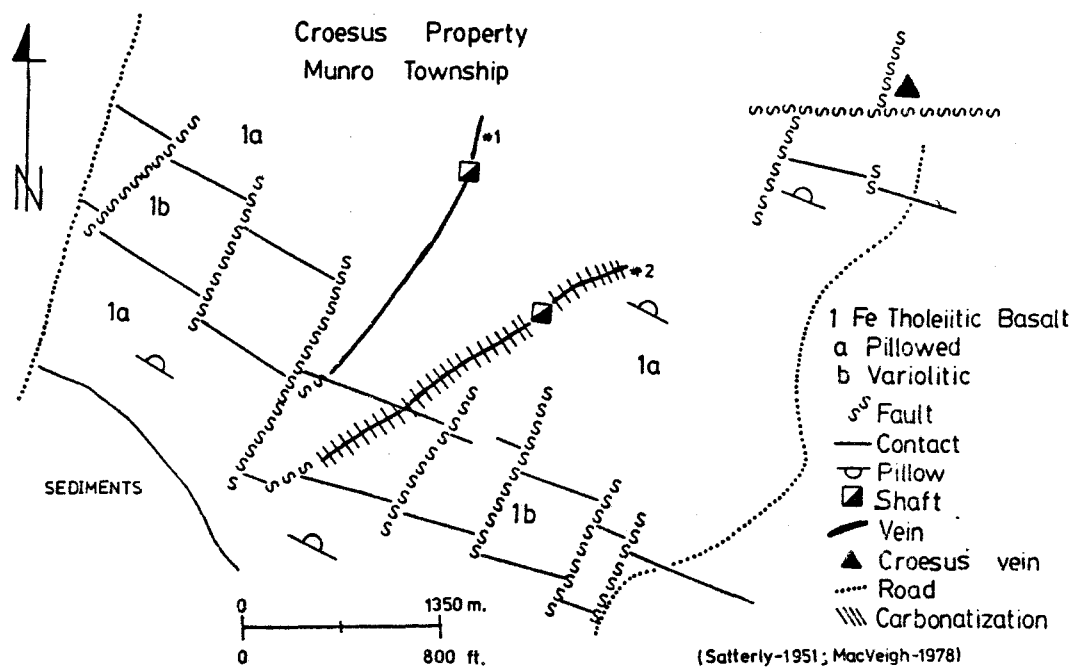


Figure 3-11: Simplified geological plan of the Croesus #2 vein, Munro Township, District of Timiskaming, illustrating a vein envelope habit of carbonatization.

dolomitized wallrock.

In general, it is unusual to observe any zone of intense dolomitization which does not contain quartz veins. However, unlike those spectacular and apparently rarely observed cases where the morphology of the carbonatization envelope is controlled by the extent of a single large quartz vein, many quartz veins in carbonatized rock consist of quartz vein arrays consisting of thin ( $<2$  cm) veins of limited strike length (Photo 3-3). These vein arrays may represent filled joint or foliation planes utilized by  $\text{CO}_2$ -rich fluids, or the vein arrays may represent indigenous free quartz remobilized from the carbonatized host rock into dilatant zones formed by brittle failure of the dolomitized rock.

Just as not all shear zones are carbonatized, neither are all quartz veins or pods accompanied by carbonatization (eg. Faymar Mine, Fig. 3-8). In general, quartz veins lacking dolomitized wallrock contain accessory calcite rather than dolomite. Detailed vein studies in the Hollinger Mine (Hurst, 1935) suggest that the quartz-calcite veins represent the last episode of quartz veining, and that they are rarely auriferous. Although other examples of quartz veins lacking carbonatized wallrock were noted during the field mapping, the vast majority of quartz veins observed in the field occur within zones of dolomitization.

Photo 3-3: Slightly folded, relatively flat quartz veins which are developed in carbonatized ultramafic flows, adjacent to a subvertical, 0.5 metre wide quartz vein (not visible in the Photo), exposed on the Beaumont property, Tisdale Township.



The precise chronology of quartz veining in the Porcupine Camp has only been systematically addressed in the Dome Mine where Roberts et al., (1978) deduced that most quartz veins were emplaced prior to, or during, the imprint of the earliest regionally penetrative fabric (D2: 040° to 070°). However, some quartz veins, such as the 55 vein on the Hollinger, clearly cross cut the regionally penetrative fabric and hence, here at least, one vein set post-dates the regional deformation (see more complete discussion of this vein system in section 5.2.1).

### 3.3. Summary of Carbonatization Habits and Fluid Access

The following carbonatization habits or environments (Fig. 3-12) have been recognized in the field: 1) intraunit; 2) shear zone; 3) dyke; 4) Unconformity; 5) contact; 6) vein envelope. Although morphologically different, the common feature of these habits, with the apparent exception of the intraunit variety, is the presence of a permeable zone which localized the CO<sub>2</sub>-bearing hydrothermal fluid and resulted in the carbonatization of the wallrock. Because the intraunit carbonatization habits also characterize the outer domains of other (eg. shear or dyke contact) carbonatization regimes, it is deduced that the pure end-member intraunit carbonatization habits are developed adjacent to unexposed, permeable conduits. That the CO<sub>2</sub>-bearing hydrothermal fluids gained access to and

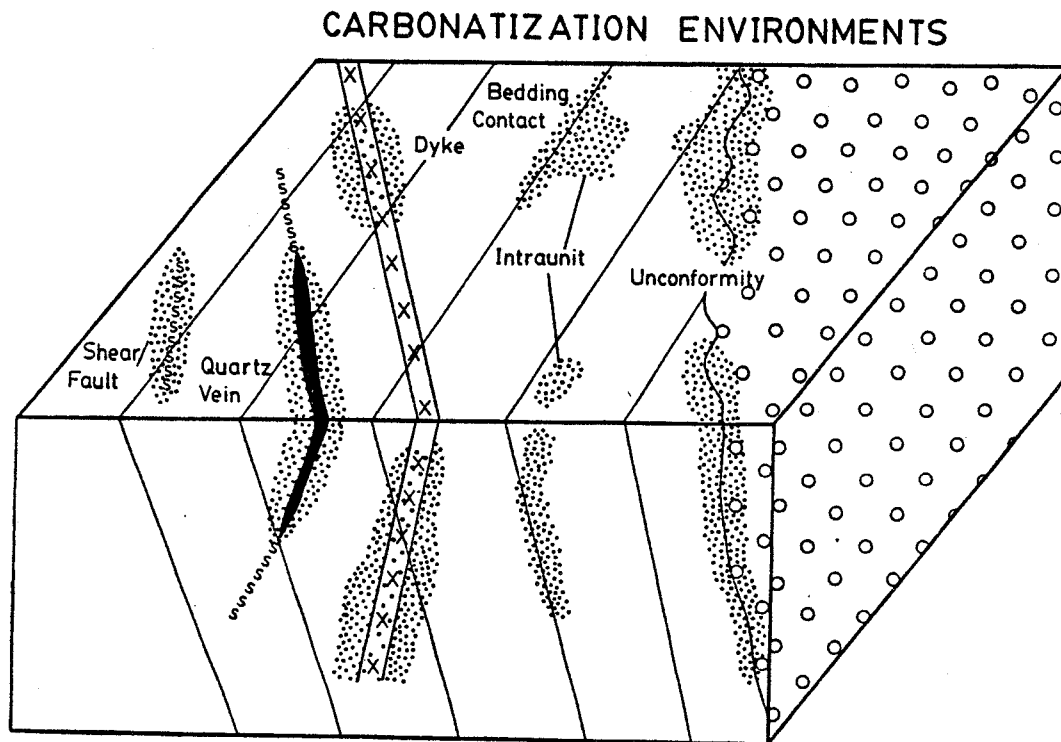


Figure 3-12: Summary of observed carbonatization environments in the Timmins area: intraunit; shear or fault; quartz vein envelope; dyke envelope; bedding plane; unconformity.

reacted with the supercrustal lithologies along permeable zones is a relationship which is observed on an outcrop scale (<10 square metres) and on a claim block scale (<1000 square metres).

It appears that the major deformation zones in the Abitibi Greenstone Belt such as the Destor-Porcupine or Larder Lake fault zones also served as large scale permeable zones through which CO<sub>2</sub>-bearing hydrothermal fluids passed leaving carbonatized rock in their wake, although this premise is somewhat more difficult to constrain quantitatively because no maps exist that show the regional distribution of carbonatized volcanic rock. However, that carbonate alteration is a fundamental characteristic of these deformation zones became apparent during the early mapping of the Abitibi Belt when the presence of carbonatized rock, coincident with broad zones of high strain and rock unit disruption, recurrently characterized the surface trace of these deformation zones (c.f. Burrows, 1912; Thomson, 1941). In a very general sense, the only empirical evidence which can be used to map the distribution of carbonatized rock regionally in the Abitibi Greenstone Belt, is the distribution of auriferous mineralization (Fig. 3-13). This statement is not meant to imply that there is a one-to-one spatial correspondence between zones of gold mineralization and the carbonatized rock, because this is not the case. However, it is well established that carbonate

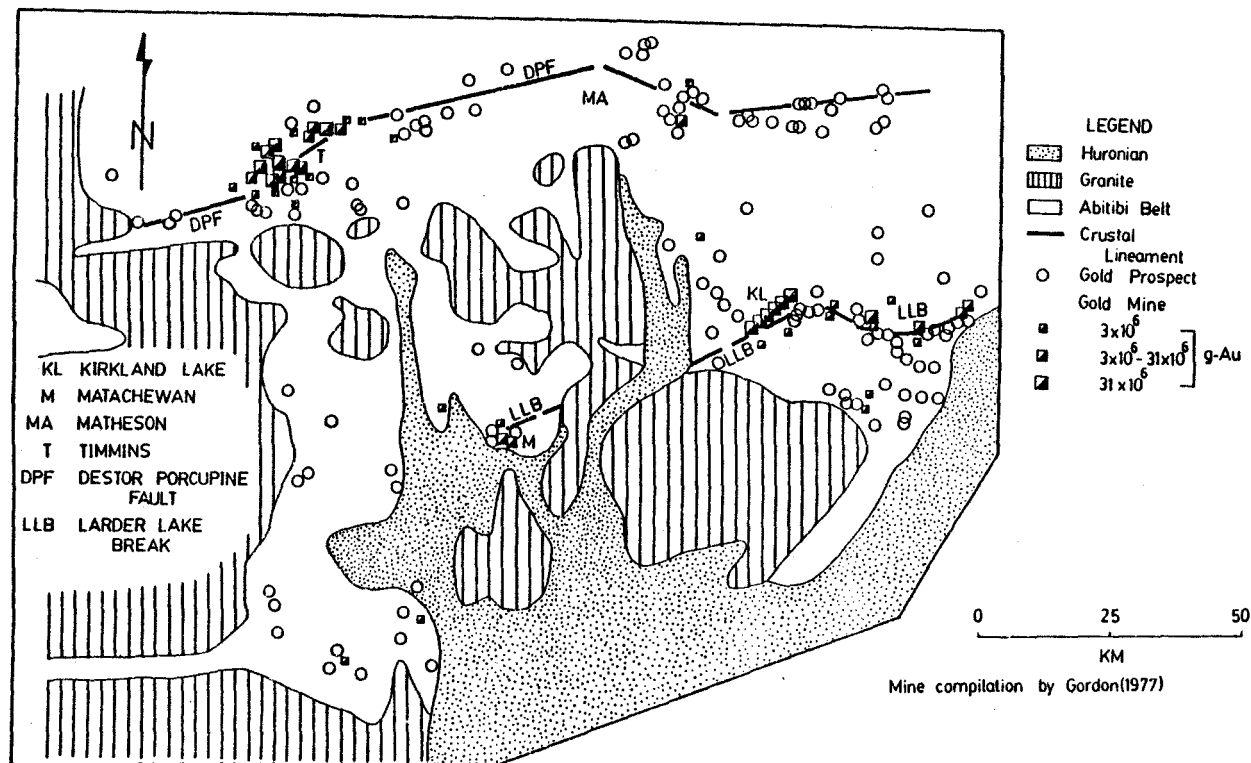


Figure 3-13: Regional spatial association between major structural lineaments and gold mines and prospects in northeastern Ontario.



alteration is a fundamental characteristic of those auriferous systems which developed in ultramafic and mafic volcanic rock within the Superior Province and which reside at greenschist metamorphic grade or lower (Colvine et al., 1984; Hodgson et al., 1983). Thus, it can be cautiously stated that the more intense, broad zones of carbonate alteration occur more frequently adjacent to the Destor-Porcupine and Larder Lake fault zones even though some major carbonate alteration zones do exist which are not proximal to either of these major fault traces (c.f. Ben Nevis Township; Grunsky, 1980).

A hierarchial scheme can be envisaged in which CO<sub>2</sub>-bearing hydrothermal fluids accessed successively smaller scale permeable conduits as they passed into and through the supercrustal volcano-sedimentary sequence (Fig. 3-14). Major deformation zones of regional extent, such as the Destor-Porcupine Fault appear to have acted as the primary loci of fluid introduction into the supercrustal sequences at a greenstone belt scale (100-10000 square kilometres). At a mining camp scale (500 square kilometres), the CO<sub>2</sub>-bearing hydrothermal fluids accessed the supercrustal rock sequences in part along the major deformation zones (such as the Destor-Porcupine fault zone), along major unconformities (eg. northern Whitney Township, Map 21) and along spur faults off the Destor-Porcupine Fault, such as the Hollinger Main and Dome Faults. At a property scale (5 kilometres

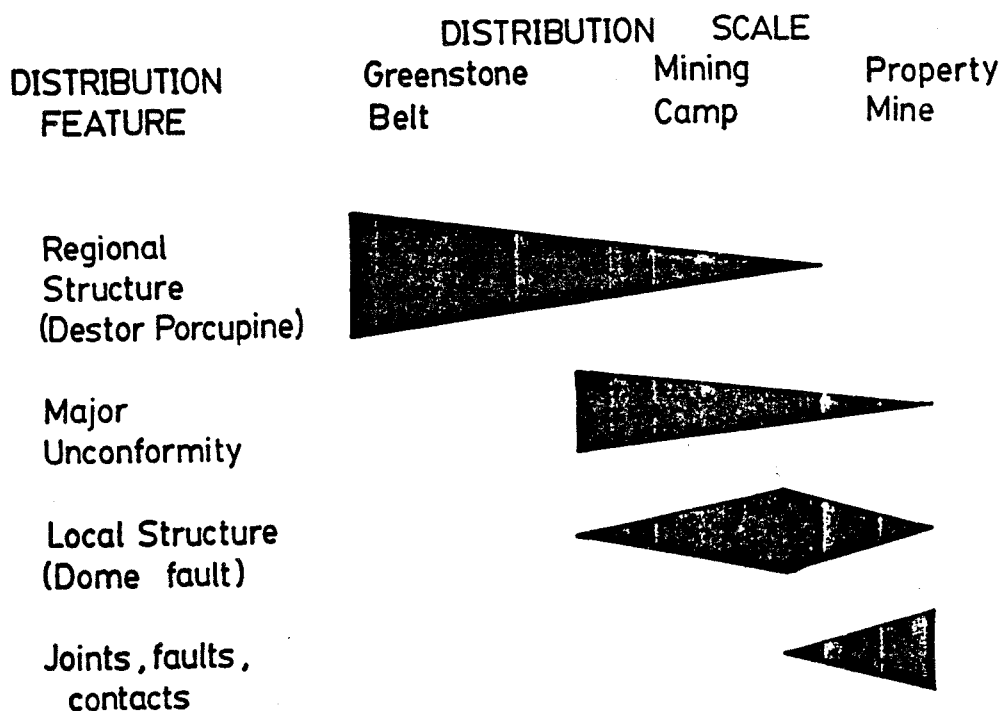


Figure 3-14: Hierarchical scheme of fluid distribution through permeable zones in the Abitibi Greenstone Belt, at various scales. Vertical thickness of bar indicates the relative importance of a particular fluid distribution feature at a considered scale. Horizontal length of bar indicates the scales at which a particular fluid distribution feature is recognizable.

square), correspondingly minor structures or planar boundaries (unit contacts, small shear zones) served as efficient fluid conduits.

### 3.4. Relationship of Carbonate Alteration Zones To Stratigraphy

Karvinen (1977) argued that two major stratigraphic horizons of carbonate-rich rock existed in the Porcupine Camp and linked the origin of these carbonate-rich rocks to synvolcanic hydrothermal activity. Implied in this model was the synvolcanic origin of the carbonate-rich rock as a result of exhalation of CO<sub>2</sub>-rich fluids of unspecified origin. Both stratabound and discordant carbonate alteration zones were permissive in this model. Fyon and Crocket (1982) demonstrated that discordant and stratabound zones of carbonate alteration occur throughout Formations IV and V of the Tisdale Group. This is an observation which has been emphatically substantiated with the more regional mapping undertaken for this thesis.

Somewhat more contentious is the origin of the regionally continuous, stratabound zones of carbonate-rich rock discussed by Karvinen (1978). It is important to emphasize that the major issue here is not the existence of stratabound zones of carbonate-rich rock, but rather the process which produced these distinctive zones. One such stratabound zone of carbonate alteration rock has been traced across the Davidson-Tisdale, Armstrong-McGibbon and

Canusa properties (Maps 10b,7) and represents one segment of the surface trace of Karvinen's Upper Carbonate Unit. The development of an intense foliation in carbonatized rock within this zone suggests that this zone actually represents the surface trace of a major shear zone which Hodgson (1983) interprets as the eastward continuation of the Hollinger Main Fault. In detail, this zone clearly cross-cuts the volcanic stratigraphy (Fig.3-15). Thus, the distribution of this carbonate-rich rock is controlled by an east-trending shear zone. A continuous zone of carbonatization, which has been traced west from the former Buffalo Ankerite through the Aunor and Delnite Mines (Map 33) represents a segment of Karvinen's Lower Carbonate Unit. Similarly, this zone also defines the surface trace of sheared and carbonatized basaltic and ultramafic flows in which relict, highly deformed pillow forms are still recognizable (Photo 3-4). In all other similar zones which were purported by Karvinen (1977) to constitute part of a regionally continuous stratabound zone, the presence of preserved volcanic textures in the carbonate-rich material, the distinctive chemistry of the carbonate-rich rock and the development of an intense foliation clearly identify the material as sheared and carbonatized volcanic rock.

Because the foliation attitudes of the highly strained, carbonatized rock are subparallel to those of the Destor-Porcupine, Dome and Hollinger Main faults, the

Photo 3-4: Intensely flattened pillows within the highly strained, auriferous south zone exposed at the west end of the open pits, Buffalo Ankerite Mine.



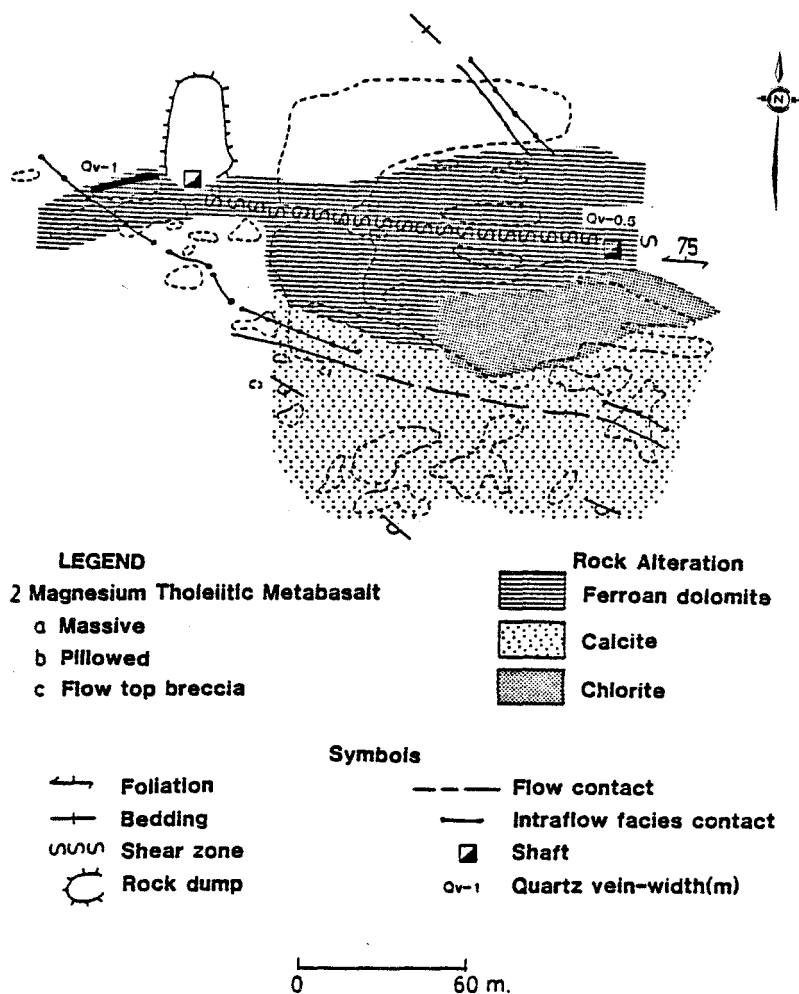


Figure 3-15: Surface geological plan of the Armstrong-McGibbon gold property, Tisdale Township. A stratabound zone of carbonate alteration is localized within a shear zone and is seen in detail to cross cut the volcanic stratigraphy.

localization of the stratabound carbonate alteration zones was the result of permeability generated by shearing that was contemporaneous with the deformation along the major deformation zones. This deformation could not have been synvolcanic, because the quartz-feldspar intrusive porphyry bodies are affected by the deformation (Ferguson et al., 1968) and attendant alteration (Fyfe et al., 1982). It follows that the stratabound alteration was not the result of a synvolcanic process.

Thus, it should now be apparent that both discordant and stratabound carbonate alteration zones occur throughout the Porcupine Camp. These major zones of continuous stratabound carbonate alteration mark the surface traces of shear zones which were active late in the volcano-tectonic history of the Timmins area, and can not be linked to a synvolcanic process.

### 3.5. Volume of Carbonatized Rock

Within the immediate Timmins area (Tisdale and northern Whitney, Deloro and Ogden Townships) an estimate of the area occupied by carbonatized mafic and ultramafic volcanic rock in the Tisdale Group and the moles of hydrothermal C that was introduced into these rocks can be made using the regional geochemical data of Whitehead et al. (1979; Fig. 3-16). In this area approximately 60% of the exposed volcanic rock contains in excess of 2 wt. % CO<sub>2</sub> (7



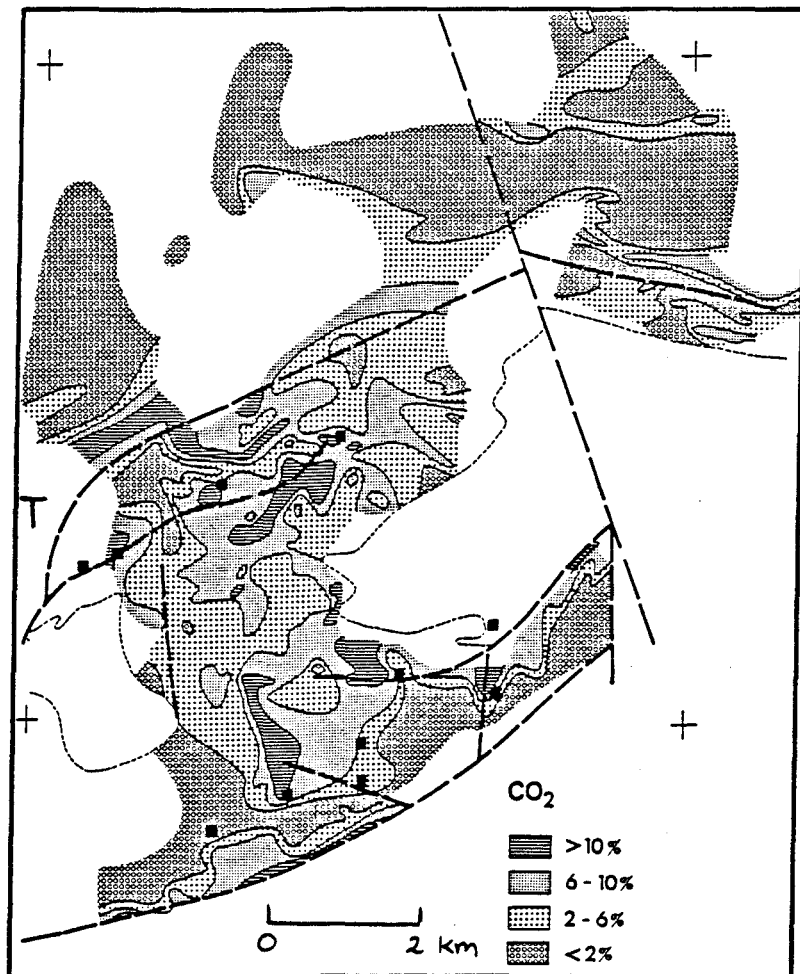


Figure 3-16: CO<sub>2</sub> abundances in volcanic rock in the Timmins area (Whitehead et al., 1981). Mines are indicated by the small squares, the city of Timmins by the letter "T".

wt.% loss on ignition-LOI) whereas 8% of volcanic rock in that area contains 10 wt. % or more  $\text{CO}_2$  ( $> 14$  wt. % LOI). Included in the area containing in excess of 2 wt. %  $\text{CO}_2$  are most of the mining properties examined for this thesis.

The quantity of hydrothermal carbon that was introduced into the Timmins area can be qualitatively estimated. Only an area enclosed by all of Tisdale Township and the north half of Whitney, Deloro and Ogden Townships, is considered for this calculation. The following assumptions are required:

1) the area being considered is 145 square kilometres. In this area better than 90% of the exposed rock consists of mafic and ultramafic flows. Approximately 60% of the mafic and ultramafic volcanic rock in this area contain at least 2 weight percent  $\text{CO}_2$  - thus, the area of mafic and ultramafic rock which contains greater than 2 weight percent  $\text{CO}_2$ , is approximately 75 square kilometres;

2) the depth to which carbonatized rocks persist in the greenstone belt is assumed to be 3 kilometres - thus, the volume of the cell of volcanic rock considered for this calculation is 225 cubic kilometres or  $2.25 \times 10^{17}$  cubic centimetres (cc);

3) assuming the cumulative density of the cell is 2.9 g/cc, the mass of rock in the cell is  $6.53 \times 10^{17}$  grams.

The mass of  $\text{CO}_2$  that was introduced into this volume

of carbonatized rock (assuming a minimum of 2 wt. %  $\text{CO}_2$  in the altered rock) is  $1.31 \times 10^{16}$  grams. This is equivalent to  $3.56 \times 10^{15}$  grams carbon that were introduced into the altered volcanic rocks in the immediate Timmins area. This figure represents a minimum, because altered volcanic rocks in the Timmins area can contain considerably more than 2 wt. %  $\text{CO}_2$ .

The amount of hydrothermal carbon that was introduced into the Destor-Porcupine and Larder Lake fault zones can be estimated assuming that the average width and length of these two zones is 1 km and 600 km respectively and that the carbonatized rock persists to a depth of 3 km. This cell has a volume of  $1.8 \times 10^{18}$  cubic centimetres and a cumulative rock mass of  $5.22 \times 10^{18}$  grams. Again assuming a minimum of 2 wt. %  $\text{CO}_2$  in the rock, the mass of  $\text{CO}_2$  in this cell is  $1.04 \times 10^{17}$  grams, equivalent to  $2.85 \times 10^{16}$  grams of Carbon. That is, each of the Destor-Porcupine and Larder Lake fault zones contains a minimum of  $2.85 \times 10^{16}$  grams of Carbon, or  $5.69 \times 10^{16}$  grams of Carbon was deposited in these two fault zones collectively.

To put these two estimates for the mass of hydrothermal carbon into perspective, it is necessary to compare the calculated masses of hydrothermal carbon present in the Timmins area and in major zones of deformation with the masses of carbon present in other, modern, terrestrial

reservoirs (Table 3-2). The mass of carbon that was introduced into the western part of the Archean Greenstone Belt ( $57 \times 10^{15}$  grams) represents about 10% of the present carbon content in the modern-day atmosphere. This is truly an impressive volume of Carbon, especially considering that the estimate represents a minimum for only the western part of the Abitibi Greenstone Belt. The process which led to the carbonatization of the Archean supercrustal sequences was thus a significant event, requiring a large source reservoir from which the  $\text{CO}_2$  was derived.

Table 3-2: Present day masses of Carbon Present In Crustal Reservoirs

| Reservoir                  | Total Carbon |       |
|----------------------------|--------------|-------|
|                            | $10^{15}$    | GRAMS |
| =====                      | =====        | ===== |
| Basaltic ocean crust       | 660,000      |       |
| Pelagic ocean sediments    | 20,160,000   |       |
| Granitic crust             | 9,050,000    |       |
| Continental sediments      | 35,640,000   |       |
| -----                      | -----        | ----- |
| Total Crust                | 65,510,000   |       |
| -----                      | -----        | ----- |
|                            | Carbon       |       |
|                            | $10^{15}$    | GRAMS |
| Atmosphere                 |              |       |
| ( $\text{CO}_2 = 329$ ppm) | 560 - 692    |       |
| Oceans                     |              |       |
| total inorganic            | 35,000       |       |
| dissolved organic          | 1,000        |       |
| -----                      | -----        | ----- |
| Data from Kempe (1979)     |              |       |

#### 4. Types of Gold Mineralization

By examining the satellite gold properties in the Timmins area, it is possible to characterize some of the salient features of the mineralization and to address the temporal relationship between the mineralization and carbonate alteration. The term "mineralization" is used in a most general way to describe a system which can consist of quartz veins, calcite, pyrite, ferroan carbonate or gold. Not all such constituents need occur together in a given area.

Table 4-1 lists the gold mineralization types observed on various properties. Not all properties contain gold reserves nor have all achieved production. The presence of a quartz-carbonate vein with or without economic concentrations of gold is included as "gold mineralization" because such an occurrence reflects a habit common to many of the productive gold mines. While individual types of gold mineralization can be classified where observed, it is much more difficult to estimate the approximate abundance of the different mineralization types present on particular properties because of limited surface and underground exposure. Also, past mining activity was selective (eg. avoidance of the carbonaceous, pyritic auriferous interflow sediments on the Hollinger) because of either metallurgical

TABLE 4-1: Habits of gold mineralization observed on the properties studied, including a lithological listing of the host rock for properties studied in the Porcupine Camp and the Stuart Abate and Croesus properties.

| Property           | Gold<br>Production<br>g x 10E6 | Vein-<br>Quartz-<br>dolomite-<br>tourmaline | Vein-<br>Quartz-<br>Calcite | Pyrite<br>Replacement | Quartz<br>vein In<br>IF | Cherty<br>Dolomite<br>Exhalit | Carbonaceous<br>Interflow<br>Sediments | Vein Host Rock |   |   |    |    |
|--------------------|--------------------------------|---------------------------------------------|-----------------------------|-----------------------|-------------------------|-------------------------------|----------------------------------------|----------------|---|---|----|----|
|                    |                                |                                             |                             |                       |                         |                               |                                        | M              | U | P | IF | CS |
| Armstrong-McGibbon | 0                              | X                                           | —                           | —                     | —                       | —                             | —                                      | X              | — | — | —  | —  |
| Aunor              | 59.097                         | X                                           | —                           | —                     | —                       | X?                            | —                                      | X              | — | — | —  | —  |
| Beaumont           | 0                              | X                                           | —                           | —                     | —                       | —                             | —                                      | X              | X | — | —  | —  |
| Broulan Reef       | 11.16                          | X                                           | —                           | —                     | —                       | —                             | —                                      | X              | — | — | —  | X  |
| Buffalo Ankerite   | 31.103                         | X                                           | —                           | X                     | —                       | X?                            | —                                      | X              | X | X | —  | —  |
| Canuse-North       | 0.031                          | X                                           | —                           | —                     | —                       | —                             | —                                      | X              | — | — | —  | —  |
| -South             | 0                              | X                                           | —                           | —                     | —                       | —                             | —                                      | X              | — | — | —  | —  |
| Carshaw            | 0.933                          | X                                           | —                           | —                     | X                       | —                             | —                                      | —              | — | — | X  | —  |
| Croesus #2 vein    | 0                              | X                                           | —                           | —                     | —                       | —                             | —                                      | X              | — | — | —  | X  |
| Crown Chartered    | 0                              | X                                           | —                           | —                     | —                       | —                             | —                                      | X              | — | — | —  | —  |
| Davidson Tisdale   | 0.062                          | X                                           | —                           | —                     | —                       | —                             | —                                      | X              | — | — | —  | —  |
| Dalnite            | 31.103                         | X                                           | —                           | —                     | —                       | X?                            | —                                      | X              | X | — | —  | —  |
| Dobell-West        | 0                              | X                                           | —                           | —                     | —                       | —                             | —                                      | X              | — | — | —  | —  |
| -East              | 0                              | X                                           | —                           | —                     | —                       | —                             | —                                      | X              | — | — | —  | —  |
| Duval- Glory hole  | 0.006                          | X                                           | —                           | —                     | —                       | —                             | —                                      | —              | — | X | —  | —  |
| - South vein       | 0                              | X                                           | —                           | —                     | —                       | —                             | —                                      | X              | — | X | —  | —  |
| Faymar             | 0.680                          | —                                           | X                           | —                     | —                       | —                             | —                                      | X              | — | X | —  | —  |
| Hallnor            | 45.722                         | X                                           | —                           | —                     | —                       | —                             | —                                      | X              | X | — | —  | X  |
| Hollinger          | 622.07                         | X                                           | —                           | X                     | —                       | X?                            | X                                      | X              | — | X | —  | X  |
| Hugh Pan           | 0                              | X                                           | —                           | —                     | —                       | —                             | —                                      | X              | — | — | —  | —  |
| Kenilworth         | 1.55                           | X                                           | —                           | X                     | —                       | —                             | —                                      | X              | X | — | —  | —  |
| Kinch              | 0                              | X                                           | —                           | —                     | —                       | —                             | —                                      | X              | — | — | —  | —  |
| Malga              | 0.467                          | X                                           | —                           | —                     | X                       | —                             | —                                      | —              | — | — | X  | —  |
| McEnaney           | 0                              | X                                           | —                           | —                     | —                       | —                             | —                                      | X              | — | — | —  | —  |
| North Whitney      | 0                              | X                                           | —                           | —                     | —                       | —                             | —                                      | X              | X | — | —  | —  |
| Pamour #1          | 62.207                         | X                                           | —                           | —                     | —                       | —                             | —                                      | X              | X | — | —  | X  |
| Porcupine Triumph  | 0                              | X                                           | —                           | X                     | —                       | —                             | —                                      | X              | X | — | —  | —  |
| Russell            | 0                              | X                                           | —                           | —                     | —                       | —                             | —                                      | X              | X | X | —  | —  |
| Stuart Abate       | 0                              | X                                           | —                           | —                     | —                       | —                             | —                                      | X              | — | — | —  | X  |

Notes: X- Indicates that mineralization habit is present.

X?- Indicates that mineralization habit either is not certainly present or that the particular habit remains controversial.

Key to host rock abbreviations: M- Basalt/gabbro IF- Chert magnetite chlorite iron formation  
U- Ultramafic flow/dyke CS- Clastic sediment  
P- Quartz feldspar porphyry  
Intrusive

or economic reasons; hence, if only production figures and geological descriptions, are available, a particular mineralization type can be overemphasized.

Several types of gold mineralization occur: 1) stratabound siliceous, ferroan dolomite-rich units; 2) pyritic, carbonaceous interflow sediments; 3) pyritic, ferroan dolomite-rich iron-rich tholeiitic basalt or "flow ore"; 4) iron formation-hosted gold; 5) quartz veins. The first three types have been argued to be syngenetic gold deposits (Fryer and Hutchinson, 1976; Karvinen, 1981; Roberts, 1981; Fyon et al., 1983a), whereas the quartz vein and iron formation related gold deposits have been argued to be epigenetic (Hurst, 1935; Ferguson et al., 1968; Fyon et al., 1983a,c). The field, petrographic and some geochemical characteristics (including oxygen and carbon stable isotopes) of only types 2 to 5 have been examined during this study. The purported exhalites (type 1, above) will not be discussed because they are best exposed in the Dome Mine and no mapping in this mine was carried for this thesis.

#### 4.1. Pyritic, Carbonaceous, Interflow Sediments

The carbonaceous units are stratiform, interflow sediments which range up to 1 metre in thickness. They serve as stratigraphic markers on the former Hollinger Mine property where they are most abundant and lie along basaltic

flow contacts. They are interpreted as chemical sediments which accumulated on the basaltic sea floor during periods of volcanic quiescence (Ferguson et al., 1968).

The sediments consist of black carbonaceous material, ferroan dolomite and fine grained (<2mm) polygonalized quartz which resembles recrystallized chert. Upto 8 percent carbon can occur in these sediments (Ferguson et al., 1968, p.106). The presence of the carbonaceous material imparts a black colour to the rock. Compositional lamination, interpreted to be bedding, is defined by changes in the proportion of very fine grained (<0.01 mm.), recrystallized quartz, ferroan carbonate and pyrite. The thickness of the laminations can exceed 1 cm. in thickness (Photo 4-1, 4-2). The quartz and carbonate-rich mesobands consist of quartz (>70%), ferroan dolomite(<20%), pyrite (<25%) and traces of carbonaceous material inferred to be graphite. The ferroan dolomite grain size seldom exceeds 0.1 mm., whereas the quartz exists as very fine grained (0.01 mm.) polygonalized arrays. Carbonaceous material occurs as fine wisps or ribbons which can be orientated either parallel to the compositional layering or to the foliation, depending on the deformation intensity. Carbonaceous units have been mined at the Moneta (Buffam, 1948), the former Hollinger (68E and 92 vein systems; Jones, 1948; Karvinen, 1981) and the former McIntyre Mine (15-26-16 stope). All these carbonaceous interflow sediments occur



Photo 4-1: Folded, pyritic, carbonaceous interflow sediment exposed in the 68E vein zone, Hollinger Mine.

Photo 4-2: Deformed microbanded pyrite contained within the carbonaceous sediment exposed in the 68E vein zone. This pyrite banding is interpreted to be bedding.



within the iron tholeiitic basalts of Formation V, Tisdale Group. Within the Porcupine Camp, interflow carbonaceous units are rare, except in an area within Formation V which contains the Dome and former McIntyre and Hollinger Mines. Carbonaceous sedimentary units appear to be more abundant in Formations II and III of the Deloro Group based on the distribution of samples collected by Cameron and Baumann (1972) and Cameron (1975), although they also occur in Hoyle Township where the new gold discoveries have been made (Kidd Creek Mine's Owl Creek and Hoyle Pond and the Canamax Bell Creek properties).

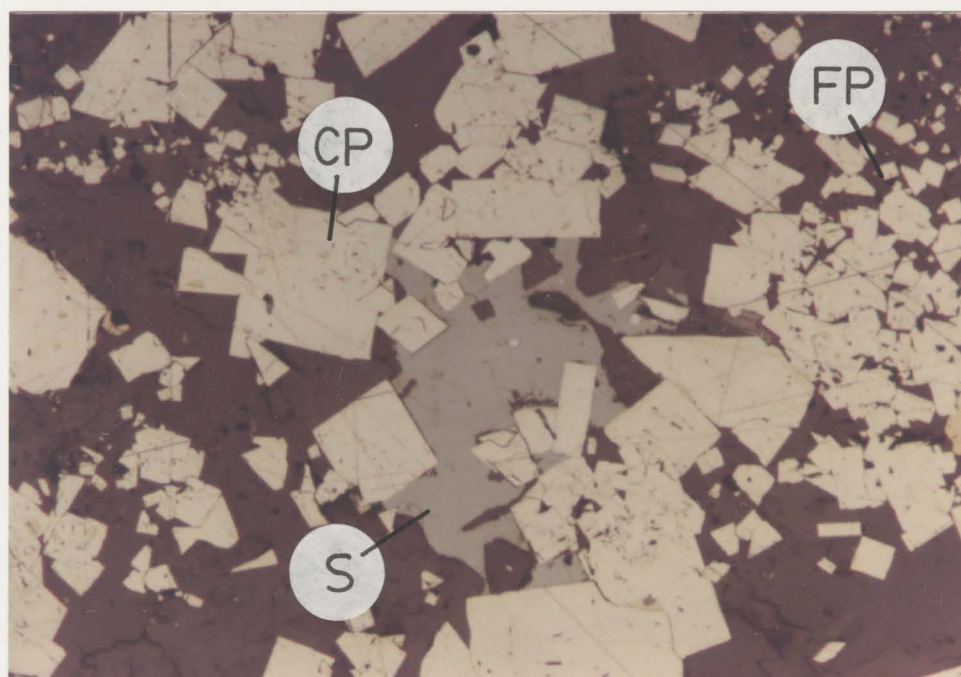
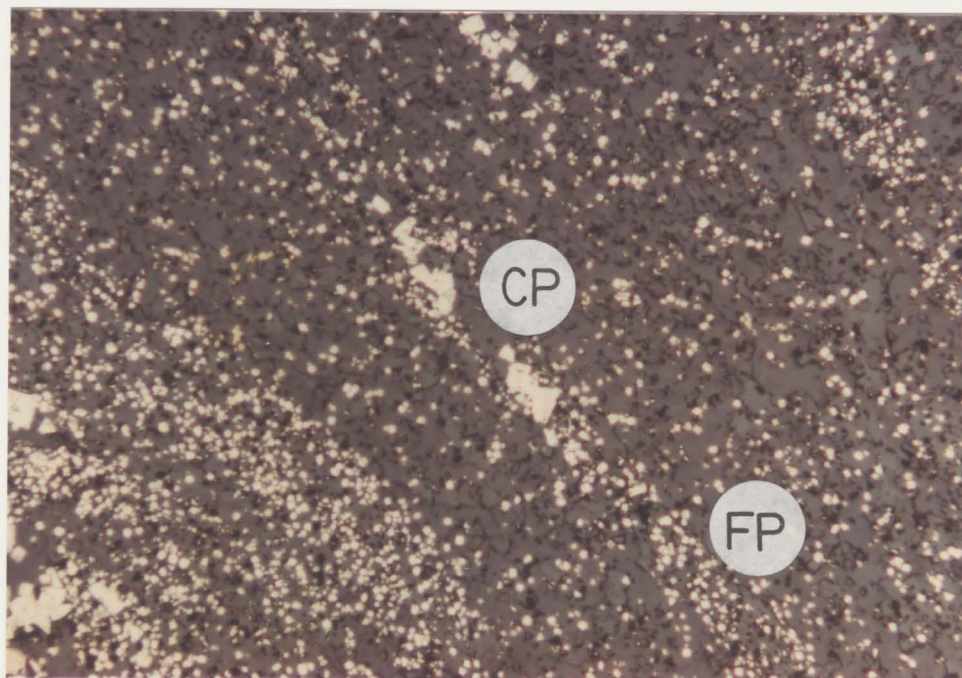
#### 4.1.1. Pyrite habits and gold tenor of the carbonaceous sediments

Within the carbonaceous sediments, pyrite occurs in two habits, dependent in part on its abundance. Where abundant ( $> 10$  modal %), pyrite occurs as very fine grained (0.01 mm) rounded grains which define linear trains resembling bedding (Photo 4-3a). In those samples where pyrite is sparse ( $< 10$  modal %) or in those pyrite-rich units where deformation, manifest as folding or shearing, has been more intense, the pyrite can occur as coarser grained (0.1 - 1 mm) porphyroblastic, euhedral cubes (Photo 4-3b). The porphyroblastic pyrite develops from the fine grained, rounded variety by progressive recrystallization and can occur as isolated cubes in the pyrite lamellae or in recrystallized, centimetre-scale, quartz-rich segregations.

Photo 4-3a: Fine grained pyrite (FP) trains interpreted to represent bedding in a carbonaceous sediment. Note coarser, recrystallized pyrite (CP) which is derived from the preexisting fine grained pyrite. (Sample H-51-2, Hollinger Mine; long axis of photo is 0.71 mm.)

Photo 4-3b: Coarse, recrystallized pyrite (CP) which has been derived by insitue recrystallization of the fine grained (FP) pyrite. Rare sphalerite (S) and chalcopyrite occur in the carbonaceous sediments also. (Sample H-51-1, Hollinger Mine; long axis of photo is 0.36 mm.)





Rarely colloform textured pyrite is present. Traces of chalcopyrite and pyrrhotite occur as minute ( $<0.005$  mm.) inclusions in the coarser pyrite. Sphalerite, where present, appears to mantle pyrite, suggesting replacement of pyrite by sphalerite.

Gold analyses of separated pyrite from the carbonaceous units are reported in Table 4-2. Highest gold concentrations occur in samples having abundant microbanded fine grained pyrite and graphite. Lowest gold concentrations occur in the black-coloured, pyrite-poor units which contain only rare porphyroblastic pyrite. Note that sulphur (equated to pyrite abundance) and reduced carbon (equated to graphite) abundances are only qualitative.

#### 4.1.2. Gold enrichment in the carbonaceous sediments

The mechanism (and therefore the timing) by which the carbonaceous sediments became enriched in gold is unclear. Generally, these units contain sufficient gold to be mined only where they had been deformed and cut by quartz veins (Fig. 4-1, 4-2; P. Walford, Senior mine geologist, Pamour Porcupine Mines Ltd., personal communication, 1982). This implies a structural and epigenetic control on the gold mineralization. That quartz veins sometimes occur in or along the contact between the carbonaceous sediments and the adjacent carbonatized basalt




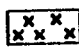
TABLE 4-2: Gold concentrations in pyrite separated from carbonaceous interflow sediments on the Hollinger Mine (Pamour Timmins Property).

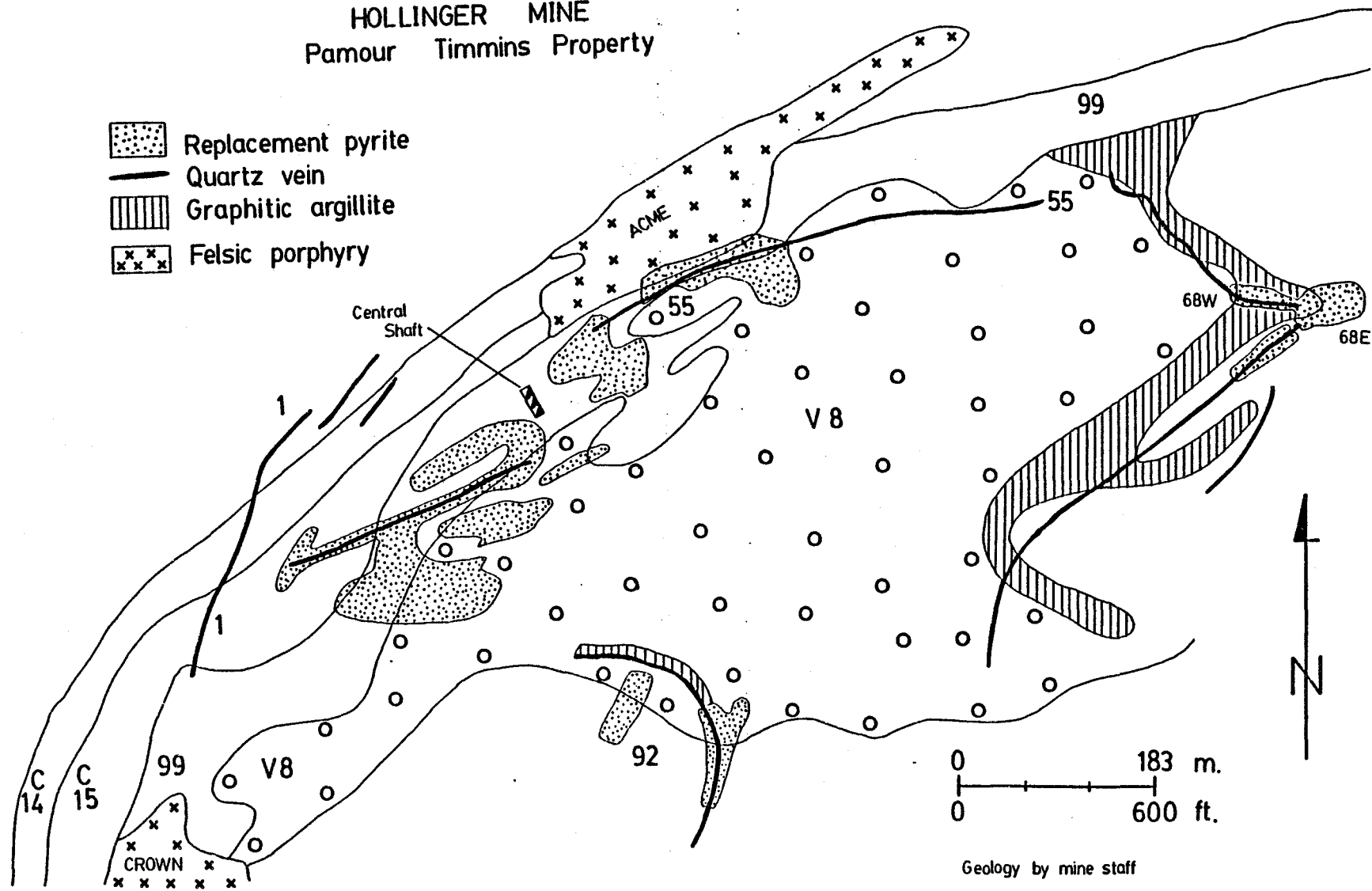
| Sample<br>Number | Description                                                                   | Au<br>ppb |
|------------------|-------------------------------------------------------------------------------|-----------|
| H-26             | Black with 20% laminated pyrite-very fine grained.                            | 1640      |
| H-22             | Black with 20% laminated pyrite-very fine grained.                            | 990       |
| H-27             | Black with <5% disseminated porphyroblastic pyrite.                           | 480       |
| H-10             | Black with 5% disseminated porphyroblastic pyrite-<br>from the 55 vein zone.  | 200       |
| H-25             | Black with 10% porphyroblastic pyrite.                                        | 75        |
| H-11             | Black with <5% disseminated porphyroblastic pyrite-<br>from the 55 vein zone. | 25        |

Figure 4-1: Simplified geological plan of the south half of the former Hollinger Mine (Pamour Mines Ltd., Timmins Property), illustrating the location of the 55 vein zone (pyritic replacement) and the 68E and 92 vein zones, both consisting of quartz veins which are localized in graphitic interflow sediments.



# HOLLINGER MINE Pamour Timmins Property

-  Replacement pyrite
-  Quartz vein
-  Graphitic argillite
-  Felsic porphyry





flows reflects the greater inherent propensity of the thin, laminated or fissile interflow sediment to fail either internally or along the contact with the adjacent basalt flows.

An alternative explanation for the auriferous nature of these sediments appeals to the syngenetic concentration of gold when pyrite was deposited. Some of the black carbonaceous sediments contain microbanded pyrite of possible syngenetic origin, suggested by the stratiform compositional banding (interpreted to be bedding) and by the presence of very fine grained (0.005 mm), rounded pyrite. It is possible that the gold associated with this fine grained pyrite (analyses of the pyrite separates listed on Table 4-2) was also syngenetically coprecipitated with the pyrite.

Empirical evidence supporting either of the gold enrichment mechanisms (syngenetic vs. epigenetic) is lacking. However several features of those segments of the interflow sediment, where gold tenor is sufficiently high to warrant mining favours an epigenetic gold enrichment mechanism. Where auriferous, the interflow sediment is invariably deformed and is cut by quartz veining of varying intensity (Fig. 4-2). This suggests that the deformation and quartz veining event was instrumental in elevating the gold tenor. Also, the gold concentration of the very fine grained pyrite alone is insufficient to account entirely for

the gold (6 ppm) in a typical mineralized black interflow sediment system defined by the pyrite plus all other constituent silicate and carbonate minerals. Hence, it must be presumed that an additional, epigenetic component of gold contributed to the overall tenor of the carbonaceous sediment system.

In this regard, influx of a CO<sub>2</sub>-rich aqueous hydrothermal fluid whose Eh was buffered by rocks not carrying reduced carbon (ie. was more oxidizing with respect to the graphite buffered system), into a graphite-dominated domain represented by the carbonaceous interflow sediments, a predictable decrease in fluid Eh would result. This would shift the proportion of hydrolyzed carbon species in favour of a reduced phase such as methane. The result might induce gold precipitation in response to the destruction of possible gold-transporting complexes, a change in solution pH resulting from the loss of CO<sub>2</sub>, and scavenging of gold on activated carbon surfaces. Some carbon isotopic data in support of this suggestion will be presented in Chapter 8.3.

#### 4.2. Pyritic, Carbonatized Tholeiitic Basalt

This type of gold mineralization has been described as "sulphide-ore", "dacite-ore", "sulphide-replacement ore", or "mineralized rock" (Ferguson et al., 1968; Furse, 1948; Jones, 1948). Grades of 3 gram Au/tonne to 19 gram Au/tonne have been reported (Furse, 1948; Langford, 1941), and the

zones of disseminated sulphide can attain widths of 12-30 metres (Furse, 1948; Langford, 1941). This type of mineralization is best exposed on the surface of the former Hollinger Mine (55 vein zone) where it occurs as an east-trending pyritic zone localized adjacent to the contact with the Acme quartz-feldspar porphyry body on the north (Fig. 4-1), in a carbonatized iron-rich tholeiitic basaltic flow unit ("99 flow" using the terminology of Ferguson et al., 1968). The pyritic zone trends roughly parallel to volcanic stratigraphy. Two carbonaceous sedimentary units occur interbedded with the basalts in this zone. Neither interflow sediment exceeds 1m in thickness and both contain only rare porphyroblastic pyrite.

The width of this mineralized zone, where mined by open pit, averaged 10 m., but gold grades across the zone averaged less than 3 gram per tonne (A. Brooks, Mine Geologist, Pamour Porcupine Mines Ltd, Timmins Property, 1982). Higher grade material (>3 gram gold per tonne) was restricted to areas where the quartz vein density was higher (vein spacing of 1-2 per metre).

#### 4.2.1. Pyrite habits

Pyrite occurs disseminated in the basalt (10-15% by mode at best; Photo 4-4) and as sulphidization envelopes which can extend up to 0.5 m. away from thin (<3 cm.) quartz veins. The quartz veins occur in a widely spaced (1-3 m.),

shallowly dipping (30 -50°dip) set (Photo 4-5), although it has been noted that the quartz veins constitute only a minor proportion (<10%) of mineable ore zone (Langford, 1941). In the quartz veins ferroan dolomite occurs as an accessory phase and visible gold is not uncommon. The margin of the Acme porphyry intrusive is strongly sheared, carries large (>1 cm) metasomatic albite crystals, but contains little pyrite.

#### 4.2.2. Gold-pyrite association

Gold concentrations in typical material from this zone (Appendix-1) vary from 5 ppb for pyrite poor samples, to 12 ppm for heavily pyritized rock. The suggested correlation between gold concentration and pyrite modal abundance implies that pyrite in the carbonatized host rock is the major gold carrier.

#### 4.2.3. Relative age of pyritic gold mineralization in the 55 vein zone

In the 55 vein zone, gold occurs in pyritic envelopes about the quartz veins and as native gold within the quartz veins. Thus the introduction of gold is clearly linked to the veining event and attendant wallrock pyritization. These quartz veins cut the well developed foliation and mullions of carbonatized wallrock (Photo 4-5) which plunge 50° northeasterly. This indicates that the quartz veins (pyritization and gold) post-dated the

Photo 4-4: Disseminated pyrite within carbonatized, iron-rich tholeiitic basalt-typical of the 55 vein zone, Hollinger Mine.

Photo 4-5: Shallowly dipping quartz veins (QV) which occur in the 55 vein zone, Hollinger Mine. The veins cut millions of carbonatized basalt, suggesting a post-deformation age for the veins.





formation of the mullions. However, the mullion formation post-dated the carbonatization event (for a review of this argument, see Chapter 2.4, point 5). Therefore, the quartz veins, with attendant pyritization and gold emplacement, apparently post-dated the intense carbonatization event - at least for this vein set in the 55 zone of the former Hollinger Mine (Pamour Timmins Property).

#### 4.2.4. Other analogues

The disseminated pyrite present in the carbonatized zone exposed on the Porcupine Triumph (Fig. 3-5) property seems to be of this type. Here carbonatized rock is cut by quartz veins and veinlets. The auriferous material, consisting of replacement pyrite and quartz veining, is restricted to a carbonatized shear zone along the contact between an ultramafic dyke and the adjacent massive calc alkaline basalt.

Assignment of mineralized material on other mining properties to this type, using literature descriptions, must be done with caution because zones of pyritized volcanic rock are associated with most auriferous quartz veins. However, disseminated, pyritic mineralization has been mined at the McIntyre (near veins 3,5,7 and 10; dacite ore), Hollinger (55 vein), Dome ("mineralized" rock; Holmes in Ferguson et al., 1968), and the Paymaster Mine (#36 zone; Karvinen, 1981).

#### 4.3. Iron Formation-Hosted Gold

The Carshaw and Malga iron formation units (Fig. 4-3) in Shaw Township contain approximately 170,000 tons which grades 3.5 gram Au/tonne (0.21 oz. Au/ton; Willars, 1982) and 80,000 tons containing 10.7 gram Au/tonne (0.34 oz. Au/ton; Anon, 1944) respectively. Two iron formation units consist of recrystallized chert, magnetite, and chlorite mesobands and lie within a sequence of pillowed and massive calc alkaline basalts. A turbiditic chert fragment-bearing conglomerate (<10 m. thickness) is interbedded with basalt flows and crops out between the Malga and Carshaw iron formations (Fig. 4-3). Ultramafic and quartz-feldspar dykes of Archean age cut the volcanic and sedimentary rocks. A Proterozoic diabase dyke is the youngest rock type.

Several alteration events affected the rocks in this area. The earliest alteration is characterized by the filling of primary porosity in the vesicular basalt flows by silica and calcite. Some of the silica fillings retain textures suggesting a chalcedony precursor and attain diameters up to 5 centimetres. Superimposed on the vesicle-filling assemblages (quartz, chlorite and calcite) is the typical ferroan dolomite-bearing assemblages of the intense carbonatization (Photo 2-2). The two iron formation units, volcanic flows and felsic and ultramafic intrusives locally carbonatized (Fig. 4-3). Carbonatization of the iron formation is characterized by the presence of abundant

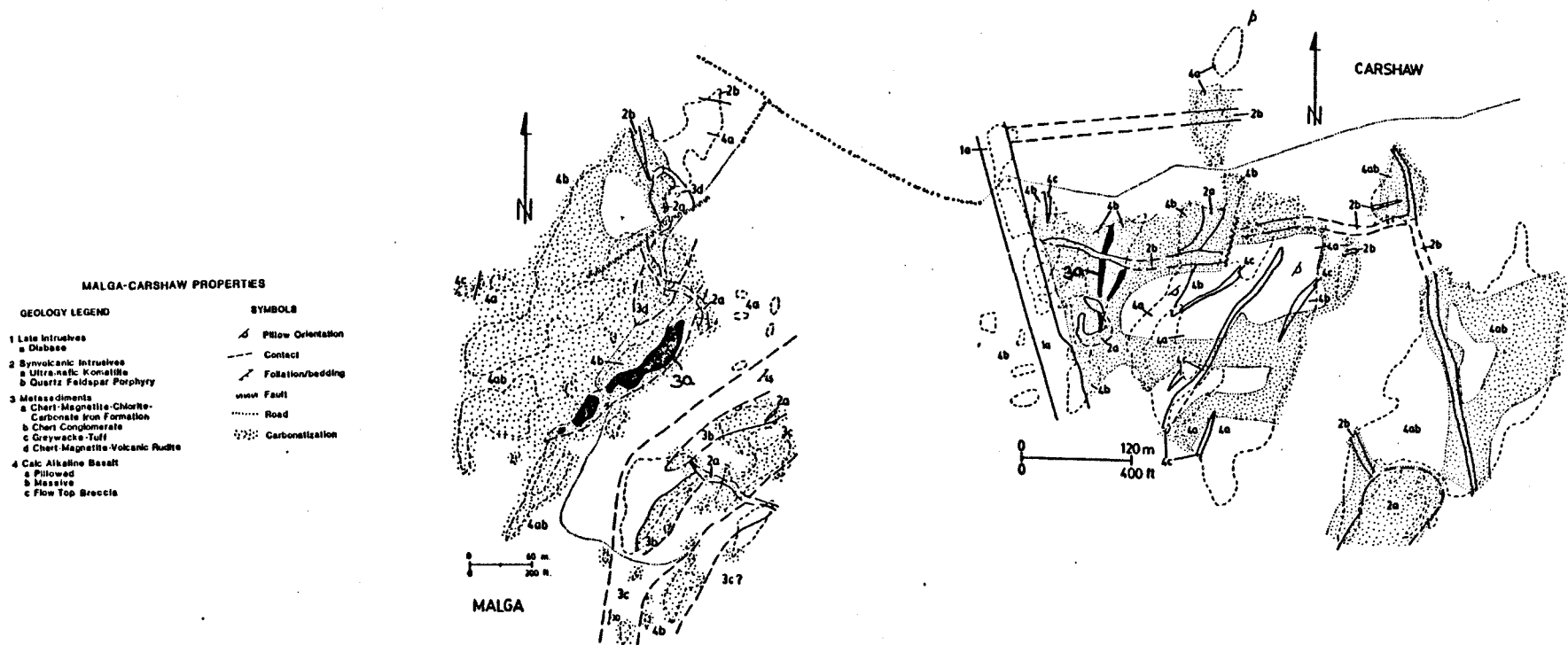


Figure 4-3: Surface geological plan of the Malga and Carshaw iron formation-hosted gold properties, Shaw Township. Sites of gold mineralization are the exposed portions of the iron formation units.

ferroan dolomite associated with magnetite-rich mesobands and less carbonate being associated with the recrystallized chert mesobands (Fyon et al., 1983c). Texturally, much of this ferroan dolomite in the iron formation appears to replace preexisting magnetite (Photo 4-6). The larger scale field relationships (Map 9), also illustrate that the zones of intense carbonatization crosscut the banded iron formations as well as the host volcanic flows and the Archean, igneous dykes. Thus, the banded iron formations and the host volcanic rocks were carbonatized contemporaneously.

#### 4.3.1. Gold mineralization

The iron formations are cut by quartz veins which average 3 centimetres in width, although exceptionally wide veins up to 1 metre in width were observed underground. The quartz veins terminate at or just beyond the contact between the iron formation and the basaltic country rocks. That is, the quartz veins were localized by brittle fracture of the iron formations. These fractures did not propagate into the basaltic country rock. Pyrite occurs as sulphidization halos adjacent to the quartz veins and preferentially replaces magnetite mesobands (Photo 4-7). The sulphidization envelopes rarely extend for more than 20 centimetres away from the outer edge of the quartz veins. Sulphidization of the magnetite-rich mesobands a metre or so

Photo 4-6: Ferroan carbonate (FC) occurs preferentially within a magnetite-rich mesoband, Carshaw iron formation. This preference suggests that the iron carbonate may have replaced the preexisting magnetite.

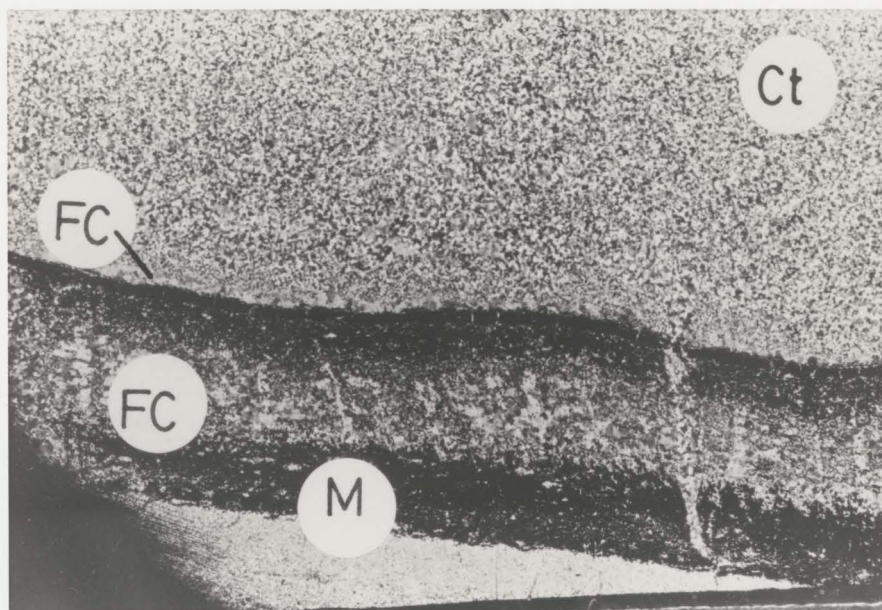
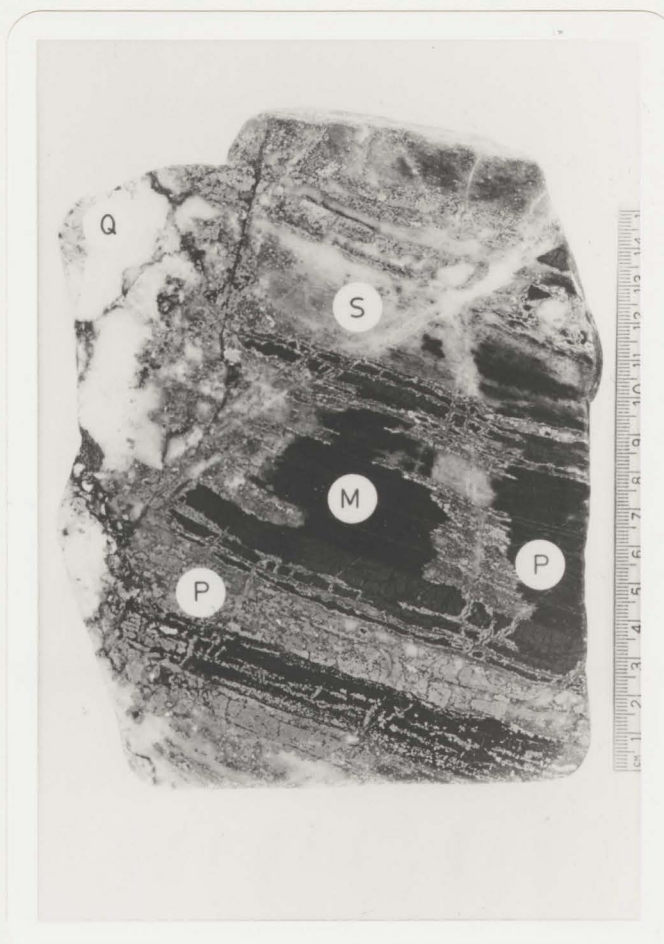


Photo 4-7: Pyrite (P) replacement of magnetite (M) mesobands adjacent to a quartz (Q) vein which cuts the Carshaw iron formation. Note the silicification (S) which accompanies the quartz vein and sulphidization (after Fyon et al., 1983c).





away from the quartz veins is much less intense. This lower intensity sulphidization is characterized by pyrite and trace pyrrhotite which occur as rare, disseminated grains, apparently replacing magnetite and ferroan dolomite.

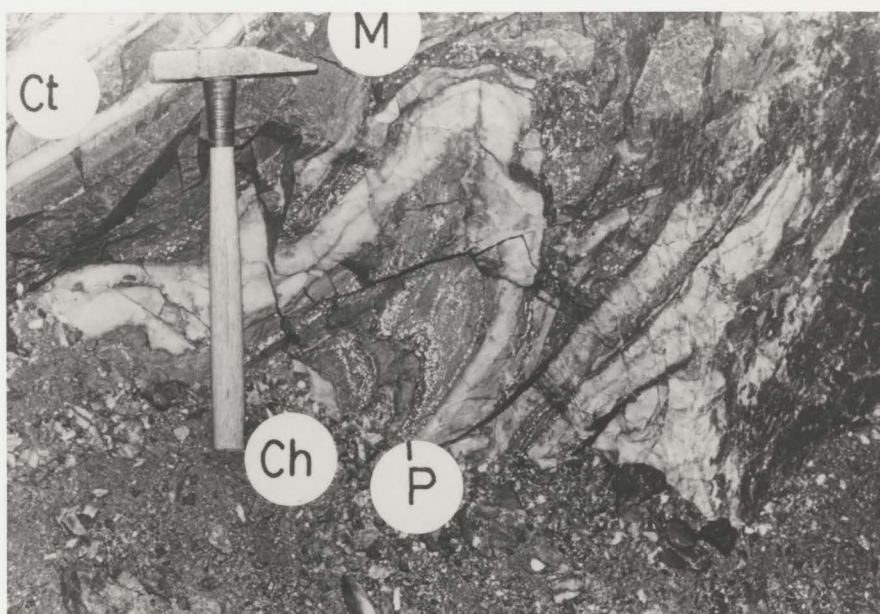
Ultramafic and felsic dikes which cut the iron formation are also cut by the quartz veins, but no pyrite sulphidization occurs in these dikes adjacent to the quartz veins even though the same veins can be traced into the adjacent magnetite-rich iron formation where the sulphidization halo is developed. This suggests that both the abundance and availability of iron played an important role in the fixation of pyrite and gold.

Stratiform pyrite occurs preferentially within chlorite-rich mesobands (Photo 4-8). Quartz veins are notably lacking in proximity to this stratiform pyrite. The stratiform, laminated habit of this pyrite and the absence of quartz veining in proximity could either reflect a syngenetic origin for the stratiform pyrite or it may represent a variant of the epigenetic sulphidization product (Fyon et al., 1983c). Insufficient field evidence is available to resolve this question.

#### 4.3.2. Gold distribution

The replacement pyrite which occurs adjacent to the quartz veins contains 20-130 ppm gold. Whole rock gold analyses of the least sulphidized iron formation material

Photo 4-8: Stratiform pyrite (P)  
microbands in a chloritic (Ch) mesoband.  
Chert (Ct) and magnetite-rich (M)  
mesobands are also folded. Underground  
at the Carshaw property (after Fyon et  
al., 1983C).



vary from 0.001 and 6.0 ppm gold (Table 4-3). The log transformed average of this material is 0.015 ppm (Fyon et al., 1981). The stratiform variety of pyrite localized primarily in chlorite-rich mesobands, averages 1-3 ppm gold. The contribution to the gold tenor of the iron formation by the stratiform pyrite is small because the chlorite-rich mesobands do not constitute a major volumetric proportion of the iron formation unit.

#### 4.3.3. Relative age of gold mineralization

The gold abundance in the iron formation is directly correlated with the sulphide abundance (Fyon et al., 1983c). Almost all of this sulphide occurs as pyrite adjacent to quartz veins. Thus, the greatest concentration of gold was fixed in the iron formation during the epigenetic quartz veining event. This quartz veining event postdated the intrusion of both ultramafic and quartz-feldspar porphyry dykes. The absolute age of these dykes is not known, but they may be assumed to be either: 1) intrusive equivalents of the Formation III or VI felsic volcanic units; or 2) equivalents to the felsic intrusive bodies (quartz-feldspar porphyry intrusives) which are abundant in the Porcupine Camp. Regardless, it is apparent that the quartz veining event was not syngenetic.

Microscopic textural relationships suggest that the pyritic sulphidization postdated the intense

TABLE 4-3: Gold concentrations of pyrite separates from ore material and mesobands from the Carshaw iron formation property.

| Sample Number                                                                        | Description                                                                                                                              | Au ppb                                         |
|--------------------------------------------------------------------------------------|------------------------------------------------------------------------------------------------------------------------------------------|------------------------------------------------|
| =====                                                                                |                                                                                                                                          |                                                |
|                                                                                      | Pyrite separate from the pyritic replacement envelope in the magnetite-rich mesobands adjacent to quartz-dolomite-chlorite-pyrite veins. |                                                |
| Car-79                                                                               |                                                                                                                                          | 75000                                          |
| Car-132                                                                              |                                                                                                                                          |                                                |
| -1                                                                                   |                                                                                                                                          | 60000                                          |
| -2                                                                                   |                                                                                                                                          | 90000                                          |
| -3                                                                                   |                                                                                                                                          | 130000                                         |
| -4                                                                                   |                                                                                                                                          | 20000                                          |
| -5                                                                                   |                                                                                                                                          | 45000, 40000                                   |
| =====                                                                                |                                                                                                                                          |                                                |
|                                                                                      | Pyrite separate from pyritized carbonate footwall carbonate breccia.                                                                     |                                                |
| Car-142                                                                              |                                                                                                                                          | 5400                                           |
| Car-143                                                                              |                                                                                                                                          | 10000, 6100                                    |
| Car-147                                                                              |                                                                                                                                          | 600                                            |
| =====                                                                                |                                                                                                                                          |                                                |
|                                                                                      | Pyrite separate from chlorite mesobands in the iron formation(possibly syngenetic pyrite).                                               |                                                |
| Car-145                                                                              |                                                                                                                                          | 3300                                           |
| Car-146                                                                              |                                                                                                                                          | 2100                                           |
| Car-152                                                                              |                                                                                                                                          | 1100, 1200                                     |
| =====                                                                                |                                                                                                                                          |                                                |
| Whole rock analysis of selected chert mesobands.<br>(log transformed population)     |                                                                                                                                          | mean 9.8 $\pm$ 0.81<br>r=0.7 to 1400<br>n= 19  |
| =====                                                                                |                                                                                                                                          |                                                |
| Whole rock analysis of selected magnetite mesobands.<br>(log transformed population) |                                                                                                                                          | mean 28.2 $\pm$ 1.14<br>r=0.9 to 5900<br>n= 12 |
| =====                                                                                |                                                                                                                                          |                                                |
| Whole rock analysis of selected carbonate mesobands.<br>(log transformed population) |                                                                                                                                          | mean 13.2 $\pm$ 0.74<br>r=1.6 to 660<br>n= 10  |
| =====                                                                                |                                                                                                                                          |                                                |

Data from Fyon et.al.(1983a)

Explanation: r- range of data; n- number of analyses.

carbonatization. Illustrated in Photos 4-9a,b are the textural features which constrain the relative timing of the carbonatization and sulphidization of the iron formation. The common habit of the secondary ferroan dolomite which replaces magnetite-rich mesobands is shown in Photo 4-6 for a sample collected well away from any quartz veining. There is no evidence of sulphidization in this sample. Shown in Photo 4-9a,b is the replacement of a magnetite mesoband (and associated secondary ferroan dolomite) by auriferous pyrite adjacent to a quartz vein. Clearly the secondary auriferous pyrite replaces the preexisting magnetite-dolomite assemblage. Thus, the gold mineralization event must have postdated the intense carbonatization event which altered both the igneous rocks and the iron formation units.

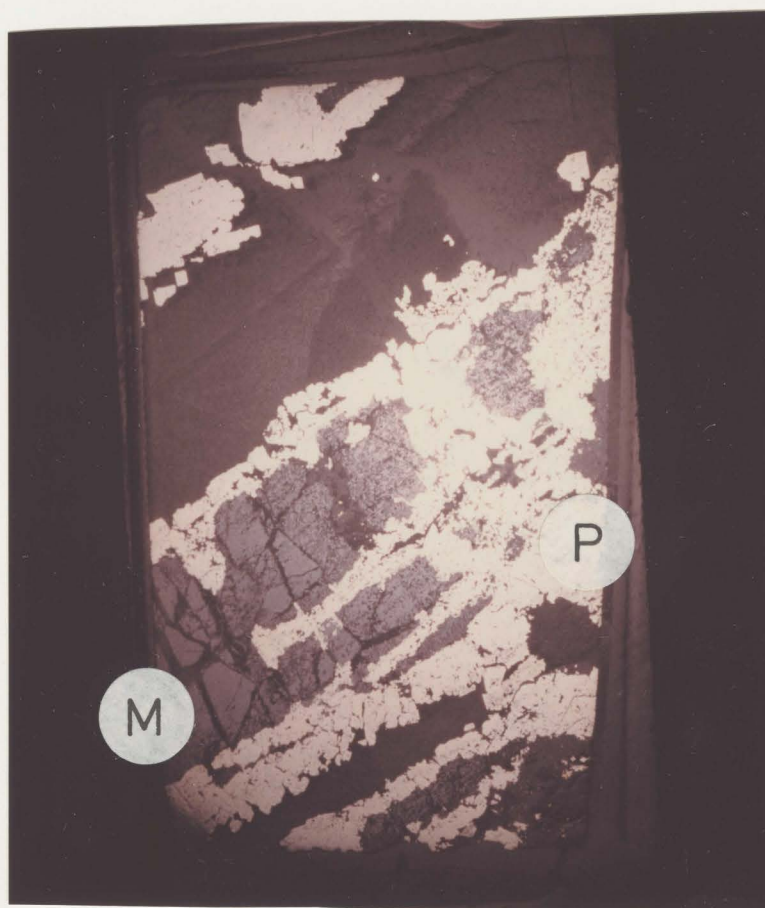
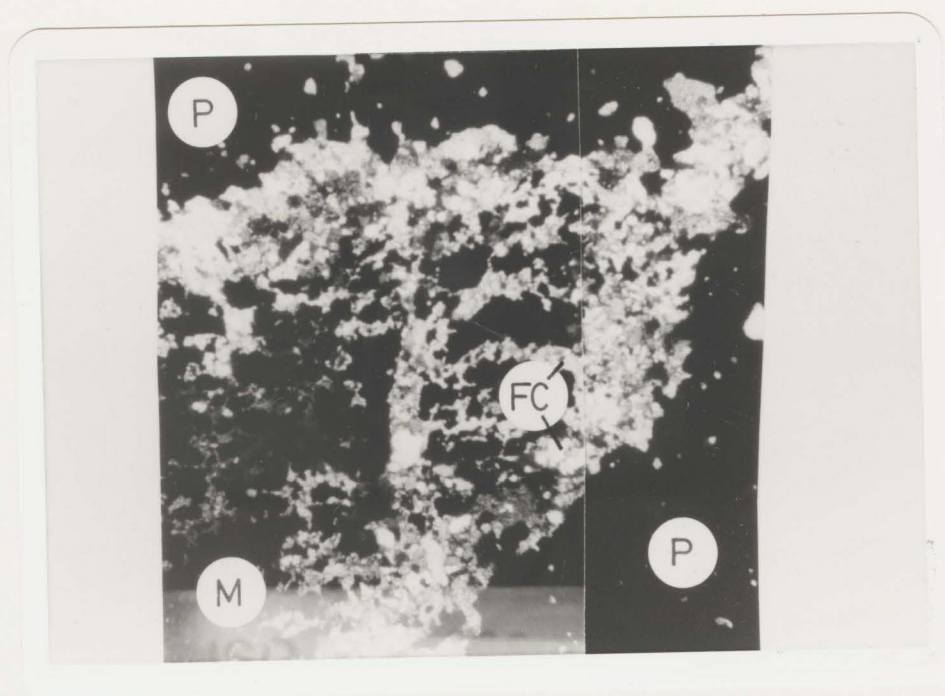
The gold-pyrite mineralization, which accompanied quartz veining, represents one of the last hydrothermal events. It is stressed that this is a relative alteration/mineralization chronology. The reconstructed alteration sequence could represent three genetically unrelated hydrothermal events, or may represent the evolution of a single hydrothermal system.

#### 4.3.4. Nature of auriferous fluids

Most if not all of the gold in the iron formations was introduced during an epigenetic quartz veining event which post-dated the intrusion of ultramafic and quartz-

Photo 4-9a: Transmitted light photograph illustrating the replacement of a preexisting ferroan dolomite-bearing (FC) magnetite (M) mesoband which is being replaced by pyrite (P) adjacent to a quartz vein (not visible in the photo). Sample from the Carshaw iron formation.

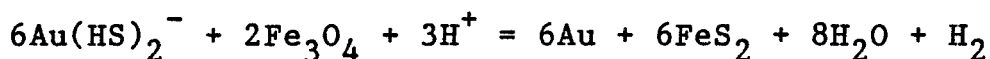
Photo 4-9b: Reflected light photograph illustrating a relict magnetite mesoband (M) which has been almost completely replaced by pyrite (P) adjacent to a quartz vein. Same sample as in Photo 4-9a.





feldspar porphyry dykes. That the gold is intimately associated with pyrite, which replaces magnetite, indicates that the precipitation of gold was induced by a reaction between magnetite in the iron formation and sulphur-bearing hydrothermal fluids. By virtue of their high iron content, magnetite mesobands were favoured sulphidization substrates.

A hypothetical reaction can be written to describe the coprecipitation of gold and pyrite resulting from reaction between magnetite ( $\text{Fe}_3\text{O}_4$ ) and reduced sulphide-bearing auriferous fluids. For near neutral solutions carrying sulphur, gold is transported as a  $\text{Au}^+$ -thio complex (Seward, 1973, 1979):



This mode of gold fixation in banded iron-formation is quite similar to that described by Phillips et al. (1984), for deposits in Western Australia.

#### 4.4. Quartz Veins In Carbonatized Mafic and Ultramafic Flows

Within the Timmins area, most quartz veins occur in carbonatized basaltic or ultramafic rock. Much less quartz veining occurs in the quartz-feldspar porphyry (Q.F.P.) bodies and virtually none occurs in the felsic pyroclastic units which constitute the top of the older Deloro and younger Tisdale Groups. A geometrical classification of vein types is given by Graton et al. (1933), Hurst (1935)

and Jones (1948) and a summary of the structural and stratigraphic control of the veins is given by Ferguson et al. (1968, p.58-60). Recent detail studies of veining history in the Dome Mine are given by Fryer et al. (1979), Roberts (1981), Roberts et al. (1978) and Roberts and Spiteri (1979).

Approximately 90 modal percent of the vein material is quartz, the remainder being composed of pyrite, white mica, calcite or ferroan dolomite. Pyrrhotite, chalcopryrite, galena, sphalerite, tellurides, chlorite, talc, albite, scheelite, siderite, selenite, and anhydrite are much less abundant in the veins (Hurst, 1935). Native gold is present as free grains in silicate or carbonate minerals and as inclusions in pyrite. Wallrocks are carbonatized adjacent to the quartz veins and chloritized further away (Bain, 1933).

#### 4.4.1. Intermineral textures within the veins

Quartz veins from several properties in the Timmins (Table 4-4) area were examined to determine if it was possible to establish the vein paragenesis on the basis of intermineral textures. Any deduced vein paragenesis establishes the geological constraints within which the stable isotopic compositions of the vein phases must be interpreted. In addition, an established vein paragenesis can be used to further constrain the temporal sequence of

TABLE 4-4: Porcupine Camp properties from which quartz vein samples were examined petrographically.

| Property          | Sample Numbers                |
|-------------------|-------------------------------|
| Aunor-1000 level  | A-33                          |
| Canusa            | Can-44, 47, 49                |
| Carshaw           | Car-60, 142, 147-1, 148, 151  |
| Dobell            | TR-395, 509                   |
| Duval(McLaren)    |                               |
| Glory hole        | Du-7                          |
| South vein        | Du-8, 14-1, 14-2              |
| Faymar            | Fa-3, 5, 10, 10-2, 15-1, 15-2 |
| Hollinger         |                               |
| #1 vein           | H-46                          |
| 68E vein          | H-23, 28                      |
| 65E vein          | H-52                          |
| 218 vein(400 pit) | H-42                          |
| 55 vein           | H-55V, 50-3                   |
| Hugh Pam          | Wh-153, 153A, 152, 152A       |
| Porcupine Triumph | DR-344                        |

wallrock alteration events. Because of the historic importance of the former Hollinger Mine (Pamour Timmins Property), intermineral textures observed in some vein systems from this property are described in more detail to categorize the variety of primary and deformation textures recognized. Other vein systems are then described only briefly to emphasize the ubiquitousness of these textures. A more complete description of the vein mineralogy and intermineral textures for vein material from the different properties is offered in Appendix-2.

#### 4.4.1.1. Hollinger vein suite

Five vein systems were examined: 1) 68E carbonaceous zone (H-23, H-28); 2) 65E vein zone (H-52); 3) 55 vein zone (H-55V, H-50-3); 4) 1 vein zone (H-46); 5) 218 vein zone, 400 pit west end (H-42). All samples were collected from vein material exposed in the open pits on surface. Although this represents a small data base, it will be demonstrated that the intermineral textural relationships and the deduced paragenetic sequence is common not only to these Hollinger vein samples, but also to samples collected from several other properties (to be discussed shortly, Table 4-4) located elsewhere in the Timmins area. Synthesized in Table 4-5 are the minerals identified in the Hollinger quartz veins, the inter- and intramineral textural relationships, and the interpreted

TABLE 4-5: Synthesis of mineral phases, their intermineral textures and the interpreted paragenetic sequence for some quartz veins on the former Hollinger Mine property.

| Sample Number                      | H-23          | H-28           | H-52     | H-42     | H-46           | H-55V | H-50-3 |
|------------------------------------|---------------|----------------|----------|----------|----------------|-------|--------|
| Vein System                        | 68E           | 68E            | 65E      | 218(400) | 1              | 55    | 55     |
| <hr/>                              |               |                |          |          |                |       |        |
| Vein Phases                        |               |                |          |          |                |       |        |
| Quartz                             | 1             | 1              | 1        | 1        | 1              | 1     | 1      |
| Dolomite                           | 2             | 2              | 2        | 2        | 2              | 2     | 2      |
| Chlorite                           | 3             | 3              | 3        | 3        | -              | -     | -      |
| White mica                         | -             | 4              | 4        | -        | 3              | -     | -      |
| Albite                             | -             | -              | -        | 1        | 1              | -     | -      |
| Pyrite-coarse                      | -             | 1              | -        | 1        | 1              | 1     | 1      |
| Chalcopryrite(a)                   | -             | -              | -        | 1        | -              | -     | -      |
| Galena(a)                          | -             | -              | -        | 1        | -              | -     | -      |
| Pyrite-fine                        | -             | -              | -        | -        | 2              | -     | -      |
| Gold                               | -             | 2-3            | -        | 1        | -              | -     | -      |
| Scheelite?                         | -             | 4              | 4        | >1(b)    | 3              | -     | -      |
| Pyrrhotite                         | -             | 1              | -        | 1        | 1              | 1     | 1      |
| <hr/>                              |               |                |          |          |                |       |        |
| Deformation                        |               |                |          |          |                |       |        |
| Textures                           |               |                |          |          |                |       |        |
| Stylolite                          | chl in<br>qtz | mica in<br>qtz | -        | -        | mica in<br>qtz | -     | -      |
| Strained quartz                    | X             | X              | X        | X        | X              | X     | X      |
| Fractured quartz                   | dol vltz      | X              | dol vltz | -        | -              | X     | -      |
| Fluid inclusion<br>trains          | X             | X              | X        | X        | X              | X     | X      |
| Sutured quartz<br>grain boundaries | X             | X              | X        | X        | X              | X     | X      |
| <hr/>                              |               |                |          |          |                |       |        |
| Annealing Textures                 |               |                |          |          |                |       |        |
| Polygonalized<br>quartz            | <5%           | 10%            | --       | <5%      | --             | <5%   | --     |
| Subgrained quartz                  | --            | --             | X        | --       | X              | --    | --     |

Notes: a) Included in coarse pyrite.  
b) Present in crushed quartz zones.  
X- Indicates texture is present.  
--: Indicates texture or mineral is absent.

#### Mineral Paragenesis

1-first;2-second;3-third;4-fourth

This is a relative chronology deduced from the intermineral textural relationships observed between the vein phases.

#### Abbreviations

chl-chlorite; qtz-quartz; cpy-chalcopryrite; dol-dolomite; vltz-veinlets  
X-indicates mineral or texture is present; <5%- less than 5% of the  
>1- indicates that the mineral in question is younger than the mineral  
precipitation event indicated.

paragenetic sequence.

The paragenetic sequence and the subsequent deformation history of the quartz vein systems follows from the interpretation of the intermineral and intramineral textures. Hence, some discussion and illustration of the textures used to arrive at these interpretations is warranted.

#### 4.4.1.1.1. Primary textures of open-space deposition

This group of textures includes those which form at the time that a mineral grows by precipitation from a hydrothermal fluid in the vein structure. They are regarded as primary textures and did not develop in response to stress modification or deformation of a pre-existing mineralogical assemblage:

i) One sample (H-55V) contains euhedral, quartz showing a comb texture which is suggestive of quartz which grew into an open fracture (Craig and Vaughn, 1981, p. 113); dolomite infills and locally embays the euhedral, stubby quartz suggesting the later infilling of the vug by dolomite (Photo 4-10a).

ii) all vein samples consist largely of coarse grained quartz (0.5-2 cm.) and less frequently albite; to attain these coarse grain sizes the minerals must have grown unimpeded in a space maintained open by hydraulic pressure.

iii) chlorite and dolomite or calcite frequently appear to fill void space about drusy quartz crystals (Photo 4-10a); this texture strongly suggests that the void filling mineral crystallized after the drusy quartz, especially where quartz crystals are coated by that later mineral (Photo 4-10b).

#### 4.4.1.1.2. Replacement textures

The following intermineral relationships are interpreted to have developed as a result of mineral replacement by fluids from which a second compositionally different mineral phase is precipitated:

1) embayment or resorption (Photo 4-11a) - the mineral being replaced lies on the convex side of the embayment surface;

2) cross-cutting or fracture-filling (Photo 4-11b) - the mineral occupying the fracture is interpreted to be younger than the fractured host mineral;

3) rafting (Photo 4-11c) - the digitate, although "scalloped", replacement surface is locally breached to produce an isolated or rafted piece of mineral undergoing replacement which is seen to be floating or enclosed completely by the "replacing" mineral.

#### 4.4.1.1.3. Deformation textures

The following intramineral textures are interpreted

Photo 4-10a: Subhedral quartz (Q) crystal grew perpendicular to vein wall (W). Ferroan dolomite (D) fills vug between quartz crystals and locally resorbs (R) quartz. (Sample H-55V, Hollinger Mine).

Photo 4-10b: Chlorite (Ch) partially fills a vug and coats a euhedral quartz crystal (Q). (Quartz vein sample from Carshaw property).



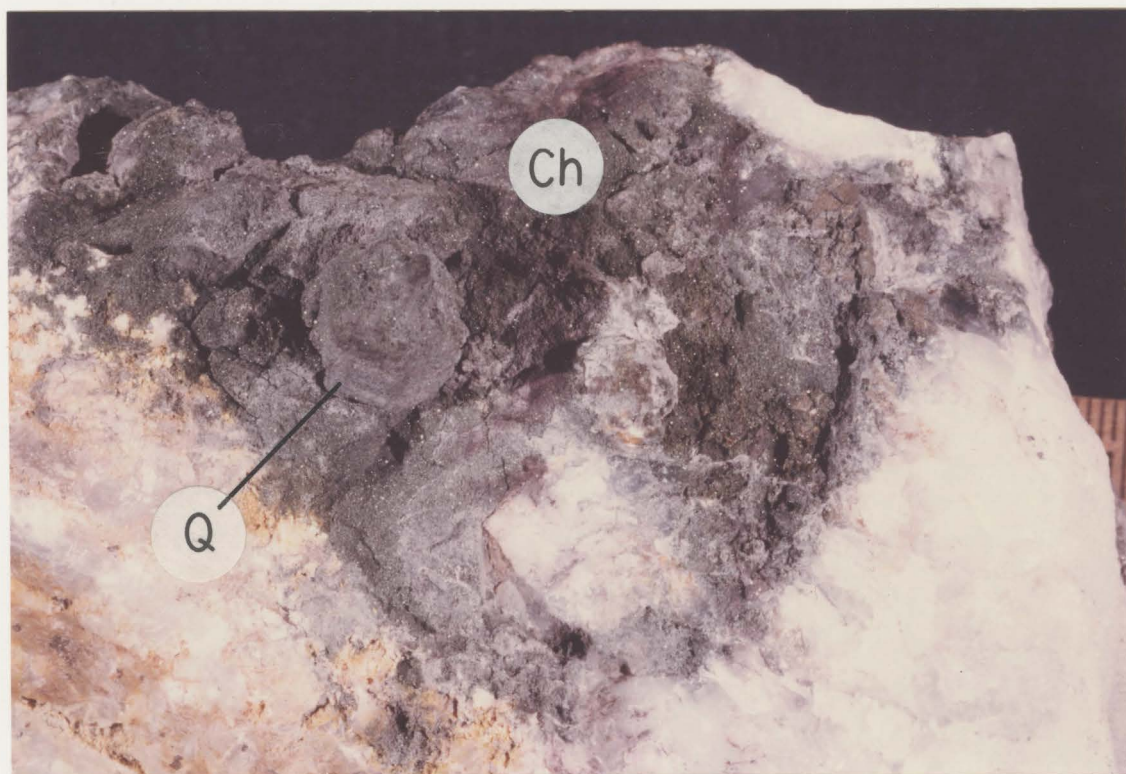
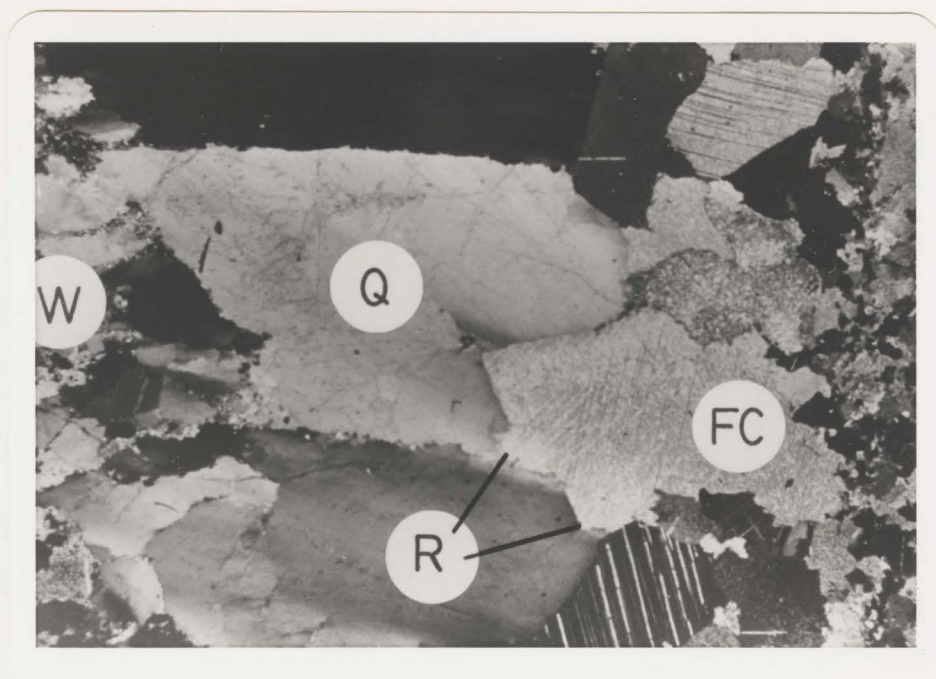


Photo 4-11a: Resorption of quartz (Q) by ferroan dolomite (FC).

Photo 4-11b: Ferroan dolomite veinlet cross cuts a quartz crystal.

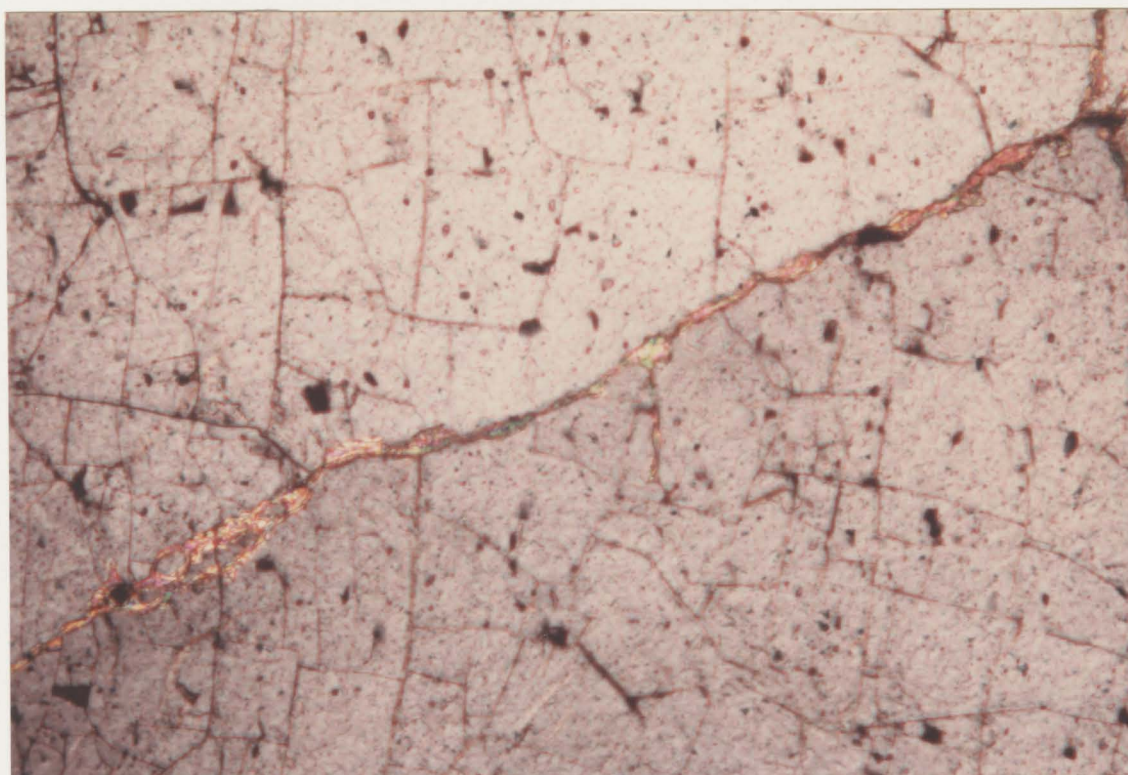
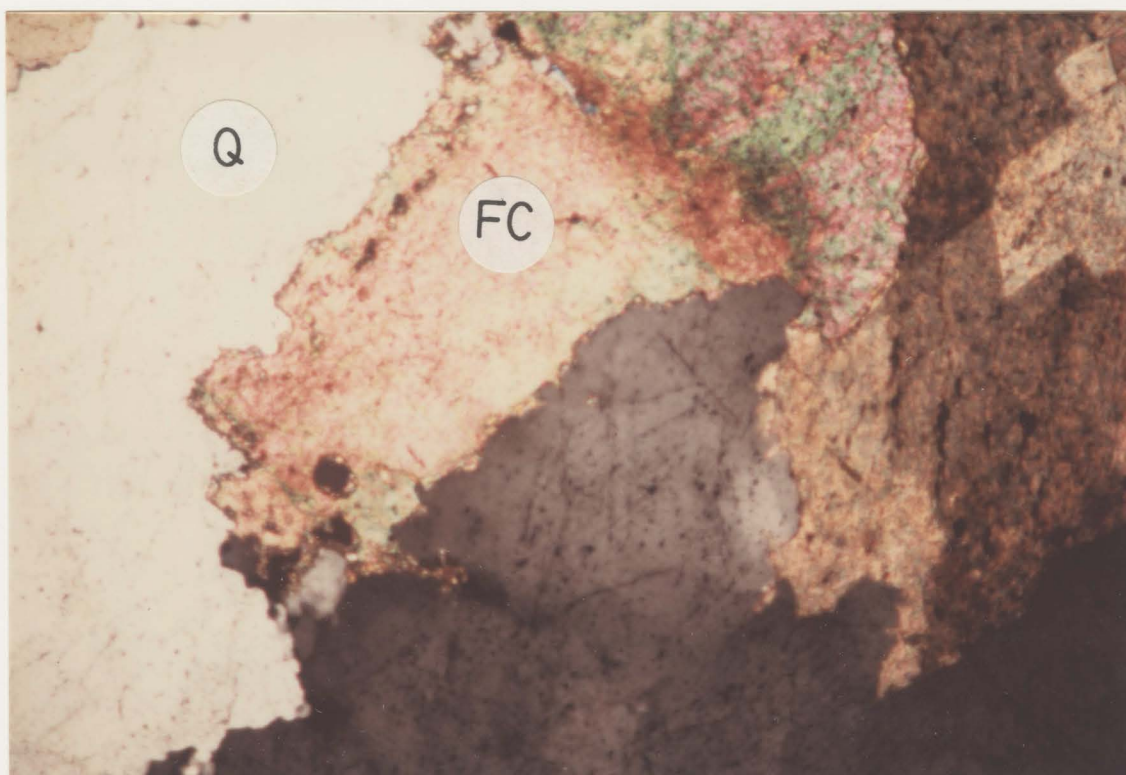
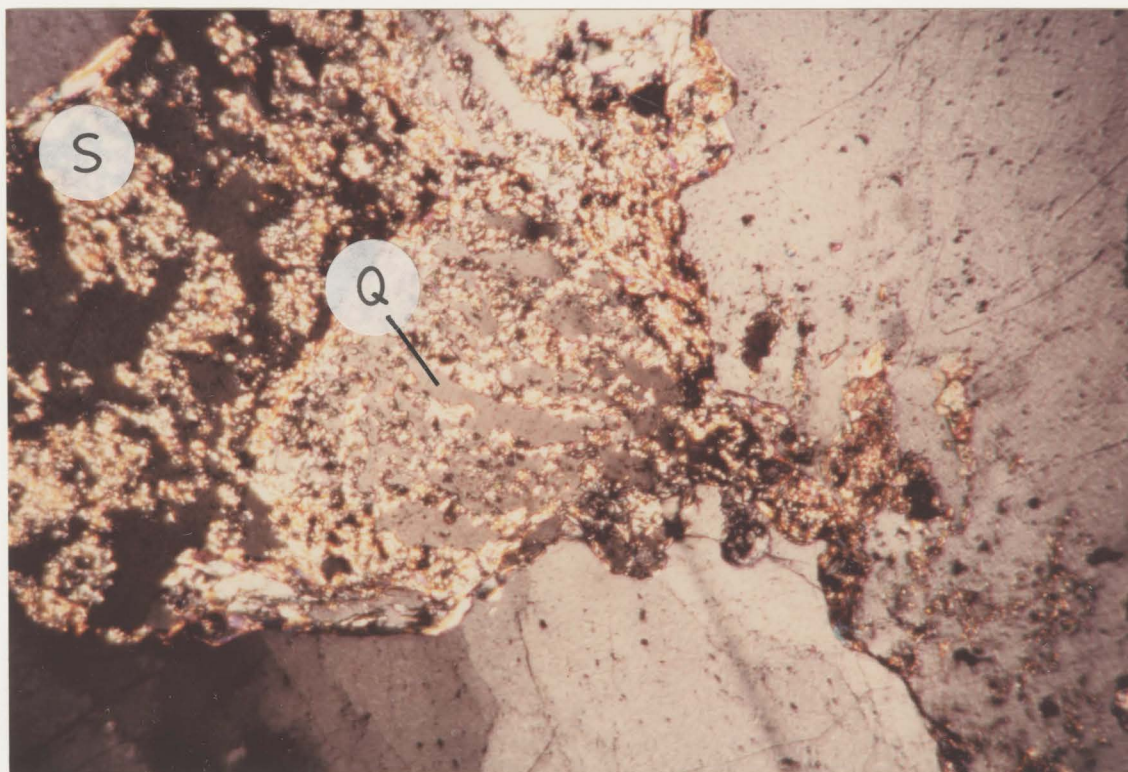


Photo 4-11c: Quartz (Q) islands  
represent pieces isolated and separated  
from the main quartz grain during the  
late introduction of white mica which  
replaces the vein quartz.





to have developed in response to applied stress and resulting deformation of the mineral phase:

i) quartz and albite exhibit strained, undulating extinction in all samples (Photo 4-12a);

ii) most quartz grains exhibit a certain degree of subgraining (Photo 4-12b); the fine grained quartz polyhedra meet with  $120^\circ$  interfacial angles (triple junctions);

iii) albite shows the development of kinked, wedge shaped domains which resemble deformation twins (Photo 4-12c);

iv) white mica-rich domains show evidence of kink banding (Photo 4-12d);

v) most samples of quartz show curved fracture planes;

vi) many different orientations of fluid inclusion trains exist in quartz and can be observed to cross cut quartz grain boundaries; some of these inclusion trains are observed to occur along or subparallel to fracture planes in quartz (Photo 4-12e);

vii) quartz grain boundaries in all samples show sutured grain boundaries (Photo 4-12a), suggestive of pressure solution;

viii) stylolites consisting of chlorite or white mica are present in some samples (Photo 4-12f; H-46; H-28, H-23). The stylolites are best developed along quartz-quartz and quartz-dolomite grain contacts whereas the sutured grain

Photo 4-12a: Undulose, strained extinction in vein quartz (Q). Note the sutured, almost stylolitic grain boundary (S) between quartz grains and the secondary fluid inclusion trains which cross cut quartz grain boundaries.

Photo 4-12b: Subgrains developed in vein quartz. Note local polygonalization of quartz adjacent to subgrain boundaries.

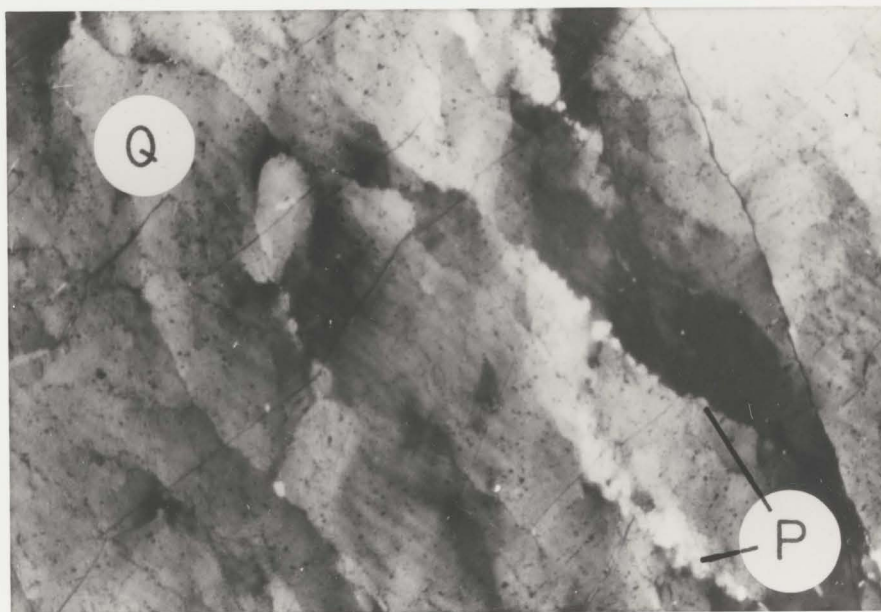
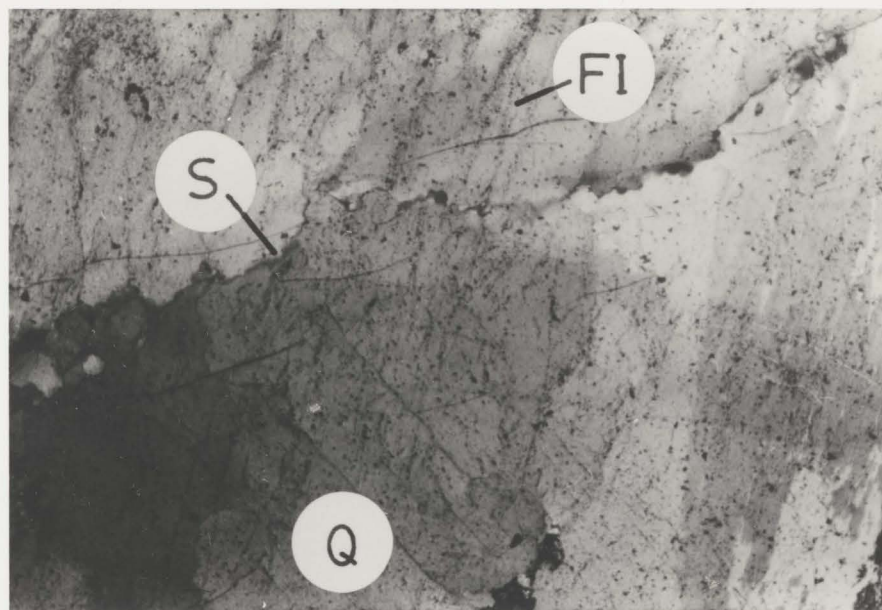




Photo 4-12c: Wedge-shaped, gently bent  
deformation twins developed in albite  
from a quartz vein.

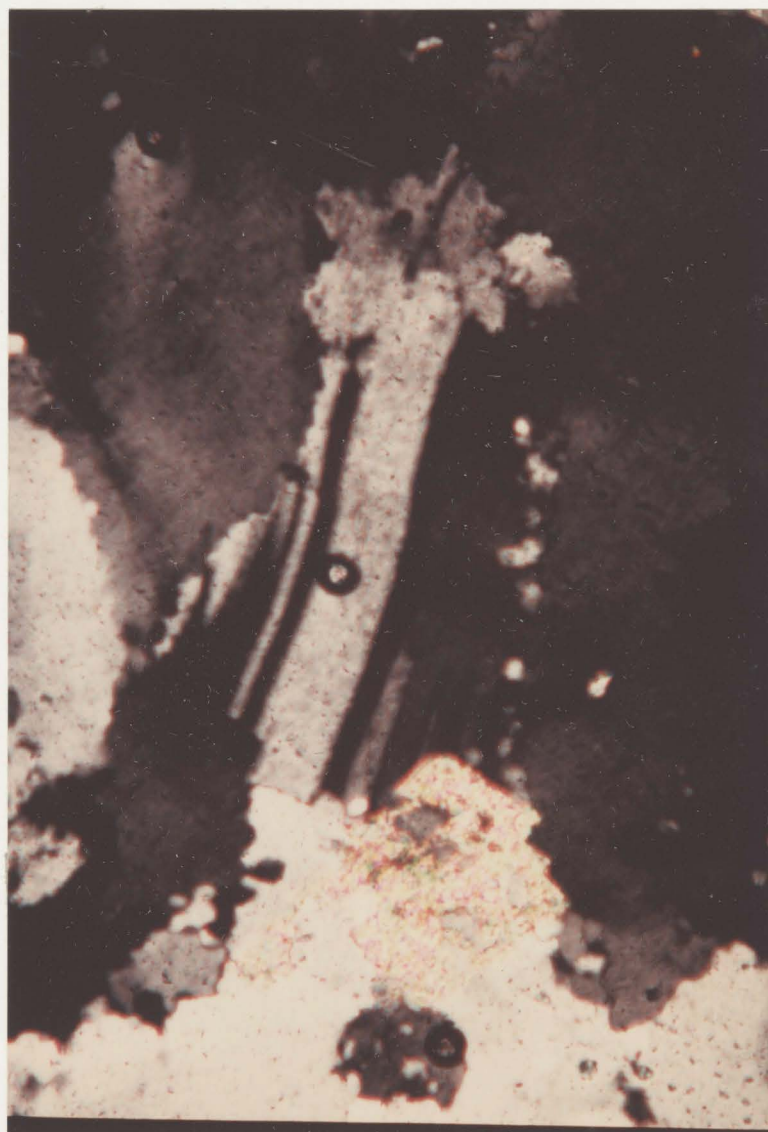


Photo 4-12d: Kinked white mica (S) present in a quartz vein exposed on the Duval, South Vein property. White mica also resorbes (R) ferroan dolomite (FC).

Photo 4-12e: Trains of fluid inclusions (FI) cross cut vein quartz (Q) grain boundaries and mark the traces of healed fractures.

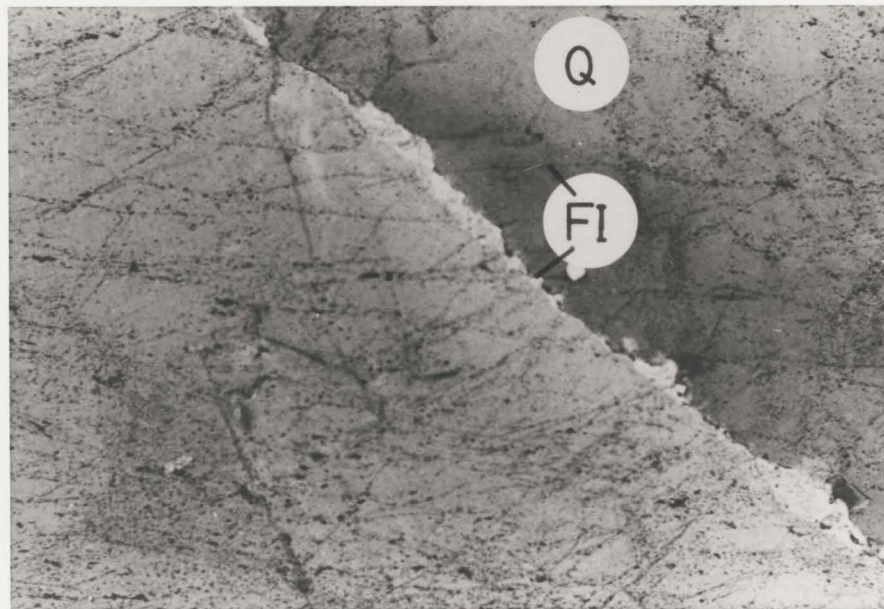
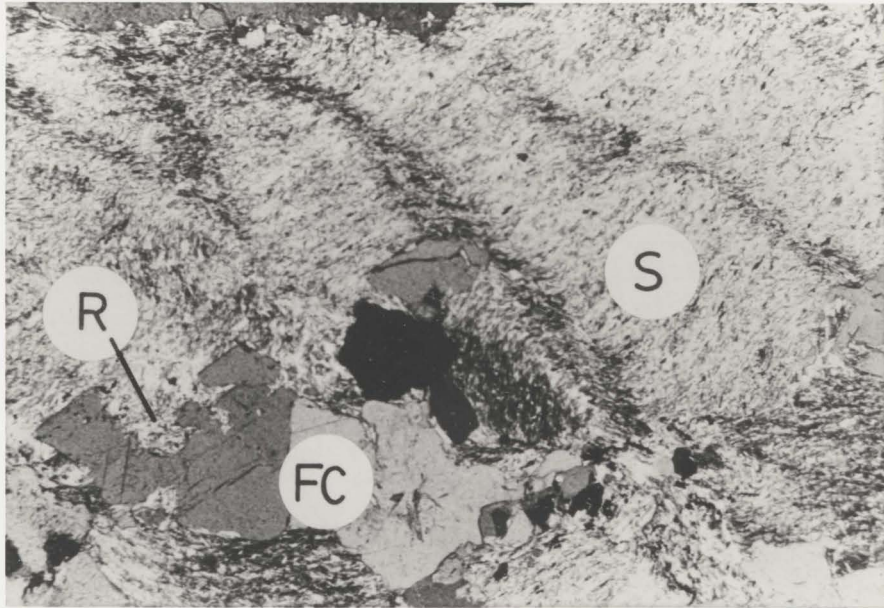
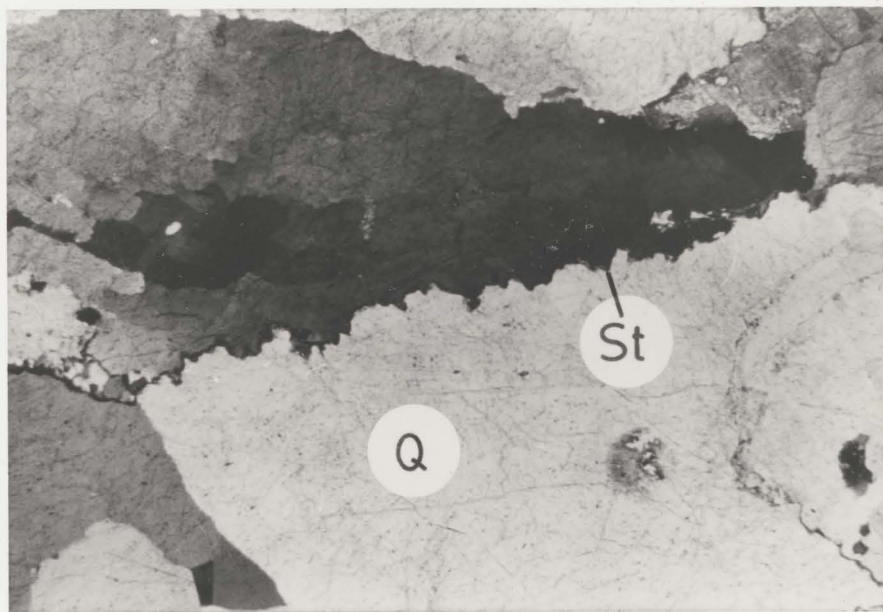


Photo 4-12f: Styolitic (St) chlorite  
developed between two quartz (Q) grains.



contacts are observed between quartz-quartz, quartz-dolomite, and dolomite-dolomite grain boundaries;

These deformation textures, including the presence of linear trains of secondary fluid inclusions, illustrate that the veins underwent deformation in the presence of at least one exotic fluid. Because detailed fluid inclusion studies on this vein material have not been carried out, the exact number of fracture and fluid incursion events is unknown, as is the constitution ( $\text{CO}_2$ ,  $\text{H}_2\text{O}$ , vapour, salt volume proportions) of the trapped fluids.

#### 4.4.1.2. Paragenesis of Hollinger veins

The deduced vein paragenesis, based on the primary and replacement textures, is common to all veins sampled from the Pamour Timmins Property (former Hollinger Mine) and is simplified in Figure 4-4. Quartz, which either coprecipitated with or postdated albite, was followed by dolomite, which were followed by chlorite which was succeeded by white mica. In general, little chlorite was observed in contact with white mica; hence, the paragenetic relationship between chlorite and white mica is less certain.

The paragenetic position of gold is not well constrained because only two samples containing microscopically visible gold were obtained (H-28, H-42). In sample H-42, gold occurs: 1) as blebby inclusions ( $<0.01$

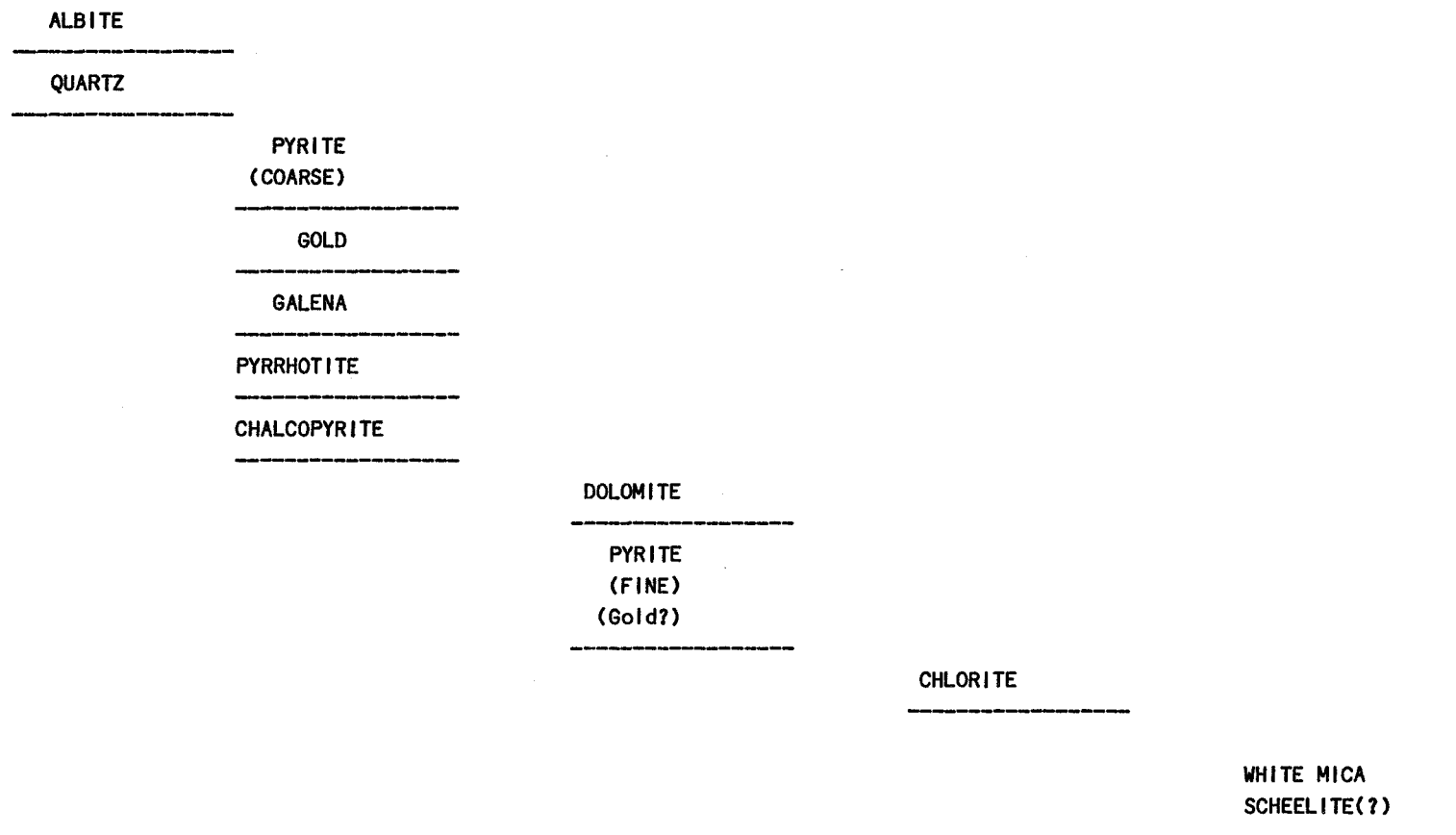


Figure 4-4: Deduced paragenetic sequence for the Hollinger vein samples.



mm.) in coarse pyrite; the pyrite is localized by cracks or fractures in quartz (Photo 4-13a); 2) along late cataclastic fractures in pyrite (Photo 4-13b); 3) as elongate grains (0.01 mm.) orientated parallel to the edge of a subhedral coarse pyrite grain associated with linear trains of galena and traces of gangue (Photo 4-13c). This last habit suggests that gold, galena and gangue were trapped onto a pyrite growth plane. The first and third habits of gold suggest that some gold was coprecipitated with pyrite. The second habit suggests the late introduction of some gold after pyrite or redistribution of gold into fractured pyrite.

The adsorption experiments by Bancroft and Jean (1982) demonstrated that gold in solution is efficiently adsorbed onto a sulphide substrate as native gold. Hence, if pyrite were to grow or recrystallize in the presence of an auriferous fluid, gold might be expected to plate out onto the pyrite growth surfaces. These experimental results have some bearing on the interpretation of gold-pyrite intermineral textures. The occurrence of gold along an apparent pyrite growth plane (Photo 4-13c) is suggestive that some gold was precipitated onto a growing pyrite growth face. However, gold which is deposited within fractures in pyrite is classically interpreted as late gold introduced into a preexisting pyrite-bearing system. In many cases good textural evidence exists to support such an

Photo 4-13a: Pyrite (P) and trace chalcopyrite (Cp) cross cut a vein quartz grain. (Sample Fa-5, Faymar Mine; long axis of photo is 0.71 mm.)

Photo 4-13b: Gold (Au) occurs in cataclastic pyrite (P). (Sample Fa-15, Faymar Mine; long axis of photo is 0.71 mm.)

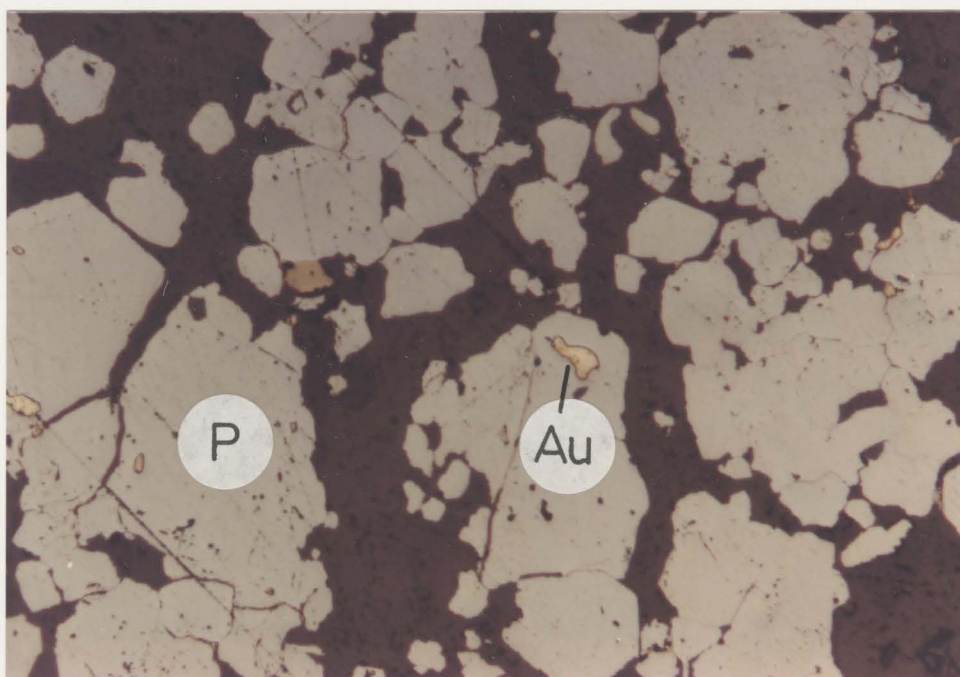
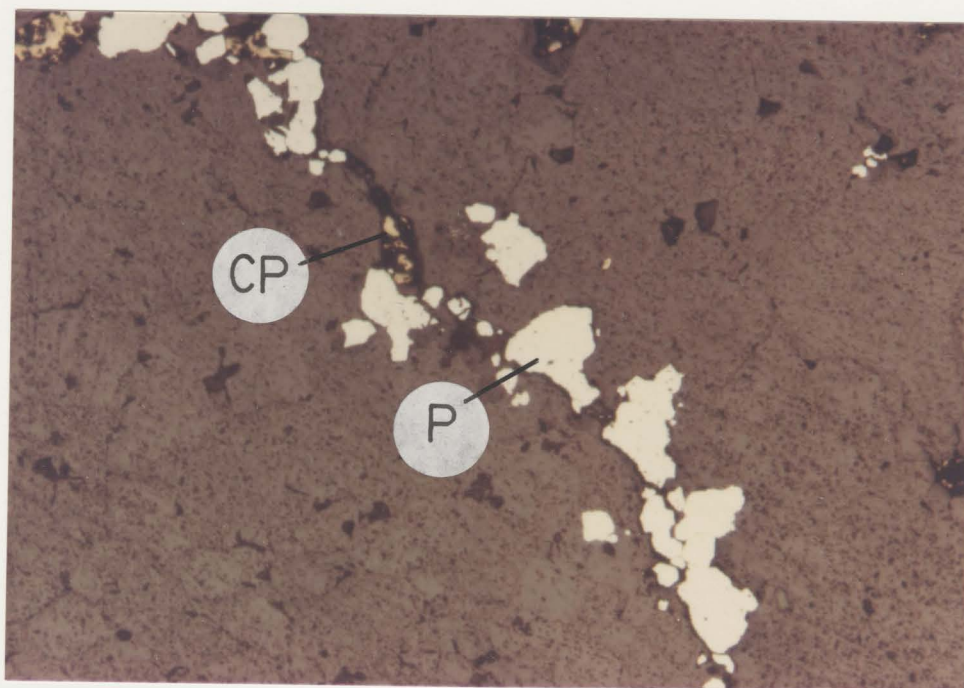
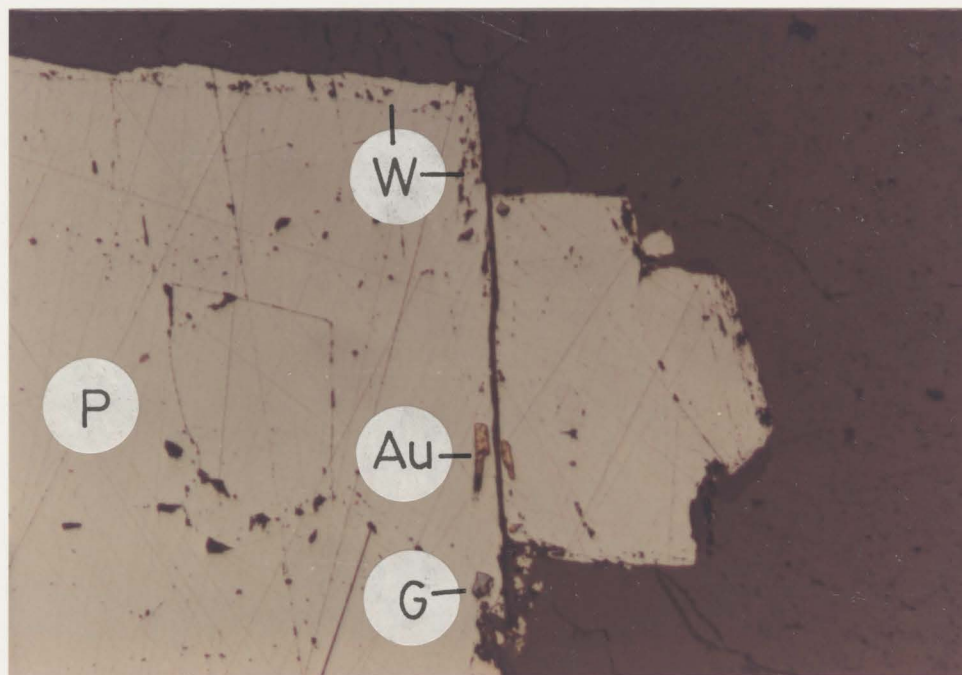


Photo 4-13c: Gold (Au), galena (G) and gangue (W) lie elongate, parallel to the outer margin of a pyrite (P) grain, suggesting that the inclusion minerals coprecipitated with the pyrite during the last (most recent) crystal growth period. (Sample H-42, Hollinger Mine. long axis of photo is 0.37 mm.)



interpretation (Ebbutt, 1948). In other cases, such as the Carshaw/Malga iron formation-hosted gold mineralization, it is difficult to divorce the gold deposition from the sulphidization event, even though some gold exists along grain boundaries between and fractures within pyrite. For this system, perhaps a Bancroft-Jean type sorption model describes the original gold precipitation. Gold could have been later redistributed during subsequent metamorphism and deformation and precipitated onto cataclastically formed pyrite fracture surfaces. This would give the textural impression that a second gold introduction event had occurred when in fact, all that occurred was an internal redistribution of indigenous gold.

Hence, the textural relationships between gold and pyrite could be interpreted in terms of two (or more) events of gold introduction, one of which resulted in the coprecipitation of gold and pyrite. Alternatively, the redistribution of gold originally indigenous to the vein system and adsorption onto pyrite surfaces, could have also produced a gold which was localized along fractures.

Regarding the age of pyrite, its association with fractures cutting coarse quartz (Photo 4-13a), implies that the coarse pyrite post-dated the vein quartz. The temporal relationship between the coarse pyrite and dolomite is less certain although the two minerals coexist in the fracture systems. Finer grained pyrite (<0.5 mm.) occurs in

disrupted zones where quartz appears to have been cataclastically deformed (H-42) or in dolomite-rich zones. No microscopically visible gold, at 400X magnification, was observed in the dolomite-associated pyrite of sample H-46.

A light grey phase having abundant honey yellow internal reflections was tentatively identified as scheelite or leucoxene. The grain size of this phase seldom exceeded 0.02 mm. and was always observed to be hosted by white mica. If this phase is actually scheelite, then it would apparently occupy a late paragenetic position, accompanied by the white mica precipitation.

Pyrrhotite and chalcopyrite are found as: 1) blebby inclusions (0.01 mm.) enclosed in coarse and fine pyrite and not obviously associated with fractures; and 2) irregular grains occurring in fractures within pyrite. Galena was only observed in sample H-42 where it occurred as: 1) inclusions (0.1-0.01 mm.) within coarse grained pyrite, not associated with fractures; and 2) irregular grains localized along fractures in cataclastic pyrite. Gold was observed in contact with one galena inclusion. These textures suggest that pyrrhotite, chalcopyrite, galena and gold were coprecipitated with coarse pyrite, but only in trace amounts.

#### 4.4.2. Paragenetic sequences for other properties

Using the inter- and intramineral textures described in detail for samples from the Hollinger Mine, paragenetic sequences for veins from other properties in the Porcupine Camp were deduced (Table 4-6). Identical paragenetic sequences are deduced for all the quartz veins. This suggests that the evolution in the vein forming fluid, reflected in the sequence of vein mineral precipitation, was experienced by all the observed vein systems regardless of their stratigraphic position or associated gold tenor.

#### 4.4.3. Intramineral textures: implications for stable isotope geothermometry

From the intermineral textures a chronological sequence of syn- and post-vein formation events can be reconstructed. This chronology began with the precipitation and unimpeded growth of the vein phases in favourable structures, presumably initiated and maintained open by hydraulic fluid fracturing. The deduced paragenesis, if correctly interpreted, is significant in that quartz, chlorite, dolomite and white mica appear not to have coprecipitated. This observation has important implications for the application of oxygen isotope geothermometry where temperatures are calculated using the oxygen isotope values of coexisting vein minerals. To obtain precipitation temperatures representative of a crystallization event, the two phases used for the oxygen isotope geothermometry must



TABLE 4-6: Summary paragenetic sequence for silicate, carbonate, and sulphide phases observed in quartz veins present within dolomite alteration zones in the Porcupine Camp.

| Property                     | Quartz | Dolomite | Calcite | White<br>Chlorite | Mica | Tourmal-<br>ine | Albite | Coarse<br>Pyrite | Fine<br>Pyrite | Gold | Cpy | Po(a) | Galena(a) |
|------------------------------|--------|----------|---------|-------------------|------|-----------------|--------|------------------|----------------|------|-----|-------|-----------|
| Aunor-1000 level             | 1      | 2        | -       | 3-4               | -    | 3-4             | -      | -                | -              | -    | -   | -     | -         |
| Canusa                       | 1      | 2        | -       | -                 | 2-3  | -               | -      | -                | -              | -    | -   | -     | -         |
| Carshaw                      | 1      | 2        | -       | 3-4               | 3-4  | -               | -      | >1               | -              | -    | -   | >1    | -         |
| Dobell                       | 1      | 2        | -       | -                 | 3    | -               | -      | -                | -              | -    | -   | -     | -         |
| Duval (McLaren<br>Porcupine) |        |          |         |                   |      |                 |        |                  |                |      |     |       |           |
| glory hole                   | 1      | 2        | -       | -                 | 2-3  | -               | -      | -                | -              | -    | -   | -     | -         |
| south vein                   | 1      | 2        | -       | -                 | 3    | -               | <2-3   | -                | -              | -    | -   | -     | -         |
| Faymar                       | 1      | -        | 2       | 3-4               | 3-4  | -               | -      | >1               | -              | >1   | >1  | >1    | -         |
| Hollinger                    |        |          |         |                   |      |                 |        |                  |                |      |     |       |           |
| #1 vein                      | 1,2    | 3        | -       | -                 | 4    | -               | <1?    | >1               | 3              | -    | -   | >1    | -         |
| 68E vein                     | 1      | 2        | -       | 3?                | 3-4  | -               | -      | >1               | -              | >1   | -   | >1    | -         |
| 65E vein                     | 1      | 2        | -       | 3                 | 4    | -               | -      | -                | -              | -    | -   | -     | -         |
| 218 vein                     | 1,2    | 3        | -       | 4                 | -    | -               | <1?    | >1               | -              | >1   | -   | >1    | >1        |
| 55 vein                      | 1      | 2        | -       | -                 | -    | -               | -      | >1               | -              | -    | -   | >1    | -         |
| Hugh Pam                     | 1      | 2        | -       | -                 | 3-4  | 3-4             | -      | >1               | 3-4            | -    | -   | >1    | -         |
| Porcupine Triumph            | 1      | 2        | -       | 3                 | -    | -               | -      | -                | -              | -    | -   | -     | -         |

Note: -: Indicates that mineral is absent.

Paragenetic Sequence:

1-first; 2-second; 3-third; 4-fourth; 5-fifth

X-X: Coprecipitation possible of the phases indicated, but the relationship is uncertain because phases in question do not exist in mutual contact or one phase is not present in sufficient quantity to establish its temporal relationship to the other phase(s).

>2: Mineral in question postdates the indicated phase.

<3: Mineral in question predates the indicated phase.

a): Mineral occurs as an inclusion in coarse pyrite.

be coeval. If the temperature of the gold precipitation event is sought, then only those phases which were coeval with gold can be used for stable isotope geothermometry. For the systems studied, quartz appears not to have coprecipitated with two or more other minerals. Thus, temperatures calculated using quartz-chlorite-muscovite oxygen isotope geothermometry may not accurately characterize any significant precipitation event. Note also that very small, blebby inclusions of pyrrhotite and chalcopyrite are hosted also within the auriferous pyrite; however, the very small grain size of the pyrrhotite and chalcopyrite inclusions ( $<0.01$  mm.) renders them virtually impossible to separate, and hence, sulphur isotope geothermometry using pyrite, pyrrhotite and chalcopyrite cannot be used to estimate the temperature of pyrite formation.

Thus, on the basis of intermineral textures, it is predicted that quartz, chlorite, dolomite and white mica would be unsuitable for oxygen isotope geothermometry because these phases were not coeval. Any temperatures calculated using mineral triplets found in the quartz veins would be difficult to interpret in terms of a specific precipitation event. Of course, if the oxygen isotope systematics of all previously precipitated phases underwent exchange during the crystallization of a later mineral phase, then geologically meaningful temperatures would be

obtained. This possibility is explored in section 8.1 dealing with the oxygen isotope geochemistry of the vein systems.

There is abundant evidence that the quartz veins have been deformed: 1) polygonal and strained quartz; 2) kinked white mica; 3) deformation twins in albite; 4) healed fractures in quartz and albite defined by linear trains of fluid inclusions. Perhaps coincident with this deformation was the development of pressure solution textures such as stylolitic chlorite and white mica, and sutured grain boundaries between: quartz-quartz, quartz-dolomite and dolomite-dolomite. These observations illustrate that the deformation of the quartz veins was achieved in the presence of a water-rich fluid (Hobbs, 1968). This observation also has certain implications regarding the application of stable isotope geochemistry to the vein system. The presence of an aqueous fluid in the vein system during deformation at least gives rise to the possibility that the oxygen (and hydrogen) isotope systematics of the vein minerals (especially dolomite, chlorite and white mica) could have undergone partial or complete isotope exchange with the pore fluid at the ambient deformation temperature. Such disruption would confuse the interpretation of the oxygen isotope geothermometry.

#### 4.5. Summary of Gold Mineralization Features

The following are considered to be important textural and chronological features of the gold mineralization:

1) gold occurs in quartz veins in a free state or as inclusions in pyrite and in the adjacent wallrock as inclusions in disseminated pyrite;

2) the proportion of vein-hosted to disseminated gold mineralization varies between deposits, but vein associated habits predominate;

3) within quartz vein systems, intermineral textures imply that quartz, dolomite, chlorite and sericite were not coeval;

4) multiple fluid inclusion trains suggest periodic multiple fluid incursions through the vein systems;

5) within the quartz vein systems, gold and pyrite precipitation postdated at least one period of quartz precipitation; in some deposits (55 vein on the Hollinger Mine and Carshaw/Malga veins) gold precipitation post dated the intense carbonatization event;

6) a possible syngenetic component of gold ( $< 2$  ppm) is associated with very fine grained, rounded pyrite ( $< 0.005$  mm.) in carbonaceous sediments on the Hollinger Mine; however, these units generally do not contain commercially exploitable ( $> 3$  ppm) gold tenors unless the carbonaceous sediments have been enriched with a later epigenetic gold

component by deformation and quartz veining.

#### 4.6. Gold/Silver Ratios of the Mineralization

##### 4.6.1. Geological regimes

Within the Tisdale Group, in the Timmins area, five geological regimes can be recognized on the basis of local geology, mineralization habit, and gold/silver ratio of the gold mineralization (Fig. 4-5). In Regime A (Table 4-7), the gold mineralization is localized primarily in iron-rich tholeiitic basalts (Formation V) and is spatially associated with quartz-feldspar porphyry intrusions and carbonaceous interflow sediments. Few ultramafic flow units are present. The gold mineralization is present as a pyritic replacement of carbonatized tholeiitic basalt (55 vein zone, Hollinger Mine), quartz veins, pyritic carbonaceous interflow sediments (68E and 92 vein zones, Hollinger Mine), and the controversial exhalative cherty dolomites found in the Dome Mine. The gold/silver ratio for the mineralization in Regime A averages 5.4 with a standard deviation of 1.2 (Table 4-7).

Regime B contains gold deposits which are hosted within sequences containing mafic and ultramafic komatiites, magnesium-rich tholeiitic basalts, and quartz-feldspar porphyry bodies. The Destor-Porcupine fault passes within 3 kilometers of these deposits which have an average

Figure 4-5: Subdivision of Timmins area into five regimes based on certain characteristics of the gold deposits. Regimes and deposits are as follows:

- Regime A:
  - 1 - Hollinger
  - 2 - McIntyre
  - 3 - Dome
  - 4 - Paymaster Porcupine
  - 5 - Coniaurum
  - 6 - Vipond
  - 7 - Moneta
  - 8 - Consolidated Gilles Lake
- Regime B:
  - 9 - Aunor
  - 10- Fuller
  - 11- Delnite
  - 12- Buffalo Ankerite
  - 13- Kenilworth (Nabob-Hayden)
  - 14- Desantis
- Regime C:
  - 15- Hoyle
  - 16- Pamour #1
  - 17- Hallnor
  - 18- Reef (Bonetal)
  - 19- Broulan Reef
  - 20- Hugh Pam
  - 21- Porcupine Lake
- Regime D:
  - 22- Davidson-Tisdale
  - 23- Faymar
  - 24- Canusa (Banner Porcupine)
- Regime E:
  - 25- Preston East Dome
  - 26- McLaren Porcupine

The surface trace of the Destor-Porcupine Fault (DPF) is illustrated.

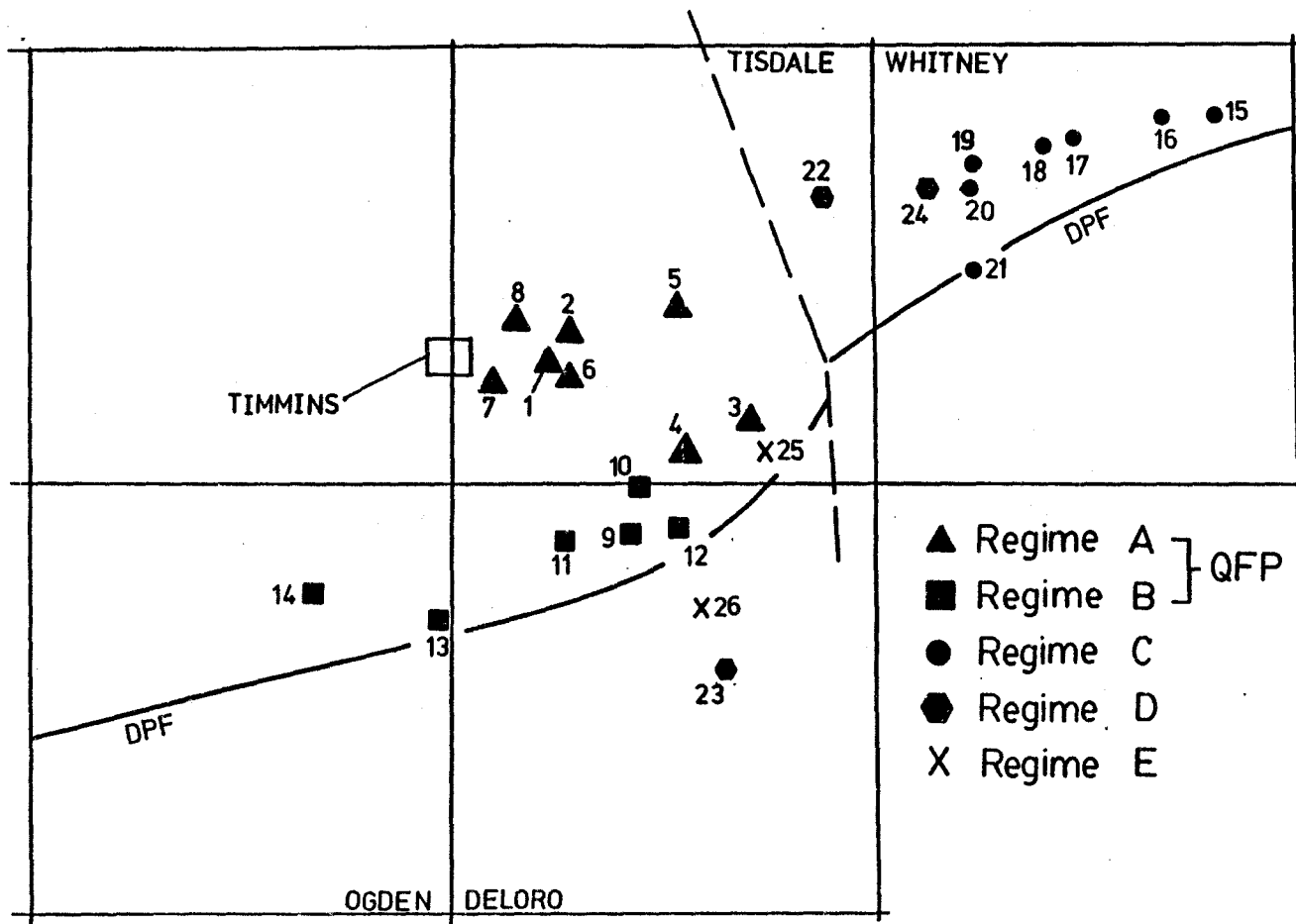


TABLE 4-7: Subdivision of mining properties in the Porcupine Camp according to geological characteristics.

| Regime                   | Mining Property           | Approximate Gold Production (oz x 1E6) | Gold/Silver Ratio     | Gold Grade (oz/ton)     |
|--------------------------|---------------------------|----------------------------------------|-----------------------|-------------------------|
| A                        | Hollinger                 | 20.00                                  | 4.50                  | 0.294                   |
|                          | McIntyre                  | 12.00                                  | 4.00                  | 0.309                   |
|                          | Dome                      | 12.00                                  | 5.60                  | 0.297                   |
|                          | Paymaster Porcupine       | 1.20                                   | 3.60                  | 0.211                   |
|                          | Coniaurum                 | 1.10                                   | 5.60                  | 0.249                   |
|                          | Vipond                    | 0.40                                   | 6.90                  | 0.265                   |
|                          | Moneta                    | 0.15                                   | 6.70                  | 0.474                   |
|                          | Consolidated Gilles       | 0.02                                   | 6.20                  | 0.280                   |
|                          | Total....                 | 46.87                                  | x= 5.40<br>s.d.= 1.2  | x= 0.297<br>s.d.= 0.078 |
| B                        | Aunor                     | 1.90                                   | 13.30                 | 0.334                   |
|                          | Delnite                   | 1.00                                   | 12.50                 | 0.239                   |
|                          | Buffalo Ankerite          | 1.00                                   | 11.90                 | 0.193                   |
|                          | Kenilworth(Naybob)        | 0.05                                   | 9.70                  | 0.167                   |
|                          | Desantis                  | 0.04                                   | 11.40                 | —                       |
|                          | Fuller                    | 0.006                                  | 820.70                | 0.149                   |
|                          | Total....                 | 3.996                                  | x= 11.80<br>s.d.= 1.4 | x= 0.216<br>s.d.= 0.074 |
| C                        | Pamour #1                 | 2.00                                   | 8.20                  | 0.103                   |
|                          | Hallnor                   | 1.47                                   | 13.50                 | 0.394                   |
|                          | Reef(Bonetal)             | 0.50                                   | 12.30                 | 0.146                   |
|                          | Broulan Reef              | 0.36                                   | 9.10                  | 0.213                   |
|                          | Hugh Pam                  | 0.12                                   | —                     | 0.188                   |
|                          | Hoyle                     | 0.08                                   | 10.60                 | 0.099                   |
|                          | Porcupine Lake            | 0.001                                  | 15.90                 | 0.127                   |
|                          | TOTAL....                 | 4.531                                  | x= 11.60<br>s.d.= 2.9 | x= 0.181<br>s.d.= 0.103 |
| D                        | Faymar                    | 0.022                                  | 1.60                  | 0.183                   |
|                          | Davidson-Tisdale          | 0.002                                  | 16.20                 | 0.260                   |
|                          | Canusa                    | 0.001                                  | 5.40                  | 2.127                   |
|                          | Total....                 | 0.025                                  |                       |                         |
| E                        | Preston East Dome         | 1.50                                   | 8.60                  | 0.248                   |
|                          | Duval (McLaren Porcupine) | 0.0002                                 | 5.40                  | 0.229                   |
|                          | Total....                 | 1.5002                                 |                       | x= 0.239<br>s.d.= 0.013 |
| Porcupine Camp Total.... |                           | 56.9209                                |                       |                         |

Notes: 1 troy ounce = 31.10348 grams gold.

x- mean gold/silver ratio; s.d. -standard deviation of mean gold/silver ratios.

Fuller property not included in the gold/silver ratio calculation for regime B.



gold/silver ratio of 11.8 (Table 4-7). The gold mineralization in this regime consists of quartz veins, some tourmaline-rich. In the Desantis and Kenilworth Mines, gold was mined from quartz vein systems in fuchsitic ultramafic zones.

Regime C, located in northern Whitney Townships, is characterized by the absence of quartz-feldspar porphyries, the abundance of mafic and ultramafic komatiitic flows, magnesium-rich tholeiitic basalts (Formation iv), and the presence of clastic sediments which in part, unconformably overlie the volcanic package. Mineralization consists of quartz veins localized in volcanic flows (eg. 51 vein of Pamour #1) and in the clastic sediments (Price and Bray, 1948). The gold/silver ratio for these deposits ranges between 8 and 16 and averages 11.6, similar to that of Regime B.

Included in Regime D are the Davidson-Tisdale, Canusa and Faymar properties, where gold was extracted from quartz veins hosted in basaltic rock. Those veins exposed on the Davidson-Tisdale and Canusa properties cut carbonatized basaltic flows. Felsic intrusions appear to be absent. Chloritization accompanies the quartz veins on the Faymar property. The gold/silver ratios for these properties ranges from 1.6 to 16.3, but because of the very small production, little significance is attributed to these values (Table 4-7).

Regime E includes the Preston East Dome and Duval glory hole deposit where gold was mined from quartz veins which cut quartz-feldspar porphyry intrusions. Their gold/silver ratios are 10 and 5.4 respectively, but again, because of the limited production, these values may not be significant.

The Cu-Mo deposit of the former McIntyre Mine (Pamour Schumacher Property) lies within the Pearl Lake quartz-feldspar porphyry intrusion (Davies and Luhta, 1978) and has a gold/silver ratio of 0.14 (Boyle, 1979).

#### 4.6.2. Metal zoning

A metal zonation is developed in the Porcupine Camp. Located in the centre of the Porcupine camp, Regime A contains Cu-Mo mineralization hosted in the Pearl Lake porphyry. The gold mineralization defines a broad envelope about the Cu-Mo core zone. A systematic change in the Au/Ag ratio appears to reflect a change in the Ag abundance in the mineralized zones. Silver tenor appears to be richest in the centre of the camp, in Regime A, and decreases in those mineralized zones which lie outward, away from this core region.

#### 4.6.3. Factors influencing the gold/silver ratio

It is apparent that the Au/Ag ratio for a cluster of mines within a given regime is relatively constant (Table 4-

7; Regimes A, B, C), even though the types of gold mineralization habits and proportion of associated rock types within a given regime are somewhat variable. Thus, the variation of the gold/silver ratio probably reflects a change in certain parameters of the hydrothermal fluid system from which the gold mineralization precipitated. Furthermore, the systematic change in the Au/Ag ratio appears to result largely from differences in the abundance of silver precipitated, because the average gold grade for all mines in the camp is about 7.7 g/t (0.25 ounces ton) or less (Table 4-7). Thus, any interpretation of the metal zonation data must account for the geological similarities or dissimilarities between the mineralized regimes as well as the absolute metal abundances.

If all the gold mineralization in the Porcupine mining camp formed more or less contemporaneously from consanguineous fluids, then two possibilities exist to explain the observed metal zoning:

- 1) the metal zoning is the result of interaction between hydrothermal fluids and rocks of different bulk composition in such a way that the precipitation of silver was enhanced by interaction with certain rock types;

- 2) the metal zoning reflects the thermal evolution of a magmatic hydrothermal system, the locus of which was centered on the Pearl Lake porphyry intrusive complex.

#### 4.6.3.1. Bulk rock composition

Some evidence suggests that the metal zoning may reflect the influence of rock type. There is an apparent dependence between the Au/Ag ratios of a group of deposits from a given regime and the bulk composition of the country rock, an observation also noted by Boyle (1979). Those deposits associated with magnesium-rich units (Regimes B and C) have high Au/Ag ratios (11-12) whereas deposits hosted in less magnesian basaltic sequences have Au/Ag ratios closer to 5 (Table 4-7). The very low Au/Ag ratio of the Cu-Mo deposit (0.14), hosted entirely within a quartz-feldspar porphyry intrusion, is consistent with the trend of decreasing Au/Ag ratio with increasing  $\text{SiO}_2/[\text{FeO} + \text{MgO} + \text{CaO}]$  of the country rock. However, because the temporal relationship between the Cu-Mo and spatially associated gold mineralization is not clear, inclusion of the Au/Ag ratio for the Cu-Mo deposit must be done cautiously.

The observation that the mineralization in the Porcupine Camp is richer in gold with respect to silver where associated with volcanic sequences containing abundant ultramafic flows, also applies to gold mineralization within the Larder Lake and Kirkland Lake fault zones (Table 4-8). In these two areas, that mineralization which is localized within volcanic sequences dominated by abundant ultramafic flows (eg. Kerr Addison and Chersterville Mines; Larder Lake Break) has the highest Au/Ag ratio (18). Conversely, that

Table 4-8: Gold and silver production figures for mines within and near the Timiskaming Group Rocks of the Kirkland Lake and Larder Lake areas.

| Mine              | Gold<br>(ounces) | Silver<br>(ounces) | Gold<br>Grade<br>(oz/ton) | Gold<br>Silver<br>Ratio | Notes |
|-------------------|------------------|--------------------|---------------------------|-------------------------|-------|
| Macassa           | 2354843          | 385458             | .44                       | 6.11                    | 1     |
| Kirkland Lake     | 1172955          | 130579             | .37                       | 8.98                    | 1     |
| Teck-Hughes       | 3688664          | 501657             | .38                       | 7.35                    | 1     |
| Lake Shore        | 8499199          | 1955132            | .51                       | 4.35                    | 1     |
| Wright-Hargreaves | 4817680          | 853643             | .49                       | 5.64                    | 1     |
| Sylvanite         | 1667520          | 337956             | .33                       | 4.93                    | 1     |
| Toburn            | 570659           | 135238             | .48                       | 4.22                    | 1     |
| Bidgood           | 160184           | 72468              | .27                       | 2.21                    | 4     |
| Moffatt-Hall      | 4768             | 1149               | .29                       | 4.15                    | 4     |
| Morris Kirkland   | 16681            | 29754              | .13                       | 0.56                    | 4     |
| Upper Canada      | 1398291          | 589696             | .30                       | 2.37                    | 4     |
| Upper Beaver      | 140709           | 59167              | .24                       | 2.38                    | 4     |
| Omega             | 214098           | 29290              | .13                       | 7.31                    | 2     |
| Chesterville      | 358615           | 19371              | .11                       | 18.51                   | 3     |
| Kerr Addison      | 9652173          | 531561             | .28                       | 18.16                   | 3     |

Notes: 1:Localized adjacent to the Kirkland Lake Break; no ultramafic rock present.

2:Localized along the Larder Lake Break, but lacks ultramafic rocks.

3:Localized along the Larder Lake Break, accompanied by abundant ultramafic rock.

4:Not associated with ultramafic rock.

Compilation by Gordon et al(1979).

mineralization which is spatially associated with syenitic intrusives or Temiskaming Group sediments and alkaline extrusive flows has a lower gold/silver ratio ( $\text{Au/Ag} < 8$ ).

Thus, it appears that interaction between an auriferous,  $\text{CO}_2$ -bearing hydrothermal fluid and ultramafic rock may influence the type and abundance of metals precipitated.

#### 4.6.3.2. Magmatic centre

The evidence linking the metal zoning to a magmatic system is circumstantial. The observed metal zonation in the Porcupine camp is Mo-Cu/Cu-Mo-Au-Ag/Au-Ag. This zoned sequence is developed outward from the Pearl Lake intrusive. Such a metal zonation is also typical of Tertiary epithermal precious metal hydrothermal systems centred on granitoid intrusives, where the silver tenor of the precipitated mineralization increases with depth within a mineralized system, in response to increased temperature of the hydrothermal system (eg. Forsythe, 1971). In the Porcupine camp, the highest silver/gold ratios (corresponding to the lowest gold/silver ratios) are characteristic of the mineralization which occurs in Regime A, where quartz-feldspar porphyry intrusive bodies are most abundant, ultramafic rock is not abundant, and carbonaceous sedimentary rock is present in minor, but persistent amounts. It is now well established that the quartz-

feldspar porphyry bodies (having an age of 2685  $\pm$  3 m.y.), which are so voluminous in the area of the former McIntyre and Hollinger Mines, were intruded much later than the youngest extrusive felsic volcanic rock (age of 2702  $\pm$  2 m.y.) at the top of the Tisdale Group (see Section 1.5). Clearly, the abundance of porphyry intrusives in this area identifies it as a major intrusive centre within the Porcupine Camp.

If the tremendous volume of gold produced from that same, small geographical area (better than 80% of the total gold that has been produced from the Porcupine Camp came from the Hollinger-McIntyre and Dome Mine areas) is considered in conjunction with the evidence that a magmatic centre existed in the Hollinger-McIntyre and Dome Mine areas, then it is reasonable to suggest that the localization of the gold mineralization in this area was related in some way to a magmatic process. In this regard, the Cu-Mo mineralization which occurs almost entirely within the Pearl Lake porphyry is interpreted to represent Archean porphyry copper-type mineralization (Davies and Luhta, 1978) and appears to represent the centre or locus of the Cu-Mo and Au-Ag hydrothermal system.

Thus, the observed metal zonation in the Porcupine Camp could reflect the evolution of a magmatic hydrothermal system as well as the influence of rock bulk composition. At present both possibilities, acting singly or

collectively, appear equally plausible, although thermal evolution of a magmatic-hydrothermal system is favoured. Further evaluation of these two possibilities is attempted in Chapter 9 when the stable isotopic data are considered.



## 5. Characterization and Evolution of the Hydrothermal Fluid Responsible For The Carbonatization

In this Chapter, the chemical characteristics and evolution of the hydrothermal fluid responsible for the carbonate alteration will be addressed using recently published fluid inclusion data and the mineralogy of the wallrock alteration assemblages. Because good experimental data exist to describe the ultramafic rock system, the alteration assemblages that developed in rocks of ultramafic composition are used to constrain certain of the fluid characteristics. These characteristics are then extrapolated to the basaltic rock system. The fluid inclusion data are examined first to establish broad constraints on the fluid composition.

### 5.1. Fluid Inclusion Constraints

Characterization of an hydrothermal fluid can also be accomplished in part through fluid inclusion studies, although relatively few such studies of Archean gold deposits exist. Roedder (1984) provides a summary of data for many different types of gold deposits of different ages. Foster (1980) provides a review of data for Archean deposits and Groves et al. (1984) tabulate data for deposits in Western Australia. Description of fluid inclusions in

Canadian lode gold deposits include Krupka et al. (1977; O'Brien Mine, Quebec), Kerrich and Fryer (1979; Dome Mine); Guha et al. (1982; Mine Doyon, Quebec), Smith et al. (1984; McIntyre-Hollinger Mines), Smith and Kesler (1985; Hollinger-McIntyre Mines, Timmins), Walsh et al. (1984; Timmins area), Wood et al. (1984; Timmins area) and Lakind (1984; Wilmar Mine and Red Lake area). Safonov et al. (1980) describe the fluid inclusion characteristics of gold mineralization in the Kolar gold field. Summarized in Table 5-1 are the fluid inclusion characteristics described in some of these studies.

Table 5-1 shows that fluid inclusions in vein quartz from Archean gold deposits are dominantly H<sub>2</sub>O, but can contain up to 70 mole % CO<sub>2</sub>. The salinity of the hydrothermal fluid was low, typically less than 3 wt.% NaCl equivalent.

Filling temperatures vary widely from 200° to 500°C, although the actual trapping temperature could have been slightly higher due to pressure corrections. Smith et al. (1984) report fluid densities of between 0.5 and 0.8 gram/cubic centimetre (g/cc) for CO<sub>2</sub> trapped in inclusions during the precipitation of gold in the McIntyre-Hollinger vein systems. Considering the filling temperatures reported for the Hollinger-McIntyre inclusions (Table 5-1), this CO<sub>2</sub> density translates to a trapping depth of 1.5 to 6 kilometre (0.5 to 2 kb.).

TABLE 5-1: Characterization of fluid inclusions from gold-quartz veins of Archean age.

| MINE (AREA)                         | INCLUSION<br>TYPE                                        | HOMOGENIZATION<br>TEMPERATURE<br>(CELCIUS) | TEMPORAL<br>RELATIONSHIP<br>TO GOLD | BOILING | SALINITY<br>WT. %<br>NaCl eq. | MOLE<br>%<br>CO <sub>2</sub> | DENSITY<br>CO <sub>2</sub><br>(g/cc) | REFERENCE                    |
|-------------------------------------|----------------------------------------------------------|--------------------------------------------|-------------------------------------|---------|-------------------------------|------------------------------|--------------------------------------|------------------------------|
|                                     |                                                          |                                            |                                     |         |                               |                              |                                      |                              |
| O'Brien<br>(Quebec)                 | G+LCO <sub>2</sub> +LH <sub>2</sub> O                    | 250-420                                    | Pre                                 | No      | High                          | High                         | —                                    | Krupka                       |
|                                     | G+LH <sub>2</sub> O                                      | 300-380                                    | Syn                                 | Yes     | Low                           | Low                          | —                                    | et al.                       |
|                                     | G+LH <sub>2</sub> O                                      | 170-330                                    | Post                                | No      | High                          | Low                          | —                                    | 1977                         |
|                                     | G+LH <sub>2</sub> O+SALT                                 | 140-270                                    | Post                                | No      | High                          | Low                          | —                                    |                              |
| Mine Doyon<br>(Quebec)              | LH <sub>2</sub> O+LCO <sub>2</sub> +GC0 <sub>2</sub>     | >500                                       | ?                                   | No      | Low                           | 10                           | —                                    | Guha                         |
|                                     | LH <sub>2</sub> O+LCO <sub>2</sub> +GC0 <sub>2</sub>     | 290-410                                    | Early Au                            | No      | Low                           | 30                           | —                                    | et al.                       |
|                                     | LH <sub>2</sub> O+LCO <sub>2</sub>                       | 310                                        | Peak Au?                            | No      | Low                           | 70                           | —                                    | 1982                         |
|                                     | LH <sub>2</sub> O+LCO <sub>2</sub>                       | —                                          | ?                                   | No      | ?                             | 95                           | —                                    |                              |
| Dome<br>(Timmins)                   | Not<br>Specified                                         | 330-370                                    | ?                                   | No      | <3                            | ?                            | —                                    | Kerrick<br>and Fryer<br>1979 |
| McIntyre-<br>Hollinger<br>(Timmins) | LCO <sub>2</sub> +LH <sub>2</sub> O+GC0 <sub>2</sub>     | 160-385                                    | Syn                                 | No      | <2                            | 3- 24                        | 0.5-0.8                              | Smith                        |
|                                     | LH <sub>2</sub> O+G                                      | 160-385                                    | Some syn                            | No      | 0-20                          | 0                            | —                                    | et al.                       |
|                                     | LH <sub>2</sub> O+LCO <sub>2</sub> +LCH <sub>4</sub> (1) | —                                          | Syn?                                | No      | 0                             | <74                          | —                                    | 1984                         |
|                                     | LCH <sub>4</sub> (1)                                     | —                                          | Post                                | No      | 0                             | 0                            | 0.3                                  |                              |
| Timmins<br>Area                     | Not<br>Specified                                         | 200-400                                    | —                                   | No      | 1.5-3.5                       | <15                          | —                                    | Walsh<br>et al.<br>1984      |
| Kolar Gold<br>Field<br>(India)      | L+G                                                      | 130-150                                    | ?                                   | No      | Low                           | ?                            | —                                    | Safonov                      |
|                                     | SALT+G+LH <sub>2</sub> O                                 | 260-280                                    | ?                                   | No      | >26                           | ?                            | —                                    | et al.                       |
|                                     | LCO <sub>2</sub> +LH <sub>2</sub> O                      | 270-305                                    | Syn                                 | No      | ?                             | ?                            | —                                    | 1980                         |

Note 1: Vein hosted in carbonaceous sediment-Smith et al. (1984).

—: Indicates information not given in reference.

?: Indicates that data was not given in the reference or the information was not clear.

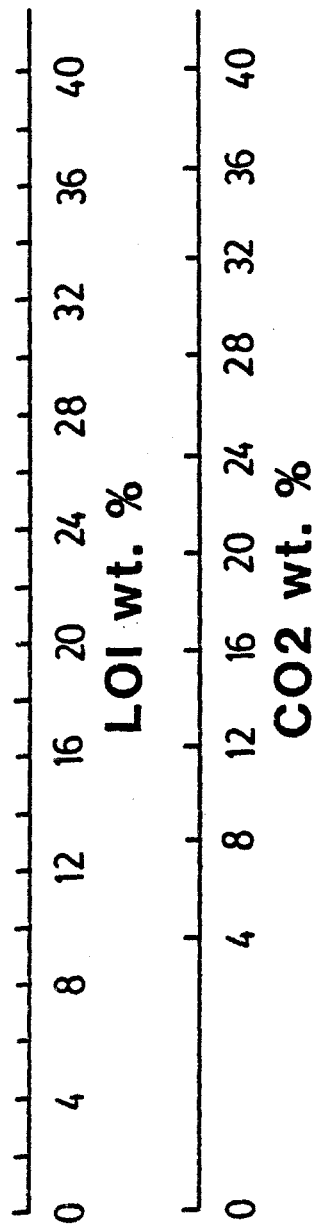
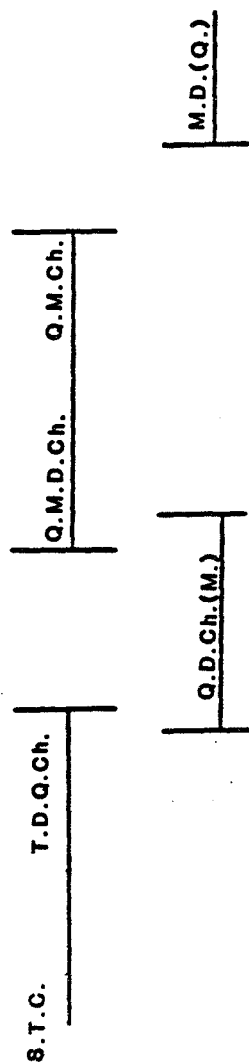
In the Hollinger-McIntyre mineralized system, methane-rich fluid inclusions occur rarely in quartz veins which are proximal to or cut carbonaceous sediments (Smith et al., 1984 and Smith and Kesler, 1985; further discussion in Chapter 7 and 9).

## 5.2. Constraints On The Fluid System Deduced From Altered Ultramafic Rock

Systematic mineralogical changes characterize the sequence of alteration assemblages which are representative of the most and least altered rock (Chapter 2, Fig. 2-2). The chemistry of the wallrock alteration assemblages (hydrous and carbonate-rich) indicate that the hydrothermal fluid can be modelled by the system  $\text{CO}_2\text{-H}_2\text{O}$ , as indicated by the fluid inclusion data. The sequential development of the alteration assemblages away from a vein or other fluid conduit may be related either to changes in the conditions under which rock alteration took place (eg. intensive parameters such as temperature (T), oxygen fugacity of the fluid ( $f\text{O}_2$ ), or hydrogen ion concentration (pH)) or to changes in the fluid composition ( $\text{CO}_2/\text{H}_2\text{O}$  molar ratio).

The secondary mineral assemblages observed in ultramafic flows are depicted in Figure 5-1, where an estimate of alteration intensity for each sample is represented by the corresponding total volatile (LOI) and  $\text{CO}_2$  abundances. This diagram is a convenient way to

Figure 5-1: Alteration assemblages in altered ultramafic flows, expressed as a function of whole rock loss on ignition (LOI wt. %) and corresponding CO<sub>2</sub> abundance (CO<sub>2</sub> wt. %). Symbols are as follows: T-talc; S-serpentine; C-calcite; D-dolomite; Q-quartz; Ch-chlorite; M-magnesite.



illustrate how the secondary assemblages change with increasing alteration intensity, as measured by either LOI or CO<sub>2</sub> abundance in the whole rock.

The change in some of the fluid parameters resulting from interaction between a CO<sub>2</sub>-bearing, aqueous hydrothermal fluid and ultramafic rock can be described qualitatively using the models of Eckstrand (1975) and Johannes (1969). The deduced chemical evolution of the hydrothermal fluid as it reacts progressively with a substrate having an ultramafic composition is summarized in Figure 5-2.

#### 5.2.1. pH

White mica coexists with ferroan dolomite in the Intensely Carbonatized Alteration Facies. The appearance of the white mica in this alteration assemblage coincides with a marked increase in the whole rock abundances of potassium, lithium and rubidium over that which typifies fresh ultramafic rock (Fyon, 1980; Davies et al., 1982; Fyon and Crocket, 1982). This indicates that the white mica is a potassium mica (sericite) and not pyrophyllite. Further, the stabilization of a potassium mica in the carbonate-rich alteration assemblages indicates that potassium was present in the hydrothermal fluid and was added to the rock while the ferroan dolomite and/or magnesite were precipitated. Thus, the pH of the hydrothermal fluid can be constrained using the experimentally deduced sericite-potassium

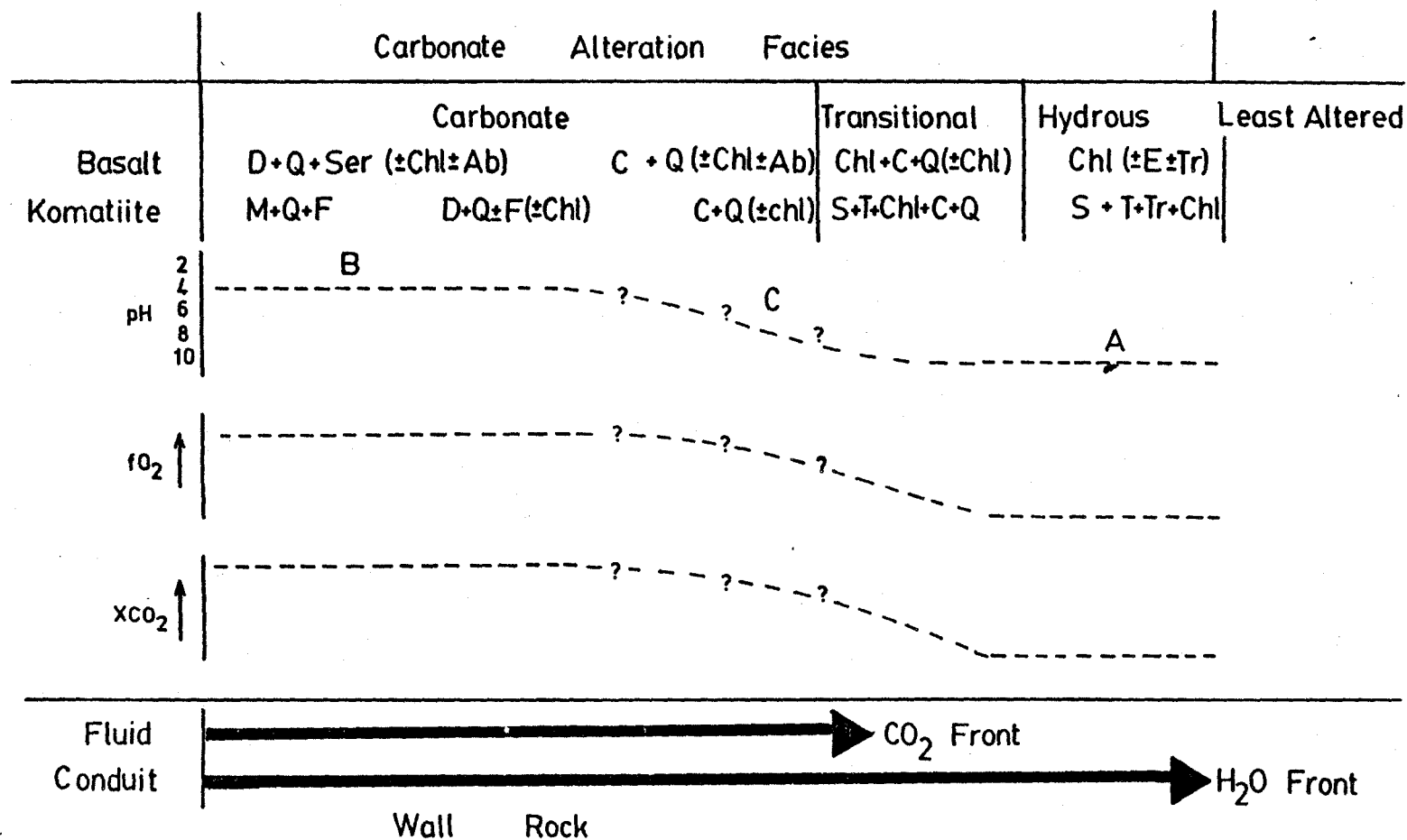
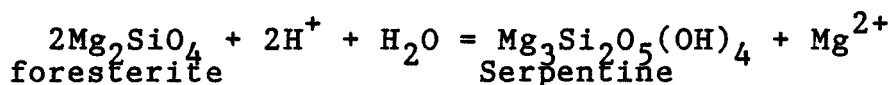


Figure 5-2: Reconstruction of the fluid evolution as it passes outward from a conduit and reacts with the adjacent wallrock. The model is based on CO<sub>2</sub>-H<sub>2</sub>O fluid reactions with ultramafic rock.



feldspar- aluminosilicate stability relationships (Hemley and Jones, 1964). That sericite and not potassium feldspar or an alumino-silicate is stable in the intensely carbonatized rock indicates that solution pH was 4 to 6 (region B, Fig. 5-2).

Unlike the conditions which prevailed during the intense carbonatization of the ultramafic rock, reactions which produced the Hydrous Alteration Facies, such as incipient serpentinization, buffered the hydrogen ion concentration in the fluid at low concentrations, producing relatively basic fluids (zone A, Fig. 5-2):

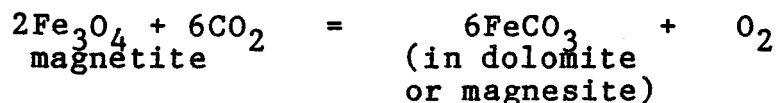


A pH gradient must have existed in the fluid-rock system between that rock domain where the potassium-bearing white mica and ferroan dolomite and/or magnesite were precipitated (Intense Carbonate Alteration Facies) and the domain where hydration minerals precipitated (Hydrous Alteration Facies).

#### 5.2.2. $f\text{O}_2$

Based on sulphide-oxide mineral stability assemblages in hydrated and carbonatized ultramafic rock, Eckstrand (1975) demonstrated that  $f\text{O}_2$  changed across the alteration facies boundaries. More oxidizing conditions were associated with the carbonate-bearing assemblage

because of oxygen-producing reactions of the type:



This reaction describes virtually all of the ferroan dolomite-bearing alteration assemblages in ultramafic rock of the Tisdale Group where magnetite is destroyed during progressive carbonatization. Hematite is stable in the Intense Carbonate Alteration Facies in some magnesite-rich ultramafic dykes which cut Deloro Group rock south of Timmins (Griffis, 1972). The presence of this secondary hematite again suggests that the fluid-rock interaction which produced the ferroan dolomite- and magnesite-bearing alteration assemblages (Intense Carbonate Alteration Facies), took place under relatively oxidizing conditions. It is probable that the hydration reactions of the Hydrous Alteration Facies took place at a relatively lower  $f\text{O}_2$  because oxygen was consumed while ferrous iron in olivine was partially oxidized and stabilized as magnetite:



This type of reaction lowers the  $f\text{O}_2$  in the aqueous phase and can liberate  $\text{H}_2$ , known to issue from some ultramafic bodies which are undergoing incipient serpentinization (Thayer, 1966). The liberated  $\text{H}_2$  assures that the incipient hydration reactions took place under relatively reducing conditions. Again, an  $f\text{O}_2$  gradient must have existed

between the Intense Carbonate Alteration Facies and the Hydrous Alteration Facies.

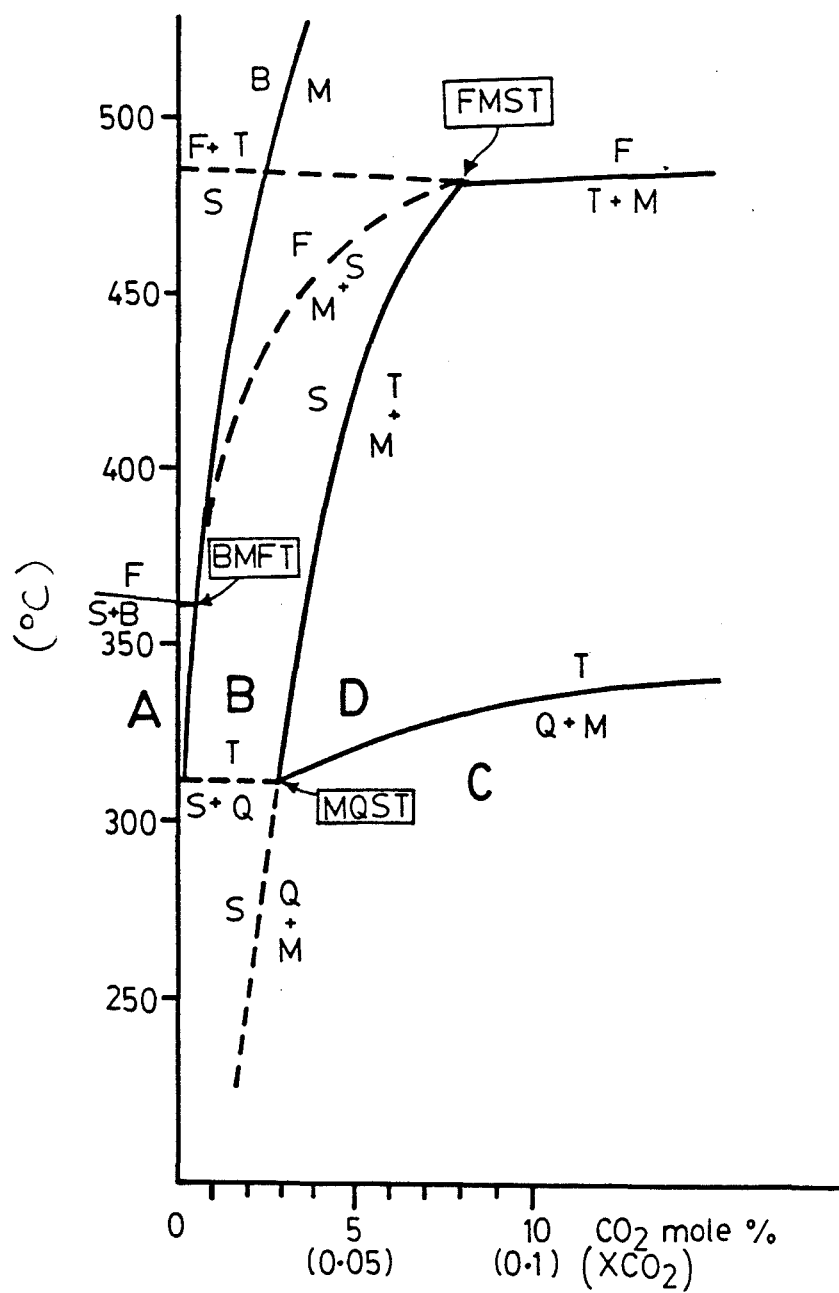
### 5.2.3. Reaction temperature and $\text{CO}_2/\text{H}_2\text{O}$ molar ratio of the hydrothermal fluid

The development of alteration assemblages in ultramafic rocks has been modelled experimentally using the  $\text{MgO-SiO}_2\text{-CO}_2\text{-H}_2\text{O}$  system (Johannes, 1969), making it possible to locate a particular alteration assemblage in an appropriate  $\text{T-XCO}_2$  space (Fig. 5-3). Note that this part of the  $\text{MgO-SiO}_2\text{-CO}_2\text{-H}_2\text{O}$  system is constructed for a total fluid pressure of 1 Kb.

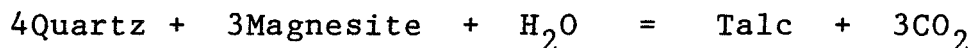
Least altered ultramafic rock consists dominantly of serpentine with minor talc (Fig. 5-1). The presence of talc indicates a minimum reaction temperature of about  $300^\circ\text{C}$  (Fig. 5-3). The presence of serpentine in this assemblage indicates that the fluid contained very little  $\text{CO}_2$  ( $\text{XCO}_2 < 0.02$ ). Thus, field A (Fig. 5-3) broadly defines the  $\text{T-XCO}_2$  space for the talc-serpentine assemblage. With increasing degree of alteration, talc is observed to coexist with quartz and dolomite and minor serpentine (Fig. 5-1). Field B (Fig. 5-3) broadly defines the  $\text{T-XCO}_2$  space for this assemblage.

Assemblages typical of more intensely carbonatized rock consist of quartz and dolomite or magnesite with no talc or serpentine (Fig. 5-1). The  $\text{T-XCO}_2$  space for this assemblage lies on the lower temperature side of the

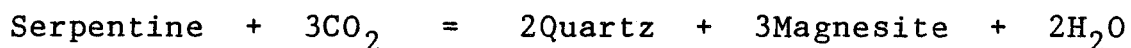
Figure 5-3: Part of the experimentally derived T-XCO<sub>2</sub> diagram for the system MgO-SiO<sub>2</sub>-CO<sub>2</sub> at total fluid pressure of 1Kb is by Johannes (1969). The mineral abbreviations are: T-talc; Q-quartz; M-magnesite; S-serpentine; B-brucite; F-foresterite. The fields A,B,D,C correspond to the domains occupied by the Least Altered, Hydrous, Transitional and Intensely Carbonatized alteration facies developed in ultramafic rock from the Porcupine Camp.



reaction:



but to the higher  $\text{XCO}_2$  side of the reaction:



as illustrated on Figure 5-3. To stabilize this assemblage the  $\text{XCO}_2$  of the ambient hydrothermal fluid had to have exceeded 0.03 or 3 mole %  $\text{CO}_2$  (field C, Fig. 5-3). Some samples contain coexisting quartz, talc, dolomite (or magnesite) and chlorite, some of which could be serpentine (Fig. 5-1). This suggests that the T- $\text{XCO}_2$  conditions of the invariant point MQST (Fig. 5-3) were approximated during the progressive reaction which produced the quartz-magnesite assemblages from the talc-bearing precursors. This suggests that reaction temperatures did not depart greatly from the 300° to 350° range. Thus, an  $\text{XCO}_2$  gradient must exist across the Transitional Alteration Facies. This is what is observed empirically in the altered ultramafic rock, where the modal proportion of carbonate decreases across the Transitional Alteration Facies illustrating that the  $\text{XCO}_2$  in the fluid decreased correspondingly.

#### 5.2.4. Summary of fluid parameter variations deduced from altered ultramafic rock and fluid inclusions

This quantitative analysis indicates that the  $\text{XCO}_2$  of the hydrothermal fluid was buffered to very low levels

(< 0.005) during the development of the Hydrous Alteration Facies. The quartz-ferroan dolomite and/or magnesite coexisted in the Intense Carbonate Alteration Facies implies that the  $X_{CO_2}$  of the hydrothermal fluid exceeded 0.03 during the intense carbonatization of the ultramafic rock. This represents a minimum estimate of the  $CO_2$  mole fraction in the hydrothermal fluid because no additional buffer reactions exist to further constrain its value. As suggested by the fluid inclusion data, the  $X_{CO_2}$  of the fluid was probably greater than this minimum value. The fluid inclusion studies show that the  $X_{CO_2}$  of the hydrothermal fluid ranged up to 0.7 for those fluids interpreted to be responsible for the wallrock alteration (Table 5-1: Smith et al., 1984). Using this value as the maximum  $X_{CO_2}$  for the hydrothermal fluid, the maximum temperature at which the Intense Carbonate Alteration assemblages could have developed was 450°C or less (Fig.5-4), assuming that the experimental description of the  $MgO-SiO_2-CO_2-H_2O$  system carried out at 2Kb fluid pressure by Johannes (1969) represents a reasonable pressure maximum for the the quartz-ferroan dolomite (or magnesite) alteration assemblage being considered. A lower total fluid pressure would require a correspondingly lower maximum carbonatization temperature.

### 5.3. Application of Model to Basalt System

Using the experimental (Johannes, 1969) and

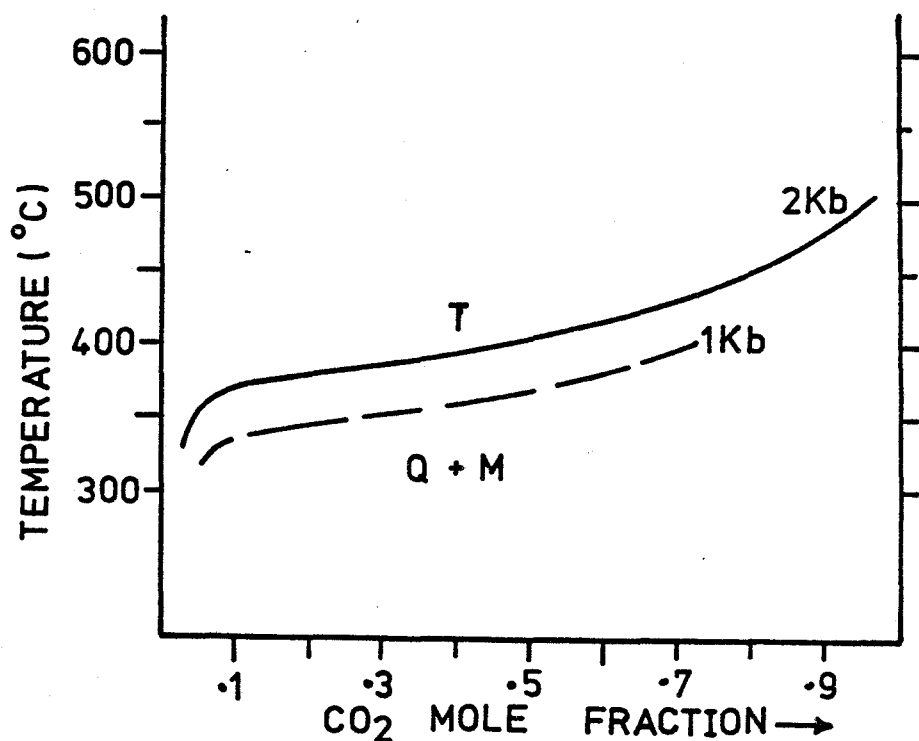


Figure 5-4: Isobaric equilibrium curves for 1 Talc + 3CO<sub>2</sub> = 4 Quartz + 3 Magnesite + 1 H<sub>2</sub>O in the T-XCO<sub>2</sub> field at Pressure (total fluid) = 1 and 2 Kb by Johannes (1969). Using the maximum CO<sub>2</sub> abundance in the hydrothermal fluid of 70 mole % (Smith and Kesler, 1974) as an upper limit on the constitution of the hydrothermal fluid, then the carbonatization can be inferred to have taken place at 450°C (2Kb) or 375°C (1Kb).



empirical qualitative (Eckstrand, 1975) models, a  $\text{CO}_2\text{-H}_2$  fluid-ultramafic rock reaction sequence can be described.

Application of the devised model, based on an ultramafic rock composition, to the basalt compositional system is somewhat more complicated because additional components, such as  $\text{CaO}$  and  $\text{Al}_2\text{O}_3$  are present and the secondary ferromagnesium silicate minerals in the alteration assemblages lack ferric iron. It can be presumed that the pH and  $f\text{O}_2$  gradients, inferred to exist across the Transitional Alteration Facies in ultramafic rock, may also exist across equivalent zones developed in basaltic rock. However, because of the different mineralogy in the basaltic flows (notably the absence of olivine), the magnitude of these gradients would have been somewhat less.

#### 5.4. Miscible or Immiscible Hydrothermal Fluid

It is of some relevance to consider if the hydrothermal fluid was supercritical and miscible or if the fluid underwent effervescence to yield separate  $\text{CO}_2$  and  $\text{H}_2\text{O}$ -rich fluids, because the state of the fluid has a direct bearing on the interpretation of stable isotopic data. The pure  $\text{CO}_2\text{-H}_2\text{O}$  solvus has been determined experimentally by Takenouchi and Kennedy (1964); however, the effect of  $\text{NaCl}$  on the  $\text{CO}_2\text{-H}_2\text{O}$  solvus must be considered as the hydrothermal fluids in question contained in general up to 3 wt.%  $\text{NaCl}$  equivalent (Table 5-1). The effect of dissolved salts on

the  $\text{CO}_2\text{-H}_2\text{O}$  solvus are not completely known. Takenouchi and Kennedy (1965) have shown that addition of NaCl to the  $\text{H}_2\text{O-CO}_2$  system expands the  $\text{H}_2\text{O}$ -rich side of the solvus.

Hollister and Burruss (1976) suggest that for a  $\text{CO}_2\text{-H}_2\text{O}$  system with 6 wt.% NaCl at 1 Kb (3km depth), the top of the solvus may be increased by at least  $75^\circ\text{C}$  (Fig 5-5). Because the hydrothermal fluids under consideration are thought to have contained less than 3 wt.% NaCl equivalent (Table 5-1), the effects of salt on the  $\text{H}_2\text{O-CO}_2$  consolute curve can be approximated by the empirical solvus established by Hendel and Hollister (1981; Fig. 5-5) and by composite T-X diagrams presented by Bowers and Helgeson (1983). It is apparent that at the P-T regime thought to be representative of wallrock reaction and vein formation ( $P=0.5\text{-}2\text{Kb}$ ;  $T=350\text{-}450^\circ\text{C}$ ) in the Timmins area, the  $\text{CO}_2\text{-H}_2\text{O}$  hydrothermal fluid would have been supercritical and miscible at the high temperature end ( $>340^\circ\text{C}$ ) or immiscible if the fluid temperature dropped below  $340^\circ\text{C}$  (Fig. 5-5).

Smith et al. (1984) reported that no fluid inclusion evidence was found for the trapping of immiscible  $\text{CO}_2\text{-}$  and  $\text{H}_2\text{O}$ -rich fluids in quartz vein samples collected from the McIntyre-Hollinger deposit. However, some oxygen isotopic evidence suggesting that the hydrothermal fluid did separate into  $\text{CO}_2\text{-}$  and  $\text{H}_2\text{O}$ -rich fractions in the Hollinger-McIntyre mineralized system will be presented in Section 8.3.2.

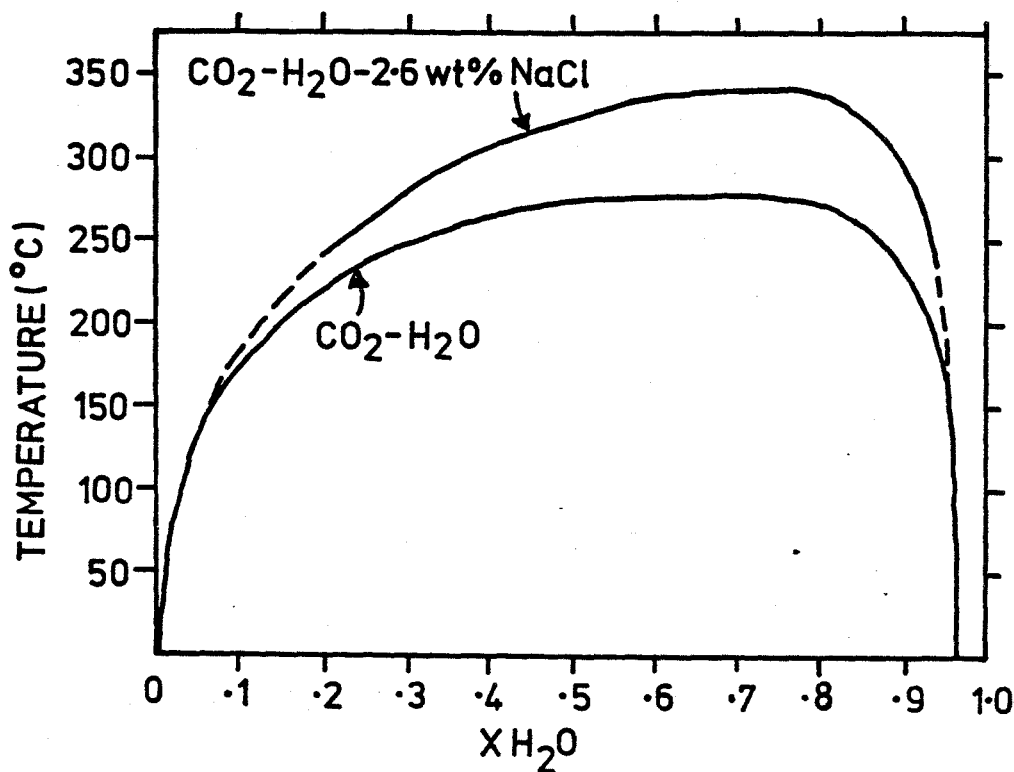


Figure 5-5: Empirical solvus for CO<sub>2</sub>-H<sub>2</sub>O with 2.6 wt.% NaCl equivalent in the aqueous phase at room temperature. This solvus is a good approximation for the hydrothermal fluid system thought to have been responsible for the carbonatization of the volcanic rocks in the Timmins area. The solvus for pure CO<sub>2</sub>-H<sub>2</sub>O of Todheide and Franck (1963) at 1 Kb is shown for comparison. Data from Hendel and Hollister (1981).

#### 5.4.1. Implications for carbon and oxygen stable isotopic studies

The super- or subcritical nature of a hydrothermal fluid has some influence on its stable isotopic characteristics. Consideration of the carbon isotopic characteristics of supercritical  $\text{CO}_2$ -rich fluids is generally straight forward. The carbon exists as  $\text{CO}_2$  under relatively oxidizing conditions or  $\text{CH}_4$  under relatively reducing conditions, and aqueous salts are highly associated. Conversely, under a subcritical regime, liquid-vapour equilibria are common and aqueous salts are highly ionized. Carbon may exist as  $\text{H}_2\text{CO}_3$ ,  $\text{HCO}_3^-$  or  $\text{CO}_3^{2-}$  under relatively oxidizing conditions, dependent on pH, or  $\text{CH}_4$  under relatively reducing conditions (Ohmoto, 1972). Thus, in general, the interpretation of the carbon isotope systematics of a system evolving in a supercritical regime is somewhat less complicated than that of a subcritical regime.

The oxygen isotope systematics of a  $\text{CO}_2$ - $\text{H}_2\text{O}$  system are inherently more complex than a pure  $\text{H}_2\text{O}$ -dominant fluid because oxygen resides in both the  $\text{CO}_2$  and  $\text{H}_2\text{O}$  molecules. Under equilibrium conditions in a miscible hydrothermal fluid, oxygen is partitioned between the  $\text{CO}_2$ ,  $\text{H}_2\text{O}$  and precipitating mineral phase. If fluid immiscibility takes place, and one of the fluid phases ( $\text{CO}_2$  or  $\text{H}_2\text{O}$ ) separates from the fluid, then the oxygen isotopes would be partitioned between the  $\text{CO}_2$ -rich and  $\text{H}_2\text{O}$ -rich fractions.

Such a separation is not likely to be immediate and complete, but rather gradual in response to gradually decreasing pressure and/or temperature. Under these conditions, the partitioning of oxygen isotopes would follow a Rayleigh fractionation process (c.f. Higgins and Kerrich, 1982).

Thus, if the a supercritical  $\text{CO}_2\text{-H}_2\text{O}$ , hydrothermal fluid did undergo immiscible separation, it would have evolved into nearly pure, but separate  $\text{CO}_2$  and  $\text{H}_2\text{O}$  fractions. The separation of these two fluid phases would have had little effect on the  $\delta^{13}\text{C}$  composition of the  $\text{CO}_2$ -rich fluid phase because of the nature of the  $\text{CO}_2$  speciation in the critical and subcritical regimes. Thus, the critical or subcritical nature of the hydrothermal fluid does not profoundly concern interpretations and predictions of the carbon isotopic characteristics of an hydrothermal fluid, but it must be considered for interpretations of oxygen isotopic data.

### 5.5. Model Summary

The universal observation that an hydrous alteration assemblage occurs on the outer margins of a quartz-carbonate alteration assemblage is convincing evidence which implicates the involvement of a single  $\text{H}_2\text{O-CO}_2$  hydrothermal fluid. The following sequence describes the fluid evolution as it reacted with mafic and ultramafic volcanic rock to

produce the carbonate-rich and hydrous alteration assemblages.

As the  $\text{CO}_2$ -rich ( $\text{CO}_2 = 20\text{-}70$  mole %) aqueous fluid infiltrates outward from a conduit into the mafic or ultramafic volcanic rock, reaction with calcium-aluminosilicate minerals produced an hydrous alteration assemblage and buffered the  $\text{XCO}_2$  of the fluid to very low values ( $\text{XCO}_2 < 0.005$ ). The mineralogy of the Hydrous Alteration Facies was determined by the bulk composition of the protolith. A critical reaction "front" separated the Hydrous from the Intense Carbonate Alteration Facies. The position of this front with respect to the fluid conduit moved further away from the conduit with continued outward migration of the fluid. The Transitional Alteration Facies represents this reaction "front" (actually a narrow zone) across which significant changes in the fluid composition, pH and  $f\text{O}_2$  take place. The hydrothermal fluid was relatively oxidizing, had a pH of 4 to 6, and contained up to 70 mole %  $\text{CO}_2$  on the conduit side of the Transitional Alteration Facies. Conversely, in the zone where hydrous minerals were precipitated (Hydrous Alteration Facies), the fluid was relatively more basic, less oxidizing, and had a lower abundance of  $\text{CO}_2$  with respect to that of the fluid in the conduit.

## 6. Stable Isotope Geochemistry

By knowing the stable isotopic relationships of coprecipitated mineral phases, it is possible to gain insight into the nature, origin and thermal evolution of a hydrothermal system. The carbon and oxygen isotope compositions of the vein and replacement carbonates and the oxygen isotope compositions of vein quartz and chlorite were measured to determine if temperatures of vein formation and alteration of adjacent wallrock could be obtained and to estimate the temperature of gold precipitation. Additional oxygen isotope data for other vein-hosted silicates from the Timmins and Yellowknife areas, reported by Kerrich and Fryer (1979), Kerrich (1981) and Kerrich and Hodder (1982), are included for comparison and to broaden the data base. From fluid inclusions hosted in some vein quartz samples,  $H_2O$  and  $CO_2$  were extracted and their hydrogen and carbon isotopic compositions respectively were determined in a limited attempt to evaluate the application of this technique to Archean quartz vein systems. Using the data collectively, it is possible to address the nature of source reservoirs for some of the hydrothermal constituents (particularly carbon) and to model some aspects of the fluid evolution.

No whole rock  $\delta^{18}\text{O}$ -values were determined because a comprehensive set of such data exists (Beaty, 1980; Kerrich and Fryer, 1979), and because calcite or dolomite are ubiquitous accessory phases in the volcanic rock. The presence of accessory carbonate minerals in sample material to be fluorinated, poses some analytical problems. Sharma and Clayton (1965) found that fluorination of carbonate (and by inference carbonate-bearing silicate material) yielded low  $\delta^{18}\text{O}$ -values because small amounts of  $\text{COF}_2$  were present in the  $\text{O}_2$  product gas. Sharma and Clayton (1965) concluded that the  $\text{COF}_2$  contaminant formed the ion  $\text{COF}^+$  in their mass spectrometer which has a mass 47. In their mass spectrometer ion collector, this ion contaminant was collected with the mass 44 ion beam giving an apparent  $^{18}\text{O}/^{16}\text{O}$  ratio that was too small.

### 6.1. Isotopic Notation

At equilibrium the isotope fractionation factor between two minerals A and B is defined as:

$$\alpha_{A-B} = R_A/R_B = (1000 + \delta_A)/(1000 + \delta_B)$$

At isotopic equilibrium, this fractionation is equal to the equilibrium isotope exchange constant  $K_{A-B}$ . In this thesis, isotope fractionations between different minerals or a mineral and water from which it equilibrated isotopically



will be expressed using the  $\Delta$ -notation:

$$\Delta_{A-B} = 1000(\ln \alpha_{A-B})$$

The stable isotopic values for minerals,  $H_2O$ , or  $CO_2$  are reported in the familiar  $\delta$ -notation relative to a reference standard (Craig, 1961):

$$\delta^{18}O = ((R_x/R_s) - 1) \times 1000 \text{ in } \text{‰}$$

where:  $R_x = {}^{18}O/{}^{16}O$  in unknown sample;

$R_s = {}^{18}O/{}^{16}O$  in standard sample

and similarly for the  ${}^{13}C/{}^{12}C$  and D/H ratios. Note that :

$$\Delta_{A-B} \approx \delta_A - \delta_B.$$

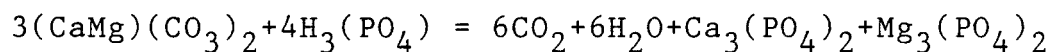
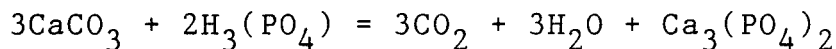
## 6.2. Analytical Methods

A more complete description of the analytical methods used to perform the stable isotopic determinations is given in Appendix-3.

### 6.2.1. $CO_2$ liberation from carbonate minerals

Carbonate minerals that were selected for isotopic analysis, came from altered (carbonatized) volcanic rock and quartz veins. Generally, the carbonate minerals in quartz veins were easily separated; however, no attempt was made to physically separate the carbonate minerals from the altered volcanic rock. Whole rock samples of carbonate-bearing

volcanic rock and vein carbonates were reacted with 100 % phosphoric acid at 25°C (McCrea, 1950):



Complete reaction for calcite took less than 24 hours, but approximately 90 hours was required for ferroan dolomite and in excess of 450 hours were required for magnesite (Fig. 6-1).

#### 6.2.1.1. Acid fractionation factor

The liberation of  $\text{CO}_2$  from carbonate minerals by the 100% phosphoric acid reaction technique releases all of the carbon as  $\text{CO}_2$ . However, only 2/3 of the oxygen originally present in the carbonate mineral is liberated and the

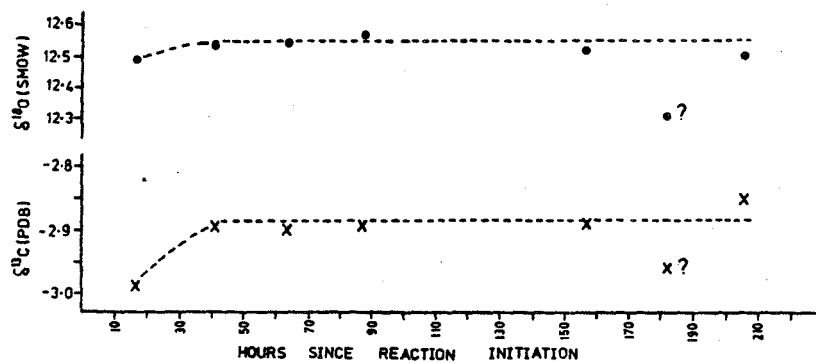
$\delta^{18}\text{O}$ -value of the liberated  $\text{CO}_2$  is about 10‰ enriched in  $^{18}\text{O}$  with respect to the total oxygen composition of the carbonate mineral, obtained by means of the  $\text{BrF}_5$  fluorination technique (Sharma and Clayton, 1965). This non-equilibrium, isotope effect is compensated by applying a carbonate-acid isotope fractionation factor ( $\alpha$ ) which is specific to each compositional type of carbonate:

$$\alpha_{\text{CO}_2\text{-Carbonate}} = \frac{(^{18}\text{O}/^{16}\text{O})_{\text{CO}_2}}{(^{18}\text{O}/^{16}\text{O})_{\text{carbonate}}}$$

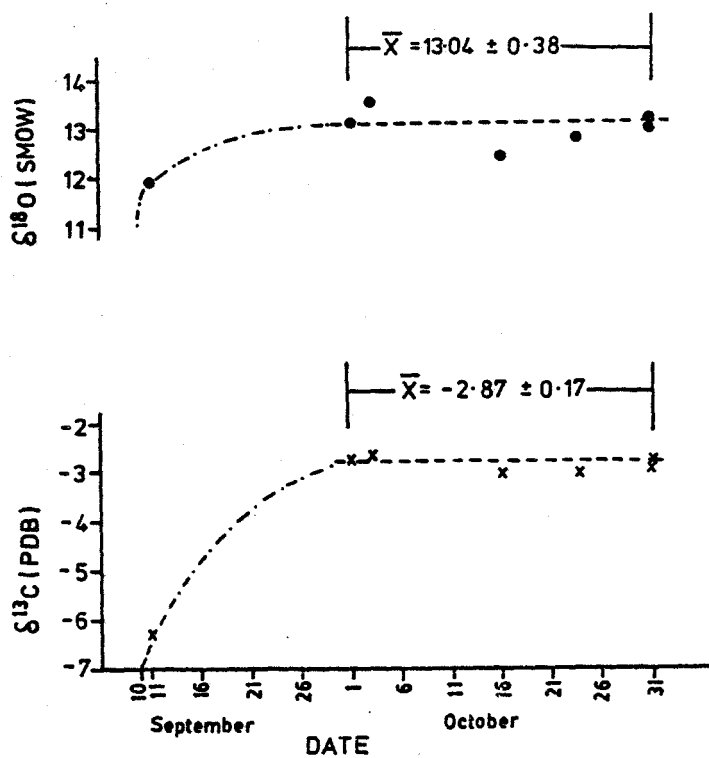
The acid isotope fractionation factors used for this study

Figure 6-1: Results of time study to determine the minimum reaction time to dissolve ferroan dolomite or magnesite, from altered volcanic rocks in the Timmins area, with 100% phosphoric acid. The reaction was assumed to have reached equilibrium when no change was observed in the isotopic value of the liberated CO<sub>2</sub> gas.

## DOLOMITE TIME STUDY



## MAGNESITE TIME STUDY



are listed in Table 6-1. Because the carbonate-acid fractionation factors are specific to each compositional type of carbonate mineral, a correction factor (row D, Table 6-1) must be applied to each dolomite, siderite and magnesite analysis before comparison can be made with calcite (Sharma and Clayton, 1965).

#### 6.2.2. Fluorination of silicate minerals

Silicate minerals were reacted with  $\text{BrF}_5$  to produce  $\text{O}_2$ . This  $\text{O}_2$  was then reacted with a carbon rod at  $550^\circ\text{C}$  to produce  $\text{CO}_2$  (Clayton and Mayeda, 1963). The  $\delta^{18}\text{O}$  and  $\delta^{13}\text{C}$  of the  $\text{CO}_2$  was analysed using a Micromass 602D mass spectrometer.

#### 6.2.3. Fluid inclusion $\text{H}_2\text{O}$ and $\text{CO}_2$

Fluid inclusion-bound  $\text{CO}_2$  and  $\text{H}_2\text{O}$  were decrepitated from acid washed, ground vein quartz ( $< 1 \text{ mm.}$ ) at approximately  $1000^\circ\text{C}$  and collected in liquid nitrogen and dry ice-iso-propyl alcohol cold traps.

#### 6.2.4. Analytical standards

The standard against which the oxygen isotope abundance ratios (whether for silicate or carbonate minerals) are reported is SMOW (Standard Mean Ocean Water; Craig, 1961). However, for routine determinations, a second standard (NBS-28-quartz sand), whose oxygen isotope ratio is

Table 6-1: Carbonate-acid isotope fractionation factors used for this study.

| A<br>mineral | B          | C<br>$10^3 \ln \alpha$<br>(CO <sub>2</sub> -carbonate) | D<br>correction factor with<br>respect to calcite |
|--------------|------------|--------------------------------------------------------|---------------------------------------------------|
| calcite      | 1.01025(1) | 10.20                                                  | -----                                             |
| ankerite     | 1.01098(4) | 10.92                                                  | -0.72                                             |
| dolomite     | 1.01109(1) | 11.03                                                  | -0.83                                             |
| siderite     | 1.01169(2) | 11.62                                                  | -1.42                                             |
| magnesite    | 1.01278(3) | 12.70                                                  | -2.50                                             |

#### Sources

- 1: Sharma and Clayton (1965) as listed by Garlick (1969)
- 2: Hangari et al. (1980)
- 3: This value represents the original reported by Sharma and Clayton, 1965, listed in Friedman and O'Neil, 1977, pp.KK6, but corrected using the revised CO<sub>2</sub>-H<sub>2</sub>O fractionation factor of 1.0412.
- 4: Becker (1971), reported in Golding and Wilson (1983).

known with respect to SMOW, is actually analysed. This enables the  $\delta^{18}\text{O}$  for the unknown sample to be expressed with respect to SMOW (see Appendix-3 for a typical calculation).

The reference standard for carbon is PDB (belemnite from the Peedee Formation; Craig, 1957); however, because this material is exhausted, NBS-20 (Solenhofen limestone), whose  $\delta^{13}\text{C}$  with respect to PDB is known to be  $-1.06\text{‰}$  (Blattner and Hulston, 1978), is now used. For routine analyses, an "in-house" standard, GCS (Grenville Marble), is used. Its  $\delta^{13}\text{C}$  with respect to NBS-20 is  $+1.750\text{‰}$  (Gascoyne, 1979).

The hydrogen isotope standard for D/H ratios is again SMOW; however, for routine analyses, a working standard (DTAP) was prepared by Dr. C.J. Yonge from distilled Hamilton tap water. Replicate analyses of this water yielded a  $\delta\text{D}$  of  $-123 \pm 4.4\text{‰}$  (SMOW). Details of the analytical method and instrumentation are described by Yonge (1982).

All oxygen and carbon stable isotopic analyses discussed in this thesis are reported with respect to SMOW or PDB respectively and these isotopic references will not follow the reported value.

#### 6.2.5. Analytical precision and accuracy

Analytical precision was determined by successive

analysis of the "in-house" laboratory standard (GCS). This material is also used as a working reference gas on the mass spectrometer. Hence, GCS, when treated as an unknown sample, should have a  $\delta^{18}\text{O}$ -value of zero when compared to the GCS reference gas. Twenty-five random analyses of GCS yielded a mean  $\delta^{18}\text{O}$ -value of  $-0.30 \pm 0.32$ . The data ranged from  $-1.34$  to  $+0.01\text{‰}$ . The mean  $\delta^{13}\text{C}$  for the same data set is  $-0.16 \pm 0.21\text{‰}$  (Table 6-2). Elimination of five extreme data pairs whose  $\delta^{18}\text{O}$  departed by more than  $0.6\text{‰}$  from the expected value ( $0\text{‰}$ ) leaves in a revised population with a mean  $\delta^{18}\text{O}$  of  $-0.15 \pm 0.09\text{‰}$  and a mean  $\delta^{13}\text{C}$  of  $-0.09 \pm 0.08\text{‰}$  (Table 6-2). Determinations for hydrothermal carbonates were corrected by these amounts.

Selective duplication of the hydrothermal carbonates contained in altered volcanic rock resulted in standard deviations which were in general smaller than  $0.3\text{‰}$  for both oxygen and carbon.

### 6.3. Equilibrium Isotope Fractionation Expressions

Listed in Table 6-3 are the "best" mineral-water and mineral-mineral oxygen isotope fractionation expressions as recommended by Clayton (1981) and Matthews and Katz (1977). Matthews et al. (1983a) presented calibrations for certain mineral-mineral oxygen isotope fractionations, but as these are high temperature expressions for mineral pairs not used in this study, those isotope fractionation expressions



TABLE 6-2: Replicate isotopic analyses of GCS marble, the in-house carbonate standard.

| Date                                    | $\delta^{18}\text{O}(\text{GCS})$ | $\delta^{13}\text{C}(\text{GCS})$ |
|-----------------------------------------|-----------------------------------|-----------------------------------|
| 21/3/80                                 | -0.30                             | -0.23                             |
| 25/3/80                                 | -0.18                             | -0.06                             |
| 26/3/80                                 | -0.03                             | -0.03                             |
| 2/4/80                                  | -0.06                             | -0.08                             |
| 7/5/80                                  | -0.20                             | -0.09                             |
| 17/6/80                                 | -0.21                             | -0.10                             |
| 7/4/81                                  | -0.14                             | -0.25                             |
| 8/5/81                                  | 0.00                              | -0.03                             |
| 29/6/81                                 | -0.30                             | -0.16                             |
| —/8/81                                  | -0.07                             | -0.01                             |
| 23/9/81                                 | -0.61                             | -0.20                             |
| 27/9/81                                 | -0.69                             | -0.28                             |
| GCS bottle baked for 24 hours at 110 C. |                                   |                                   |
| 29/9/81                                 | -0.09                             | -0.05                             |
| 30/9/81                                 | -0.02                             | -0.04                             |
| —/11/81                                 | -0.16                             | -0.12                             |
| 2/1/82                                  | -0.17                             | -0.10                             |
| 1/2/82                                  | -0.28                             | -0.10                             |
| 6/2/82                                  | -0.91                             | -0.47                             |
| 19/2/82                                 | -0.20                             | -0.12                             |
| 8/4/82                                  | -0.16                             | -0.13                             |
| 8/4/82                                  | -0.64                             | -0.29                             |
| 27/4/82                                 | -0.10                             | +0.12                             |
| 10/1/83                                 | -1.34                             | -0.99                             |
| 5/2/83                                  | -0.24                             | -0.08                             |

#### STATISTICS

all data, n=24

|   |       |       |
|---|-------|-------|
| x | -0.30 | -0.09 |
| s | 0.32  | 0.21  |

eliminate samples falling outside 1s, n=19

|   |       |       |
|---|-------|-------|
| x | -0.15 | -0.09 |
| s | 0.09  | 0.08  |

NOTE: x- mean value; s- standard deviation

TABLE 6-3: Mineral-water and mineral-mineral oxygen isotope fractionation expressions relevant to Archean Gold Quartz Vein systems.

171

| SYSTEM                            | 1000 ln $\alpha$<br>( $T=1E6/K^2$ )<br>( $t=1000/K$ ) | Calibrated<br>Temperature<br>Range(C) |
|-----------------------------------|-------------------------------------------------------|---------------------------------------|
| =====                             |                                                       |                                       |
| Quartz-Water                      |                                                       |                                       |
| Clayton et al.(1972)              | 3.38T-3.40(5)                                         | 200-500                               |
|                                   | 3.38T-2.90(3)                                         | 200-500                               |
| Matsuhisa et al.(1979)            | 3.34T-3.31(1)                                         | 250-500                               |
| Matthews and Beckinsale<br>(1979) | 3.05T-2.09                                            | 265-465                               |
| -----                             |                                                       |                                       |
| Dolomite-Water                    |                                                       |                                       |
| Sheppard and Schwarcz<br>(1970)   | 3.23T-2.89(1,4)                                       | 200-600                               |
| Matthews and Katz(1977)           | 3.06T-3.24                                            | 252-295                               |
| -----                             |                                                       |                                       |
| Calcite-Water                     |                                                       |                                       |
| O'Neil et al.(1969)               | 2.78T-3.39Z(5)                                        | 0-500                                 |
|                                   | 2.78T-2.89(1,3)                                       | 0-500                                 |
| Calcite-CO2                       |                                                       |                                       |
| Bottinga(1968)                    | 1.8T-10.61+2.78(1)                                    |                                       |
| Dolomite-CO2                      |                                                       |                                       |
|                                   | 2.25T-10.61+2.38(1,7)                                 |                                       |
| -----                             |                                                       |                                       |
| Chlorite-Water                    |                                                       |                                       |
| Wenner and Taylor(1971)           | 1.56T-4.70(2,5)                                       |                                       |
| Recast expression                 | 1.72T-4.29(1,3)                                       |                                       |
| -----                             |                                                       |                                       |
| Sericite-Water                    |                                                       |                                       |
| O'Neil and Taylor(1969)           | 2.38T-3.89(1)                                         | 400-650                               |
| -----                             |                                                       |                                       |
| Quartz-chlorite(6)                | 1.62T+0.98(1)                                         |                                       |
| Quartz-sericite(6)                | 0.96T+0.58(1)                                         |                                       |
| Quartz-calcite(6)                 | 0.56T-0.42(1)                                         |                                       |
| Quartz-dolomite(6)                | 0.11T-0.02(1)                                         |                                       |
| Dolomite-calcite(6)               | 0.45T-0.40(1)                                         |                                       |
| Calcite-chlorite                  | 1.06T+1.40(1)                                         |                                       |
| Dolomite-chlorite                 | 1.51T+1.40(1)                                         |                                       |
| Muscovite-chlorite                | 0.66T+0.40(1)                                         |                                       |
| =====                             |                                                       |                                       |

- NOTES: 1:Expressions used in this study for mineral-fluid and mineral-mineral expressions.
- 2:Clayton(1981) and Matthews and Katz(1977) express some doubt about the accuracy of this expression.
- 3:Modified expression using CO2-H2O oxygen isotope fractionation factor of 1.0412.
- 4:Derived by linearly combining the calcite-water with the dolomite-water expression given by Sheppard and Schwarcz(1970).
- 5:Original expression reported by authors using CO2-H2O oxygen isotope fractionation factor of 1.0407 at 25 C.
- 6:Based on the Matsuhisa et al. Quartz-water expression.
- 7:Linear combination of Calcite-CO2 (Bottinga,1968) and Calcite Dolomite (Sheppard and Schwarcz,1970) expressions.

listed in Table 6-3 are used in this thesis.

The  $\Delta_{\text{dolomite-water}}$  derived by Sheppard and Schwarcz (1970) has been substituted in place of the earlier experimental fractionation expression derived by Northrop and Clayton (1966) which was used in calculations reported by Fyon et al. (1983d). This substitution was made because:

1) Northrop and Clayton (1966) determined their  $\Delta_{\text{dolomite-water}}$  experimentally by reacting dolomite powder with a 0.55 M  $\text{NH}_4\text{Cl}$  solution. The effects of dissolved salts on the activity of isotopic species of  $\text{H}_2\text{O}$  (Truesdell, 1974) would tend to increase the  $\Delta_{\text{dolomite-water}}$  (Matthews and Katz, 1977).

2) Sheppard and Schwarcz (1970) found that the Northrop and Clayton  $\Delta_{\text{dolomite-water}}$  fractionation, when linearly combined with the  $\Delta_{\text{calcite-water}}$  fractionation expression (O'Neil et al. 1969), yielded a  $\Delta_{\text{dolomite-calcite}}$  which gave anomalously high temperatures when applied to the thermometry of coexisting metamorphic dolomite and calcite.

3) The  $\Delta_{\text{dolomite-water}}$  fractionation expression deduced experimentally by Matthews and Katz (1977) is similar to that proposed by Sheppard and Schwarcz (1970); however, the Sheppard and Schwarcz fractionation expression is preferred because it incorporates empirical data from a wide range of temperatures.

The  $\Delta_{\text{quartz-water}}$  used in this thesis is that of Matsuhisa et al. (1979), although all three listed in Table 6-3 yield nearly identical results. Note also that the slope of the  $\Delta_{\text{quartz-dolomite}}$  fractionation expression is almost flat and therefore this mineral pair is not a sensitive geothermometer. Also, the use of the Northrop-Clayton  $\Delta_{\text{dolomite-water}}$  fractionation expression, linearly combined with the Matsuhisa et al.  $\Delta_{\text{quartz-water}}$  fractionation expression, requires that dolomite should be about 1‰ enriched in  $\delta^{18}\text{O}$  with respect to coprecipitated quartz at equilibrium in the 300-500 °C temperature range. Conversely, dolomite would be about 0.6‰ depleted with respect to coprecipitated quartz if the preferred Sheppard-Schwarcz (and Matthews-Katz)  $\Delta_{\text{dolomite-water}}$  fractionation expression is linearly combined with the Matsuhisa et al.  $\Delta_{\text{quartz-water}}$  fractionation.

The  $\Delta_{\text{chlorite-water}}$  fractionation expression reported in Table 6-3 differs from that reported by Wenner and Taylor. The original Wenner and Taylor (1971) has been corrected using the new  $\text{CO}_2$ -water fractionation factor of 1.0412, and linearly combined with the Matsuhisa et al. (1979)  $\Delta_{\text{quartz-water}}$  fractionation expression. The revisions are explained in more detail in Section 6.4.2.2..

Clayton (1981) states that the  $\Delta_{\text{chlorite-water}}$  and any other  $\Delta_{\text{mineral-chlorite}}$  fractionation expressions to be the least reliable of those listed on Table 6-3, because of

the "boot-strap" empirical approach used by Wenner and Taylor (1971) to derive the function (see Section 6.4.2.2 for a detailed explanation). Wenner and Taylor (1971) established the  $\Delta_{\text{quartz-chlorite}}$  fractionation by plotting  $\Delta_{\text{quartz-chlorite}}$  against  $\Delta_{\text{quartz-ilmenite}}$  for low grade metamorphic rocks to obtain the relationship:

$$\Delta_{\text{quartz-chlorite}} = 0.59(\Delta_{\text{quartz-ilmenite}}).$$

Deines (1977) discussed these concordancy plots and found that spurious correlations can result when  $\Delta_{AB}$  is plotted against  $\Delta_{AC}$ , where the isotopic enrichments are in the order  $S_A > S_B > S_C$ .

The  $\Delta_{\text{muscovite-water}}$  fractionation (O'Neil and Taylor, 1969) is considered by Clayton (1981) to be the best available for that mineral. It was calibrated experimentally using 3 different methods, all of which yielded nearly identical results (O'Neil and Taylor, 1969).

Listed in Table 6-4 are the equilibrium isotopic fractionation factors of carbon compounds with respect to  $\text{CO}_2$ , as compiled by Ohmoto and Rye (1979). Note that experimental determinations of equilibrium carbon-isotope fractionations are lacking for that temperature range relevant to hydrothermal ore deposit formation (200-700°C). However, uncertainties in the values for the  $\Delta_{\text{CaCO}_3-\text{CO}_2}$  system are probably accurate to +/- 10 percent (Ohmoto and Rye, 1979). This error estimate may be cautiously extended

TABLE 6-4: Equilibrium carbon isotopic fractionation expressions for some carbon compounds with respect to CO<sub>2</sub>.

$$10^3 \ln \alpha_{i-\text{CO}_2} = \frac{A}{T^3} \times 10^8 + \frac{B}{T^2} \times 10^6 + \frac{C}{T} \times 10^3 + D$$

| Compound                               | A      | B      | C      | D    | T(°C)<br>Range |
|----------------------------------------|--------|--------|--------|------|----------------|
| Dolomite(a)                            | -8.914 | 8.737  | -18.11 | 8.44 | <600           |
| Calcite(b)                             | -8.914 | 8.557  | -18.11 | 8.27 | <600           |
| H <sub>2</sub> CO <sub>3</sub> (ap)(c) | 0      | 0      | 0      | 0    | <350           |
| Methane(d)                             | 4.194  | -5.210 | -8.93  | 4.36 | <700           |
| C(graphite)(d)                         | -6.637 | 6.921  | -22.89 | 9.32 | <700           |

Notes:

- a) Based on empirical dolomite-calcite fractionation factors by Sheppard and Schwarcz(1970).
- b) Polynomial fit to values calculated by Bottinga(1969) fitted by Ohmoto and Rye(1979).
- c) Estimated by Ohmoto(1972) on the premise that H<sub>2</sub>CO<sub>3</sub>(apparent) = CO<sub>2</sub>(apparent) + H<sub>2</sub>CO<sub>3</sub>.
- d) Polynomial fit to values calculated by Bottinga(1968) fitted by Ohmoto and Rye(1979).

to the  $\Delta_{\text{dolomite-CO}_2}$  system, only because carbon isotopic fractionation between dolomite and calcite at temperatures above 200°C is probably less than 1‰ (Sheppard and Schwarcz, 1970). The dolomite-calcite pair is no longer considered to be a sensitive geothermometer (Ohmoto and Rye, 1979). Thus, in the absence of cogenetic CO<sub>2</sub> gas data, the carbon isotopic compositions of hydrothermal carbonate minerals can be best used to infer the  $\delta^{13}\text{C}$  of the hydrothermal fluid and hence to identify possible source reservoirs. However, it must be emphasized that the  $\delta^{13}\text{C}$  of coexisting CO<sub>2</sub> can only be qualitatively estimated because the partitioning of carbon isotopes between CO<sub>2</sub> and carbonate minerals is not known very accurately.

#### 6.4. Error Analysis of Oxygen Isotope Fractionation Expressions

To use the isotope fractionation expressions for geothermometry, it is imperative to evaluate the cumulative error associated with each expression. This has been attempted in detail for the  $\Delta_{\text{quartz-water}}$  oxygen isotope fractionation expression derived by Matsuhisa et al. (1979). Less quantitative error analysis is provided, where sufficient reported data exists, for the other experimentally derived oxygen isotope fractionation expressions. The empirically-derived isotope fractionation expressions are less amenable to error analysis and will be considered only briefly.

#### 6.4.1. Experimentally derived isotope fractionation expressions

To derive by experimental methods the isotope fractionation between a mineral and water, the mineral and water, whose  $\delta^{18}\text{O}$ -values are known by previous analysis, are heated at a fixed temperature to effect an isotope exchange. Following this reaction, the  $\delta$ -values of the exchanged mineral and water are analysed to calculate the  $\alpha_{\text{mineral-water}}$ :

$$\alpha_{\text{M-W}} = \frac{\delta_{\text{M}} + 1000}{\delta_{\text{W}} + 1000}$$

Errors are associated with the  $\delta$ -analyses of the mineral and water prior to and after the isotope exchange reaction and with the estimation of the temperature at which the reaction took place. The error in  $\Delta_{\text{mineral-water}}$  resulting from the analytical errors in  $\delta$ -mineral (m) and  $\delta$ -water (w) is calculated as follows (Bevington, 1969, p. 61):

$$\sigma_{\Delta}^2 = \sigma_{\text{m}_1}^2 + \sigma_{\text{m}_2}^2 + \sigma_{\text{w}_1}^2 + \sigma_{\text{w}_2}^2,$$

where  $\sigma_{\text{mineral}_1}^2$  or  $\sigma_{\text{water}_1}^2$  and  $\sigma_{\text{mineral}_2}^2$  or  $\sigma_{\text{water}_2}^2$  are the analytical errors (variance) on the  $\delta$ -mineral or  $\delta$ -water analyses prior (1) to and after (2) the exchange reaction respectively.

To illustrate how this error may be estimated, the  $\Delta_{\text{quartz-water}}$  fractionation expression by Matsuhisa et al. (1979) is analysed. Reproduced in Table 6-5 are the



TABLE 6-5: Detailed error analysis of the experimentally-derived Quartz-Water oxygen isotope fractionation expression, using the data of Matsuhisa *et al.* (1979).

| T(°C) | (1E6/K) | Quartz<br>$\delta^{18}\text{O}$ | Water<br>$\delta^{18}\text{O}$ | (1)               | A                 | B C              |                   |                                                            |
|-------|---------|---------------------------------|--------------------------------|-------------------|-------------------|------------------|-------------------|------------------------------------------------------------|
|       |         |                                 |                                | Delta<br>$\Delta$ | Sigma<br>$\Delta$ | Mean<br>$\Delta$ | Sigma<br>$\Delta$ | Temperature<br>Error<br>(10 <sup>3</sup> /K <sup>2</sup> ) |
| ===== |         |                                 |                                |                   |                   |                  |                   |                                                            |
| 800   | 0.859   | 9.59                            | -0.56                          | 0.63              | 0.20              |                  |                   |                                                            |
|       |         | 9.59                            | 14.52                          | 0.64              | 0.20              | 0.635            | 0.28              | 0.0085                                                     |
| ----- |         |                                 |                                |                   |                   |                  |                   |                                                            |
| 700   | 1.056   | 20.86                           | 9.75                           | 1.11              | 0.20              |                  |                   |                                                            |
|       |         | 20.86                           | 28.33                          | 1.16              | 0.20              |                  |                   |                                                            |
|       |         | 9.59                            | -0.56                          | 1.22              | 0.20              |                  |                   |                                                            |
|       |         | 9.59                            | 14.52                          | 0.88              | 0.20              |                  |                   |                                                            |
|       |         | 9.59                            | -0.56                          | 1.93              | 0.20              |                  |                   |                                                            |
|       |         | 9.59                            | 14.52                          | 1.41              | 0.20              |                  |                   |                                                            |
|       |         | 9.59                            | 14.52                          | 0.91              | 0.20              |                  |                   |                                                            |
|       |         | 9.59                            | 14.52                          | 1.03              | 0.20              |                  |                   |                                                            |
|       |         | 9.59                            | -0.56                          | 1.22              | 0.20              | 1.208            | 0.60              | 0.0105                                                     |
|       |         | -----                           |                                |                   |                   |                  |                   |                                                            |
| 600   | 1.312   | 9.59                            | -0.56                          | 1.23              | 0.20              |                  |                   |                                                            |
|       |         | 9.59                            | 9.75                           | 1.14              | 0.20              |                  |                   |                                                            |
|       |         | 9.59                            | 28.33                          | (-0.02)           | —                 |                  |                   |                                                            |
|       |         | 20.86                           | 9.75                           | 1.58              | 0.20              |                  |                   |                                                            |
|       |         | 20.86                           | 28.33                          | 1.58              | 0.20              |                  |                   |                                                            |
|       |         | 20.86                           | 9.75                           | 1.58              | 0.20              |                  |                   |                                                            |
|       |         | 20.86                           | 28.33                          | 1.74              | 0.20              | 1.475            | 0.49              | 0.0148                                                     |
| ----- |         |                                 |                                |                   |                   |                  |                   |                                                            |
| 500   | 1.674   | 9.59                            | -0.56                          | 4.20              | 0.20              |                  |                   |                                                            |
|       |         | 9.59                            | 14.52                          | (0.60)            | —                 |                  |                   |                                                            |
|       |         | 9.59                            | -0.56                          | 3.26              | 0.20              |                  |                   |                                                            |
|       |         | 9.59                            | 14.52                          | 1.45              | 0.20              |                  |                   |                                                            |
|       |         | 20.86                           | 9.75                           | 1.95              | 0.20              |                  |                   |                                                            |
|       |         | 20.86                           | 28.33                          | 2.54              | 0.20              | 2.662            | 0.45              | 0.0219                                                     |
| ----- |         |                                 |                                |                   |                   |                  |                   |                                                            |
| 400   | 2.208   | 20.86                           | 9.75                           | 4.14              | 0.20              |                  |                   |                                                            |
|       |         | 20.86                           | 28.33                          | 4.11              | 0.20              |                  |                   |                                                            |
|       |         | 20.86                           | 14.52                          | 4.21              | 0.20              |                  |                   |                                                            |
|       |         | 9.59                            | -0.56                          | 6.37              | 0.20              |                  |                   |                                                            |
|       |         | 9.59                            | 14.52                          | 1.24              | 0.20              |                  |                   |                                                            |
|       |         | 9.59                            | 4.78                           | 3.72              | 0.20              | 3.965            | 0.49              | 0.0326                                                     |
| ----- |         |                                 |                                |                   |                   |                  |                   |                                                            |
| 300   | 3.046   | 20.86                           | 4.78                           | 6.68              | 0.20              |                  |                   |                                                            |
|       |         | 20.86                           | 14.52                          | 6.60              | 0.20              | 6.64             | 0.28              | 0.0527                                                     |
| ===== |         |                                 |                                |                   |                   |                  |                   |                                                            |

Note: Data in ( ) was not used in the error analysis or to determine the mean  $\Delta$ .

Columns: A-Error on  $\Delta$  arising from analytical uncertainty on  $\delta$  for mineral and water.

B-Sum of analytical errors on the mean value of  $\Delta$ .

C-Temperature uncertainty based on measurement accuracy of  $\pm 5^\circ\text{C}$ .

1-Delta ( $\Delta$ ) Quartz-Water calculated from the  $\delta$ -minerals after the exchange reaction. These data were not listed by Matsuhisa *et al.* (1979).

Error on one  $\delta$ -analysis reported to have been  $\pm 0.10\%$

experimental data reported by Matsuhisa et al. (1979) with the corresponding detailed error analysis. In Table 6-5, Column A lists the error on each individual  $\Delta_{\text{quartz-water}}$  calculation and is derived as follows, using the reported analytical error on one S-analysis of  $\pm 0.1\%$  (Matsuhisa et al., 1979):

$$\begin{aligned} G_{\Delta}^2 &= G_{m_1}^2 + G_{m_2}^2 + G_{w_2}^2 + G_{w_1}^2 \\ &= (0.1)^2 + (0.1)^2 + (0.1)^2 + (0.1)^2 \\ &= 0.04 \end{aligned}$$

or

$$G_{\Delta} = 0.20 \%$$

That is, the error on  $\Delta_{\text{quartz-water}}$  attributed to analytical uncertainty is  $\pm 0.2\%$ , or:

$$\Delta_{\text{quartz-water}}^{300^{\circ}\text{C}} = 6.64 \pm 0.20 \%$$

To determine the oxygen isotope fractionation expression, it is necessary to plot the  $\Delta$ -values against their corresponding temperature, expressed as ( $10^6/\text{K}^2$ ).

Matsuhisa et al. (1979) averaged the replicate  $\Delta$ -values for a given temperature to obtain a single value. This averaged  $\Delta$ -value has a cumulative error equal to:

$$G^2 = G_{\Delta_1}^2 + G_{\Delta_2}^2 + \dots + G_{\Delta_n}^2,$$

where  $G_{\Delta_n}^2$  is the error associated with a single  $\Delta_{\text{quartz-water}}$  determination (Column A, Table 6-5). For the  $300^{\circ}\text{C}$  runs, the cumulative error on the averaged  $\Delta_{\text{quartz-water}}$

is calculated as follows:

$$\begin{aligned} \epsilon_{\Delta}^2 &= (0.20)^2 + (0.20)^2 \\ &= 0.08 \end{aligned}$$

or

$$\epsilon_{\Delta} = 0.28 \text{ ‰}$$

That is, the mean  $\Delta_{\text{quartz-water}}$  of 6.64 has an associated error of  $\pm 0.28 \text{ ‰}$  which is attributed to the experimental procedure. The total experimental error on the other mean  $\Delta$ -values is tabulated in Column B, Table 6-5. The error in the temperature measurement is reported by Matsuhisa et al. (1979) to be  $\pm 5^{\circ}\text{C}$ , and this error is listed in Column C, Table 6-5, in the form  $(10^6/\text{K}^2)$ .

The remaining step in the data treatment is to regress a line through the  $\Delta$ -( $10^6/\text{K}^2$ ) array. To calculate the error on the slope and intercept of the linearly regressed line through the data points, a version of YORKFIT (York, 1969) was used. Two errors are associated with each point - temperature (Column C, Table 6-5) and the cumulative experimental error for the mean  $\Delta$ -determination (Column B, Table 6-5). The resulting linear regression expression derived for the Matsuhisa et al. (1979) data is listed in Table 6-6 along with similarly derived, error analysed, linear regression oxygen isotope fractionation expressions for other fractionation expressions. The slopes and intercepts of the reported experimentally derived and error analysed linear regressions are similar. From such an error

TABLE 6-6: Estimation of the minimum cumulative error associated with some oxygen isotope fractionation expressions, considering experimental, curve fitting errors.

| System           | Matauhisa <i>et al.</i><br>Quartz-water                                                                                                                                                                                          | Matthews and Beckinsale<br>Quartz-water | O'Neill <i>et al.</i><br>Calcite-water | O'Neill and Taylor<br>Muscovite-water | Sheppard and Schvarcz<br>Dolomite-Calcite | Dolomite-Water | Chlorite-Water |
|------------------|----------------------------------------------------------------------------------------------------------------------------------------------------------------------------------------------------------------------------------|-----------------------------------------|----------------------------------------|---------------------------------------|-------------------------------------------|----------------|----------------|
| Reported         | 3.34T-3.31                                                                                                                                                                                                                       | 3.05T-2.09                              | 2.78T-2.89                             | 2.38T-3.89                            | 0.45T-0.40                                |                | 1.72T-4.29     |
| YORKFIT          | 2.94T-2.36                                                                                                                                                                                                                       | 3.12T-2.23                              | 2.85T-3.57                             | 2.46T-4.17                            | 0.46T-0.47                                | 3.26T-3.92     |                |
| Error            |                                                                                                                                                                                                                                  |                                         |                                        |                                       |                                           |                |                |
| Slope            | 0.16                                                                                                                                                                                                                             | 0.20                                    | 0.11                                   | 0.12                                  | 0.02                                      | —              | —              |
| Intercept        | 0.42                                                                                                                                                                                                                             | 0.55                                    | 0.30                                   | 0.27                                  | 0.07                                      | —              | —              |
| Temperature (°C) | Minimum experimental and curve fitting error on $\Delta$ (‰)                                                                                                                                                                     |                                         |                                        |                                       |                                           |                |                |
| 500              | 0.50                                                                                                                                                                                                                             | 0.64                                    | 0.35                                   | 0.34                                  | 0.08                                      | 0.36           | 0.64           |
| A 400            | 0.55                                                                                                                                                                                                                             | 0.71                                    | 0.39                                   | 0.38                                  | 0.08                                      | 0.39           | 0.67           |
| 300              | 0.64                                                                                                                                                                                                                             | 0.82                                    | 0.45                                   | 0.45                                  | 0.09                                      | 0.46           | 0.78           |
|                  | Minimum temperature error resulting from minimum experimental, and curve fitting error on $\Delta$ (°C).                                                                                                                         |                                         |                                        |                                       |                                           |                |                |
| 500              | 39                                                                                                                                                                                                                               | 47                                      | 28                                     | 32                                    | 40                                        | 26             | 84             |
| B 400            | 29                                                                                                                                                                                                                               | 35                                      | 21                                     | 25                                    | 26                                        | 18             | 58             |
| 300              | 20                                                                                                                                                                                                                               | 25                                      | 15                                     | 17                                    | 18                                        | 13             | 41             |
|                  | Minimum error on $\Delta$ (‰) resulting from cumulative error analysis (experimental, curve fitting and hypothetical analytical error of 0.2 ‰ on each $\delta$ -value for a silicate mineral and 0.15‰ for carbonate minerals). |                                         |                                        |                                       |                                           |                |                |
| 500              | 0.54                                                                                                                                                                                                                             | 0.67                                    | 0.40                                   | 0.39                                  | 0.23                                      | 0.46           | 0.68           |
| C 400            | 0.59                                                                                                                                                                                                                             | 0.74                                    | 0.44                                   | 0.43                                  | 0.23                                      | 0.50           | 0.70           |
| 300              | 0.67                                                                                                                                                                                                                             | 0.84                                    | 0.49                                   | 0.49                                  | 0.23                                      | 0.54           | 0.81           |
|                  | Minimum temperature error resulting from cumulative error analysis (°C).                                                                                                                                                         |                                         |                                        |                                       |                                           |                |                |
| 500              | 42                                                                                                                                                                                                                               | 50                                      | 32                                     | 37                                    | 115                                       | 33             | 89             |
| D 400            | 30                                                                                                                                                                                                                               | 36                                      | 24                                     | 27                                    | 76                                        | 23             | 60             |
| 300              | 21                                                                                                                                                                                                                               | 25                                      | 16                                     | 19                                    | 47                                        | 16             | 43             |

analysis it is possible to determine the minimum cumulative error on  $\Delta$  resulting from the experimental and curve-fitting steps at each specified temperature. The relationship:

$$\Delta_{\text{quartz-water}} = 2.96T - 2.37,$$

can be expressed in the form:

$$\Delta = T (m) - c,$$

where  $T = 10^6/K^2$ ,  $M =$  slope and  $C =$  intercept. For expressions of this form, the error on  $\Delta$  is calculated as follows (Bevington, 1969, p. 61):

$$\sigma_{\Delta}^2 = T^2(\sigma_m)^2 + \sigma_c^2$$

The error on the slope ( $m$ ),  $\sigma_m$ , and intercept ( $c$ ),  $\sigma_c$ , is  $\pm 0.16$  and  $\pm 0.42$  respectively (Table 6-6) for the Matsuhisa et al. (1979)  $\Delta_{\text{quartz-water}}$  fractionation expression. Thus, at  $400^\circ\text{C}$  the minimum experimental and curve-fitting error on  $\Delta$  is:

$$\begin{aligned}\sigma_{\Delta}^2 &= (2.208)^2(0.16)^2 + (0.42)^2 \\ &= 0.30\end{aligned}$$

or

$$\sigma_{\Delta} = 0.55\%.$$

Similar sets of calculations for the other oxygen isotope fractionation expressions at 300°, 400° and 500°C are listed in Table 6-6, Row A.

The minimum error on  $\Delta$  (‰) can be translated to a minimum temperature error using the relationship (Clayton, 1981):

$$\Delta = M(10^6/K^2) - C$$

$$(d\Delta)/(dt) = (-2)(M)(10^6)(K^{-3})$$

A set of minimum temperature errors have been calculated for each of the oxygen isotope fractionation expressions and are listed in Table 6-6 (Row B). For the Matsuhisa et al. (1979)  $\Delta_{\text{quartz-water}}$  data, minimum temperature errors attributed to the experimental and curve-fitting errors are +/- 39°, +/- 29° and +/- 20°C at 500°C, 400° and 300°C respectively.

To this point, the error analysis has considered only those errors which arose during the experimental derivation of the  $\Delta$ -values and the linear regression of a line through the  $\Delta - (10^6/K^2)$  data array. That is, this is the cumulative error attributed only to the experimental derivation (calibration) of a particular oxygen isotope fractionation expression. It may be considered as the "hidden" or inherent error for a particular isotope fractionation expression. The routine application of any such fractionation expression involves not only the inherent

experimental error, but one additional element of error must also be considered - namely, the analytical error associated with the routine laboratory determination of the  $\delta$ -values for samples. From these  $\delta$ -values,  $\Delta$  is calculated, and its value is substituted into an oxygen isotope fractionation expression to obtain a temperature. The magnitude of this additional error and its contribution to the cumulative error on a fractionation expression is considered in the following section.

#### 6.4.1.1. Error component related to laboratory analyses

For routine laboratory determinations, an analytical uncertainty is associated with each  $\delta$ -value obtained. This error, or precision, is estimated by successive analysis of a given sample. The magnitude of the error varies between 0.1 and 0.3‰ for  $\delta^{18}\text{O}$  determinations, depending on the nature of the sample material, the analyst, his technique and the mass spectrometer characteristics. The best precision obtained during the course of this thesis for replicate analyses of silicate material, was  $\pm 0.2\text{‰}$  on the quartz standard NBS-28. In general replicate analyses of other silicate material yielded comparable or worse precisions. For the exercise at hand, the  $\pm 0.2\text{‰}$  precision will be used to calculate a minimum temperature error which combines the cumulative experimental errors, outlined in section 6.4.1, as well as the analytical errors

incurred during the treatment of unknown samples.

As a simple geothermometry example, using the error analysed  $\Delta_{\text{quartz-water}}$  isotope fractionation expression of Matsuhisa et al. (1979), and assuming an individual  $\delta$ -value is known to  $\pm 0.2\%$ , the resulting uncertainty in  $\Delta$  can be treated as follows. The analytical uncertainty associated with the determination of one  $\delta$ -value is  $\pm 0.20\%$ . This analytical uncertainty must be summed with the previously determined minimum experimental uncertainty on (Table 6-6). Using the Matsuhisa et al. (1979)  $\Delta_{\text{quartz-water}}$  data, the minimum experimental uncertainty on  $\Delta$  was determined to be  $\pm 0.55\%$  at  $400^\circ\text{C}$ . Therefore, the total error on  $\Delta_{\text{quartz-water}}$  is:

$$\begin{aligned}\sum G_{\Delta}^2 &= (0.55)^2 + (0.20)^2 \\ &= 0.34\end{aligned}$$

or

$$\sum G_{\Delta} = 0.59\%$$

Again, using the fractionation expression for the Matsuhisa et al. (1979)  $\Delta_{\text{quartz-water}}$  data:

$$\Delta_{\text{qw}} = 2.94(10^6 / \text{K}^2) - 2.36$$

$$(d\Delta)/(dt) = (-5.88)(10^6)(\text{K}^{-3}).$$



Using the value of  $\pm 0.59$  for the total cumulative error in estimating  $\Delta_{\text{quartz-water}}$ , the resulting error in estimating temperature at  $400^{\circ}\text{C}$  is approximately  $\pm 30^{\circ}\text{C}$ . Similar calculations for the other experimentally derived oxygen isotope fractionation expressions are reported in Table 6-6 (Row D) as the minimum temperature error resulting from the cumulative error analysis (Row C). Such a detailed error analysis illustrates that the greatest source of error derives collectively from the experimental determinations and the curve fitting procedure. This collective error is generally ignored or at least not considered by most stable isotopic treatises.

#### 6.4.2. Empirically-derived isotope fractionation expressions

Two empirically-derived oxygen isotope fractionation expressions are included in Table 6-6- $\Delta_{\text{dolomite-water}}$  and  $\Delta_{\text{chlorite-water}}$ . The error analysis of these expressions is somewhat less precise than that followed for the experimentally-derived expressions.

##### 6.4.2.1. Dolomite-water

The  $\Delta_{\text{dolomite-water}}$  expression is derived by linearly combining the empirical  $\Delta_{\text{dolomite-calcite}}$  (Sheppard and Schwarcz, 1970) and experimental  $\Delta_{\text{calcite-water}}$  (O'Neil et al, 1969) expressions, where C, W, and D

correspond to calcite, water and dolomite respectively:

$$\begin{aligned}\Delta_{D-W} &= \Delta_{D-C} + \Delta_{C-W} \\ &= [(0.45)(10^6/K^2) - 0.40] + [(2.78)(10^6/K^2) - 2.89] \\ &= 3.23(10^6/K^2) - 3.29.\end{aligned}$$

Hence, the cumulative error on the dolomite-water expression ( $\epsilon^2_{D-W}$ ) is the sum of the cumulative errors on the dolomite-calcite ( $\epsilon^2_{D-C}$ ) and calcite-water ( $\epsilon^2_{C-W}$ ) expressions. The minimum experimental error on  $\Delta$  for  $\Delta_{\text{dolomite-calcite}}$  expression is 0.08% in the 300-500°C range (Table 6-6). Therefore at 500°C the total minimum experimental error on the  $\Delta_{\text{dolomite-water}}$  expression is:

$$\begin{aligned}\epsilon^2_{D-W} &= \epsilon^2_{D-C} + \epsilon^2_{C-W} \\ &= (0.08)^2 + (0.35)^2 \\ &= 0.13\end{aligned}$$

or

$$\epsilon_{D-W} = 0.36 \text{ at } 500^\circ\text{C}.$$

The other errors on  $\Delta_{\text{dolomite-water}}$  are +/- 0.39% at 400°C and +/- 0.46% at 300°C (Table 6-6; Row C). Replicate analyses of an "inhouse" carbonate standard yielded an analytical error of 0.15%. Using this value for demonstrative purposes, the minimum cumulative error on for  $\Delta_{\text{dolomite-water}}$  is calculated to be +/- 0.46% at 500°C, +/- 0.50% at 400°C and +/- 0.54% at 300°C (Table 6-6; Row D). This error translates to a temperature

uncertainty of  $\pm 33^\circ$  at  $500^\circ\text{C}$  and  $\pm 16^\circ$  at  $300^\circ\text{C}$  (Table 6-6; row D).

#### 6.4.2.2. Chlorite-water

The procedure used by Wenner and Taylor (1971) to calculate  $\Delta_{\text{chlorite-water}}$  was as follows.  $\Delta_{\text{quartz-chlorite}}$  was plotted against  $\Delta_{\text{quartz-ilmenite}}$  to obtain the relationship:

$$\Delta_{\text{quartz-chlorite}} = 0.59 (\Delta_{\text{quartz-ilmenite}}).$$

The actual  $\Delta_{\text{quartz-chlorite}}$  and  $\Delta_{\text{quartz-ilmenite}}$  data were not included in their paper and hence a rigorous error analysis of this step is not possible. However, the minimum pooled error would be  $\pm 0.17\%$  - derived totally from an analytical error of  $\pm 0.1\%$  on a single  $\delta$ -analysis.

Next, it was determined that:

$$\Delta_{\text{quartz-muscovite}} = 0.35 (\Delta_{\text{quartz-ilmenite}}).$$

Again, the minimum pooled error in this step would be  $\pm 0.17\%$ , based totally on analytical uncertainty on a single  $\delta$ -value. Again, no curve fitting error can be estimated because the original data set was not listed. Now:

$$(\Delta_{\text{quartz-chlorite}})/(0.59) = (\Delta_{\text{quartz-muscovite}})/(0.35)$$

or

$$\Delta_{\text{quartz-chlorite}} = (1.69) (\Delta_{\text{quartz-muscovite}}).$$

The  $\Delta_{\text{quartz-muscovite}}$  term can be recast in terms of

$\Delta_{\text{quartz-water}}$  and  $\Delta_{\text{muscovite-water}}$ . In their calculation, Wenner and Taylor (1971) used the  $\Delta_{\text{quartz-water}}$  expression reported by Clayton et al. (1972). However, to experimentally determine the  $\Delta_{\text{quartz-water}}$  expression, Clayton et al. (1972) measured the  $\delta$ -value of the water that was reacted with quartz, using the  $\text{CO}_2\text{-H}_2\text{O}$  equilibration method. The old oxygen isotope fractionation factor value of 1.0407 was used. Friedman and O'Neil (1977) recommend the adoption of 1.0412 as the  $\text{CO}_2\text{-H}_2\text{O}$  fractionation factor. I have recalculated the original  $\Delta_{\text{quartz-water}}$  expression of Clayton et al. (1971) using this new value. The recalculated expression is:

$$10^3 \ln \alpha = 3.38 (10^6 T^{-2}) - 2.90 \quad (200\text{-}500^\circ\text{C})$$

Because a detailed error analysis has been carried out on the Matsuhisa et al. (1979)  $\Delta_{\text{quartz-water}}$ , this reported expression is used in subsequent calculations, where Q, W, C and M correspond to quartz, water, chlorite and muscovite respectively:

$$\begin{aligned} \Delta_{\text{Q-C}} &= (1.69)(\Delta_{\text{Q-W}}) - (\Delta_{\text{M-W}}) \\ &= (1.69)(0.96T + 0.58) \\ &= 1.62T + 0.98 \end{aligned}$$

An error on  $\Delta_{\text{quartz-chlorite}}$  can be calculated from the previously established errors on the  $\Delta_{\text{quartz-water}}$  and

$\Delta$  muscovite-water expressions:

$$\begin{aligned}\sigma^2_{Q-C} &= \sigma^2_{Q-W} + \sigma^2_{M-W} \\ &= (0.50)^2 + (0.34)^2 \\ &= 0.37\end{aligned}$$

or

$$\sigma_{Q-C} = 0.60\text{‰ at } 500^\circ\text{C}.$$

The  $\Delta$  chlorite-water is calculated from  $\Delta$  quartz-water of Matsuhisa et al. (1979) as follows:

$$\begin{aligned}\Delta_{C-W} &= \Delta_{Q-W} - \Delta_{Q-C} \\ &= (3.34T - 3.31) - (1.62T + 0.98) \\ &= 1.72T - 4.29.\end{aligned}$$

The uncertainty on  $\Delta$  chlorite-water is determined from the known errors on  $\Delta$  quartz-water and  $\Delta$  quartz-chlorite as follows:

$$\begin{aligned}\sigma^2_{C-W} &= \sigma^2_{Q-W} + \sigma^2_{Q-C} \\ &= (0.50)^2 + (0.60)^2 \\ &= 0.61\end{aligned}$$

or

$$\sigma_{C-W} = 0.78\text{‰ at } 500^\circ\text{C}.$$

Listed in Table 6-6 (Row A) are the other calculated errors for  $\Delta$  chlorite-water including their effect on a temperature uncertainty. A set of calculations have been carried out assuming a routine analytical error of  $\pm 0.2\text{‰}$  on a  $\delta$ -determination to illustrate the minimum cumulative temperature error based on this approximate error analysis (Row D).

This analysis for  $\Delta$  chlorite-water only yields a minimum error on  $\Delta$  because some of the data required to

perform a more rigorous analysis were not reported by Wenner and Taylor (1972). However, the exercise serves to illustrate the order of magnitude for the cumulative error on  $\Delta_{\text{chlorite-water}}$ .

#### 6.4.3. Linearly combined isotope fractionation expressions

The cumulative sum of errors for linearly combined mineral-mineral isotope fractionation expressions are listed on Table 6-7. They were derived by summing the squares of the minimum error on  $\Delta$  for each of the two expressions used. For example, the minimum experimental and curve-fitting error on the  $\Delta$  for  $\Delta_{\text{quartz-calcite}}$  calculated using the  $\Delta_{\text{quartz-water}}$  expression from Matsuhisa et al. (1979) and  $\Delta_{\text{calcite-water}}$  of O'Neil et al. (1969) at 500°C is:

$$\begin{aligned}\sigma^2_{Q-C} &= \sigma^2_{Q-W} + \sigma^2_{C-W} \\ &= (0.50)^2 + (0.35)^2 \\ &= 0.37\end{aligned}$$

or

$$\sigma_{Q-C} = 0.61\%$$

The corresponding minimum uncertainty in temperature is also indicated. Note that this analysis has not included an estimate of analytical error, unlike the error analysis presented in Table 6-6. This type of calculation will be reported as required when actual data determined for this thesis are discussed.

TABLE 6-7: Estimation of the minimum cumulative error on  $\Delta$   
and corresponding temperature uncertainty attributed  
to experimental and curve fitting errors.

| Expression         | Function     | Minimum Error on $\Delta$<br>(Temperature error at<br>300, 400, 500°C) |               |                |
|--------------------|--------------|------------------------------------------------------------------------|---------------|----------------|
|                    |              |                                                                        |               |                |
| Quartz-muscovite   | $0.96T+0.58$ | 0.78<br>(76)                                                           | 0.67<br>(106) | 0.60<br>(144)  |
| Quartz-calcite     | $0.56T-0.42$ | 0.78<br>(131)                                                          | 0.67<br>(182) | 0.61<br>(252)  |
| Quartz-dolomite    | $0.11T-0.02$ | 0.79<br>(676)                                                          | 0.67<br>(928) | 0.62<br>(1302) |
| Dolomite-muscovite | $0.85T+1.00$ | 0.64<br>(71)                                                           | 0.54<br>(97)  | 0.50<br>(136)  |
| Quartz-chlorite    | $1.62T+0.98$ | 1.01<br>(159)                                                          | 0.87<br>(82)  | 0.81<br>(115)  |
| Dolomite-chlorite  | $1.51T+1.40$ | 0.91<br>(57)                                                           | 0.78<br>(79)  | 0.73<br>(112)  |
| Calcite-chlorite   | $1.06T+1.40$ | 0.90<br>(80)                                                           | 0.78<br>(112) | 0.73<br>(159)  |

Expressions used are listed table 6-3. See table 6-6 for error analysis.

Linearly combined quartz-mineral expressions are based on the Matsuhisa *et al.* (1979) quartz-water expression.

## 7. Oxygen Isotopic Characteristics Of Quartz Vein Systems

It is possible to calculate the temperature at which a mineral assemblage precipitated in a vein and the wallrock if the minerals all coprecipitated and if the  $\delta^{18}\text{O}$ -values of the coprecipitated minerals is known. Previous oxygen isotopic studies in the Timmins area (Kerrick and Fryer, 1979; Kerrich and Hodder, 1982) attempted to address these questions using sample material from the Dome and Aunor Mines. Their data are also incorporated into this study for comparative purposes and to broaden the data base.

Before considering the oxygen isotope data, some underlying assumptions behind the application of oxygen isotope geothermometry must be emphasized. If isotope geothermometry is to be used to calculate the temperature at which a particular vein-filling assemblage formed, the vein-filling phases must have coprecipitated in isotopic equilibrium with each other and the hydrothermal fluid. Further, those minerals must have retained their initial oxygen isotopic values. If the minerals did not coprecipitate, they must have all subsequently undergone equilibrium oxygen isotope exchange during a later hydrothermal event. In this later case, the temperature obtained by isotope geothermometry describes the hydrothermal event during which the equilibrium isotope exchange took place and not necessarily the temperature at



which the vein formed. If the precipitation temperature of a specific mineral (such as gold) is sought, then it must be demonstrated that the minerals used for the isotope geothermometry coprecipitated with gold or that the minerals underwent oxygen isotope re-equilibration during the gold precipitation event.

### 7.1. Equilibrium Mineral Assemblages

Regarding the contemporaneity of the silicate and carbonate phases in typical quartz veins from the Timmins area, evidence was presented in Section 4.4.2 to indicate that the minerals in the quartz veins (Table 4-6; gold, albite, quartz, dolomite, calcite and chlorite-white mica) do not represent a coprecipitated assemblage. Additional, independent evidence in support of this observation is offered by Boyle (1979) and Ebbutt (1948), who demonstrated that gold in Archean-aged quartz veins from many different deposits, often occupies fractures which cross cut several phases, including quartz; hence, in many Archean quartz vein systems the precipitation of gold postdated the precipitation of some quartz. This is an important fact because quartz is the most voluminous mineral in the veins. In all oxygen isotope studies of Archean quartz veins from the Abitibi Greenstone Belt (c.f. Kerrich and Hodder, 1982), the oxygen isotope values of vein quartz were used to calculate a temperature inferred to represent that at which

gold precipitated. The observations regarding the temporal relationship between the precipitation of gold and the other vein minerals imply that the derived temperatures, calculated using the oxygen isotope systematics of coexisting quartz-white mica-chlorite-carbonate assemblages, may not represent either the temperature of vein formation or of gold precipitation because these phases did not coprecipitate.

This intent of the first part of this chapter is to test the hypothesis that the minerals in the quartz veins did not coprecipitate. This hypothesis is evaluated using the the oxygen isotopic characteristics of the silicate and carbonate minerals collected from several vein systems in the Porcupine camp.

#### 7.1.1. Equilibrium Tests

Two approaches have been used to test for oxygen isotope equilibrium in the quartz veins. The first involves the calculation of a temperature using the  $\delta^{18}\text{O}$ -values of two coexisting minerals, assuming that they had coprecipitated and have retained their initial isotopic ratios. For this approach, the following criteria, considered collectively, serve as a test for isotopic equilibrium within the vein mineral system: 1) the calculated temperature must be geologically reasonable; 2) all possible combinations of mineral pairs should yield

nearly identical temperatures; 3) the calculated  $\delta^{18}\text{O}$  of the water from which each of the minerals precipitated should be nearly identical. If differences are observed in points "2" and "3" above, they must be accommodated by the experimental uncertainty in the mineral-water isotope fractions. Use of this approach presumes that the intermineral textures, indicative of disequilibrium, discussed in Chapter 4.4.1, have been incorrectly interpreted. An alternative test for isotopic equilibrium involves the manipulation of mineral triplets to determination if they are isotopically concordant.

The oxygen isotope data for several vein systems from the Timmins area are listed in Table 7-1. For these systems the general sequence of  $^{18}\text{O}$ -enrichment is  $\delta_{\text{quartz}} > \delta_{\text{dolomite}} > \delta_{\text{calcite}} > \delta_{\text{chlorite}}$ , which is consistent with that sequence generally observed in rock systems (Taylor, 1968; Garlick and Epstein, 1967). No temperatures can be calculated utilizing the  $\Delta_{\text{quartz-dolomite}}$  fractionation because oxygen isotope fractionation between these two minerals is relatively insensitive to temperature (Table 6-3).

#### 7.1.1.1. Isotopic equilibrium assumed

Considering the Faymar data (Table 7-1), the calculated temperatures range from  $416 \pm 125^\circ\text{C}$  (Fa-10; calcite-chlorite) to  $244 \pm 95^\circ\text{C}$  (Fa-13; quartz-calcite).

TABLE 7-1: Oxygen isotope geochemistry of some quartz vein systems from the Timmins Area.

| Mining<br>Property   | Sample<br>Number | $\delta^{18}\text{O}$ Mineral<br>(‰) | $\alpha_{\text{A-B}}$ | Temperature Calculation |          |          |           | CALCULATED(1)<br>$\delta^{18}\text{O}$ WATER |       |       |       |
|----------------------|------------------|--------------------------------------|-----------------------|-------------------------|----------|----------|-----------|----------------------------------------------|-------|-------|-------|
|                      |                  |                                      |                       | Qts-chl                 | Qts-C    | D-Chl    | C-Chl     | Qts-chl                                      | Qts-C | C-Chl | D-Chl |
| Faymar               | Fa-10            | 10.70 $\pm$ 0.05 (Q)                 | 1.69 (Q-C)            | 338                     | 242      | --       | 416       | 5.1                                          | 1.4   | 6.0   | --    |
|                      |                  | 9.01 (C)                             | 3.32 (Q-chl)          | $\pm$ 40                | $\pm$ 87 | --       | $\pm$ 123 | --                                           | --    | --    | --    |
|                      |                  | 5.38 (chl)                           | 3.63 (C-chl)          | --                      | --       | --       | --        | --                                           | --    | --    | --    |
|                      | Fa-13            | 11.04 $\pm$ 0.30 (Q)                 | 1.65 (Q-C)            | 253                     | 244      | --       | 257       | 2.3                                          | 1.9   | 2.4   | --    |
|                      |                  | 9.37 (C)                             | 6.84 (Q-chl)          | $\pm$ 37                | $\pm$ 95 | --       | $\pm$ 74  | --                                           | --    | --    | --    |
|                      |                  | 4.20 $\pm$ 0.47 (chl)                | 5.14 (C-chl)          | --                      | --       | --       | --        | --                                           | --    | --    | --    |
|                      | Fa-14            | 10.60 $\pm$ 0.44 (Q)                 | 1.46 (Q-C)            | --                      | 273      | --       | --        | --                                           | 2.7   | --    | --    |
|                      |                  | 9.14 (C)                             | --                    | $\pm$ 120               | --       | --       | --        | --                                           | --    | --    | --    |
| Duval<br>south vein  |                  | 10.78 $\pm$ 0.32 (Q)                 | 1.48 (Q-D)            | --                      | --       | --       | --        | --                                           | --    | --    | --    |
|                      |                  | 9.30 (D)                             | --                    | --                      | --       | --       | --        | --                                           | --    | --    | --    |
| Carshaw              | Car-143          | 13.14 $\pm$ 0.26 (Q)                 | 2.64 (Q-D)            | 200                     | --       | 329      | --        | 1.5                                          | --    | --    | 4.5   |
|                      |                  | 10.50 (D)                            | 5.37 (D-chl)          | $\pm$ 26                | --       | $\pm$ 63 | --        | --                                           | --    | --    | --    |
|                      |                  | 4.93 $\pm$ 0.45 (chl)                | 8.21 (Q-chl)          | --                      | --       | --       | --        | --                                           | --    | --    | --    |
| Malga                | Car-147          | 11.44 $\pm$ 0.11 (Q)                 | 6.28 (Q-chl)          | 280                     | --       | --       | --        | 3.8                                          | --    | --    | --    |
|                      |                  | 5.16 $\pm$ 0.98 (chl)                | --                    | $\pm$ 60                | --       | --       | --        | --                                           | --    | --    | --    |
| Beaumont             |                  | 13.53 $\pm$ 0.32 (Q)                 | 1.29 (Q-D)            | --                      | --       | --       | --        | --                                           | --    | --    | --    |
|                      |                  | 12.25 $\pm$ 0.09 (D)                 | --                    | --                      | --       | --       | --        | --                                           | --    | --    | --    |
| McNameey             |                  | 13.16 (Q)                            | 0.16 (Q-D)            | --                      | --       | --       | --        | --                                           | --    | --    | --    |
|                      |                  | 13.00 $\pm$ 0.43 (D)                 | --                    | --                      | --       | --       | --        | --                                           | --    | --    | --    |
| Kinch                |                  | 12.73 $\pm$ 0.18 (Q)                 | 1.15 (Q-D)            | --                      | --       | --       | --        | --                                           | --    | --    | --    |
|                      |                  | 11.58 $\pm$ 0.12 (D)                 | --                    | --                      | --       | --       | --        | --                                           | --    | --    | --    |
| Dobell               |                  | 13.14 (Q)                            | 1.48 (Q-D)            | --                      | --       | --       | --        | --                                           | --    | --    | --    |
|                      |                  | 11.66 (D)                            | --                    | --                      | --       | --       | --        | --                                           | --    | --    | --    |
| Hollinger<br>55 Vein |                  | 14.02 (Q)                            | 2.01 (Q-D)            | --                      | --       | --       | --        | --                                           | --    | --    | --    |
|                      |                  | 12.02 (D)                            | --                    | --                      | --       | --       | --        | --                                           | --    | --    | --    |
| 68W Vein             |                  | 14.90 (Q)                            | 0.10 (Q-D)            | --                      | --       | --       | --        | --                                           | --    | --    | --    |
|                      |                  | 14.80 (D)                            | --                    | --                      | --       | --       | --        | --                                           | --    | --    | --    |
| 68E Vein             |                  | 15.10 (Q)                            | 1.00 (Q-D)            | --                      | --       | --       | --        | --                                           | --    | --    | --    |
|                      |                  | 14.10 (D)                            | --                    | --                      | --       | --       | --        | --                                           | --    | --    | --    |

Mineral Abbreviations:  
Qts-quartz; C-calcite; D-dolomite; Chl-chlorite

NOTE:  
O of water calculated using the temperature deduced from the indicated mineral(1)-mineral(2) fractionation and substituting this temperature into the mineral(1)-water fractionation expression Table 6-3 to obtain a value for delta ( ).  
Temperature error represents the sum of the experimental (Table 6-7) and laboratory errors. Where only 1 determination was made, an uncertainty of  $\pm 0.2$  was used for the error calculation.

The mineral-mineral geothermometers incorporating the chlorite analysis in sample Fa-10 consistently yield high temperatures. If this chlorite analysis is not used in any of the isotopic calculations, the remaining data cluster in the 240°-280°C range. The one sigma standard deviation on this data cluster include temperatures from 160° to approximately 340°C. The clustering of these data, regardless of the mineral pair used, is consistent with the conjecture that oxygen isotopic equilibrium exists in the data set (ignoring the chlorite analysis in Fa-10). The three Carshaw/Malga data yield different temperatures. The highest temperature (329 +/-65°C) is obtained using the dolomite-chlorite geothermometer (Table 7-1). The two quartz-chlorite data sets yield lower temperatures (200 +/-25°C; Car-143 and 280 +/-60°C; Car-147). Note that the two quartz-chlorite data overlap within the minimum error assigned to their temperatures.

All calculated temperatures are geologically reasonable and hence are consistent with the conjecture that the mineral assemblages attained isotopic equilibrium. However, if oxygen isotopic equilibrium was achieved and preserved, then all possible geothermometers should should yield similar temperatures. Considering the Faymar and Carshaw data, where several different minerals were analysed, it is apparent that this is true of the Faymar data, if the chlorite analysis from Fa-10 is omitted. The

temperatures obtained using different mineral pairs from the Carshaw/Malga system are variable. Now, there is no a priori reason why the chlorite analysis from Fa-10 should be ignored. If it is included in the calculations, the different geothermometers in the Faymar data set also yield different temperatures.

Additional evidence pointing to inconsistency within the Faymar and Carshaw data sets comes from the variation in the calculated  $\delta^{18}\text{O}$ -values of the water from which the different minerals precipitated (Table 7-1), which range from +1.9 to +6.0‰ and +1.5 to +4.5‰ respectively.

That different geothermometers yield different temperatures is not unique to my small data suite. Compiled in Table 7-2 is a summary of recent oxygen isotope data for other Archean gold-quartz veins from the Timmins and Yellowknife areas reported by Kerrich and Hodder (1982). From these data the quartz-sericite, quartz-chlorite and sericite-chlorite fractionations (Table 7-2; Column C) and corresponding temperatures (Table 7-2; Columns D, E and F) are calculated. The temperatures reported in Column F (Table 7-2; Kerrich and Hodder, 1982) were calculated using the preliminary  $\Delta_{\text{quartz-water}}$  and  $\Delta_{\text{muscovite-water}}$  oxygen isotope fractionation expressions determined by Clayton et al. (1972) and O'Neil and Taylor (1969) respectively which were personally communicated to Wenner and Taylor (1971). The temperatures reported in Columns D and E (Table 7-2)

TABLE 7-2: Oxygen isotope geothermometry for some quartz veins from the Timmins and Yellowknife areas.

| Area        | Mine      | (A)                   | (B)                   | (C)               | (D)              | (E)      | (F)         |
|-------------|-----------|-----------------------|-----------------------|-------------------|------------------|----------|-------------|
|             |           | $\delta^{18}\text{O}$ | $\delta^{18}\text{O}$ | $10^3 \ln \alpha$ | Temperatures(°C) |          |             |
| =====       |           |                       |                       |                   |                  |          |             |
|             |           | Quartz                | Mineral               | (A-B)             | Calc.(1)         | Calc.(2) | Reported(3) |
| =====       |           |                       |                       |                   |                  |          |             |
| Yellowknife |           |                       |                       |                   |                  |          |             |
|             | Campbell  | 12.53                 | 6.58(CH)              | 5.89              | 359              | 301      | 440         |
|             |           | 11.50                 | 5.97(CH)              | 5.48              | 393              | 327      | 480         |
|             |           | 11.59                 | 7.03(M)               | 4.52              | 259              | 221      | 320         |
|             | Con       | 11.50                 | 5.97(CH)              | 5.48              | 393              | 327      | 480         |
| -----       |           |                       |                       |                   |                  |          |             |
| Timmins     |           |                       |                       |                   |                  |          |             |
|             | Dome      | 14.74                 | 10.98(M)              | 3.71              | 333              | 281      | --          |
|             |           | 14.41                 | 11.28(M)              | 3.09              | 417              | 345      | --          |
|             |           | 14.37                 | 10.78(M)              | 3.55              | 352              | 296      | 430         |
|             |           | 14.52                 | 10.54(M)              | 3.93              | 310              | 262      | 380         |
|             |           | 14.19                 | 8.05(CH)              | 6.07              | 347              | 291      | 420         |
|             |           | 15.09                 | 9.21(CH)              | 5.81              | 366              | 306      | 440         |
|             |           | 15.17                 | 9.38(CH)              | 5.72              | 373              | 312      | 450         |
|             |           | 14.53                 | 8.99(CH)              | 5.48              | 393              | 327      | 480         |
|             |           | 14.87                 | 9.31(CH)              | 5.49              | 392              | 326      | 480         |
|             | McIntyre  | 15.02                 | 10.62(M)              | 4.34              | 273              | 232      | 340         |
|             |           | 14.81                 | 10.80(M)              | 3.96              | 307              | 260      | 380         |
|             | Paymaster | 14.87                 | 9.17(CH)              | 5.63              | 380              | 317      | 460         |
| =====       |           |                       |                       |                   |                  |          |             |

## Averaged Data From Each Camp

|           | Yellowknife   | Timmins       |
|-----------|---------------|---------------|
| Quartz    | 11.78 +/-0.50 | 14.72 +/-0.31 |
| Muscovite | 7.03          | 10.83 +/-0.27 |
| Chlorite  | 6.17 +/-0.35  | 9.02 +/-0.49  |

| =====  |      |      |      |      |      |      |
|--------|------|------|------|------|------|------|
| Mean   | YN   | T(2) | TIM  | T(2) | DOM  | T(2) |
| A-B(G) |      |      |      |      |      |      |
| Q-M    | 4.75 | 207  | 3.82 | 371  | 4.71 | 209  |
| Q-Chl  | 5.61 | 320  | 5.63 | 317  | 5.56 | 322  |
| M-Chl  | 0.86 | 925  | 1.79 | 416  | 0.85 | 938  |
| =====  |      |      |      |      |      |      |

All raw data in columns A,B,C, and F come from Kerrich and Hodder (1981).

Column G: Obtained using  $\Delta AB = 10^3 \ln \alpha (AB)$ Temperature Calculations: 1) Using recast  $\Delta$ Quartz-water expression of Clayton et al.(1972), listed in Table 6-3.2) Using Matsuhisa et al.(1979)  $\Delta$ Quartz-water expression.  
 $\Delta$ Quartz-chlorite=(1.69)(( $\Delta$ Quartz-water)-( $\Delta$ Muscovite-water)), from Wenner and Taylor (1971).

3) Temperatures reported by Kerrich and Hodder (1981).

Abbreviations: M-Muscovite; CH-Chlorite; YN-Yellowknife; TIM-Timmins  
Q-Quartz

were obtained by processing the same isotopic data reported by Kerrich and Hodder (1982; Table 7-2, Columns A and B) with the more recently revised Clayton et al. (1972)

$\Delta_{\text{quartz-water}}$  (column D) and Matsuhisa et al. (1979)

$\Delta_{\text{quartz-water}}$  (column E) expressions, linearly combined with the  $\Delta_{\text{muscovite-water}}$  (O'Neil and Taylor, 1969) expression:

$$\Delta_{\text{quartz-chlorite}} = 1.69[(\Delta_{\text{Quartz-water}}) - (\Delta_{\text{muscovite-water}})]$$

$$\Delta_{\text{quartz-muscovite}} = (\Delta_{\text{Quartz-water}}) - (\Delta_{\text{muscovite-water}})$$

and

$$\Delta_{\text{muscovite-chlorite}} = (\Delta_{\text{Quartz-chlorite}}) - (\Delta_{\text{Quartz-muscovite}})$$

The temperatures reported in Columns D and E (Table 7-2) are considered to be more accurate because they are based the best available experimental oxygen isotope partition functions, listed by by Clayton (1981). Ideally, the temperatures reported in Columns D and E should be identical. That they differ reflects the effect of minor differences in the experimentally derived partition function for oxygen isotopes between quartz and water. For the following discussions, those oxygen isotope fractionation expressions based on the Matsuhisa et al. (1979)



$\Delta_{\text{quartz-water}}$  system will be considered (eg. Column E, Table 7-2).

For the data set reported by Kerrich and Hodder (1982), it is apparent that different temperatures are calculated using different geothermometers, yet the minerals analysed came from the same vein system. This lack of consistency between calculated temperatures, is characteristic of: 1) oxygen isotope disequilibrium in the vein systems; or 2) inaccurate mineral-water oxygen isotope fractionation expressions.

It may be appealing to cite the relatively small variance of the  $\Delta A-B$  (Table 7-2) as evidence of isotopic equilibrium and the precipitation of the minerals at a relatively constant temperature from a fluid of constant  $\delta^{18}\text{O}$ . For this scenario the difference in calculated temperatures for different geothermometers must reflect the inherent inaccuracy of the isotope fractionation expressions. An assessment of this uncertainty was given in Tables 6-4 and 6-5. In general, the geothermometers are associated with a temperature uncertainty of  $\pm 100^\circ\text{C}$  at  $400^\circ\text{C}$ .

Thus, considering only the mineral-mineral oxygen isotope fractionation relationships, it is not possible to unequivocally prove or disprove that oxygen isotope equilibrium existed in the quartz vein systems because the inconsistency in calculated temperatures could reflect

either isotope disequilibrium or uncertainty associated with the isotope partition function.

#### 7.1.1.2. Concordancy test

A second more definitive test of isotope equilibrium involves mineral triplets which are tested for isotope concordancy. The  $\delta$ -value of each mineral is determined and then a plot of  $\Delta_{AB}$  vs.  $\Delta_{BC}$  is constructed. On such a diagram (eg. Fig. 7-1), the data points must fall along an empirically or theoretically deduced equilibrium line constructed using the intermineral oxygen isotope fractionation expressions (Table 6-3), since each  $\Delta$  is a function of temperature (Clayton and Epstein, 1961). Departures from the expected concordancy line are indications of disequilibrium, whereas adherence to a smooth curve is not in itself a sufficient test of equilibrium if the temperature dependencies of  $\Delta_{AB}$  and  $\Delta_{BC}$  are not independently known (Clayton, 1981). Note that certain disequilibrium conditions can produce systematic relationships on concordancy plots (Clayton, 1981). This may occur if partial isotopic readjustment has taken place in a systematic manner. Examples of this are given by Clayton (1981) and Deines (1977) and will be discussed later in this Chapter.

Initially, data published by Kerrich and Hodder (1982) for Archean gold veins systems in the Timmins area

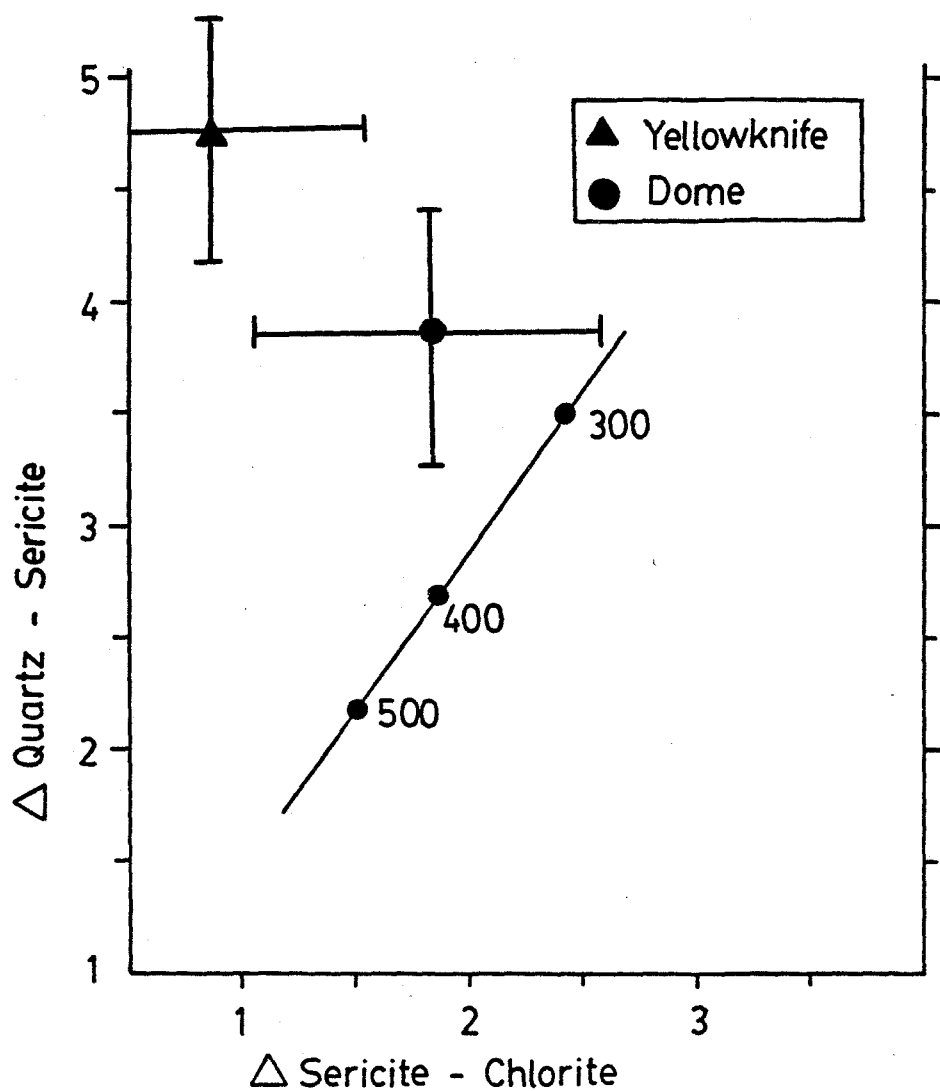


Figure 7-1: Quartz-sericite-chlorite oxygen isotope concordancy plot for samples from the Yellowknife and Dome Mine (Timmins) areas. Data published by Kerrich and Fryer (1979).

and elsewhere were plotted to test for isotope concordancy. For these data, where mineral triplets from a single hand sample were not available, the mean of all quartz, sericite and chlorite analyses from a mine (Dome Mine) or mine level (Yellowknife data) were used to obtain a triplet point. This approach is less satisfactory than having a triplet set from one hand sample; however, the relatively small variance of  $\delta$ -values for a given mineral such as quartz (better than 0.41) on a mine scale justifies this approach, at least to a first approximation. By treating the data in this way, it is assumed that the precipitation of a given mineral was widespread in a mine and took place from a fluid having a constant  $\delta^{18}\text{O}$  value. It does not necessarily assume that all minerals coprecipitated.

The quartz-sericite-chlorite concordancy plot (Fig. 7-1) was constructed using the  $\Delta_{\text{quartz-water}}$ ,  $\Delta_{\text{sericite-water}}$ , and the recast  $\Delta_{\text{chlorite-water}}$  expressions of Matsuhisa et al. (1979) and O'Neil and Taylor (1969) respectively (Table 6-3). The Dome and Yellowknife data depart from the constructed concordancy line (Fig. 7-1). This observation is consistent with: 1) oxygen isotope disequilibrium within the data sets; or 2) use of inaccurate geothermometers.

Plotted on Figure 7-2 is the one datum from the Carshaw Mine on a quartz-dolomite-chlorite concordancy diagram. The datum plots significantly off the expected

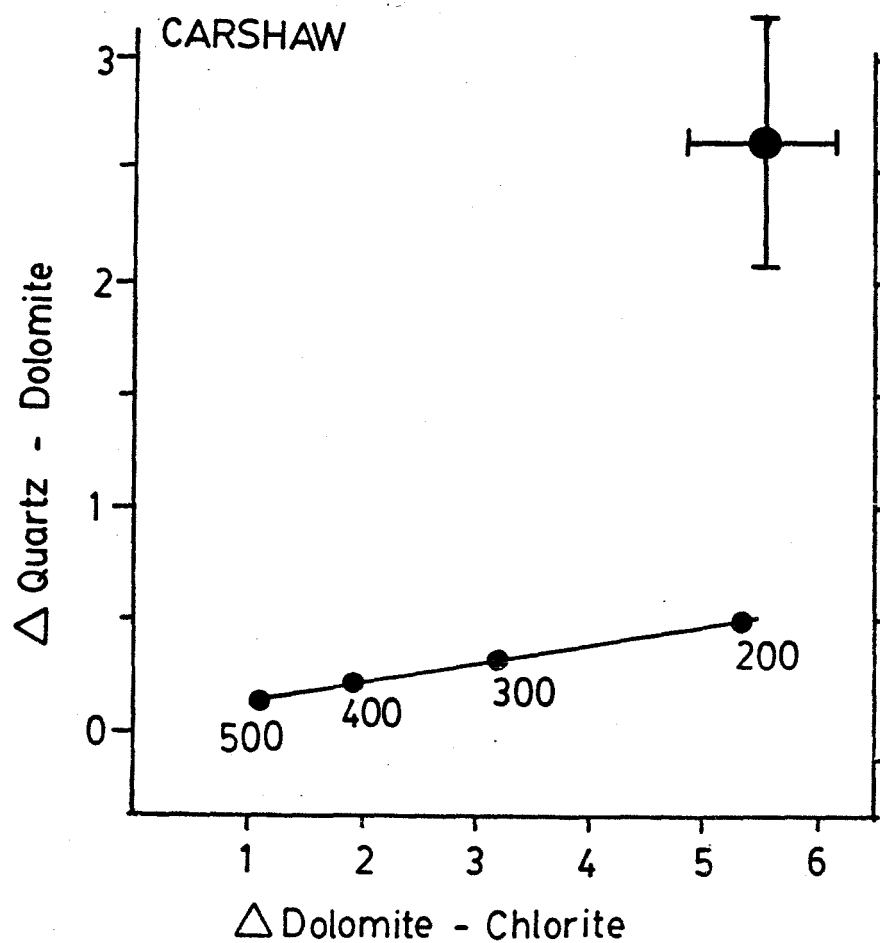


Figure 7-2: Quartz-dolomite-chlorite oxygen isotope concordancy plot for one sample from the Carshaw Mine.

concordancy line. One of the two data from the Faymar vein system (Fa-10) falls off the expected quartz-calcite-chlorite concordancy line (Fig. 7-3), while sample Fa-13 falls on the concordancy line.

#### 7.1.2. Discussion of the equilibrium tests

The conclusions drawn by considering the concordancy plots and the mineral pair geothermometers are equivocal. The evidence presented (particularly the lack of agreement between geothermometers) is consistent with the following two alternatives: 1) oxygen isotope equilibrium was not attained or preserved in the vein systems; or 2) the difference between different geothermometers reflects the uncertainty with which the partitioning of oxygen isotopes between certain silicate and carbonate minerals is known. That some  $\Delta_{\text{mineral-water}}$  oxygen isotope fractionation expressions are not well constrained is certainly true, particularly for the chlorite-water system. If chlorite is deemed unsuitable for oxygen isotope geothermometry, then quartz, sericite, and carbonates remain as the only minerals present in the quartz veins from the Timmins area which can be used for geothermometry. Unfortunately, insufficient amounts of sericite were present in the quartz veins to acquire quartz-sericite-carbonate triplets with which to test for oxygen isotope equilibrium.

It is attractive to view the relatively tight

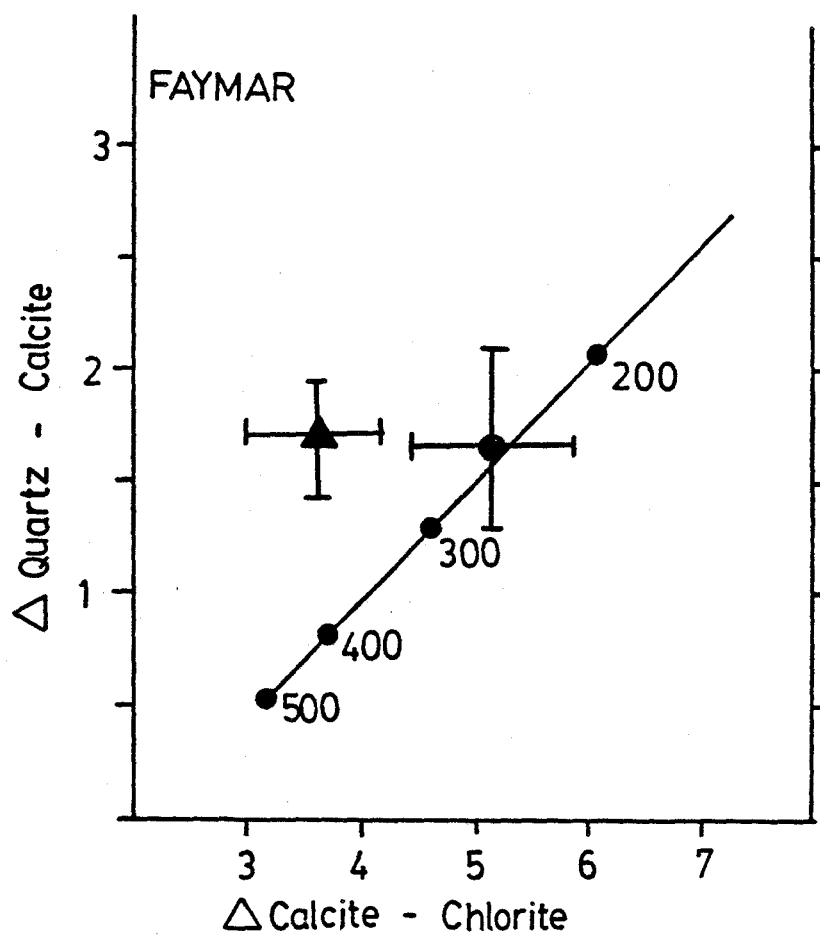


Figure 7-3: Quartz-calcite-chlorite oxygen isotope concordancy plot for samples from the Faymar Mine.

clustering of  $\Delta_{\text{quartz-muscovite}}$  and  $\Delta_{\text{quartz-chlorite}}$  values from the Timmins vein systems as evidence in favour of isotopic equilibrium within the data set. However, Clayton (1981) has cited cases where a tight clustering of data can result from systematic disruptive processes. For example, in a study of metamorphosed clastic sediments in the Iltay Dalradians of southwest Scotland, Kerrich et al. (1977) found that five of eight mineral triplet data fell on or close to the expected quartz-muscovite-iron oxide concordancy line. The authors concluded that the five samples represented equilibrium assemblages. However, for these data, the  $\Delta_{\text{quartz-muscovite}}$  geothermometer yields temperatures that are 100° to 200°C lower than the  $\Delta_{\text{quartz-hematite}}$  geothermometer. The  $\Delta_{\text{quartz-muscovite}}$  fractionations are low by 1-2‰. Regarding these data, Clayton (1981) concludes that these muscovite samples must have been disturbed in a fairly systematic way to produce what are really disequilibrium assemblages. For the Iltay Dalradian data set, the  $\delta$ -values of the muscovite average +9.67‰ with a variance of 0.55. The data define a relatively tight cluster with a variance that is similar to that of the quartz, sericite, and chlorite data from the Timmins quartz veins (c.f. Tables 7-1 and 7-2). Thus, coherence within a stable isotopic data array can be fortuitous, resulting from processes which systematically establish isotope disequilibrium between coexisting phases.



## 7.2. Summary Statement

The intent of this Chapter was to test the hypothesis that certain minerals (notably quartz, sericite, and chlorite) did not coprecipitate by assessing if oxygen isotopic equilibrium existed between the minerals. This hypothesis was formulated in Chapter 4 on the basis of intermineral textures from which it was concluded that the precipitation sequence of the vein minerals was complex and could not be described in a single precipitation event.

The following salient observations summarize the important textural and oxygen isotopic characteristics of the vein minerals which are relevant to the question of coprecipitation:

- 1) different isotope geothermometers yield significantly different calculated temperatures, which may reflect isotope disequilibrium or inaccuracy in some of the  $\Delta$ mineral-water oxygen isotope fractionation expressions (notably  $\Delta$ chlorite-water);

- 2) departures from quartz-sericite-chlorite, quartz-dolomite-chlorite and quartz-calcite-chlorite oxygen isotopic concordancy is consistent with oxygen isotope disequilibrium in the quartz veins;

- 3) intermineral textural relationships observed in thin section suggest that quartz, albite, dolomite, calcite and chlorite-sericite did not coprecipitate. Chlorite and sericite may have coprecipitated but few

examples of coexisting grains in mutual contact were found;

4) wallrock alteration assemblages adjacent to quartz veins support the interpretation that dolomite did not coprecipitate with either albite or chlorite because both silicate phases are destroyed by progressive carbonatization.

The oxygen isotopic data acquired from these veins cannot be interpreted unambiguously and thus, the isotopic data cannot unequivocally refute or support the contention that the vein minerals did not coprecipitate and now coexist in isotopic disequilibrium. Because the oxygen isotope systematics of the quartz vein minerals from the Timmins (and by implication in the Yellowknife) area are, at the very least, consistent with the hypothesis that the vein minerals do not now exist in oxygen isotope equilibrium (other alternate explanations are equally permissive), and on the weight of the petrographic data presented in Sections 4.4.1 to 4.4.4, I conclude that quartz, chlorite, muscovite, and the carbonate minerals did not all coprecipitate and that oxygen isotopic disequilibrium exists within the quartz vein system.

Based on this conclusion and the uncertainty in the geothermometers, it is proposed that the temperature of vein formation, wallrock alteration and gold precipitation cannot be deduced unambiguously using oxygen isotope geothermometry

for the vein systems considered in the Timmins area. Temperatures can be calculated using the oxygen isotope geothermometry, but identification of the thermal event(s) to which the temperatures apply is ambiguous.

### 7.3. $\delta^{18}\text{O}$ of Vein Quartz and Stratigraphic Position

Compiled in Table 7-3 are the  $\delta^{18}\text{O}$  values for vein quartz from several properties in the Timmins area. Fyon et al. (1982) reported a positive correlation between  $\delta^{18}\text{O}$  of vein quartz and stratigraphic position of the sample (Fig. 7-4). The  $\delta^{18}\text{O}$ -values of vein quartz average +11, +13.2 and +14.8‰ in Formation II, Deloro Group, Formation IV, Tisdale Group, and Formation V, Tisdale Group respectively. The overall range in  $\delta^{18}\text{O}$ -values for vein quartz is +10.5 to +15‰. Vein quartz from the most gold-rich deposits (Hollinger, Dome, Buffalo Ankerite Mines; Fig. 7-4) is more  $^{18}\text{O}$ -enriched with respect to vein quartz from the smaller gold deposits.

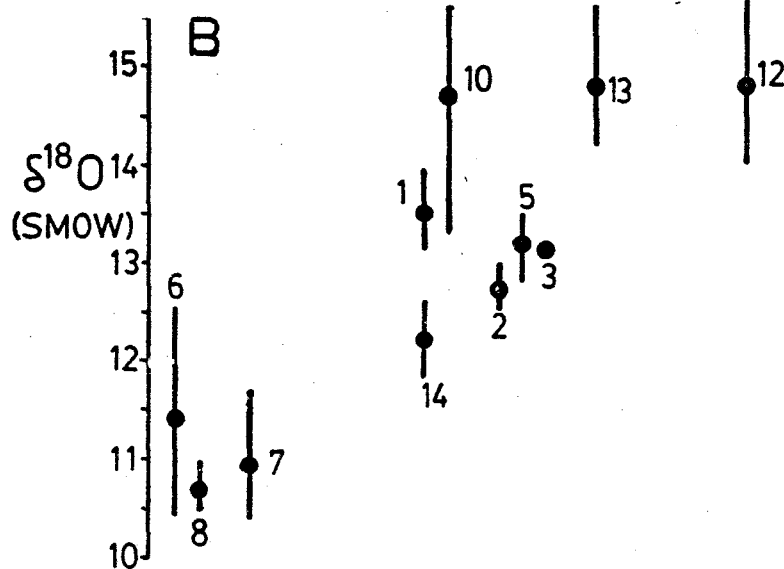
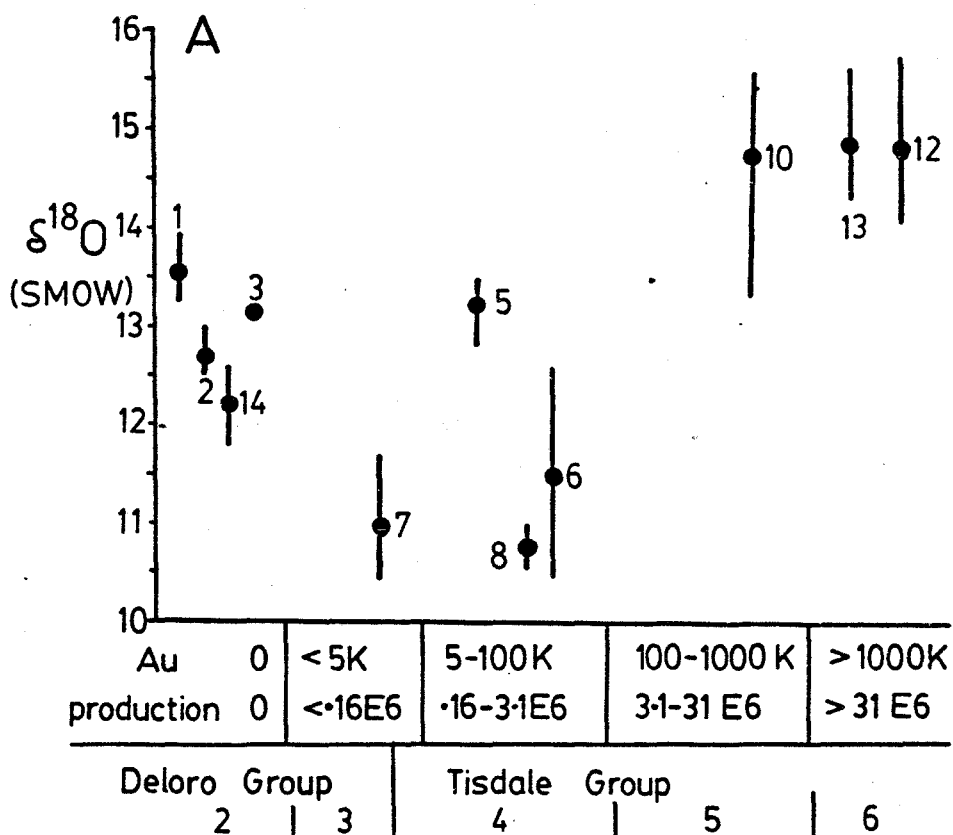
A similar correlation between stratigraphic position and the  $\delta^{18}\text{O}$  of the whole rock was previously noted by Beaty (1980) who attributed this covariation to decreasing reaction temperatures between a sea water-derived hydrothermal fluid and the rock with increasing stratigraphic height. It is not possible to distinguish whether the increasing  $\delta^{18}\text{O}$  of vein quartz identified here reflects: 1) decreasing precipitation temperatures; 2)

TABLE 7-3: Oxygen and carbon isotopic-values of hydrothermal ferrous dolomite and vein quartz  
Only the data for ferrous dolomite in the quartz veins or immediately adjacent in the wallrock is tabulated here, except for the Faymar Mine, where vein-hosted calcite is the only carbonate present.

| Mine<br>Property                       | Vein Carbonate<br>RHEAN |                        | Replacement<br>Carbonate |                          | Mineralogy            | $\delta^{18}\text{O}$<br>Vein<br>Quartz | Host<br>Rock<br>Formatio |
|----------------------------------------|-------------------------|------------------------|--------------------------|--------------------------|-----------------------|-----------------------------------------|--------------------------|
|                                        | $\delta^{13}\text{C}$   | $\delta^{18}\text{O}$  | $\delta^{13}\text{C}$    | $\delta^{18}\text{O}$    |                       |                                         |                          |
| Carshaw/Maige                          |                         |                        | -3.43<br>+/-0.31<br>n=31 | 10.76<br>+/-0.60<br>n=31 | Dolomite              | 11.36<br>+/-0.58<br>n=14                | II                       |
| Faymar                                 | -3.29<br>+/-0.14<br>n=3 | 9.0<br>+/-0.77<br>n=3  | --                       | --                       | Calcite               | 10.8<br>n=3                             | II                       |
| Porcupine Triumph                      | -4.87<br>+/-0.06<br>n=2 | 9.1<br>+/-0.3<br>n=2   | -4.14<br>+/-0.23<br>n=3  | 10.63<br>+/-0.25<br>n=3  | Dolomite              | --                                      | II                       |
| Duval<br>south vein                    | -4.60<br>n=1            | 9.3<br>n=1             | -3.99<br>n=2             | 9.63<br>n=2              | Dolomite              | 10.78<br>+/-0.32<br>n=4                 | II                       |
| glory hole                             | --                      | --                     | -4.19<br>n=2             | 9.21<br>n=2              |                       | 11.67<br>n=1                            |                          |
| Beaumont                               | --                      | --                     | -3.36<br>+/-0.41<br>n=14 | 12.79<br>+/-0.5<br>n=14  | Dolomite              | 13.31<br>+/-0.32<br>n=3                 | IV                       |
| Kinch                                  | --                      | --                     | -4.01<br>+/-0.29<br>n=8  | 11.58<br>+/-0.12<br>n=8  | Dolomite              | 12.73<br>+/-0.18<br>n=5                 | IV                       |
| Dobell                                 | --                      | --                     | -4.09<br>n=1             | 11.66<br>n=1             | Dolomite              | 13.14<br>n=1                            | IV                       |
| Canusa                                 | --                      | --                     | -3.04<br>n=2             | 12.09<br>n=2             | Dolomite              | --                                      | IV                       |
| Davidson-Tisdale                       | --                      | --                     | -3.07<br>+/-0.39<br>n=19 | 11.91<br>+/-0.70<br>n=19 | Dolomite              | --                                      | IV                       |
| Aunor                                  | -2.20<br>n=1            | 13.2<br>n=1            | -3.63<br>+/-0.43<br>n=13 | 12.56<br>+/-0.47<br>n=13 | Dolomite              | --                                      | IV                       |
| Armstrong<br>McGibbon                  |                         |                        | -3.1<br>+/-0.6<br>n=4    | 11.3<br>+/-0.3<br>n=4    | Dolomite              |                                         | IV                       |
| Crown<br>Chartered                     |                         |                        | -3.3<br>+/-0.4<br>n=2    | 11.3<br>+/-0.3<br>n=2    | Dolomite              |                                         | IV                       |
| Delnite                                | --                      | --                     | -2.91<br>+/-0.41<br>n=7  | 13.17<br>+/-0.50<br>n=7  | Dolomite              | --                                      | IV                       |
| Buffalo Ankerite                       | -3.60<br>+/-0.40<br>n=3 | 12.9<br>+/-0.1<br>n=3  | -3.2<br>+/-0.5<br>n=11   | 12.3<br>+/-0.6<br>n=11   | Dolomite              | 14.73<br>+/-1.03<br>n=6                 | IV                       |
| McInaney                               | -3.02<br>+/-0.72<br>n=3 | 13.0<br>+/-0.43<br>n=3 | -3.90<br>+/-0.52<br>n=10 | 12.66<br>+/-0.22<br>n=10 | Dolomite              | 13.16<br>+/-0.43<br>n=2                 | IV                       |
| Famous #1<br>(includes 35 vein)        | -1.9<br>+/-0.5<br>n=14  | 12.6<br>+/-0.2<br>n=14 | -1.97<br>+/-0.46<br>n=4  | 11.94<br>+/-0.6<br>n=4   | Dolomite              | --                                      | IV                       |
| North Whitney Mine                     |                         |                        | -1.73<br>+/-0.7<br>n=4   | 12.1<br>+/-0.3<br>n=4    |                       | 12.2<br>+/-0.37<br>n=2                  |                          |
| Wallinor                               | --                      | --                     | -2.42<br>+/-0.38<br>n=6  | 11.1<br>+/-0.3<br>n=6    | Dolomite<br>Magnesite | --                                      | IV                       |
| Dome Mine<br>(Kerrick and Fryer, 1979) |                         |                        |                          |                          |                       | 14.81<br>+/-0.35<br>n=47                | V                        |
| McIntyre                               |                         |                        | -1.1<br>+/-1.4<br>n=6    | 13.2<br>+/-0.4<br>n=6    | Dolomite              |                                         | V                        |
| Coniaurum                              |                         |                        | -1.6<br>+/-1.6<br>n=2    | 13.6<br>+/-0.9<br>n=2    | Dolomite              |                                         | IV, V                    |
| Hollinger<br>35 vein                   | -1.3<br>n=1             | 12.0<br>n=1            | -0.64<br>+/-0.46<br>n=17 | 12.66<br>+/-0.50<br>n=17 | Dolomite              | 14.02<br>n=1                            | V                        |
| 6RE vein                               | -0.7<br>+/-0.6<br>n=4   | 14.1<br>+/-0.7<br>n=4  | -0.37<br>+/-0.21<br>n=6  | 14.44<br>+/-0.33<br>n=4  | Dolomite              | 13.1<br>n=2                             | V                        |
| 6RW vein                               | -0.2<br>n=1             | 14.8<br>n=1            | +0.33<br>n=1             | 13.52<br>n=1             | Calcite               | 14.9<br>n=1                             | V                        |

Figure 7-4:  $\delta^{18}\text{O}$ -values of vein quartz expressed as a function of gold tenor of the property (7-4A) and stratigraphic position of the sample (7-7B). The mean and range of the data is indicated by a large dot and bar respectively. The property identification labels are: 1-Beaumont; 2-Kinch; 3-Dobell; 5-McEnaney; 6-Carshaw/Malga; 7-Duval; 8-Faymar; 10-Buffalo Ankerite; 12-Hollinger; 13-Dome; 14-North Whitney Mine. Dome data taken from Kerrich and Fryer (1979).

## Quartz Veins



uniform precipitation temperatures, but buffering of the  $\delta^{18}\text{O}$  of the hydrothermal fluids by the previously sea water-altered volcanic rocks; or 3) the influence of an  $^{18}\text{O}$ -enriched water (such as magmatic water).

The possibility that at least two hydrothermal fluids existed is postponed until Chapter 8-5 when the  $\delta^{18}\text{O}$  data for the hydrothermal dolomite and magnesite are considered.

#### 7.4. $\delta^{18}\text{O}$ and $\delta^{13}\text{C}$ of Vein and Wallrock Replacement Carbonate

Compiled in Table 7-3 are the oxygen and carbon isotopic values of hydrothermal ferroan dolomite and magnesite collected from properties in the Timmins area. A complete data list is included in Appendix-1. The only calcite reported in this table comes from the Faymar Mine veins where no ferroan dolomite is present. No intense carbonatization is exposed on surface at the Faymar. Calcite from the Intense Carbonate Alteration Facies was analysed, but these data are reported and discussed in chapter 8.2.2.1. They have not been included on Table 7-3. The reported isotopic values of the hydrothermal dolomite and/or magnesite represents the average  $\delta^{13}\text{C}$  value of samples taken across the Intense Carbonate Alteration Facies where dolomite or magnesite (in ultramafic rock) are the only carbonates present.

In general, the  $\delta^{13}\text{C}$  values of both vein and

replacement dolomites are very similar, although there is a tendency for the vein dolomites to be lighter by about 0.5‰. The similarity of these data is not surprising since the source of the hydrothermal fluid was the vein conduit and therefore, the vein and adjacent replacement ferroan carbonate precipitated from the same hydrothermal fluid.

More detailed consideration of the isotopic characteristics of the vein carbonate is deferred to Chapter 8 where these data are integrated into a discussion of the wallrock replacement carbonate.

#### 7.4.1. Covariation of quartz vein gold tenor with $\delta^{13}\text{C}$ and $\delta^{18}\text{O}$ of vein carbonate

Possible covariation between vein gold tenor,  $\delta^{13}\text{C}$  and  $\delta^{18}\text{O}$  of vein carbonate has been examined in the 51 vein, Pamour #1 Mine, where the gold grade is known to vary along strike (Fig. 7-5). Only ferroan dolomite that precipitated in the quartz vein was sampled; no wallrock replacement carbonate has been included. This study was initiated to determine if any isotopic characteristic of the vein carbonate correlated with gold tenor in the vein. Such a correlation could arise if gold precipitation resulted from a process which would simultaneously impart a distinctive isotopic signature to the precipitated dolomite. Precipitation in response to temperature decrease or fluid boiling would induce corresponding  $\delta^{18}\text{O}$  and  $\delta^{13}\text{C}$  shifts in the precipitated dolomite. Methane stabilization would



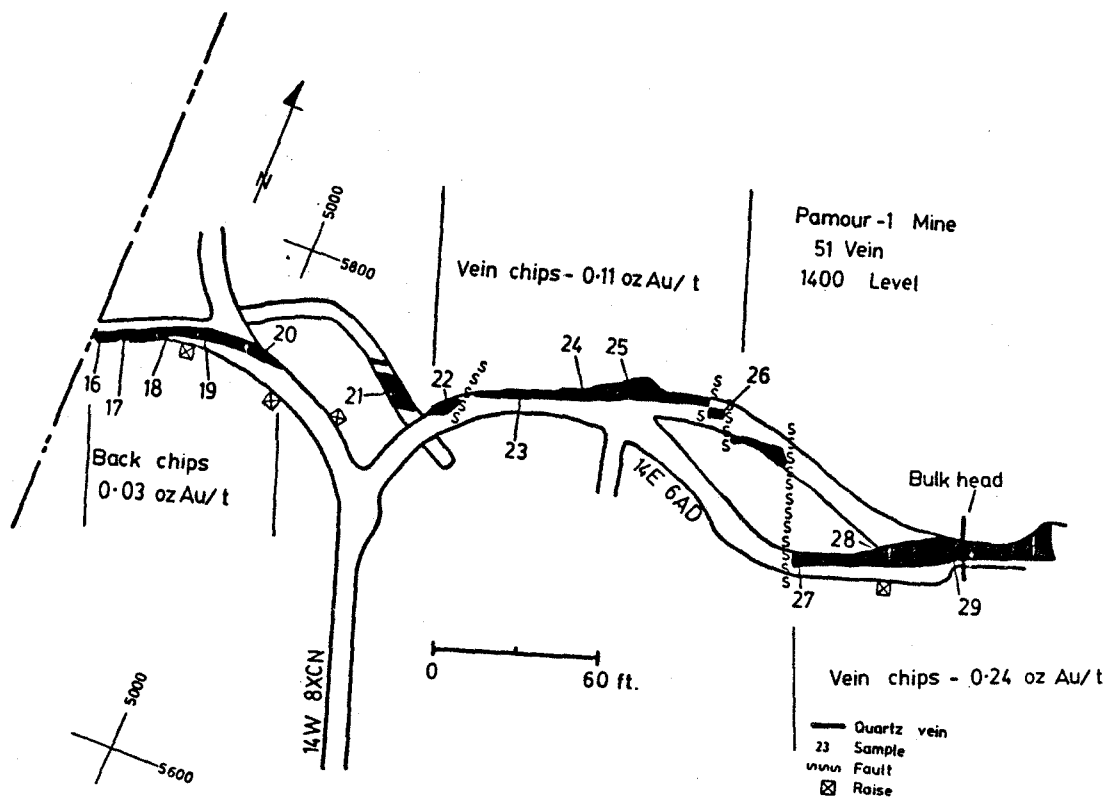


Figure 7-5: Simplified 1400 level plan showing the location of 51 vein, Pamour #1 Mine. Gold tenors increase from west to east.

produce  $^{13}\text{C}$ -enriched  $\text{CO}_2$  and hence would produce  $^{13}\text{C}$ -enriched dolomites.

No correlation exists between either  $\delta^{13}\text{C}$  or  $\delta^{18}\text{O}$  of the vein dolomite and gold tenor (Fig. 7-6). In fact, these isotopic variables are remarkably uniform along the 100 m of vein sampled, over the nearly ten fold increase in the gold tenor. Although it is conceivable that a gold precipitation mechanism was operative which did not affect the  $\delta^{13}\text{C}$  of the hydrothermal system, such as the immiscible separation of  $\text{CO}_2$  from the  $\text{CO}_2$ - $\text{H}_2\text{O}$  fluid, the lack of correlation of both  $\delta^{18}\text{O}$  and  $\delta^{13}\text{C}$  of the carbonate with gold tenor suggests that the gold and carbonate precipitation events were not contemporaneous. This lack of correlation is not surprising in light of the paragenetic and field textures described in Section 4.4.1 which suggest that gold may not have coprecipitated with quartz or dolomite in the vein.

#### 7.5 $\delta\text{D}$ and $\delta^{13}\text{C}$ of Fluid Inclusions From Vein Quartz

Before discussing these data some consideration is required of the extent to which the methodology of fluid extraction from the inclusion can affect the analytical data. As described in Section 4.4.3, the vein quartz is cut by many secondary fluid inclusion arrays. Because the inclusions were decrepitated from 5-7 grams of vein quartz, it is impossible to discriminate between different populations of fluid inclusions present in the vein quartz.

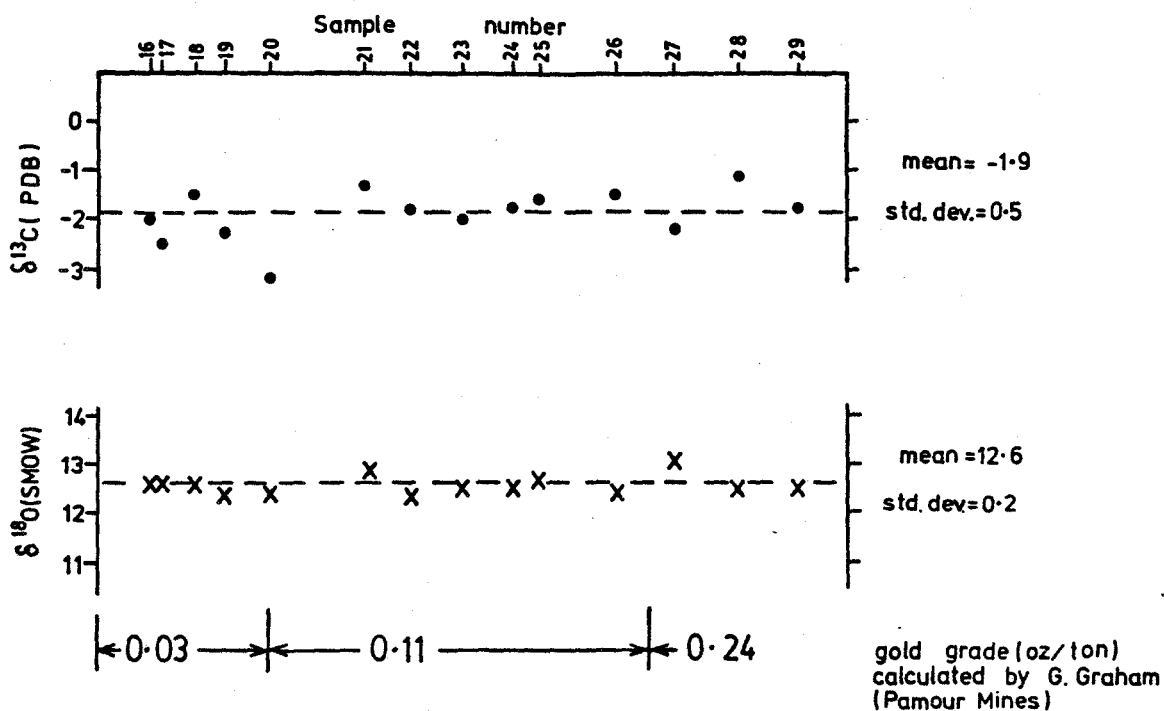


Figure 7-6: Covariation of  $\delta^{18}\text{O}$  and  $\delta^{13}\text{C}$  of hydrothermal vein-hosted dolomite with geographical position of the sample from the 51 vein, Pamour #1 Mine. No correlation exists between either  $\delta^{18}\text{O}$  or  $\delta^{13}\text{C}$  and gold tenor of the quartz vein.

Secondly, the method of gas collection described in Appendix-3 precluded the trapping of any gas which did not condense in either the liquid nitrogen or alcohol-dry ice baths. Methane is such a gas. For all experiments, a small but variable amount of non-condensable gas was observed.

Of these two major limitations, the first is most serious. Multiple fluid inclusion arrays clearly indicate the incursion of at least one exotic fluid following the precipitation of quartz. The number of distinct fluid incursions is not known, nor is the composition of the fluid(s) known as no apparatus was available with which to conduct detailed microscopic fluid inclusion studies.

However, the vein paragenesis described in Section 4.4.3 infers that fluids of quite different constitution passed through and precipitated minerals in the vein system following the precipitation of quartz. It is likely that several different fluids were trapped as fluid inclusions and hence any batch decrepitation of a large mass of vein quartz (3-7g) would yield a composite condensate. The stable isotopic compositions of this composite fluid could likewise be difficult or impossible to interpret.

Given the severity of these reservations, the experiments were undertaken with the hope that a correlation might exist between the Au tenor of a vein system and an isotopic characteristic of the fluid. Such a correlation might have developed as a result of a particular gold

precipitation mechanism. For example, precipitation of gold in a vein structure can be induced by solution boiling, a change in fluid equilibria in passing from one rock type to another, or a drop in temperature. If evidence of the precipitation process is preserved and can be identified, then such evidence would assist in the evaluation of possible gold precipitation mechanisms.

The carbon and hydrogen stable isotopic data are presented in Table 7-4. No duplicate analyses of  $\delta^{13}\text{C}$  were made. The mean and standard deviation for the  $\delta\text{D}$  data are also tabulated as well as the pooled variance and standard deviation determinations for each property.

For two samples (Car-23, Car-55) the presence, together with  $\text{CO}_2$ , of an additional liquid  $\text{N}_2$  condensable gas was detected during the mass spectrometry. The presence of this trace gas caused sufficient instrument drift, that such samples could not be analysed isotopically without prior reaction of the liquid  $\text{N}_2$  condensable fraction with  $\text{CuO}$ . The carbon isotopic compositions of the liquid  $\text{N}_2$  condensable fractions for these two samples were determined after reaction with  $\text{CuO}$ .

Plotted on Figure 7-7 are the ranges of  $\delta\text{D}$  analyses expressed as a function of property stratigraphic position and gold tenor. For individual properties, the intra-site variation in  $\delta\text{D}$  varies from 5‰ (McEnaney) to about 50‰ (Faymar). The respective ranges overlap to an extent that

TABLE 7-4:  $^{13}\text{C}/^{12}\text{C}$  and D/H determinations for fluid inclusions hosted in vein quartz.

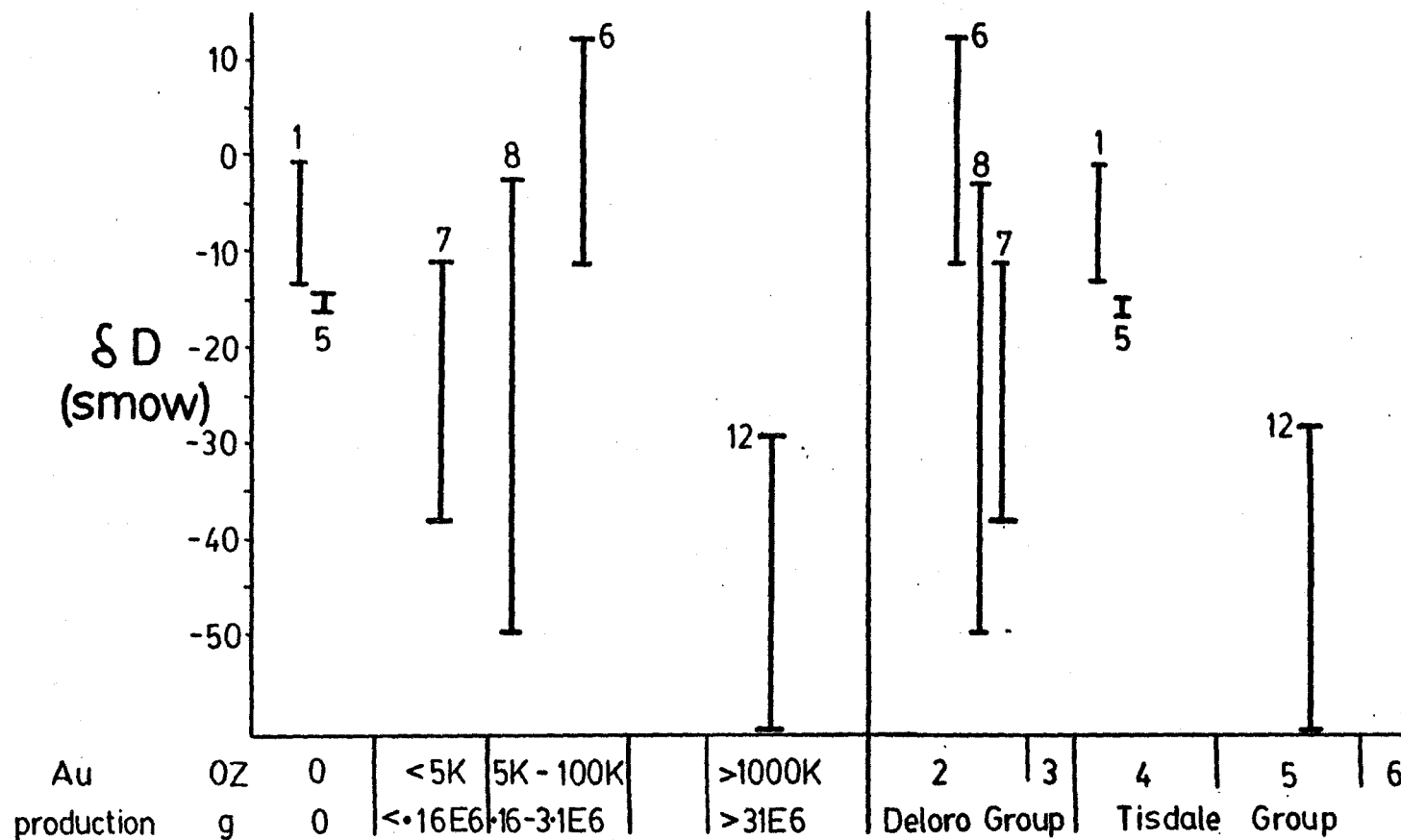
inclusions hosted in vein

| Mine Property<br>Sample Number | $\delta^{13}\text{C}$<br>(PDB) | $\delta\text{D}$<br>(SMOW) | $\bar{X}$ | $\delta\text{D}$ |             |    |
|--------------------------------|--------------------------------|----------------------------|-----------|------------------|-------------|----|
|                                |                                |                            |           | $\text{Sp}^2$    | $\text{Sp}$ | R  |
| Carshaw                        |                                |                            |           |                  |             |    |
| Car-23                         | -6.6(a)                        | —                          | —         |                  |             |    |
| 55                             | -7.1(a)                        | +5,-1                      | +2+4.2    |                  |             |    |
| 59                             | -1.7                           | -7,-1,-12                  | -6.7+5.5  |                  |             |    |
| 79                             | -1.9                           | -5,-6                      | -5.5+0.7  |                  |             |    |
| 81A                            | -4.8                           | —                          | —         | 14.5             | 3.8         | 14 |
| 82                             | -3.0                           | —                          | —         |                  |             |    |
| 91                             | -1.7                           | -12,-12                    | -12       |                  |             |    |
| 92                             | -4.4                           | +14,+10                    | +12+2.8   |                  |             |    |
| Duval                          |                                |                            |           |                  |             |    |
| Du-7                           | —                              | -33,-39                    | -36+4.2   |                  |             |    |
| 8                              | +0.2                           | -39,-34,-41                | -38+3.6   |                  |             |    |
| 11                             | +0.1                           | -21,-12                    | -16+6.4   | 14.4             | 3.8         | 27 |
| 12                             | —                              | -9,-14,-10                 | -11+2.6   |                  |             |    |
| 14                             | —                              | -13,-11                    | -12+1.4   |                  |             |    |
| Faymar                         |                                |                            |           |                  |             |    |
| Fa-1                           | —                              | -40,-38                    | -39+1.4   |                  |             |    |
| 3                              | —                              | -50,-50                    | -50       |                  |             |    |
| 5                              | —                              | -17,-23                    | -20+4.2   |                  |             |    |
| 9                              | —                              | -26,-23                    | -24+2.1   | 5.0              | 2.2         | 47 |
| 10                             | —                              | -2,-5                      | -3.5+2.1  |                  |             |    |
| 13                             | -2.8                           | -16,-12,-16                | -15+2.3   |                  |             |    |
| 14                             | —                              | -19,-20                    | -20+0.7   |                  |             |    |
| Beaumont†                      |                                |                            |           |                  |             |    |
| B-44                           | —                              | -15,-13                    | -14+1.4   |                  |             |    |
| 46                             | —                              | -2,-1                      | -1.5+0.7  | 1.3              | 1.1         | 13 |
| McEnaney                       |                                |                            |           |                  |             |    |
| M-40                           | —                              | -16                        | -16       |                  |             |    |
| 41                             | —                              | -14,-17,-15                | -15+1.5   |                  |             | 1  |
| Hollinger                      |                                |                            |           |                  |             |    |
| H-30                           | —                              | -35,-35,-30,-28            | -32+3.6   |                  |             |    |
| 31                             | —                              | -60,-60,-48                | -56+6.9   |                  |             | 24 |

Note: a) Liquid nitrogen condensate reacted with  $\text{CuO}$  at  $550^\circ\text{C}$ .Explanation:  $\bar{X}$ — Mean value;  $\text{Sp}^2$ — Variance;  $\text{Sp}$ — Standard deviation; R— Range

Figure 7-7 :  $\delta D$  values of water from vein quartz-hosted fluid inclusions expressed as a function of property gold tenor and stratigraphic position. Property identification labels as follows: 1-Beaumont; 5-McEnaney; 6-Carshaw; 7-Duval; 8-Faymar; 12-Hollinger.

# Quartz veins: fluid inclusion water



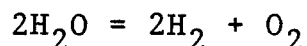


$\delta D$  is not a useful tool to discriminate between auriferous and barren quartz veins, nor is there any correlation between  $\delta D$  of the composite fluid and the stratigraphic position of the vein.

The  $\delta^{13}C$  of the inclusion  $CO_2$  are generally heavier than -5‰ (Table 7-4). The two Carshaw samples whose liquid  $N_2$  condensable fraction was reacted with  $CuO$  contain  $CO_2$  with a  $\delta^{13}C$  value approximating -7‰.

#### 7.5.1. Discussion of fluid inclusion isotopic results

The large range of  $\delta D$  analyses observed in some vein systems is of interest as is the tendency for the lightest  $\delta D$  values to cluster between -45 and -60‰ (SMOW; Fig. 7-7). The extremely wide range of  $\delta D$  typical of some vein systems (eg. Faymar) could be attributed to the mixing of two fluids or the formation of methane ( $CH_4$ ) or hydrogen ( $H_2$ ) from  $H_2O$  and  $CO_2$  in an hydrothermal fluid resulting from an internal equilibria shift:



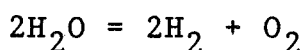
Alternatively, carbonaceous material in interflow sediments might have reacted to produce  $CH_4$  when encountered by a  $CO_2$ - $H_2O$  bearing hydrothermal fluid:



Because  $\text{CH}_4$  and  $\text{H}_2$  are enriched in the light isotope H, the remaining unreacted water would become isotopically enriched in D (Fig. 7-8). Assuming a closed system where all  $\text{CH}_4$  or  $\text{H}_2$  is produced from the C-O-H fluid in response to an internal redox shift:



or



the stabilization of as little as 10 mole %  $\text{H}_2$  or as much as 50 mole %  $\text{CH}_4$  could induce shifts in  $\delta\text{D}(\text{H}_2\text{O})$  of the magnitude observed. That no  $\delta\text{D}$  analyses are lighter than -60‰ suggests that this value might have been the initial  $\delta\text{D}$  value of the hydrothermal fluid before substantial  $\text{CH}_4$  or  $\text{H}_2$  was stabilized. This value lies within the field of magmatic and metamorphic fluids. Unfortunately,  $\delta\text{D}$  alone cannot adequately distinguish between magmatic or metamorphic fluids.

The lightest  $\delta^{13}\text{C}$ -values of the  $\text{CO}_2$  from the fluid inclusions lie in the range -6 to -7‰ (Table 7-4), within the field of magmatic carbon. Like the shift to heavier  $\delta\text{D}$  values, the presence of heavy  $\delta^{13}\text{C}$  values in the fluid inclusion  $\text{CO}_2$  may reflect the closed system stabilization of a reduced carbon-bearing species such as methane ( $\text{CH}_4$ ). This  $\text{CH}_4$  would be enriched in  $^{12}\text{C}$ , leaving the remaining  $\text{CO}_2$

Figure 7-8: Hypothetical closed system model to illustrate the magnitude of D partitioning between  $\text{H}_2\text{O}$ ,  $\text{CH}_4$  or  $\text{H}_2$ , resulting from a C-O-H equilibria shift which stabilizes either  $\text{H}_2$  or  $\text{CH}_4$  in a  $\text{CO}_2$ - $\text{H}_2\text{O}$  fluid at the expense of  $\text{H}_2\text{O}$ .

The calculation is carried out at  $350^\circ\text{C}$ ,  $\delta^{\text{D}}$  of the water in the original fluid is  $-50\text{‰}$  and the  $\Delta_{\text{H}_2\text{O}-\text{CH}_4}$  and  $\Delta_{\text{H}_2\text{O}-\text{H}_2}$  fractionation factors are  $+75\text{‰}$  and  $+450\text{‰}$  respectively, using the calculated Water-Methane and Water-Hydrogen carbon isotope fractionation expressions of Bottinga (1969). The equation used to model the effect of  $\text{CH}_4$  or  $\text{H}_2$  stabilization in a closed system, where  $\text{H}_2$ ,  $\text{CH}_4$  and  $\text{H}_2\text{O}$  remain captive in the fluid is (Ohmoto and Rye, 1979):

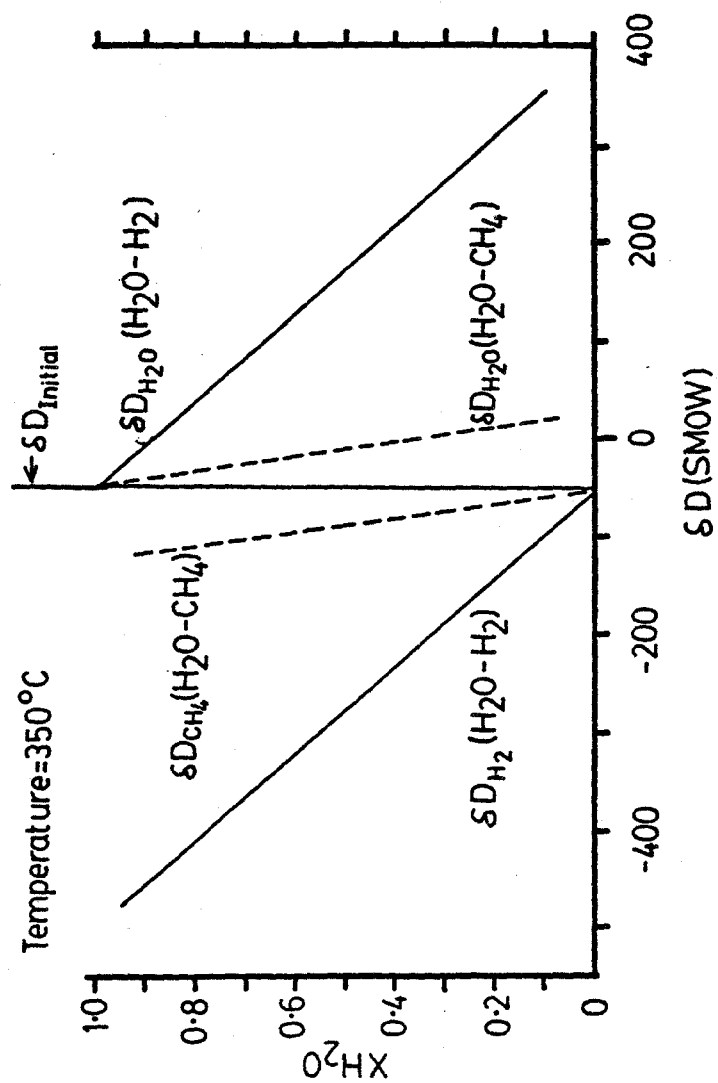
$$\delta^{\text{D}}_{\text{A}} = \delta^{\text{D}}_{\text{FLUID}} - \Delta_{\text{B-A}} (R_{\text{B/A}} / (1 + R_{\text{B/A}}))$$

where

$R$  = mole fraction B/A

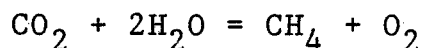
$A$  =  $\text{H}_2\text{O}$

$B$  =  $\text{CH}_4$  or  $\text{H}_2$



enriched in  $^{13}\text{C}$  (Fig. 7-9). The stabilization of 30 mole %  $\text{CH}_4$  would shift the  $\delta^{13}\text{C}$  of the remaining  $\text{CO}_2$  by as much as 6‰ at 350°C from a value of -5 to +1.5‰.

Plotted on Figure 7-10 are the corresponding  $\delta\text{D}$  and  $\delta^{13}\text{C}$  values for  $\text{H}_2\text{O}$  and  $\text{CO}_2$  respectively that was liberated from the fluid inclusions in quartz. A negative correlation exists between  $\delta\text{D}$  and  $\delta^{13}\text{C}$  which when tested with the t-test at the 95% significance level, is statistically significant. If methane had formed in a hydrothermal  $\text{CO}_2$ - $\text{H}_2\text{O}$  fluid closed to C and H, at the expense of  $\text{H}_2\text{O}$  and  $\text{CO}_2$ , a positive correlation between  $\delta\text{D}$  and  $\delta^{13}\text{C}$  would result (trend line A, Fig 7-10):



This positive correlation would result because  $\text{CH}_4$  is depleted in H and  $^{13}\text{C}$  with respect to the coexisting  $\text{H}_2\text{O}$  and  $\text{CO}_2$ . The slope of trend line A would be difficult to determine because it is dependent on the temperature of the reaction, the fraction of  $\text{CO}_2$ , and hence  $\text{H}_2\text{O}$ , converted to  $\text{CH}_4$  and the maintenance of isotopic equilibrium.

The regression line represented in Figure 7-10 could arise from mixing between two end members, each having  $\delta\text{D}_{\text{H}_2\text{O}}$  and  $\delta^{13}\text{C}_{\text{CO}_2}$  compositions of -40 and +3‰ and +10 and -7‰ respectively. The end member having a  $\delta\text{D}$  and  $\delta^{13}\text{C}$  of -40‰ and +3‰ respectively resembles metamorphically derived  $\text{CO}_2$  and  $\text{H}_2\text{O}$  (Sheppard and Schwarcz, 1970; Sheppard,

Figure 7-9: Hypothetical closed system model to illustrate the magnitude of  $\delta^{13}\text{C}$  shift in residual  $\text{CO}_2$  resulting from an equilibria shift which stabilizes  $\text{CH}_4$  at the expense of  $\text{CO}_2$  in a C-O-H fluid. The calculation was carried out at  $350^\circ\text{C}$ , the  $\delta^{13}\text{C}$  of the total dissolved carbon in the original fluid is  $-5\text{‰}$ , using a  $\Delta_{\text{Carbon dioxide-Methane}}$  carbon isotope fractionation factor of  $+21.7\text{‰}$  (Bottinga, 1969). The equation used to model the effect of  $\text{CH}_4$  stabilization is (Ohmoto and Rye, 1979):

$$\delta^{13}\text{C}_{\text{CO}_2} = \delta^{13}\text{C}_{\Sigma\text{C}} - \Delta_{\text{CH}_4-\text{CO}_2} \left( \frac{1}{1 + \frac{m_{\text{CO}_2}}{m_{\text{CH}_4}}} \right)$$

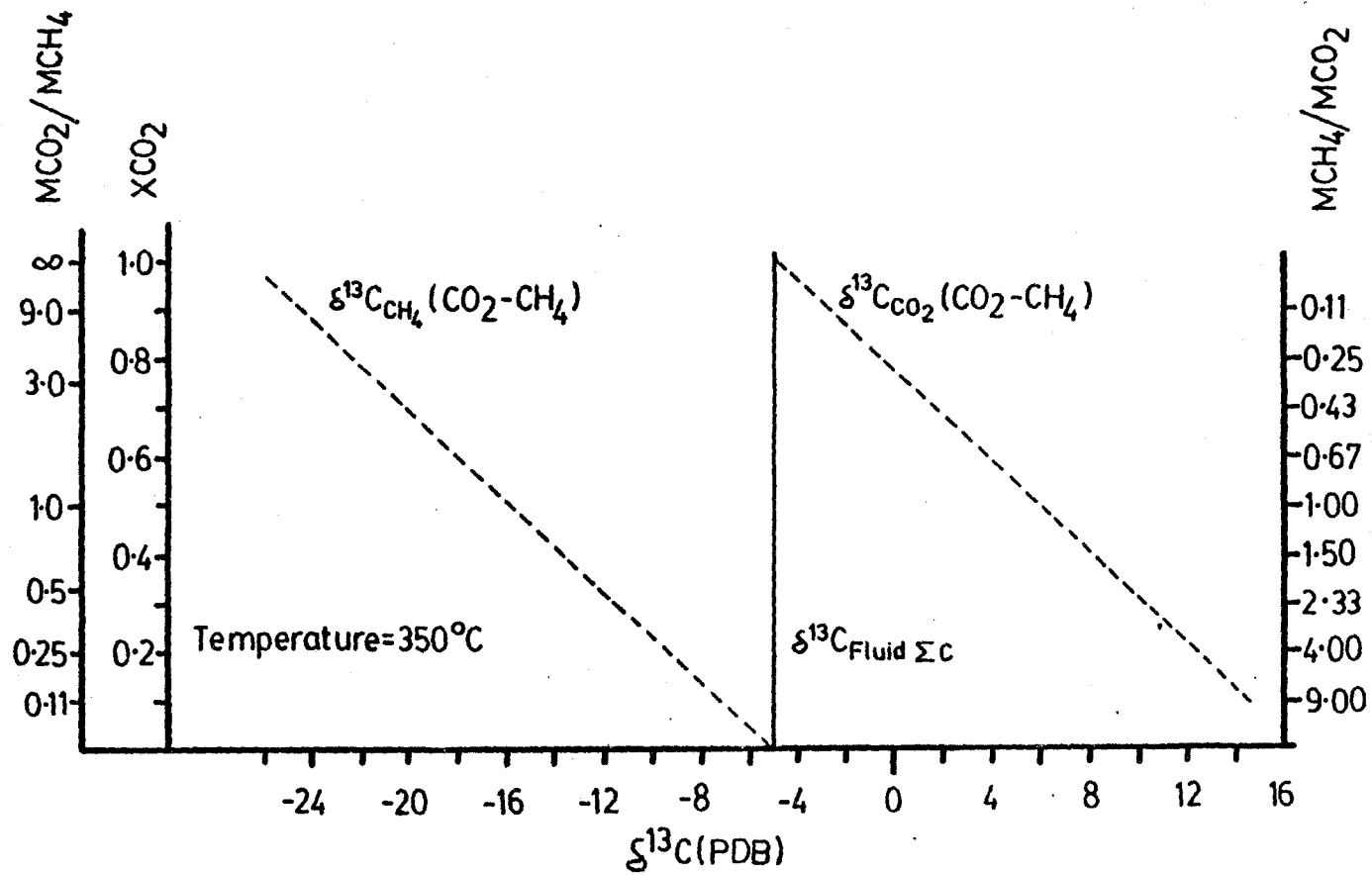
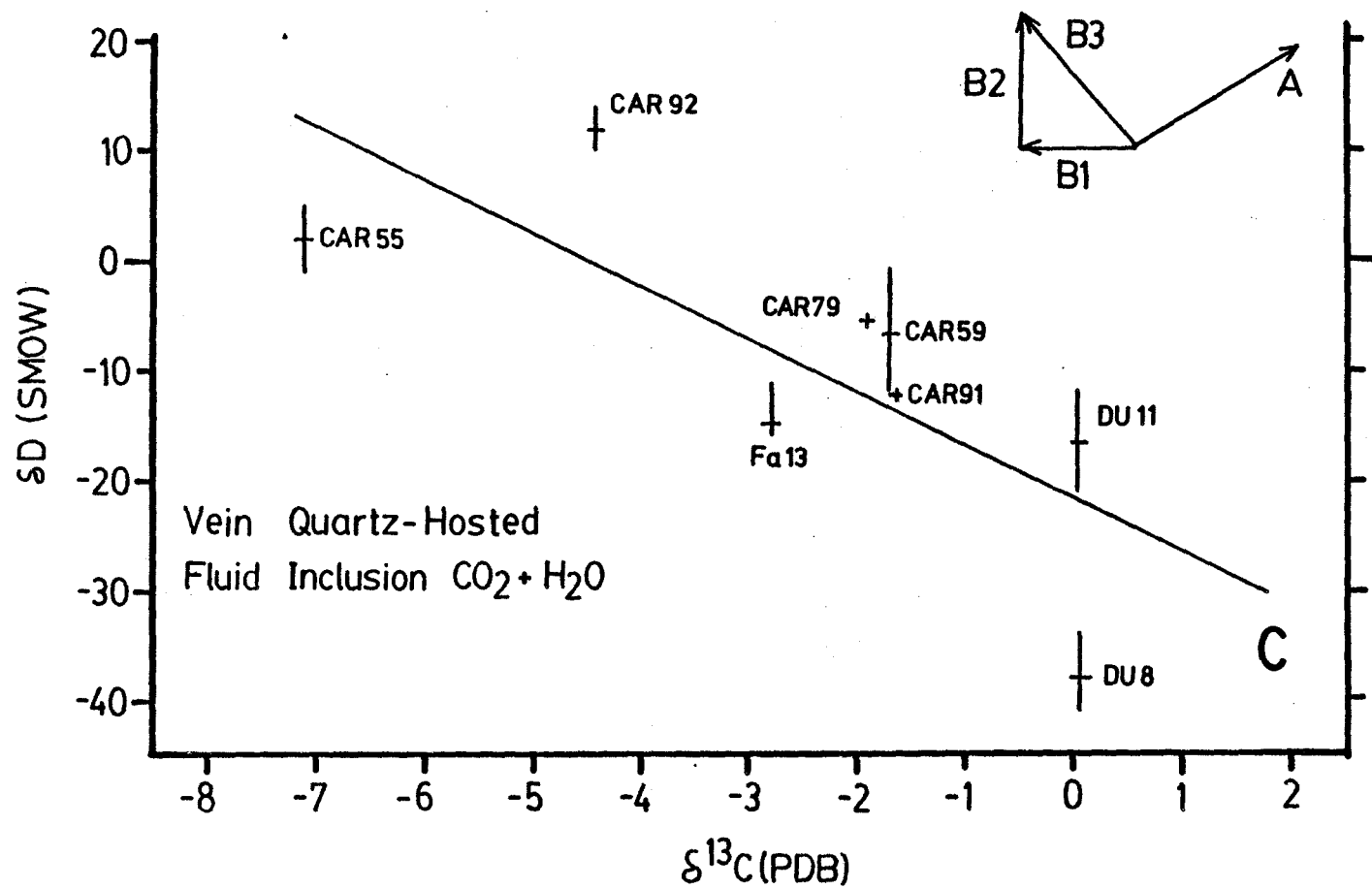


Figure 7-10: Covariation between  $\delta D$  and  $\delta^{13}C$  of vein quartz-hosted fluid inclusion water and  $CO_2$  respectively. Vector B1 illustrates the direction of  $\delta^{13}C$  shift if  $^{12}C$ -enriched  $CO_2$  is mixed with  $^{13}C$ -enriched  $CO_2$ . Vector B2 illustrates the direction of shift if D-rich water mixed with H-rich water. Vector B3 represents the sum of vectors B1 and B2. Vector A represents the expected direction of  $\delta D$  and  $\delta^{13}C$  shift if  $CH_4$  formed in a closed system at the expense of  $CO_2$  and  $H_2O$  in a hydrothermal fluid.

If the regressed line is the result of mixing, an original fluid may be represented by the  $\delta^{13}C$  and  $\delta D$  values of region C.

The regressed line through the data array has a slope of -4.8, a y-intercept of -21.4 and a correlation coefficient of 0.77, which is statistically significant at the 95% confidence level.





1977). The other hypothetical end member has a  $\delta^{13}\text{C}$  typical of magmatic  $\text{CO}_2$  (-7 to -5‰), but the  $\delta\text{D}$  of the hypothetical  $\text{H}_2\text{O}$  phase (+10‰) does not resemble any normal terrestrial water. Therefore, this model does not seem very probable.

A negative correlation between  $\delta\text{D}$  and  $\delta^{13}\text{C}$  of  $\text{H}_2\text{O}$  and  $\text{CO}_2$  respectively in a fluid mixture would also result from the addition of an exotic  $\text{CH}_4$ - $\text{CO}_2$ - $\text{H}_2\text{O}$  fluid, generated and equilibrated externally in a reducing environment, to a  $\text{CO}_2$ - $\text{H}_2\text{O}$  hydrothermal fluid. Graphite reacts with  $\text{H}_2\text{O}$  to produce  $\text{CH}_4$  and  $\text{CO}_2$ :



The  $\text{CO}_2$  produced at 350-600°C would be 3 to 12‰ enriched in  $\delta^{13}\text{C}$  with respect to the graphite depending on the proportion of graphite consumed and whether isotopic equilibrium is established between the remaining graphite and the  $\text{CO}_2$  produced (Ohmoto and Rye, 1979). Thus, hydrolysis of carbonaceous material, having a  $\delta^{13}\text{C}$  of -25‰ should yield  $\text{CO}_2$  having a  $\delta^{13}\text{C}$  in the range of -20 to -10‰.

If the hydrolysis reaction was nearly complete, the  $\delta\text{D}$  of the residual water would be about 70‰ enriched in deuterium with respect to the coexisting  $\text{CH}_4$  if equilibrium is attained (Ohmoto and Rye, 1979). Mixture of such a fluid, having a  $\delta^{13}\text{C}$  of -15‰ and  $\delta\text{D}$  of +20‰, with an

hydrothermal fluid, having a  $\delta^{13}\text{C}$  of +3‰ and  $\delta\text{D}$  of -50‰, would reproduce the mixing trend shown on Figure 7-10. The carbon isotope composition of the D- and  $^{13}\text{C}$ -rich fluid is similar to that of metamorphically derived  $\text{CO}_2$  and  $\text{H}_2\text{O}$  (Sheppard, 1977; Sheppard and Schwarcz, 1970), but is much richer in  $^{13}\text{C}$  than that inferred to have been involved in the carbonatization of the ultramafic and basaltic rocks (see Chapter 8).

The discussion of the fluid inclusion isotopic data is all predicated on the assumption that only one fluid inclusion population has been sampled and that the phase and isotope exchange reactions ceased at the time of trapping, leaving the system closed for 2.7 billion years. As considered in the preamble to this section, it is more likely that several fluid inclusion populations have been sampled by the decrepitation technique. Perhaps the large variability within a vein system reflects the presence of more than one fluid inclusion population and the line on Figure 7-10 may be a mixing trend between these populations.

#### 7.6. Summary

The following general interpretations may be deduced from the oxygen and carbon isotopic relationships observed in the quartz vein systems:

- 1) oxygen isotopic fractionation between coexisting vein-hosted quartz, dolomite, chlorite and sericite are

suggestive of disequilibrium, consistent with the intermineral textural relationships; consequently, no temperature can be calculated for gold precipitation or wallrock carbonatization events using the oxygen isotopic relationships of the coexisting quartz vein silicates or carbonates;

2) the  $\delta D$  and  $\delta^{13}C$  values of  $H_2O$  and  $CO_2$  respectively for  $H_2O$  and  $CO_2$  from fluid inclusions in vein quartz show a large degree of variability within and between different vein systems; this variability is consistent with the generation of some methane (< 50 mole %) or  $H_2$  (< 10 mole %) in the hydrothermal fluid;

3) the lightest  $\delta D$  and  $\delta^{13}C$  values for the fluid inclusion  $H_2O$  and  $CO_2$  have minimum values of -50‰ and -7‰ respectively, which is consistent with a magmatic origin for the hydrothermal fluids; however, the lightest  $\delta D$ -values coexist with the heaviest  $\delta^{13}C$ -values and hence a simple magmatic origin is unsatisfactory;

4) covariation between  $\delta D$  and  $\delta^{13}C$  analyses of fluid inclusion water and  $CO_2$  respectively shows a negative correlation which is not explained easily by a closed system  $CH_4$  stabilization at the expense of  $CO_2$  and  $H_2O$ ; such a result could be produced by mixing between two fluids, one produced by decarbonatization of dolomite having a  $\delta^{13}C$  of -5 to -2‰, the other being  $H_2O$ -poor, produced by reaction between graphite and  $H_2O$ . Alternatively, the fluid

inclusion isotopic analyses could be interpreted in terms of mixing of several fluid inclusion populations during the decrepitation step;

5) the similarity in  $\delta^{18}\text{O}$  and  $\delta^{13}\text{C}$  between the vein-hosted and adjacent wallrock replacement hydrothermal carbonates implies they had a common origin, which will be further discussed in Chapter 8;

6) on a single vein scale, neither  $\delta^{13}\text{C}$  nor  $\delta^{18}\text{O}$  of vein carbonate correlates with the vein gold tenor, consistent with the paragenetic relationships which suggested that gold did not coprecipitate with the carbonate.

## 8. Isotope Geochemistry Of Replacement Carbonates From Volcanic Rock

Carbonate-rich rocks of quite different origins exist in the Timmins area, and a brief review is relevant prior to discussing their stable isotopic characteristics. A stratiform dolomite unit of possible sedimentary origin crops out on the Buffalo Ankerite Mine property (Maps 5,6). This material represents the only possible sedimentary carbonate recognized during this study, although certain carbonate-rich units in the Dome Mine (Fryer and Hutchinson, 1976; Roberts, 1981) and Aunor Mines (Kerrich and Fryer, 1979) have been argued to be sedimentary, but their origin remains controversial (Hodgson, 1983).

The remainder of carbonate that occurs in the volcanic rocks was introduced by hydrothermal processes. This hydrothermal carbonate exists as: 1) calcite, which fills vesicles and is referred to as "dispersed calcite"; and 2) replacement calcite, dolomite, or magnesite, which depending on alteration intensity and initial whole rock composition, occur within the Intense Carbonate Alteration zones (Chapter 3).

### 8.1. Sedimentary Marine Carbonate

Exposed on the former Buffalo Ankerite Mine property (Maps 5 and 6), is a buff-coloured, carbonate-rich, stratiform, dolomitic unit which is interpreted to be a metamorphosed sedimentary, marine sediment. The unit rarely exceeds 0.5 metre in thickness, is composed of dolomite and quartz, and chemically is unlike any carbonatized volcanic rock in the Timmins area (Table 8-1). Its distinctive  $\delta^{13}\text{C}$  value of -0.5 to +1.0‰ (Table 8-1) falls within the range for other Archean, marine carbonate sediments (Schidlowski et al., 1975; Veizer and Hoefs, 1976).

The  $\delta^{18}\text{O}$  of this dolomite (+16.5‰) falls within the range of  $\delta^{18}\text{O}$  for other Archean marine dolomites (Schidlowski et al., 1973; Veizer and Hoefs, 1976), but is 5 to 10‰ lighter than Phanerozoic marine dolomites. If its  $\delta^{18}\text{O}$  of +16.5‰ represents the value obtained at the time of precipitation, it would represent a precipitation temperature of about 150°C, assuming the  $\delta^{18}\text{O}$  of the ambient sea water was approximately 0‰. This is a considerably higher than the 60-70°C temperature proposed by Knauth and Epstein (1976) to represent ambient Archean sea water. Either the local sea water reservoir from which the dolomite precipitated was thermally anomalous or the  $\delta^{18}\text{O}$  of the dolomitic sediment represents an exchanged value.

A local thermal anomaly, perhaps maintained by vigorous submarine volcanism or hydrothermal discharge,

TABLE 8-1: Representative chemical analyses of a siliceous dolomitic marine sediment exposed on the Buffalo Ankerite Mine property, Deloro Township.

---

Chemical Analyses

| Major element<br>weight percent    |       | Minor element<br>ppm |      |
|------------------------------------|-------|----------------------|------|
| SiO <sub>2</sub>                   | 10.7  | As                   | <1.0 |
| Al <sub>2</sub> O <sub>3</sub>     | 1.5   | Ba                   | 70.0 |
| Fe <sub>2</sub> O <sub>3</sub> (T) | 4.8   | Bi                   | <0.1 |
| MgO                                | 12.6  | Co                   | 10.0 |
| CaO                                | 27.6  | Cr                   | 15.0 |
| Na <sub>2</sub> O                  | <0.01 | Cu                   | <5.0 |
| K <sub>2</sub> O                   | 0.2   | Li                   | <5.0 |
| TiO <sub>2</sub>                   | 0.07  | Ni                   | 15.0 |
| MnO                                | 0.1   | Pb                   | 25.0 |
| P <sub>2</sub> O <sub>5</sub>      | 0.2   | Sb                   | 0.1  |
| L.O.I.                             | 42.3  | Zn                   | 65.0 |
| TOTAL                              | 99.5  |                      |      |
| CO <sub>2</sub>                    | 42.7  |                      |      |
| S                                  | <0.01 |                      |      |

---

Stable Isotopic Data

$\delta^{18}\text{O} = +16.5\% \pm 0.1$  (SMOW)

$\delta^{13}\text{C} = +0.3\% \pm 0.2$  (PDB)

4 Analyses

---

Data for Early Precambrian marine marbles and dolomites:

$\delta^{18}\text{O} = +25\%$  to  $6\%$  (SMOW)

$\delta^{13}\text{C} = -1\%$  to  $+2.5\%$  (PDB) (Schidlowski et al., 1975;  
Velzer and Hoefs, 1976)



might be an appealing mechanism to induce inorganic precipitation of dolomitic sediment, in that the solubility of carbonate minerals in water is inversely proportional to temperature (Ellis, 1959). However, it would be difficult to maintain water temperature differences on the order of 80°C for extended periods of time because the superheated sea water, of normal salinity, would disperse convectively into the reservoir of cooler sea water. Even if dolomite precipitation occurred in a small, anomalously hot restricted basin, surface temperatures would not significantly exceed 100°C and if deeper waters were hotter, convection would occur. In short, the  $\delta^{18}\text{O}$ -values of the dolomite could represent precipitation from an anomalously hot marine reservoir (around 150 °C), but a basin having a minimum depth of 50 metres would have been required to prevent boiling (Haas, 1971).

Isotope exchange is a second process capable of producing relatively light  $\delta^{18}\text{O}$ -values in sedimentary marine carbonates (Keith and Weber, 1964; Schidlowski et al., 1975). Oxygen isotopic exchange between the primary dolomitic marine sediment and isotopically lighter metamorphic pore fluids, derived from hydrated mafic volcanic rock by prograde dehydration reactions, could have dragged down the  $\delta^{18}\text{O}$  of the dolomite from a primary value of +20 to +30‰ to +16‰.

Decarbonatization is known to deplete carbonate

protoliths in the heavier isotopes (Sheppard and Schwarcz, 1970; Shieh and Taylor, 1969), but such a process cannot explain the light  $^{18}\text{O}/^{16}\text{O}$  ratios for this dolomitic unit because no calc-silicate minerals (wollastonite- $\text{CaSiO}_3$ ; tremolite- $\text{Ca}_2\text{Mg}_5\text{Si}_8\text{O}_{22}(\text{OH})_2$ ; diopside- $\text{CaMgSi}_2\text{O}_6$ ) are present in the siliceous dolomite. Furthermore, there is no corroborative depletion in  $\delta^{13}\text{C}$ .

Thus, it seems most reasonable that the light  $\delta^{18}\text{O}$ -values of the sedimentary dolomite reflects post-precipitation exchange with isotopically light metamorphic waters, although higher temperature ( $150^\circ\text{C}$ ) precipitation cannot be ruled out.

## 8.2. Hydrothermal Carbonate

The textural and temporal relationships of the dispersed calcite and the replacement carbonates were described in Chapter 2.1 and 2.2. The dispersed calcite co-exists with quartz and chlorite in vesicles in the least altered volcanic rocks whose volatile content does not exceed 5 weight percent loss on ignition (L.O.I.). This calcite is interpreted to have precipitated during the low temperature, sea water alteration of the basalt flows. Superimposed upon this dispersed calcite-bearing assemblage are the zones of intense carbonate alteration which consist in part of calcite- and dolomite- or magnesite-rich assemblages depending on alteration intensity and bulk rock

composition (Chapter 2.2 and 2.4; Fig. 2-2). The carbon and oxygen isotope geochemistry of these two systems is discussed separately.

#### 8.2.1. Dispersed calcite

Dispersed calcite has variable  $\delta^{13}\text{C}$  values ranging from -3.5 to 0‰, with a mode at -1.7‰ (Fig. 8-1). The  $\delta^{18}\text{O}$ -values of this calcite are quite variable, and range from +8 to +16.5‰, with a mode of 11.3‰ (Fig. 8-2).

The textural and paragenetic characteristics of this calcite (Chapter 2.1, 2.4), suggest that it partly filled primary porosity during the early, low temperature, sea water hydrothermal alteration of the basalt flows. The  $\delta^{13}\text{C}$  of this calcite, ranging from -3.5 to 0‰ (mode at -1.7‰), is about 1‰ lighter than the modal  $\delta^{13}\text{C}$  of Archean marine limestones and marbles, but lies well within the range of values reported for Archean, marine carbonate (Veizer and Hoefs, 1976; Schidlowski et al, 1975). The range in  $\delta^{13}\text{C}$  for the dispersed hydrothermal calcite is compatible with its precipitation from sea water in the volcanic rock at temperatures in the range of 50° to 150°C. This precipitation presumably took place in response to sea water recharge into an oceanic crust composed of volcanic rock where  $\text{pCO}_2$  in the sea water hydrothermal fluid would be buffered to very low levels by reaction with zeolite and clay minerals (Thompson, 1971).

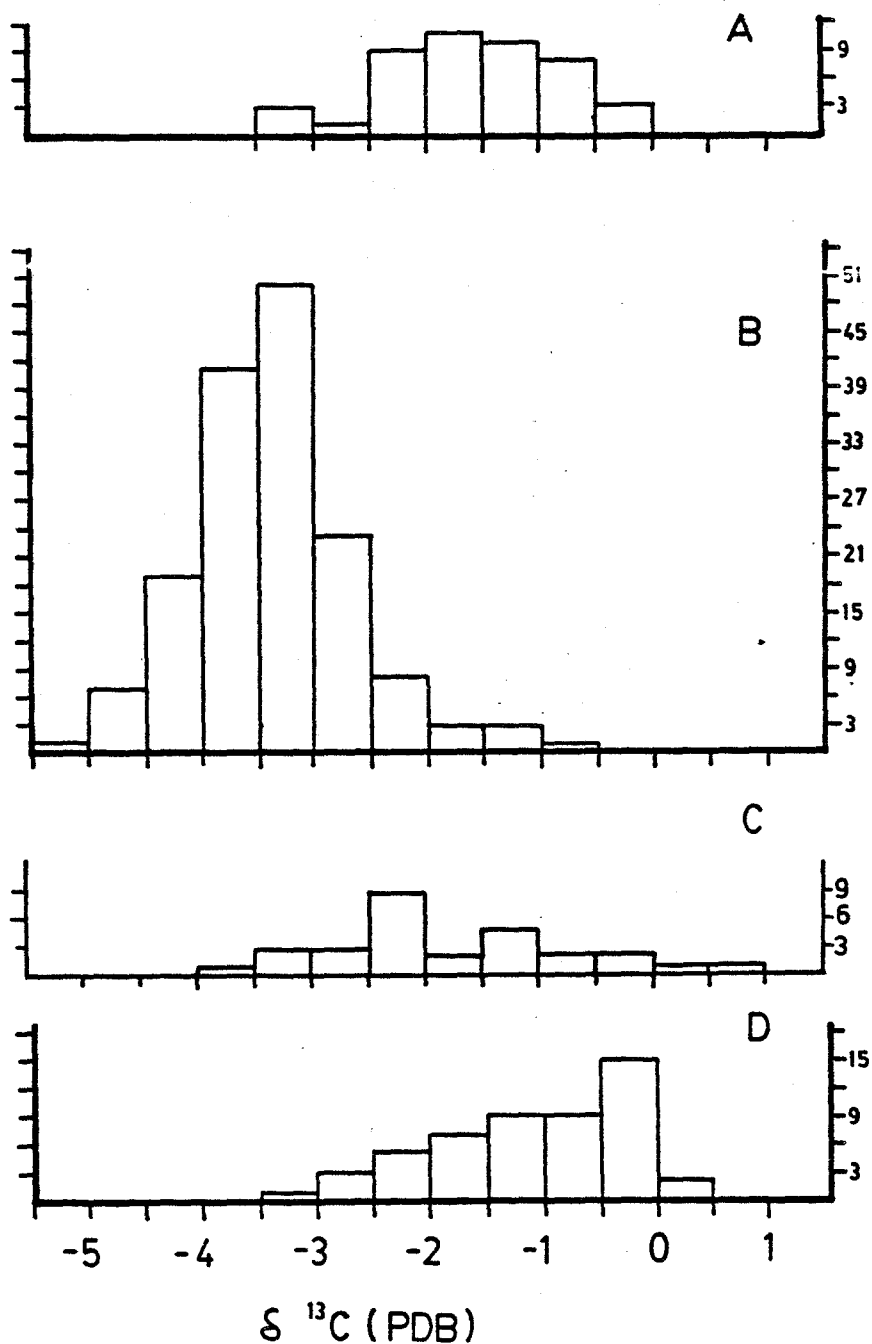


Figure 8-1: Histograms of  $\delta^{13}\text{C}$  compositions for:  
 A - disseminated, vesicle-filling calcite  
 B - hydrothermal ferroan dolomite not proximal to carbonaceous sediments.  
 C - hydrothermal calcite adjacent to ferroan dolomite zone.  
 D - hydrothermal dolomite from properties proximal to carbonaceous sediments (Hallnor, Pamour #1, North Whitney, and Hollinger Mines).

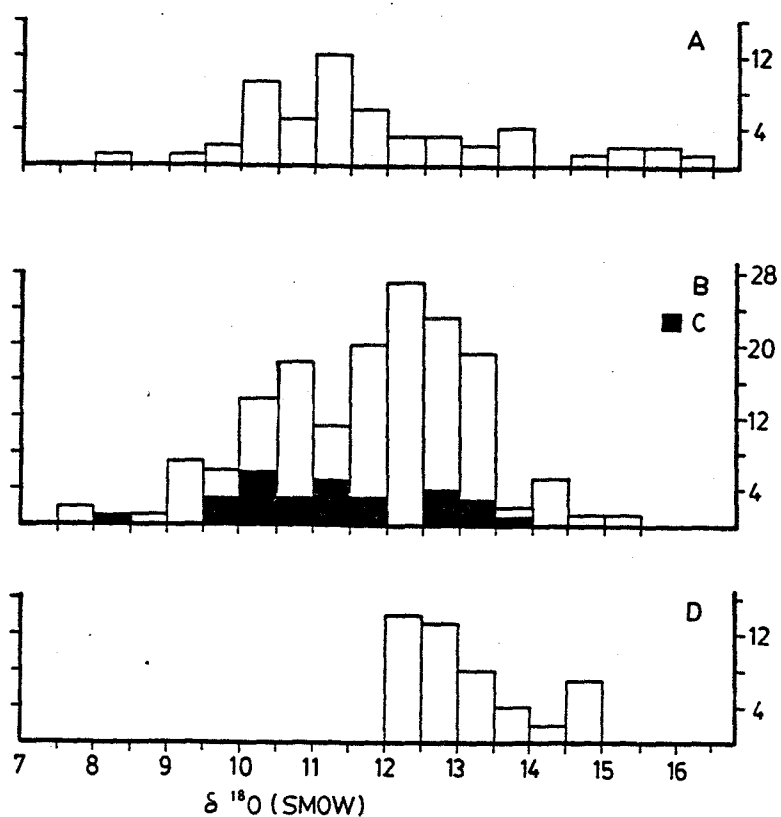


Figure 8-2: Histograms of  $\delta^{18}\text{O}$  compositions for:  
 A - disseminated, vesicle-filling calcite  
 B - hydrothermal ferroan dolomite not proximal to carbonaceous sediments.  
 C - hydrothermal calcite adjacent to ferroan dolomite facies.  
 D - hydrothermal ferroan dolomite from properties proximal to carbonaceous sediments (Hallnor, Pamour #1, North Whitney, and Hollinger Mines).

The variable  $\delta^{18}\text{O}$ -values of the dispersed calcite (range from +8 to +16.5‰; Fig. 8-2) are lighter than expected for low or moderate temperature (<200 °C) precipitation of calcite from sea water. Three processes, acting collectively or singly, could have been responsible for the variable  $\delta^{18}\text{O}$ -values of the dispersed calcite: 1) variable precipitation temperature; 2) variable water/rock ratio during calcite precipitation; 3) post precipitation exchange between the dispersed calcite and an aqueous metamorphic fluid.

If it is assumed that the variable  $\delta^{18}\text{O}$  of the dispersed calcite is a primary feature, then, the variation could reflect precipitation from sea water having a  $\delta^{18}\text{O}$  of 0‰ at temperatures ranging from 100°C to 235°C. These temperatures are well within those expected for low temperature, sea water alteration of basalt.

An additional degree of  $\delta^{18}\text{O}$ -variability during precipitation of the dispersed calcite could have resulted from changes in the water/rock (W/R) ratio during the sea water alteration event. The effect of varying W/R ratio during the precipitation event can be approximated assuming a closed system, where given amounts of water and rock are allowed to equilibrate. If W/R is expressed in terms of oxygen in each reservoir, then W/R can be

related to the other reactants as follows (Sheppard et al., 1969):

$$W/R = \frac{\delta_{\text{rock}}^f - \delta_{\text{rock}}^i}{\delta_{\text{H}_2\text{O}}^i - (\delta_{\text{rock}}^f - \Delta)} \quad ; \quad \Delta = \delta_{\text{rock}}^f - \delta_{\text{H}_2\text{O}}^f$$

where  $\delta_{\text{rock}}^f$  and  $\delta_{\text{rock}}^i$  correspond to the final and initial  $\delta^{18}\text{O}$ -values of the rock respectively,  $\delta_{\text{H}_2\text{O}}^i$  and  $\delta_{\text{H}_2\text{O}}^f$  correspond to the initial and final  $\delta^{18}\text{O}$ -values of the fluid respectively, and  $\Delta$  is the oxygen isotope fractionation factor between the rock and fluid. This expression has been rearranged to yield  $\delta_{\text{H}_2\text{O}}^f$  as a function of the other parameters (Fig. 8-3). To solve for  $\delta_{\text{H}_2\text{O}}^f$  as a function of varying W/R (Fig. 8-3), the following whole rock oxygen isotopic data from Beaty (1980), describing the altered basalts from the Timmins area, have been used: ( $\delta_{\text{rock}}^i = +5\%$ ,  $\delta_{\text{rock}}^f = +11\%$ , and  $\delta_{\text{H}_2\text{O}}^i = 0\%$ ). Note that the final  $\delta^{18}\text{O}$  of the rock (+11‰) is the mean of data which range from +9 to +14‰ and that this range can itself be related to W/R ratio changes. Hence, this approach permits only a very approximate model of  $\delta_{\text{H}_2\text{O}}^f$ . Nevertheless, a solution for  $\delta_{\text{H}_2\text{O}}^f$  is given on Figure 8-3 (line A) for the constraints imposed, and illustrates that very light  $\delta^{18}\text{O}$ -values of hypothetical sea water hydrothermal fluid result when the W/R ratio drops below 4. The calculated  $\delta^{18}\text{O}$  for calcite, precipitated from the hypothetical sea water hydrothermal fluid at 150°C (line B)

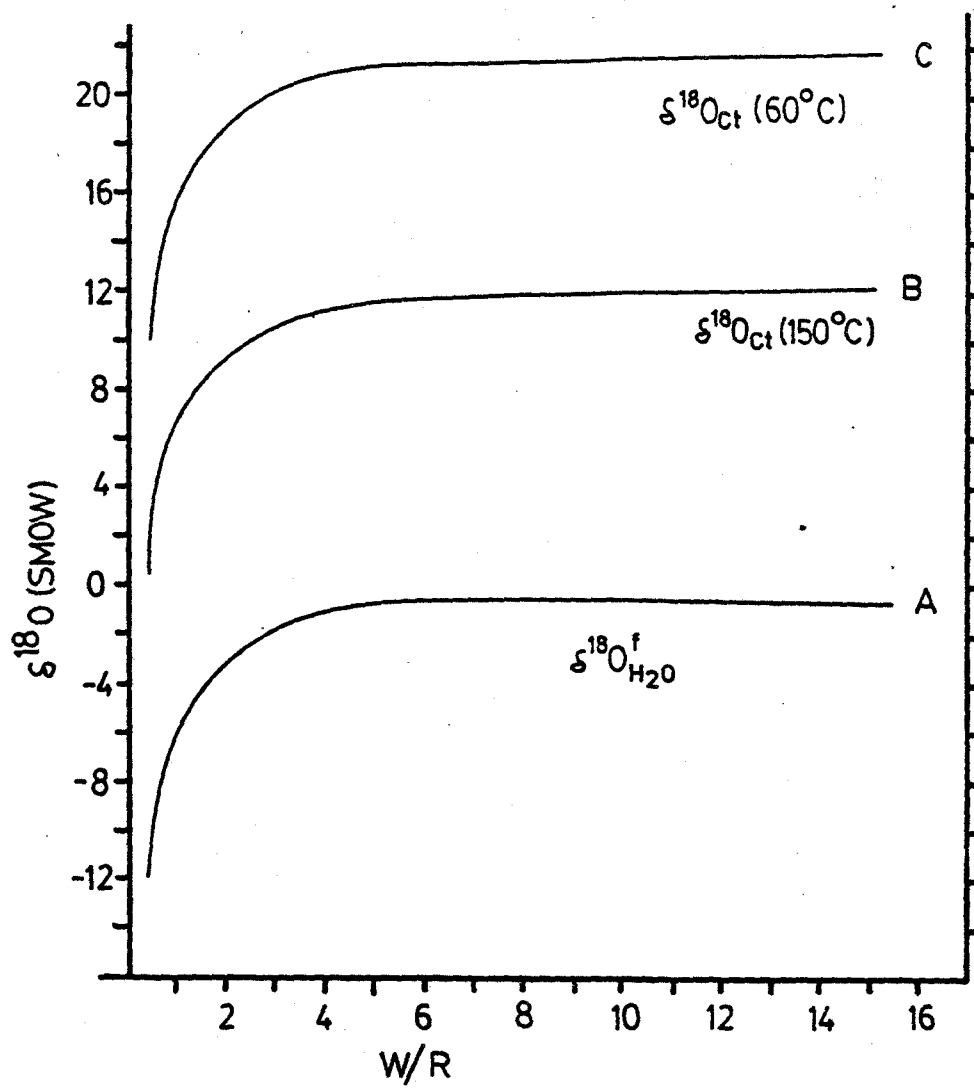
Figure 8-3: Calculated  $\delta^{18}\text{O}$  of the fluid (line A) which reacted with basalt in the Timmins area to impart an elevated  $\delta^{18}\text{O}$  whole rock value of +11‰ (SMOW), as a function of varying water/rock ratio. A closed system was modelled and the  $\Delta_{\text{feldspar-water}}$  was used to approximate the  $\Delta_{\text{rock-water}}$  (Sheppard et al., 1969). Lines B and C represent the  $\delta^{18}\text{O}$  of calcite precipitated from a fluid having a  $\delta^{18}\text{O}$  represented by Line A at 150°C and 60°C respectively and enclose the field occupied by the  $\delta^{18}\text{O}$  of the disseminated calcite in the Timmins area. This model illustrates that the variation of  $\delta^{18}\text{O}$  of the disseminated calcite in the Timmins area could have resulted from either temperature or water/rock ratio fluctuations acting singly or in tandem during the low temperature sea water alteration.

$$\delta_{\text{H}_2\text{O}}^{\text{f}^{18}} = \delta_{\text{H}_2\text{O}}^{\text{i}^{18}} - \left[ \frac{\delta_{\text{RX}}^{\text{f}^{18}} - \delta_{\text{RX}}^{\text{i}^{18}}}{\text{W/R}} \right]$$

$$\delta_{\text{RX}}^{\text{i}^{18}} = +5\text{‰}$$

$$\delta_{\text{RX}}^{\text{f}^{18}} = +11\text{‰}$$





and 60°C (line C), illustrates the combined effect of both temperature and W/R variation. The field bounded by curves B and C (Fig. 8-3) encloses virtually all  $\delta^{18}\text{O}$ -values for the dispersed calcite. Thus, either temperature or W/R ratio fluctuations acting singly or collectively could account for the variable  $\delta^{18}\text{O}$ -values of the dispersed calcite.

If the interpretation that the dispersed calcite was precipitated during an early sea water alteration event is correct, then the calcite must have experienced the regional contact metamorphism described by Jolly (1979, 1980). Therefore, it is conceivable that a component of the large variance in  $\delta^{18}\text{O}$  for the dispersed calcite could be attributed to variable degrees of oxygen isotope exchange with an aqueous, metamorphic fluid. The dolomitic sediment must have also experienced the greenschist metamorphism, but it apparently did not undergo the same degree of recrystallization. The greater variance in  $\delta^{18}\text{O}$  of the dispersed calcite may have resulted because the basaltic rock, which is host to the dispersed calcite, is dominated by hydrous silicates, whereas the dolomitic sediment is essentially anhydrous. That is, the activity of  $\text{H}_2\text{O}$  (exchangeable oxygen reservoir) within the hydrous basaltic rock would have exceeded that in the core of the dolomitic sediment. It has been recognized in metamorphic terranes that in general, oxygen isotope exchange between a mineral

and a metamorphic pore fluid is enhanced if the host rock is hydrous (Taylor et al., 1963; Rye et al., 1976). In addition, because the dispersed calcite constitutes only a small modal proportion of an otherwise hydrous silicate mineral assemblage and if metamorphic conditions of low water/rock ratio prevailed, the dominant process controlling the  $\delta^{18}\text{O}$  of the dispersed calcite would have been the redistribution of oxygen between calcite and the vast silicate mineral reservoir at various temperatures. Conversely, in the dolomitic sediment (and by implication in the intensely carbonatized alteration zones), the volume of carbonate mineral greatly exceeds that of the silicate minerals and hence, it is the  $\delta^{18}\text{O}$  of the carbonate mineral which essentially buffers the  $\delta^{18}\text{O}$  of the fluid. It has also been observed in metamorphic terranes that dolomite is less susceptible than calcite to oxygen isotope exchange (Sheppard and Schwarcz, 1969).

In summary, variation in temperature and W/R ratio during initial precipitation and then superimposed later greenschist metamorphic exchange processes could all, either acting singly or collectively, have contributed to the variability of the  $\delta^{18}\text{O}$  of the disseminated calcite.

#### 8.2.2. Replacement carbonate in intense carbonate alteration zones

As discussed in Chapter 2.2 (Fig. 2-2), the carbonate mineral species stabilized within the intense

carbonate alteration facies closest to the fluid conduit is ferroan dolomite if the host rock is basaltic, or magnesite where the host rock is ultramafic. Calcite occurs farther out from the fluid conduit. The replacement calcite present in the intense carbonate alteration zones can be distinguished from the dispersed calcite using the characteristics listed on Table 8-2. The oxygen and carbon isotopic values for these hydrothermal carbonates are listed in Appendix-1 and in Figures 8-1 and 8-2.

#### 8.2.2.1. Replacement calcite

Although many fewer data exist, the  $\delta^{13}\text{C}$  of this hydrothermal calcite ranges from -3.2 to +0.5‰ with a mode at -2.3‰ (Fig. 8-1).  $\delta^{18}\text{O}$  for this calcite ranges from +8.2 to +13.8‰ (Fig. 8-2).

#### 8.2.2.2. Replacement dolomite and magnesite

The carbon and oxygen isotopic values of hydrothermal dolomite and magnesite, developed within any given alteration zone in ultramafic rock, are nearly identical (Fig. 8-4) and hence, the magnesite and dolomite isotopic data are grouped together for the remainder of the discussion.

On the scale of a discrete carbonate alteration zone, isotopic variations exist which correlate with variations in alteration intensity. For example,

TABLE 8-2: Criteria to distinguish the dispersed calcite variety from the replacement variety present in Carbonatization Zones (Transitional and Hydrous alteration facies).

| Criteria                    | Dispersed<br>Calcite                                                                 | Replacement Calcite<br>in Intense Carbonatization<br>Alteration Zones                    |
|-----------------------------|--------------------------------------------------------------------------------------|------------------------------------------------------------------------------------------|
| =====                       |                                                                                      |                                                                                          |
| Host rock bulk<br>chemistry |                                                                                      |                                                                                          |
| L.O.I.                      | <5 wt. %                                                                             | 6 to 12 wt. %                                                                            |
| CaO                         | 8 to 11 wt. %                                                                        | 13 to 18 wt. %                                                                           |
| -----                       |                                                                                      |                                                                                          |
| Petrography                 | <5 modal % calcite<br>epidote present,<br><20 modal % chlorite,<br>tremolite present | 5 to 20 modal % calcite<br>epidote absent,<br>> 20 modal % chlorite,<br>tremolite absent |
| -----                       |                                                                                      |                                                                                          |
| Habit                       | Vesicle-filling<br>Veinlet locally                                                   | Whole scale replacement<br>of rock.                                                      |
| =====                       |                                                                                      |                                                                                          |

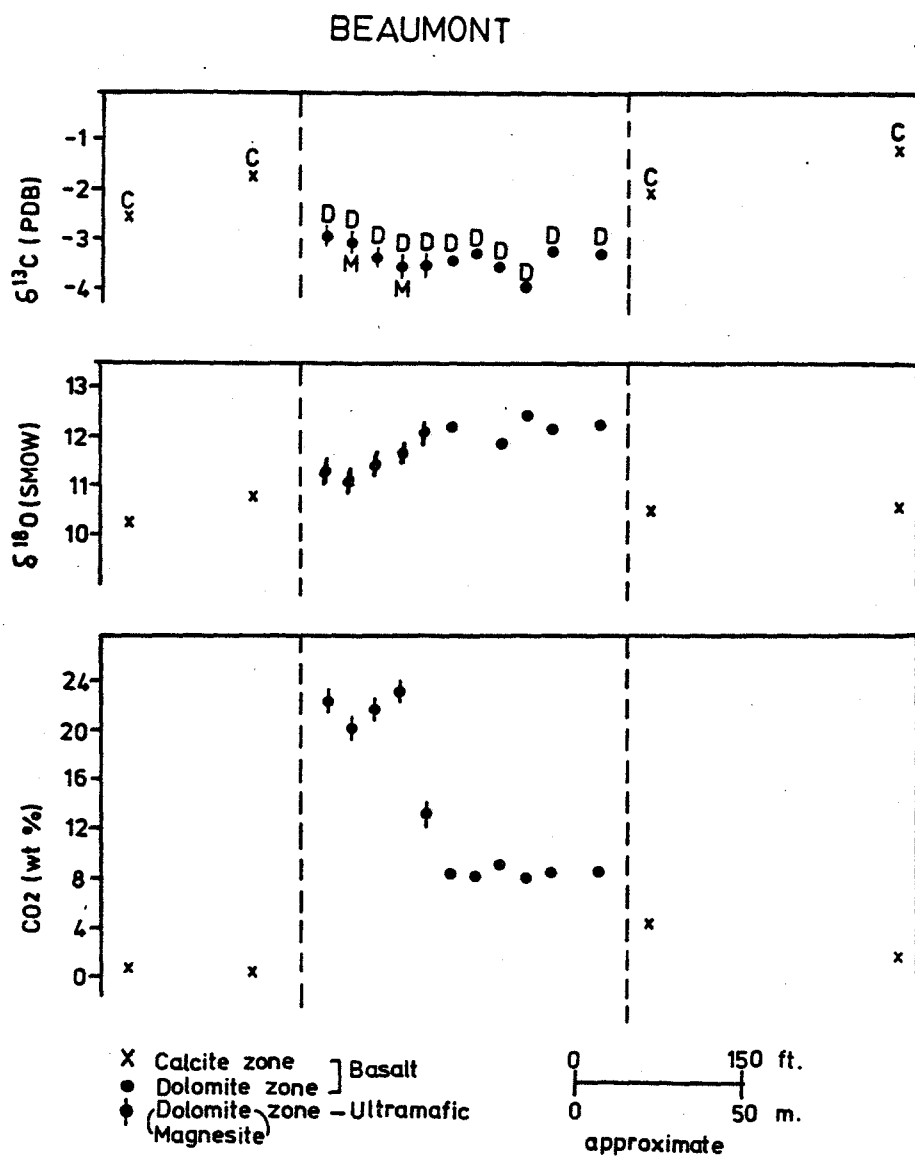


Figure 8-4:  $\delta^{13}\text{C}$  and  $\delta^{18}\text{O}$  profiles of hydrothermal carbonates and whole rock  $\text{CO}_2$  wt.% across the Beaumont carbonate alteration zone. Mineral symbols are: C-calcite; D-ferroan dolomite; M-magnesite.

illustrated on Figure 8-5 are oxygen and carbon isotopic values of hydrothermal carbonate across various zones of intense carbonatization. The following general relationships apply on the scale of a single alteration zone:

1) the  $\delta^{13}\text{C}$  values are lightest, but remain relatively uniform within the more intensely altered zone where magnesite or ferroan dolomite are present. There is no correlation between percent  $\text{CO}_2$  in the whole rock and  $\delta^{13}\text{C}$  of the dolomite and/or magnesite in this part of the alteration zone, despite large changes in  $\text{CO}_2$  abundance;

2) the  $\delta^{13}\text{C}$ -values become increasingly heavier by 3 or 4 ‰ towards the outer edge of the alteration zone where calcite, and not dolomite, is stable, but rarely exceeds about 0 ‰. This change is accompanied by an order of magnitude change in the  $\text{CO}_2$  abundance in the whole rock.

3) the  $\delta^{18}\text{O}$  of the hydrothermal dolomite and magnesite, present in the more intensely altered core of the zone, either is identical to that of the hydrothermal calcite (most of the Davidson-Tisdale profiles, Fig. 8-5A) or exceeds that of the calcite by 1 to 2 ‰ (McEnaney profiles, Fig. 8-5B).

### 8.2.3. Explanation for the stable isotopic profiles

For those carbonate alteration zones which do not occur in proximity to carbonaceous sediments, the  $\delta^{13}\text{C}$  of

Figure 8-5A: Variation of  $\delta^{13}\text{C}$ - and  $\delta^{18}\text{O}$ -values of hydrothermal carbonate and whole rock  $\text{CO}_2$  wt.% across different facies of the carbonate alteration zone exposed on the Davidson Tisdale property. See Map 11 in Appendix-1 for sample locations. Symbols as follows: RD-replacement ferroan dolomite zone; RC-replacement calcite zone; DC-disseminated calcite. Note that  $\delta^{18}\text{O}$  of the carbonate generally remains uniform across alteration facies boundaries.





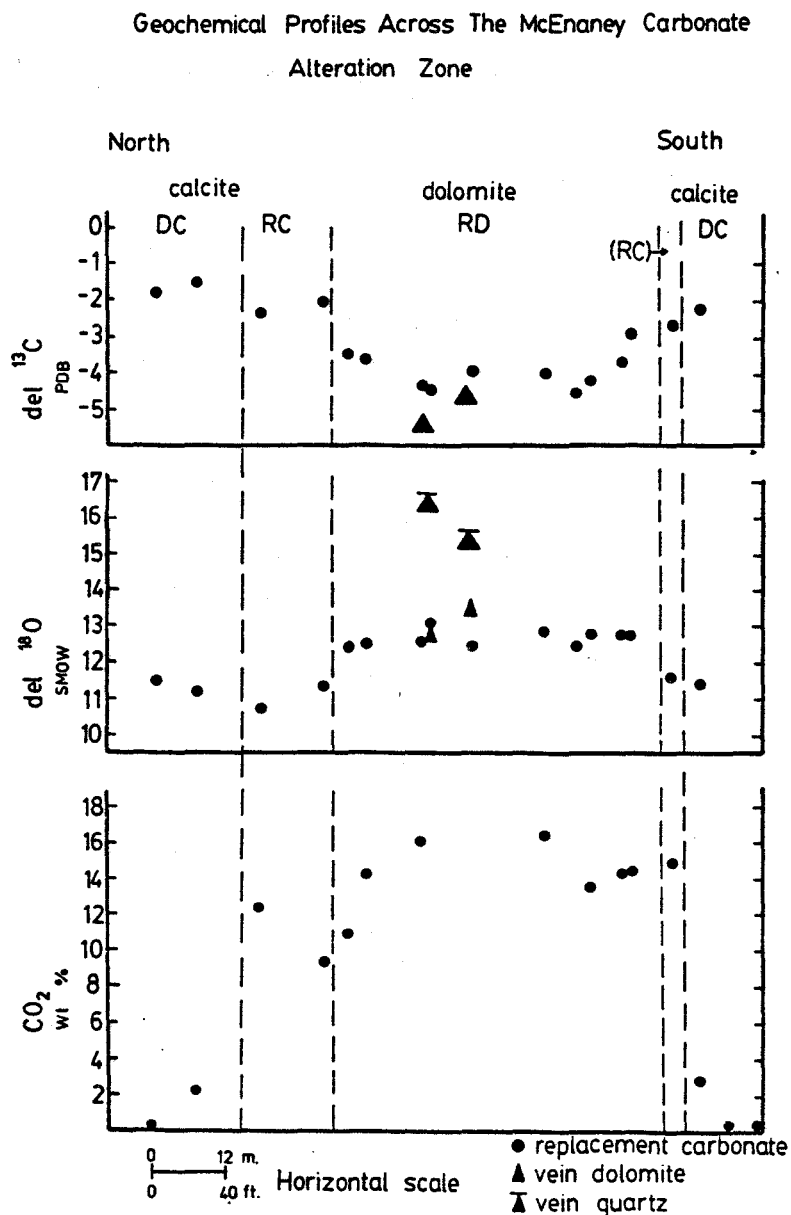


Figure 8-5B: Variations in  $\delta^{13}\text{C}$ - and  $\delta^{18}\text{O}$ -values and  $\text{CO}_2$  abundances across the carbonate alteration zone exposed on the McEnaney property, Ogden Township. The  $\delta^{18}\text{O}$  of the hydrothermal calcite is about 1‰ lighter with respect to the that of the hydrothermal dolomite.

the hydrothermal carbonate ranges between -3 to -4‰ within the Intense Carbonate Alteration Facies where dolomite and magnesite are stable, but increases to about -1‰ in the Transitional and Hydrous Alteration Facies where calcite is present (Fig. 8-5). It is unlikely that the heavier  $\delta^{13}\text{C}$  of the replacement calcite reflects solely the presence of dispersed calcite (or vesicle calcite) which has been overprinted by the replacement calcite of the Transitional Alteration Facies, because the volcanic rock containing the dispersed calcite has whole rock abundances of less than 1 wt. %  $\text{CO}_2$ , while the replacement calcite assemblage can have up to 12 wt. %  $\text{CO}_2$  (Fig. 8-5B). This replacement calcite, formed during the intense carbonatization, would simply outweigh any trace quantities of dispersed calcite present. However, the presence of relict dispersed calcite (precipitated during the lower temperature sea water alteration) in the outer fringes of the Hydrous Alteration Facies could influence the  $\delta^{13}\text{C}$  of the carbonate fraction, because the whole rock  $\text{CO}_2$  abundance of this less altered rock is low (< 2 wt. %). Thus, the change in  $\delta^{13}\text{C}$  of the replacement carbonate from -4‰, where magnesite or dolomite is stable, to -1‰, where replacement calcite is stable, reflects a change in an alteration parameter and is not an isotopic relict of the disseminated calcite that was precipitated earlier during the sea water alteration event.

This change in  $\delta^{13}\text{C}$  could be related to the change

in carbonate mineralogy that takes place across the alteration zone (Fig. 2-2) or to change in one or more of the intensive (temperature, pH,  $fO_2$ ) or extensive ( $CO_2/H_2O$  mole ratio) parameters which describe the alteration system (Chapter 5.5). The effects of changes in some of these parameters on the isotopic composition of precipitated carbonate are discussed and evaluated in the following sections.

#### 8.2.3.1. Change in carbonate mineralogy

The mineralogy of the replacement carbonate in the alteration zones changes from ferroan dolomite, located closest to the fluid conduit, to calcite farther out. Generally this change takes place across the Transitional Alteration Facies where the isotopic shift occurs. At a given temperature, calcite and dolomite do not have the same oxygen and carbon isotopic  $\Delta$  values. For example, if calcite and dolomite coprecipitate from the same fluid at 300° to 500°C, then dolomite should be enriched in  $^{18}O$  by 0.5 to 1‰ and in  $^{13}C$  by 0.5‰ with respect to the calcite (Sheppard and Schwarcz, 1970). Therefore, it is possible that the change in isotope values across the carbonate alteration zone reflects a change in the proportion of these different carbonates. If this were the case, then it could be predicted that a change in oxygen and carbon isotopic value would accompany the change from dolomite to calcite

precipitation, if both were to precipitate from a single hydrothermal fluid having a constant isotopic value. The magnitude and direction in which the oxygen and carbon isotopic values of the precipitated carbonate would change is: 1) 1‰ decrease in  $\delta^{18}\text{O}$  of the precipitated carbonate; 2) 0.5‰ decrease in the  $\delta^{13}\text{C}$  of the precipitated carbonate. However, the  $\delta^{13}\text{C}$ -values of the hydrothermal carbonates increase by 4‰ across the alteration zone, which is opposite to that which would be expected. Thus, the magnitude and direction of the observed  $\delta^{13}\text{C}$  shift cannot be attributed simply to the change from ferroan dolomite to calcite precipitation across the alteration zone. Conversely, the observed  $\delta^{18}\text{O}$ -values of the hydrothermal carbonates either remain approximately constant or decrease by 1‰ where calcite becomes stable, and ferroan dolomite is absent. The direction and magnitude of this trend is consistent with that which would be expected for a change in the type of carbonate that precipitated.

#### 8.2.3.2. Temperature

The temperature of a hydrothermal fluid could have decreased as it infiltrated out away from the fluid conduit into the wallrock. Hydrothermal carbonate that precipitated early from a hotter hydrothermal fluid would be isotopically different compared to carbonate that precipitated later from the same, but cooler hydrothermal fluid, assuming that the

isotopic composition of the fluid remained constant and the volume of fluid (both  $\text{CO}_2$  and  $\text{H}_2\text{O}$  components) remained large with respect to the volume of rock. The magnitude of this temperature effect on carbon isotope fractionation between  $\text{CO}_2$  and dolomite is illustrated on Figure 8-6. If all other conditions describing the hydrothermal fluid remained constant as the cooling and carbonate precipitation took place, then the  $\Delta_{\text{dolomite-CO}_2}^{13\text{C}}$  curves also model the  $\delta^{13\text{C}}$  of the precipitated dolomite, if for convenience, the  $\delta^{13\text{C}}$  of the  $\text{CO}_2$  is arbitrarily set to 0‰.

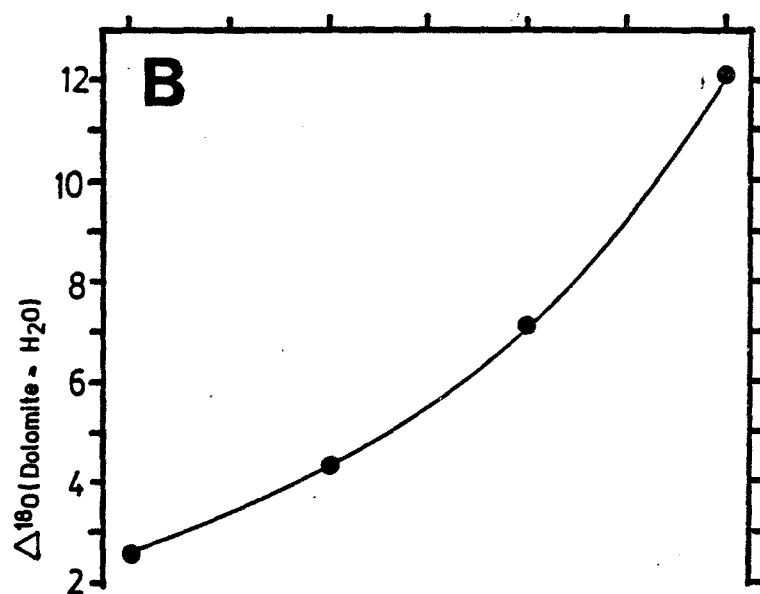
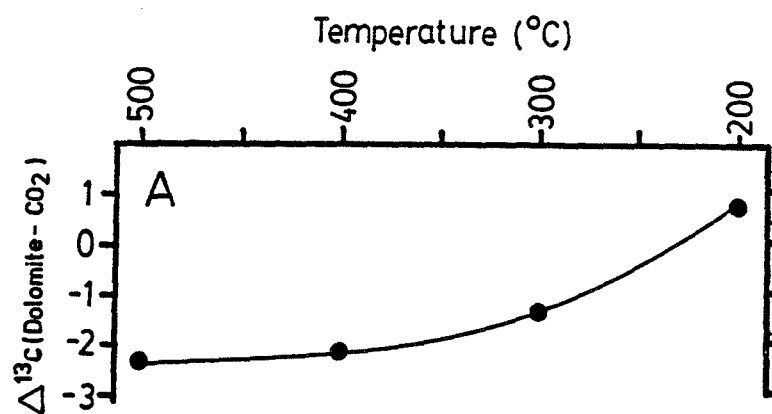
The  $\Delta_{\text{dolomite-CO}_2}^{13\text{C}}$  fractionations (Fig.8-6) are relatively temperature insensitive above  $350^\circ\text{C}$ . Thus, a hydrothermal fluid that infiltrated away from a conduit while precipitating dolomite, could cool to  $350^\circ\text{C}$  before a significant change in the  $\Delta_{\text{dolomite-CO}_2}^{13\text{C}}$  or in  $\delta^{13\text{C}}$  of the precipitated carbonate would occur. Therefore, if the observed 3 or 4‰ change in  $\delta^{13\text{C}}$ -values of the replacement carbonate across the carbonate alteration zone is to be attributed to the effect of decreased reaction temperature, this change would have occurred abruptly across the Transitional Alteration Facies (where calcite becomes stable) and correspond to a drop in temperature below  $350^\circ\text{C}$ . A decrease in temperature from  $350^\circ\text{C}$  to  $225^\circ\text{C}$  during carbonate replacement of the volcanic rock could account for both the magnitude and direction of change in  $\delta^{13\text{C}}$  of the replacement carbonate.

Figure 8-6:

A) Change in  $\Delta^{13}\text{C}_{\text{Dolomite-Carbon dioxide}}$  as a function of temperature.

B) Change in  $\Delta^{18}\text{O}_{\text{Dolomite-Water}}$  as a function of temperature.

The  $\Delta_{\text{Dolomite-Carbon dioxide}}$  carbon isotope fraction expression is based on the  $\Delta_{\text{Dolomite-Water}}$  fractionation expression (Sheppard and Schwarcz, 1970) and  $\Delta_{\text{Calcite-Carbon dioxide}}$  fractionation expression (Bottinga, 1969).





However, if a temperature decrease is solely responsible for the observed increase in  $\delta^{13}\text{C}$  of the precipitated carbonate, then a corresponding increase in  $\delta^{18}\text{O}$  of the hydrothermal carbonate should also be observed (Fig. 8-6). However, the  $\delta^{18}\text{O}$  of the hydrothermal carbonate either remains relatively constant or decreases across the carbonate alteration zone (Fig. 8-5). Thus, these carbon and oxygen isotopic trends are not consistent with a simple model of decreasing precipitation temperature across the carbonate alteration zone.

Assuming the oxygen isotopic composition of the water in the hydrothermal fluid remained constant during the precipitation of the dolomite within the more intensely altered core of a zone, then the uniform  $\delta^{18}\text{O}$ -values of dolomite across the intense carbonate alteration facies indicates that the hydrothermal fluid remained essentially isothermal, at least in this alteration facies.

Thus, it seems that a temperature decrease cannot adequately explain the increasing  $\delta^{13}\text{C}$  and decreasing or uniform  $\delta^{18}\text{O}$  values of the hydrothermal carbonate observed across the Transitional Alteration Facies.

#### 8.2.3.3. $\text{CO}_2/\text{H}_2\text{O}$ molar ratio

Continuous reaction between a  $\text{CO}_2$ -rich aqueous hydrothermal fluid and mafic or ultramafic rock which results in the precipitation of hydrothermal carbonate, will

will consume  $\text{CO}_2$  from the fluid and reduce the  $\text{CO}_2/\text{H}_2\text{O}$  molar ratio, unless mass transfer from the fluid conduit to the leading edge of alteration is rapid and efficient.

Empirical evidence, in the form of the abruptly decreased carbonate (calcite) abundance across the Transitional Alteration Facies (Fig. 8-5), indicates that an abrupt decrease in the  $\text{CO}_2/\text{H}_2\text{O}$  molar ratio of the hydrothermal fluid did take place. Fluid inclusion studies (Chapter 5.1) show that the  $X_{\text{CO}_2}$  of the hydrothermal fluid could have been as high as 0.7 in and immediately adjacent to the fluid conduit (Intense Carbonate Alteration Facies); however, experimental mineral-fluid studies (discussed in Chapter 5) demonstrate that the  $X_{\text{CO}_2}$  of the hydrothermal fluid decreased by as much as 2 orders of magnitude, to less than 0.05 in the outer edges of the Hydrous Alteration Facies where calcite is stable. Fluids in equilibrium with assemblages bearing calcium-aluminosilicates (mineralogically characteristic of the outer edges of the Hydrous Alteration Facies; Fig. 2-2) are buffered to very low  $\text{CO}_2$  concentrations (c.f. Johannes, 1969:  $\text{MgO}-\text{SiO}_2-\text{H}_2\text{O}-\text{CO}_2$ ; Metz and Trommsdorff, 1968: siliceous dolomite; Thompson, 1971:  $\text{CaO}-\text{Al}_2\text{O}_3-\text{SiO}_2-\text{CO}_2-\text{H}_2\text{O}$ ; Schuiling and Vink, 1967: Titanium minerals- $\text{H}_2\text{O}-\text{CO}_2$ ). Thus, the  $X_{\text{CO}_2}$  of the hydrothermal fluid must have decreased in passing from the fluid conduit, through the Intense Carbonate Alteration Facies, outward toward the outer fringes of the Hydrous Alteration Facies.

Continuous depletion of  $\text{CO}_2$  from the hydrothermal fluid resulting from precipitation of carbonate will be accompanied by changes in the  $\delta^{13}\text{C}$  of the fluid which will follow a Rayleigh distillation trend, if the composition of the fluid cannot be maintained by diffusion from the conduit. To model such a carbon isotopic Rayleigh fractionation process, the following assumptions have been made: 1) the  $\delta^{13}\text{C}$  of the starting fluid is taken to be -5‰; 2) for simplicity, only calcite is precipitated, because virtually all of the observed change in  $\delta^{13}\text{C}$  takes place across the Transitional and Hydrous Alteration Facies where only calcite was precipitated; 3) precipitation temperature is held at a constant 400°C; 4) the precipitation takes place under equilibrium conditions; 5) once precipitated, the calcite does not undergo further isotopic exchange with the ambient hydrothermal fluid; 6) the stable and dominant dissolved C-bearing species in solution is  $\text{CO}_2$  (ie  $X\text{CO}_2 \gg X\text{HCO}_3 + X\text{CO}_3$ ); 7)  $\Delta_{\text{calcite-CO}_2}^{13\text{C}}$  remains constant through the precipitation process.

The equilibrium precipitation of calcite from a  $\text{CO}_2$ -rich fluid can be described by the following expression:

$$R/R_0 = f^{(\alpha - 1)}$$

where  $R = {}^{13}\text{C}/{}^{12}\text{C}$  ratio of the remaining fluid

$R_0 = {}^{13}\text{C}/{}^{12}\text{C}$  ratio of the fluid before

crystallization begins

$f$  = fraction of fluid remaining

$\alpha$  = isotope fractionation factor  $R_{cc}/R_v$

$R_{cc}$  =  $^{13}\text{C}/^{12}\text{C}$  ratio of the calcite

$R_v$  =  $^{13}\text{C}/^{12}\text{C}$  ratio of the fluid.

The conversion of isotope ratios  $R$  and  $R_o$  to the  $\delta$ -notation is accomplished using:

$$\alpha = \frac{R_{cc}}{R_v} = \frac{\delta^{13}\text{C}_{cc} + 1000}{\delta^{13}\text{C}_o + 1000}$$

ie

$$\frac{R}{R_o} = \frac{\delta^{13}\text{C} + 1000}{(\delta^{13}\text{C})_o + 1000}$$

Therefore,

$$\delta^{13}\text{C}_f = [(\delta^{13}\text{C}_o) + 1000] f^{(\alpha-1)} - 1000$$

The  $\delta^{13}\text{C}$  of the precipitated calcite that is in equilibrium with the fluid at any given instant is given by:

$$\delta^{13}\text{C}_{cc} = \alpha [(\delta^{13}\text{C}_f) + 1000] - 1000$$

The  $\Delta$  Calcite-Carbon dioxide carbon isotope fractionation by Bottinga (1969) is used in the subsequent calculations:

$$10^3 \ln \alpha_{\text{CC-CO}_2} = -8.9(10^8 \text{K}^{-3}) + 8.56(10^6 \text{K}^{-2}) - 18.11(10^3 \text{K}^{-1}) + 8.27$$

At 400°C,  $\alpha_{\text{CC-CO}_2}^{^{13}\text{C}}$  is 0.99734 which means that the fluid

is enriched in  $^{13}\text{C}$  by approximately 2.7‰ with respect to the precipitated calcite.

The effect of Rayleigh distillation is to produce a  $^{13}\text{C}$ -enriched residual fluid, if the rock/ $\text{CO}_2$ -rich fluid reaction takes place above 200°C (Fig. 8-7). Precipitated calcite will be correspondingly  $^{13}\text{C}$ -enriched. If the observed decrease in hydrothermal calcite modal abundance across the Transitional Alteration Zone (Fig. 8-5) corresponds to a decrease in the  $\text{CO}_2/\text{H}_2\text{O}$  molar ratio in the hydrothermal fluid due to precipitation of a carbonate phase, then such a Rayleigh distillation process describes the direction of the observed carbon isotopic trends across the outer edge of the carbonate alteration zone

To model the  $\delta^{18}\text{O}$  evolution of such a system is more difficult because of the abundance of oxygen-bearing silicate phases in the rock, each capable of exchanging with the evolving fluid, and the probable changes in water/rock ratio, resulting in changes in  $\delta^{18}\text{O}$  of the water and  $\text{CO}_2$  components in the hydrothermal fluid. In this regard, recall that the  $\delta^{18}\text{O}$ -values of the hydrothermal carbonate are relatively uniform across the alteration facies (Fig. 8-5), which suggests that: 1) the  $\delta^{18}\text{O}$  of the hydrothermal fluid was quite uniform, and therefore, variation in  $\delta^{18}\text{O}$  across the carbonate alteration zone reflects the change in carbonate mineralogy (see Section 8.2.3.1); or 2) the  $\delta^{18}\text{O}$  of the carbonate represents an "exchanged" value, resulting

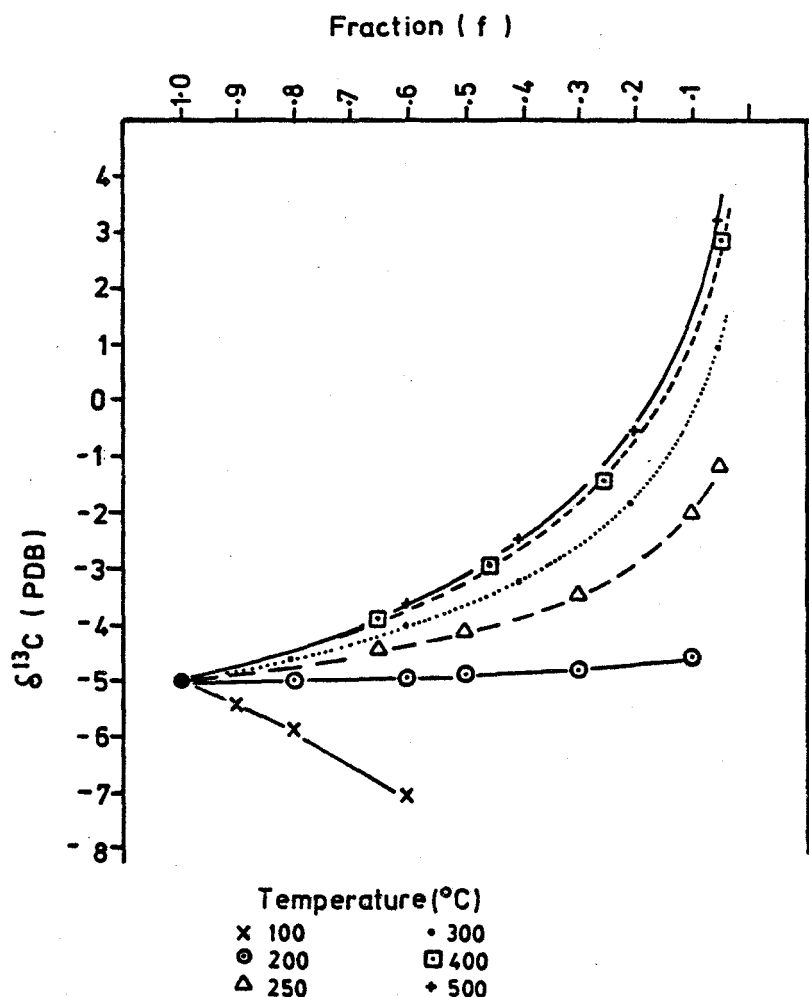


Figure 8-7: Effect of Rayleigh distillation on  $\delta^{13}\text{C}$  composition of a  $\text{CO}_2$  fluid as a function of temperature. Rayleigh distillation or removal of  $\text{CO}_2$  from the fluid is induced by reaction between a mafic rock and the fluid resulting in carbonatization. For all calculations, the fluid started with an initial  $\delta^{13}\text{C}$  composition of  $-5\text{‰}$  (PDB). At temperatures above  $200^\circ\text{C}$ , Rayleigh distillation of  $\text{CO}_2$ , by calcite precipitation, enriches the fluid in  $^{13}\text{C}$ . Subsequently precipitated calcite would be correspondingly enriched in  $^{13}\text{C}$ . Fraction (f) corresponds to the fraction of hydrothermal fluid remaining.

from interaction with an aqueous, metamorphic fluid.

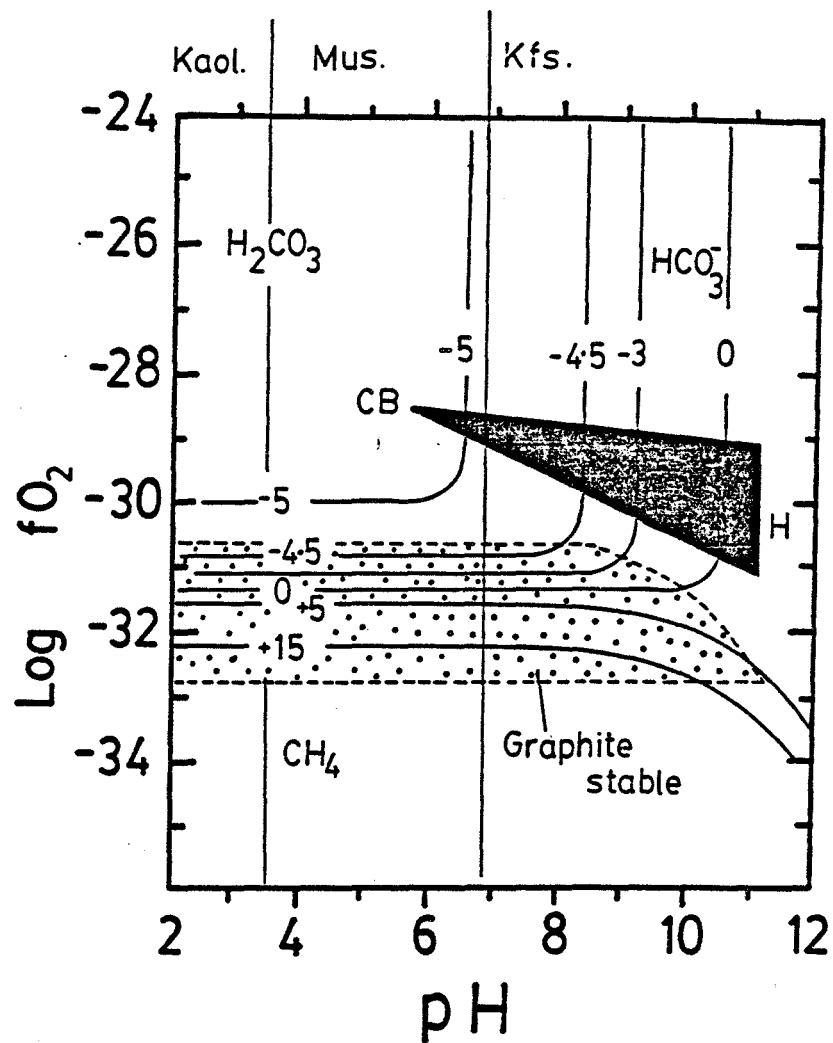
#### 8.2.3.4. pH and $fO_2$

As described in Chapter 5, the pH and  $fO_2$  of the hydrothermal fluid are buffered by and can be constrained using the alteration mineral assemblages. The pH and  $fO_2$  trajectory mapping of the fluid evolution as a function of alteration assemblage is indicated on Figure 8-8. This model is based on the development of alteration assemblages in a rock having an ultramafic bulk composition, as described in Chapter 5. Also indicated are the contours for  $\delta^{13}C_{CO_2}$  taken from Ohmoto (1972) for a  $CO_2$ -bearing aqueous fluid at  $350^\circ C$  with  $\delta^{13}C_{\Sigma C} = -5\%$ . The sericite-dolomite assemblage of the Intense Carbonatization Facies developed under relatively oxidizing, near neutral pH (region "CB"; Fig. 8-8) whereas the incipient hydration (Hydrous Alteration Facies) developed under more basic, less oxidizing conditions (region "H"; Fig. 8-8), as discussed in Chapter 5.1.

Now, the  $fO_2$ -pH gradient that must exist across the boundary between the Hydrous and Intense Carbonatization Alteration Facies also corresponds to a shift in the nature of carbon speciation in the aqueous fluid from  $CO_2$  in the sericite-dolomite stable field to  $HCO_3^-$  or  $CO_3^{2-}$  dominant under the more basic regime of hydrous alteration. The change in  $^{13}C$ -partitioning between the carbon species

Figure 8-8: pH-log  $fO_2$  trajectory for a  $CO_2$  bearing, subcritical aqueous hydrothermal fluid which reacts with ultramafic rock to produce the Hydrous (H) and Intense Carbonatization (CB) Alteration Facies. The plot is constructed at  $350^\circ C$ , using a  $\delta^{13}C$  of the total dissolved carbon of  $-5\text{‰}$  (PDB). Stability field for graphite calculated for  $\Sigma C$  at 3 moles/Kg  $H_2O$ . Muscovite-K-felspar boundary at  $K^+=0.001$  moles/Kg  $H_2O$  and kaolinite-muscovite at  $K^+=0.1$  moles/Kg  $H_2O$ . This represents a maximum field for muscovite stability (Ohmoto, 1972).





$T=350^\circ C : \delta^{13}C_{\Sigma C} = -5$  (magmatic)

Contours for  $\delta^{13}C$  of dissolved  $CO_2$   
in solution.

results in an increased  $\delta^{13}\text{C}$  of the residual  $\text{CO}_2$  under basic conditions, when  $\text{CO}_3^{2-}$  is dominant; however,  $\delta^{13}\text{C}_{\text{CO}_2}$  approaches that of the total dissolved carbon under the near neutral, oxidizing conditions deduced for the sericite-dolomite assemblage (region CB; Fig. 8-8). That is, the  $\delta^{13}\text{C}$  of the precipitated hydrothermal carbonate should become progressively heavier as the fluid passes from the inner sericite-dolomite facies, developed closest to the fluid conduit, out through the Transitional Alteration Facies into the Hydrous Alteration Facies. Thus, pH and  $f\text{O}_2$  changes in the hydrothermal fluid, in response to wallrock-fluid reactions, could account for the observed increase in  $\delta^{13}\text{C}$  of the hydrothermal carbonate across the alteration zone (Fig. 8-5).

#### 8.2.4. Summary

An increase in  $\delta^{13}\text{C}$  of the hydrothermal carbonate, from -4 to -1‰ takes place across the carbonate alteration zone (Fig. 8-5). This change could be related to a decrease in the  $\text{CO}_2/\text{H}_2\text{O}$  molar ratio of the fluid or a change in the pH and  $f\text{O}_2$  of the fluid. Considering the nature and mineral proportions in the alteration assemblages suggests that all three factors were operative and were collectively responsible for the observed systematic  $\delta^{13}\text{C}$  variation of the hydrothermal carbonate. The effect of pH and  $f\text{O}_2$  changes on the  $\delta^{13}\text{C}_{\text{CO}_2}$  of the hydrothermal fluid is

expected to have been more profound for the reactive ultramafic rocks and less influential for the relatively less reactive basaltic rocks. Notwithstanding the effects of pH and  $fO_2$ , the empirical data indicate that the hydrothermal fluid became progressively depleted in  $CO_2$  as it passed outward from conduit (ferroan dolomite- or magnesite-bearing alteration assemblages), through the calcite-bearing and ultimately, into the carbonate-free assemblages. It is highly probable that this fluid evolution was accompanied by a Rayleigh fractionation effect, which accounted for the largest part of the change in  $\delta^{13}C$  of the hydrothermal carbonate (from -4 to 0‰).

The Rayleigh fractionation model predicts that the  $\delta^{13}C$  of the fluid (and hence of the precipitated carbonate) should become extremely heavy as the fraction of fluid remaining decreases below about 20% of the initial amount (Fig. 8-7). However, the measured  $\delta^{13}C$  of the replacement calcite in the Transition and Hydrous Alteration Facies rarely exceeds 0‰, even though the mole fraction of  $CO_2$  in the fluid must have approached a minuscule amount. The absence of extreme  $^{13}C$ -enrichment in the calcite at the outer edges of the alteration zone may reflect: 1) the dominance in the rock of the pre-existing dispersed calcite, whose  $\delta^{13}C$  does not exceed 0‰; 2) a nonequilibrium, kinetic isotope exchange between the outward moving  $CO_2$ -bearing hydrothermal fluid and the pre-existing dispersed

calcite (precipitated during the sea water alteration) such that the difference between the  $\delta^{13}\text{C}$  of the hydrothermal fluid at that point and its starting  $\delta^{13}\text{C}$  reaches a plateau. Both these possible explanations point to the presence of the dispersed calcite.

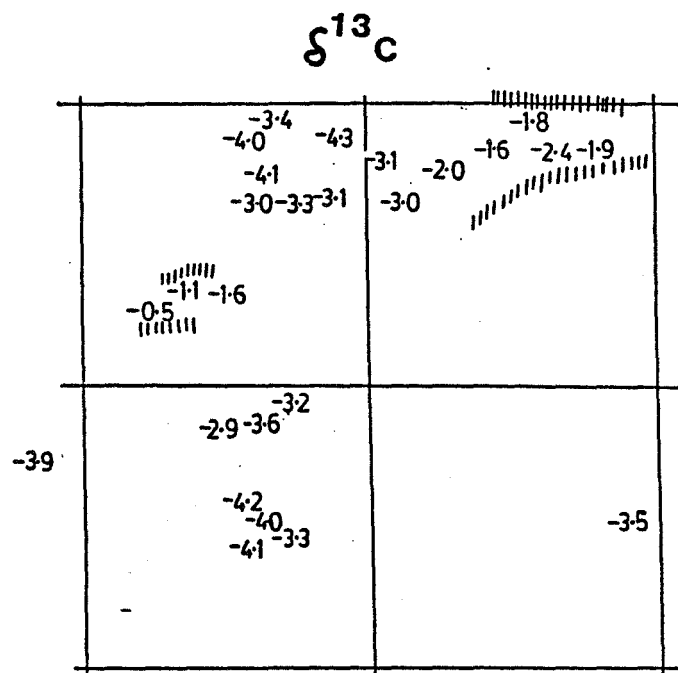
### 8.3. Regional Isotopic Variation of Hydrothermal Dolomite or Magnesite

A wide variation of  $\delta^{13}\text{C}$  and  $\delta^{18}\text{O}$  characterizes the hydrothermal dolomite and magnesite from the Timmins area (Figs. 8-1 and 8-2). The  $\delta^{13}\text{C}$  and  $\delta^{18}\text{O}$  values of these carbonates show a geographical dependence (Fig. 8-9 and 8-10). The heaviest  $\delta^{13}\text{C}$ -values are found in central Tisdale Township in an area which includes the Hollinger, McIntyre and Coniaurum Mines and in northern Whitney Township on the Pamour #1 and Hallnor properties. The heaviest  $\delta^{18}\text{O}$  values occur in an area centred on the Hollinger mineralized zone. Several processes could give rise to the isotopic variation. The carbon isotopic data are considered first.

#### 8.3.1. Methane stabilization

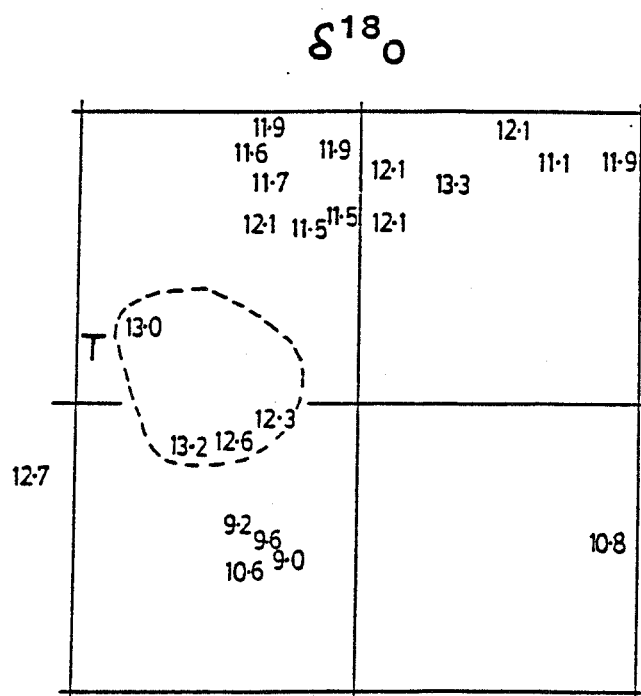
A clue to the geographical dependence of  $\delta^{13}\text{C}$  comes from the types of associated rock types near and within the zones of carbonate alteration. The regional distribution of carbonaceous sediments is illustrated on Figure 8-9. These sediments are manifest as thin, (<1m) interflow units on the

Figure 8-9: Regional variation of  $\delta^{13}\text{C}$ -values of hydrothermal vein and wallrock replacement ferroan dolomite and magnesite from properties in the Timmins area. Heaviest  $\delta^{13}\text{C}$ -values occur in areas where carbonaceous sediments (depicted by the short vertical lines) are present. This spatial correspondence between heavy  $\delta^{13}\text{C}$ -values of hydrothermal dolomite and magnesite and carbonaceous sediments suggests that the C-O-H hydrothermal fluid underwent an equilibria change, induced by the reduced carbon in the sediments, which produced some methane at the expense of  $\text{CO}_2$  and  $\text{H}_2\text{O}$ .

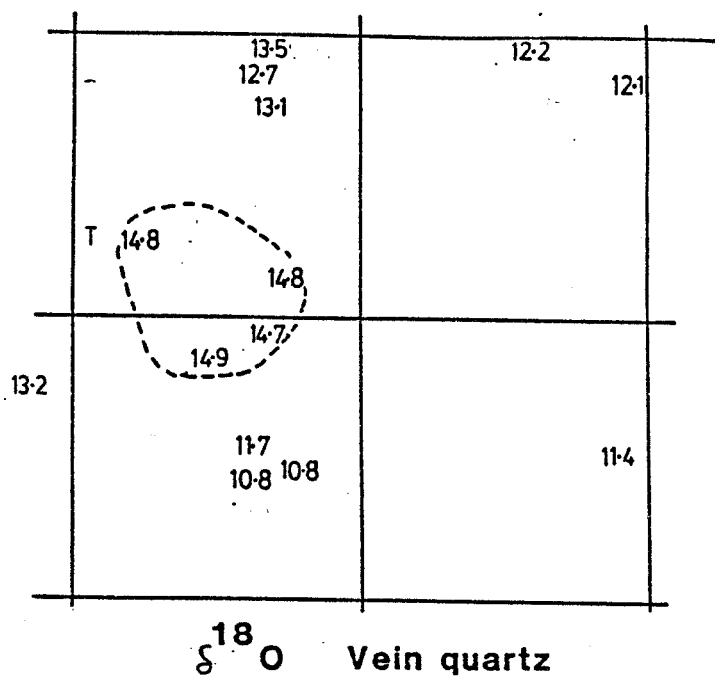


Hydrothermal dolomite and/or magnesite

Figure 8-10: Regional variation of  $\delta^{18}\text{O}$ -values for hydrothermal ferroan dolomite and magnesite and vein quartz in the Timmins area. Heaviest  $\delta^{18}\text{O}$ -values of vein quartz define an area of "anomalous" values (enclosed within the dashed circle), centred on the Hollinger-McIntyre-Dome mineralized systems, where intrusive quartz-feldspar porphyry bodies are most abundant. This " $\delta^{18}\text{O}$ -anomalous" area is less definitively defined by the  $\delta^{18}\text{O}$ -values of the ferroan dolomite. The city of Timmins is marked by the letter "T", and the blocked areas represent township boundaries.



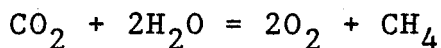
Hydrothermal dolomite and/or magnesite





Hollinger and McIntyre properties (see Chapter 4.1) or as carbonaceous slates in the wackes of the Porcupine Group exposed in northern Whitney Township, to the north in Hoyle Township and to the west in Mountjoy Township.

If a  $\text{CO}_2\text{-H}_2\text{O}$  hydrothermal fluid reacted with the carbonaceous sediments, some methane might have formed by the reaction (Ferry and Burt, 1982):



Decreased  $f\text{O}_2$  because of the presence of carbonaceous material would drive the reaction to the right to produce some methane ( $\text{CH}_4$ ). Residual  $\text{CO}_2$  in the hydrothermal fluid would be  $^{13}\text{C}$ -enriched. Carbonate minerals, when precipitated from such a hydrothermal fluid, would be similarly  $^{13}\text{C}$ -enriched. This effect is shown on Figure 8-8, where contours of higher  $\delta^{13}\text{C}$  are encountered in the field of low  $f\text{O}_2$ , where graphite is stable. The spatial influence of the carbonaceous sediments on the  $\delta^{13}\text{C}$  of the hydrothermal carbonate is emphasized in Figure 8-11, where  $\delta^{13}\text{C}$  of the hydrothermal dolomite and magnesite in carbonatized ultramafic flows in northern Whitney Township increases as the carbonaceous slates in the Porcupine Group sediments are approached.

In addition to the effect on the  $\delta^{13}\text{C}$  of the precipitated hydrothermal carbonate, the interaction between carbonaceous sediments and the  $\text{CO}_2\text{-H}_2\text{O}$  hydrothermal fluid

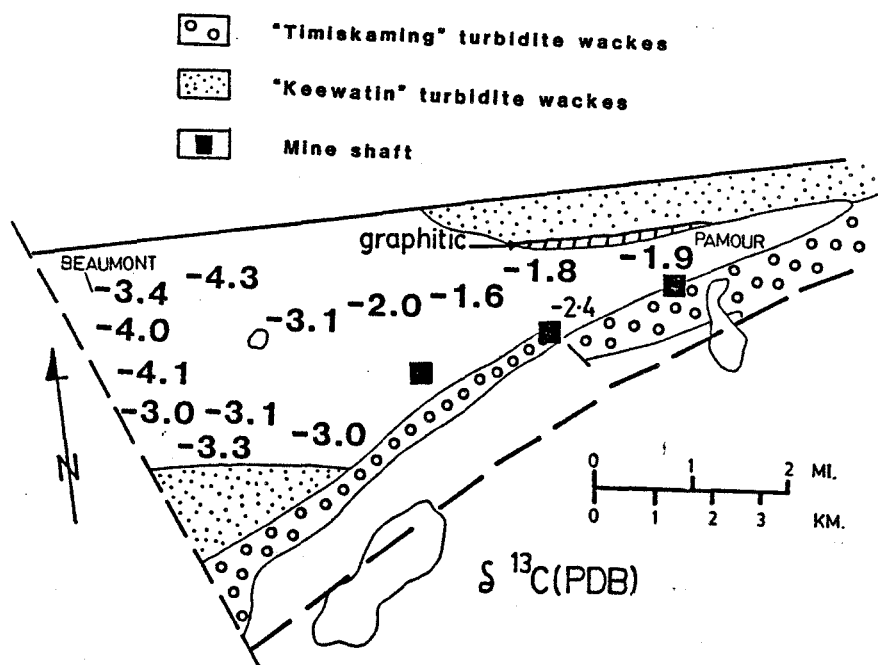


Figure 8-11: Regional variation of  $\delta^{13}\text{C}$  in hydrothermal dolomite and magnesite in mafic and ultramafic flows in northern Whitney Township. The heaviest  $\delta^{13}\text{C}$ -values occur closest to the gold mine locations (black square), and reflects the influence of the carbonaceous material in the slates of the Porcupine Group turbidite sequence.

also appears to have some effect on the gold tenor of a mineralized area. Shown in Figure 8-12 is the relationship between gold tenor of a property and the  $\delta^{13}\text{C}$  of the local hydrothermal carbonate. Two data populations are present. Hydrothermal carbonates in Population B deposits have uniform  $\delta^{13}\text{C}$ -values (-3 to -4.5‰), regardless of stratigraphic position, size or gold tenor of the alteration zone. Carbonates from deposits in Population A have  $\delta^{13}\text{C}$ -values which are generally heavier than -3‰ and are positively correlated with gold tenor.

Using the carbon isotope compositions of the hydrothermal carbonate that was precipitated in proximity to the carbonaceous sediments, it is possible to qualitatively model of the isotope shift associated with the proposed interaction using the following formula taken from Ohmoto and Rye (1979):

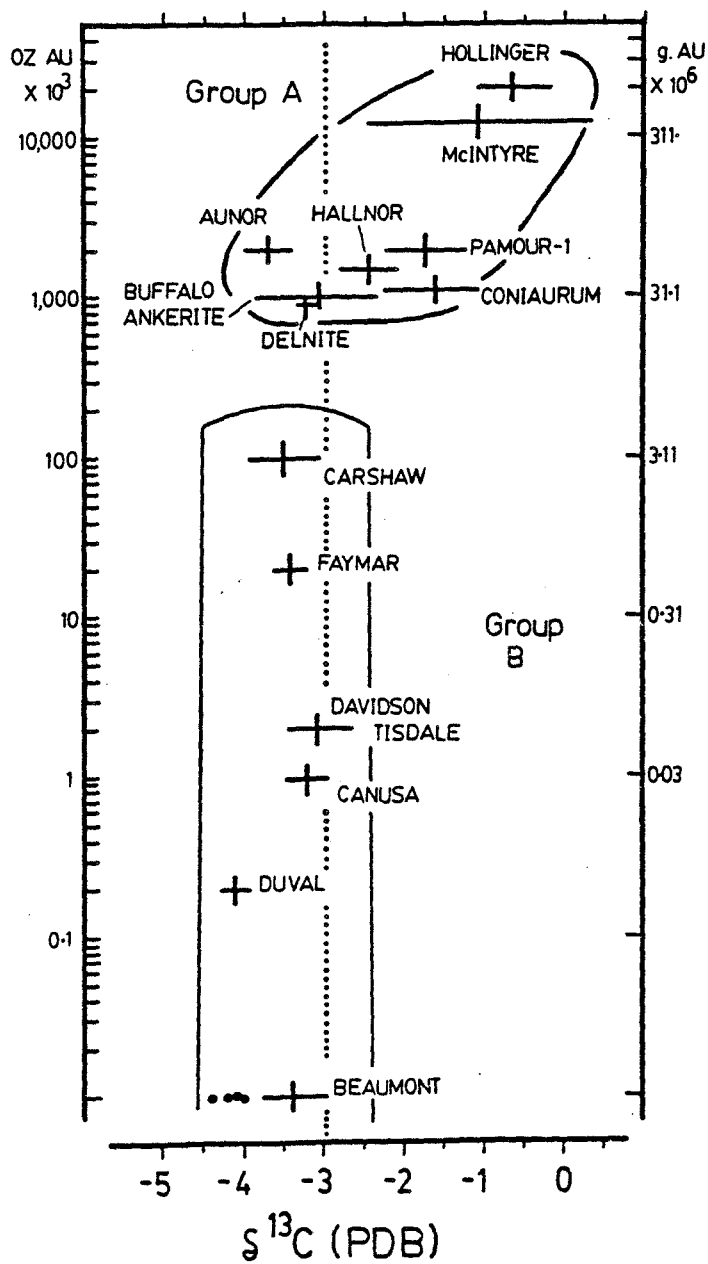
$$\begin{aligned}\delta^{13}\text{C}_{\text{F1}} &= (\delta^{13}\text{C}_{\text{CO}_2})(X\text{CO}_2) + (\delta^{13}\text{C}_{\text{CH}_4})(X\text{CH}_4) \\ &= (\delta^{13}\text{C}_{\text{CO}_2}) + (\Delta_{\text{CH}_4-\text{CO}_2})(R/1+R)\dots\dots\dots (1)\end{aligned}$$

where R is the mole fraction ( $\text{CH}_4/\text{CO}_2$ ) in the fluid and  $\Delta_{\text{CH}_4-\text{CO}_2}$  represents the  $^{13}\text{C}/^{12}\text{C}$  fractionation between  $\text{CH}_4$  and  $\text{CO}_2$  at a given temperature. Rearranging this equation yields equation (2):

$$(R/1+R) = (\delta^{13}\text{C}_{\text{F1}} - \delta^{13}\text{C}_{\text{CO}_2}) / (\Delta_{\text{CH}_4-\text{CO}_2}) \dots (2)$$

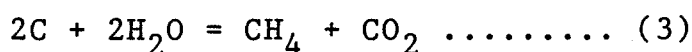
allows for the solution of R.

Figure 8-12:  $\delta^{13}\text{C}$ -values of hydrothermal dolomite and magnesite (calcite in the case of Faymar) plotted against the gold tenor of properties from the Timmins area. Group A deposits have  $\delta^{13}\text{C}$ -values which are positively correlated with gold tenor and occur within or in proximity to carbonaceous sediments. Group B deposits have  $\delta^{13}\text{C}$ -values which are not correlated with gold tenor and these properties are not proximal to carbonaceous sediments.



Now, some assumptions have been made to facilitate the calculations that follow. The temperature of  $\text{CH}_4$  stabilization has been modeled at 300°, 400° and 500°C for which the corresponding  $\Delta_{\text{CH}_4-\text{CO}_2}^{13\text{C}}$  values of -25, -19 and -16 respectively were used. The total dissolved carbon in the hydrothermal fluid is estimated to have had a  $\delta^{13}\text{C}_{\text{Total}}$  carbon of approximately -4‰. This follows from the general relationship that  $\delta^{13}\text{C}_{\text{Fluid}}$  approximately equals  $\delta^{13}\text{C}_{\text{Total}}$  under relatively oxidizing (graphite-free) conditions and  $\text{pH} < 6$  (Fig. 8-8; further discussion in Chapter 9).  $\delta^{13}\text{C}_{\text{Total}}$  carbon approximately equals the  $\delta^{13}\text{C}$  of the precipitated carbonate under these conditions (Fig. 8-8; Ohmoto and Rye, 1979; Ohmoto, 1972). This value of -4‰ represents the  $\delta^{13}\text{C}$  of the total dissolved carbon in the hydrothermal fluid before it entered the carbonaceous-bearing domains and is estimated from the  $\delta^{13}\text{C}$  of hydrothermal dolomite which precipitated away from carbonaceous sediments. The  $\delta^{13}\text{C}$  of  $\text{CO}_2$  from which the hydrothermal carbonate precipitated in the carbonaceous-bearing domain is estimated to have been approximately 0‰, deduced from the  $\delta^{13}\text{C}$  of the hydrothermal dolomite on the Hollinger Property. Substituting these values into equation (2), the following  $(\text{CH}_4/\text{CO}_2)$  mole ratios for the hydrothermal fluid are derived at 300°, 400° and 500°C respectively; 0.19, 0.27 and 0.37. The results of this approach are identical to that summarized in Figure 7-11.

Theoretical estimates of the speciation in C-O-H-S fluid systems are summarized by Ohmoto and Kerrick (1977), Ferry and Burt (1982) and Holloway (1981). These studies showed that the composition of C-O-H-S fluids in equilibrium with graphite in pelitic schists could be dominated by CH<sub>4</sub>, although CO<sub>2</sub> was often present. The CH<sub>4</sub> and CO<sub>2</sub> in these fluids can be produced by the reaction (Ferry and Burt, 1982):

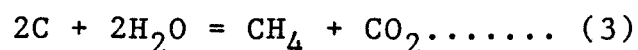


For example, log fO<sub>2</sub> determined by the QFM buffer would be fixed at approximately -30 at 400-350°C (Eugster, 1981). If, in the presence of graphite, log fO<sub>2</sub> was buffered at 2 log units below the QFM buffered value (eg. log fO<sub>2</sub> = -32), then a C-O-H fluid would consist almost entirely of CH<sub>4</sub> with virtually no CO<sub>2</sub> (see Fig.2 in Ferry and Burt, 1982). Clearly, the stabilization of this amount of CH<sub>4</sub> is not consistent with the proportion predicted from the stable isotope data. Further, recent fluid inclusion studies on quartz vein material from the McIntyre-Hollinger system, reported by Smith et al. (1984), show only one of twelve samples to have a (CH<sub>4</sub>/CO<sub>2</sub>) molar ratio in excess of 1.0 (sample MJ-23; CH<sub>4</sub>/CO<sub>2</sub>=1.06). The remaining eleven samples had CH<sub>4</sub>/CO<sub>2</sub> molar ratios averaging 0.06. It appears that substantial lowering of fO<sub>2</sub> due to the presence of carbonaceous material was only effective on a local scale

(cm.) where a quartz vein was actually hosted by a carbonaceous sediment.

The proposed model of closed system  $\text{CH}_4$  stabilization resulting from the reaction between an exotic C-O-H fluid and carbonaceous matter quantitatively explains the heavy (0‰)  $\delta^{13}\text{C}$ -values of hydrothermal carbonate which precipitated in proximity to carbonaceous sediments. However, ( $\text{CH}_4/\text{CO}_2$ ) mole fraction of the hydrothermal fluid is required to lie in the range of 0.2 to 0.3. This conflicts with the quantitative measurements of fluid inclusion hosted gases (Smith et al., 1984) which show the ( $\text{CH}_4/\text{CO}_2$ ) mole ratio not to exceed 0.07 except in one case where a quartz vein was hosted by carbonaceous sediment. Explanation of this discrepancy may lie in the analytical procedure used by Smith et al. (1984) where fluid inclusions were decrepitated from 20-30 gram of clean vein quartz. The gas fraction produced by such a technique must represent an integration of all fluid inclusion types present (discussion in Chapter 7.4). Hence, low ( $\text{CH}_4/\text{CO}_2$ ) molar ratios may represent a dilution effect by nearly pure  $\text{CO}_2$  or  $\text{H}_2\text{O}$  fluids.

Note that this model differs from one where  $\text{CH}_4$  and  $\text{CO}_2$  are formed by reaction between the carbonaceous matter and water from the hydrothermal fluid;





Both the  $\text{CH}_4$  and  $\text{CO}_2$  formed this way would be isotopically light ( $^{12}\text{C}$ -enriched). Addition of these components to the indigenous  $\text{CO}_2$  in the hydrothermal fluid result in a net lowering of the  $\delta^{13}\text{C}$  of the total  $\text{CO}_2$  in the mixture. The following arguments suggest that reaction (3) did not contribute large quantities of  $^{12}\text{C}$ -enriched  $\text{CO}_2$  to the hydrothermal fluid from which the hydrothermal carbonates on the Hollinger Mine property precipitated. The  $\delta^{13}\text{C}$  of the  $\text{CO}_2$  in the hydrothermal fluid, inferred from the  $\delta^{13}\text{C}$  of the precipitated carbonate, increases when the fluid entered the domain where carbonaceous matter was present (Fig. 8-9), as predicted in Figure 8-8. This is indicated by the 4‰ increase in the  $\delta^{13}\text{C}$  of the replacement and vein dolomites near the Pamour # 1 and Hollinger properties. Thus, it appears that little  $\text{CO}_2$  was transferred to the hydrothermal system directly from the carbonaceous units by oxidation of reduced carbon. In addition, equal amounts of  $\text{CO}_2$  and  $\text{CH}_4$  are produced as a result of reaction "3", but the fluid inclusion inclusion analysis (Smith et al., 1984; Smith and Kesler, 1985) show that none of the none of the samples contained equal amounts of these carbon species. This does not preclude the possibility that a minor proportion of the  $\text{CO}_2$  and  $\text{CH}_4$  in the hydrothermal fluid was not formed by reaction "3", but the isotopic arguments limit the contribution of that carbonaceous-derived component to a very small proportion of the total fluid.

Although it is not possible to model exactly the interaction between C-O-H fluids and carbonaceous material for the system described in the thesis area, the distinct spatial association between  $^{13}\text{C}$ -enriched hydrothermal carbonates and carbonaceous matter (Fig. 8-9) is evidence that the carbonaceous sediments did influence the carbon isotope systematics of the hydrothermal fluid.

Stabilization of  $\text{CH}_4$  within a  $\text{CO}_2\text{-H}_2\text{O}$  hydrothermal fluid is the preferred model to account for the increase in  $\delta^{13}\text{C}$  of the precipitated hydrothermal dolomite, rather than one which derives substantial  $\text{CO}_2$  and  $\text{CH}_4$  by hydrolysis of reduced carbon.

#### 8.3.2. $\delta^{18}\text{O}$ -rich hydrothermal dolomite and vein quartz

Fyon et al. (1983d) pointed out that the  $\delta^{18}\text{O}$ -values of vein quartz and hydrothermal dolomite (eg. Fig. 7-4) showed an increase with increasing stratigraphic position of the sample. Although correct in the context of the figure, this correlation and resulting interpretations were misleading in that the geological context of the samples was not considered. The same data, with some additions, are recast on Figure 8-10. When viewed in their geographical context, the  $^{18}\text{O}$ -rich vein quartz and hydrothermal dolomite lie concurrently in the spectacularly auriferous domain which hosts the Hollinger, McIntyre, Coniaurum, Dome, Buffalo Ankerite, Delnite, Aunor and Paymaster Porcupine Mines. This domain will be henceforth referred to as the

" $^{18}\text{O}$ -anomalous" zone. This rock domain yielded approximately 90% of the total gold produced from the Porcupine camp. It must be emphasized that sampling gaps do not allow for precise location of the boundary of the " $^{18}\text{O}$ -anomaly". The presence of two populations of vein quartz and hydrothermal carbonate in the Porcupine Camp, recognized on the basis of their  $\delta^{18}\text{O}$ -values, (Fig. 8-10) could represent: 1) the presence of two isotopically distinct aqueous fluids (one  $^{18}\text{O}$ -rich and the other  $^{18}\text{O}$ -poor); 2) a process, such as immiscible separation of  $\text{CO}_2$  from a  $\text{CO}_2$ - $\text{H}_2\text{O}$  fluid, that operated within the relatively restricted area of the Hollinger-McIntyre-Dome-Buffalo Ankerite Mines; or 3) a change in the precipitation temperature.

#### 8.3.2.1. Temperature change

If the  $\delta^{18}\text{O}$  of the hydrothermal water in the  $\text{CO}_2$ - $\text{H}_2\text{O}$  fluid remained relatively constant, the  $\delta^{18}\text{O}$ -values of vein quartz and hydrothermal dolomite within the Hollinger-McIntyre-Dome mineralized zone are consistent with their lower temperature precipitation with respect to dolomite and quartz precipitated outside this zone. From fluid inclusion studies, the precipitation temperature of vein quartz within the Hollinger-McIntyre mineralized zone is estimated to be  $160^\circ$  to  $400^\circ\text{C}$  (Smith et al., 1984; Smith and Kesler, 1985; see also Table 5-1). Data from the Pamour #1 Mine (Walsh et al., 1984), located in northeast Whitney Township, and the

Dome Mine (Kerrick and Fryer, 1979) span the same range (Table 5-1). Although no vein quartz from any other deposit has had its fluid inclusion population characterized, there seems to be no evidence pointing to lower temperature precipitation of hydrothermal quartz or dolomite in the Hollinger-McIntyre mineralized zone. Therefore, differences in precipitation temperature is an unlikely explanation for the  $^{18}\text{O}$ -enriched hydrothermal quartz and carbonate.

#### 8.3.2.2. Two different fluids

The presence of  $^{18}\text{O}$ -rich hydrothermal quartz and dolomite in the " $^{18}\text{O}$ -anomalous" zone could signal the involvement of an  $^{18}\text{O}$ -rich hydrothermal fluid. An estimate of  $\delta^{18}\text{O}$  of the  $\text{H}_2\text{O}$  component of this fluid can be obtained using the precipitation temperatures provided by the fluid inclusion studies. The  $\delta^{18}\text{O}$  of vein quartz from the Hollinger Mine (+15‰) is combined with the the range of filling temperatures reported by Smith et al. (1984) for inclusions trapped in vein quartz (225° to 325°C), to calculate  $\delta^{18}\text{O}$  of the  $\text{H}_2\text{O}$  component in the fluid using the  $\Delta_{\text{quartz-water}}$  oxygen isotope fractionation expression of Matsuhisa et al., (1979). The calculated  $\delta^{18}\text{O}$  of the water is +5 to +9‰. Conversely, using the same temperature range (justification for same precipitation temperature given in Section 8.3.2.1) and the  $\delta^{18}\text{O}$  of vein quartz from deposits which lie outside the " $^{18}\text{O}$ -anomalous" zone, the calculated

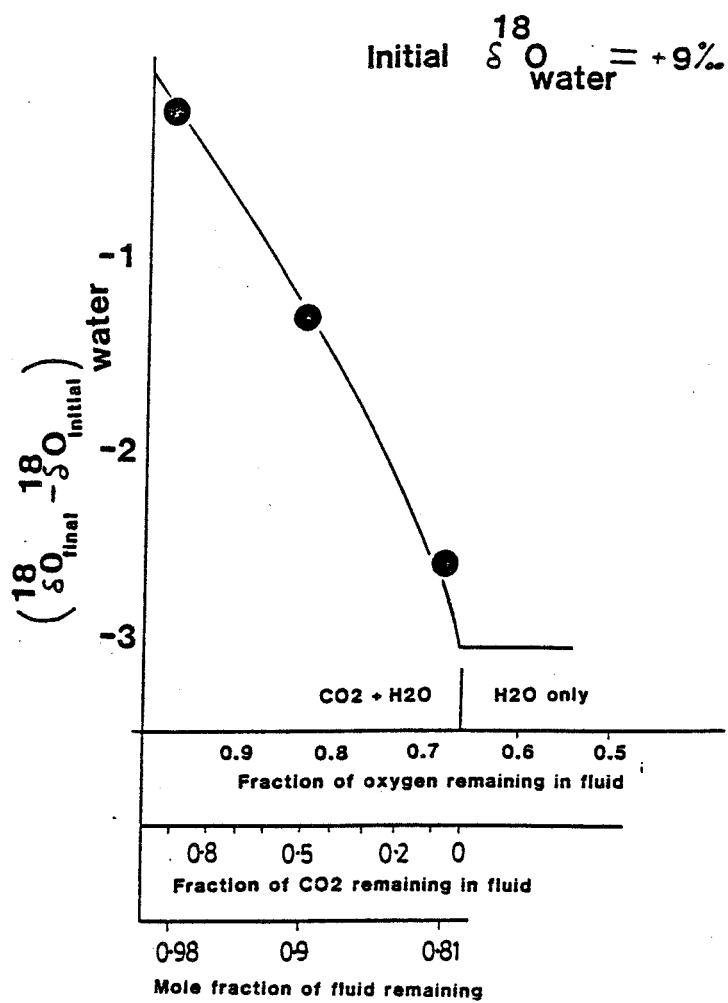
$\delta^{18}\text{O}$  of the water ranges from +3 to +7‰. Although the calculated  $\delta^{18}\text{O}$  of the water component of the hydrothermal fluids overlap, the isotopic data are consistent with the involvement of two isotopically different fluids.

#### 8.3.2.3. Fluid immiscibility

The immiscible separation of a significant volume of  $\text{CO}_2$  from an initially miscible  $\text{CO}_2$ - $\text{H}_2\text{O}$  fluid could affect the  $\delta^{18}\text{O}$  of the residual  $\text{H}_2\text{O}$ , because  $\text{CO}_2$  is  $^{18}\text{O}$ -enriched with respect to coexisting  $\text{H}_2\text{O}$  at given temperature (Bottinga, 1968). However, the degree of  $^{18}\text{O}$ -enrichment in the residual  $\text{H}_2\text{O}$  will depend on both the temperature at which separation takes place as well as the volume of  $\text{CO}_2$  that leaves the fluid. For example, the complete separation of  $\text{CO}_2$  from a fluid in which the original  $\text{CO}_2/\text{H}_2\text{O}$  molar ratio was very small is not likely to profoundly affect the  $\delta^{18}\text{O}$  of the residual  $\text{H}_2\text{O}$ . The separation of  $\text{CO}_2$  from  $\text{H}_2\text{O}$  may not significantly affect the  $\delta^{13}\text{C}$  of the  $\text{CO}_2$ , because almost all the carbon, on a molecular basis, resides in the  $\text{CO}_2$  phase.

The oxygen isotopic evolution of the  $\text{H}_2\text{O}$  that remains after the immiscible separation of  $\text{CO}_2$  will follow a Rayleigh distillation model. The magnitude of the  $^{18}\text{O}$ -enrichment in the fluid  $\text{H}_2\text{O}$  is quantified on Figure 8-13, for the immiscible separation of  $\text{CO}_2$  from an  $\text{H}_2\text{O}$ - $\text{CO}_2$  fluid mixture. The calculation was carried out at 400°C using a

Figure 8-13: Rayleigh distillation system modelling the immiscible separation of  $\text{CO}_2$  from an originally miscible  $\text{CO}_2\text{-H}_2\text{O}$  fluid. The ordinate axis records the relative increase or decrease in  $\delta^{18}\text{O}$  of the residual Water with respect to its initial value after the separation of an aliquot of  $\text{CO}_2$ . The initial  $\delta^{18}\text{O}$  of the Water component in the fluid was arbitrarily set at  $+9\text{‰}$ . The calculation was carried out at  $400^\circ\text{C}$ , using a  $\delta^{18}\text{O}_{\text{Carbon dioxide-Water}}$  of  $6.7\text{‰}$  (Bottinga, 1968). For the calculation, the different molar proportions of oxygen contained in  $\text{CO}_2$  and  $\text{H}_2\text{O}$  were compensated for by translating each mole of  $\text{CO}_2$  that was removed from the fluid into its molar equivalent of oxygen.



$\Delta^{18}\text{O}_{\text{CO}_2\text{-H}_2\text{O}} = 6.72$ , calculated from the theoretical curve of Bottinga (1968), listed by Friedman and O'Neil (1977). For the calculation, the different molar proportions of oxygen contained in  $\text{CO}_2$  and  $\text{H}_2\text{O}$  were compensated for by translating each mole of  $\text{CO}_2$  that was removed from the fluid, into its molar equivalent of oxygen. For the calculation illustrated in Figure 8-13, the starting mole fraction of  $\text{CO}_2$  in the initially miscible  $\text{H}_2\text{O}$ - $\text{CO}_2$  fluid was set at 0.2, as this represents the lower limit for fluids from which hydrothermal carbonate is interpreted to have precipitated (Smith et al., 1984; Smith and Kesler, 1985). They also reported  $\text{XCO}_2$  values higher than this, but because very  $\text{CO}_2$ -rich fluids may represent the product of immiscible separation, a  $\text{CO}_2$ -rich ( $\text{XCO}_2 > 50$  mole %) fluid composition was not used to model the Rayleigh fractionation process. Note that the abscissa on Figure 8-13 is expressed as fraction of oxygen remaining in the fluid. For comparative purposes, the fraction of  $\text{CO}_2$  and fluid remaining is also illustrated. For this quantitative example, the fluid remains a mixture of  $\text{CO}_2$  and  $\text{H}_2\text{O}$  until immiscible separation of  $\text{CO}_2$  removes 44 % of the fluid (or 66 % of the fluid remains). At this point, all of the  $\text{CO}_2$  component has been completely removed and the fluid consists of pure  $\text{H}_2\text{O}$ .

This model calculation (Fig. 8-13) illustrates that the residual  $\text{H}_2\text{O}$  should become  $^{18}\text{O}$ -depleted as  $\text{CO}_2$  is progressively separated. Carbonate (or quartz) that



precipitated in equilibrium with the  $H_2O$  in the fluid, during the immiscible separation of  $CO_2$ , should show a corresponding decrease in  $\delta^{18}O$ . This model would explain the 3‰ change in  $\delta^{18}O$  of the vein quartz and the 1 or 2‰ change of dolomite (Fig 8-10) only if the  $\delta^{18}O$ -rich minerals, located in the " $^{18}O$ -anomalous" zone, were precipitated from the miscible  $H_2O$ - $CO_2$  fluid, whereas the  $\delta^{18}O$ -poor carbonates and quartz (Fig. 8-10) would have to represent material that precipitated from the  $^{18}O$ -depleted,  $H_2O$ -rich, immiscible residue. The variable mole ratios of  $CO_2$  reported in fluid inclusions from quartz veins in the Hollinger-McIntyre Mines (Table 5-1) may be evidence of the trapping of a fluid undergoing immiscible phase separation, although Smith and Kesler (1985) state that no fluid inclusion evidence was seen to support such immiscibility.

### 8.3.3. Discussion

The spread in  $\delta^{13}C$  values for the hydrothermal carbonate could be related to their precipitation in a reducing environment established by the presence of carbonaceous sedimentary material. Within the reducing domain, some  $CH_4$  was stabilized, leaving  $^{13}C$ -enriched residual  $CO_2$  from which  $^{13}C$ -enriched hydrothermal carbonate precipitated.

$\delta^{18}O$ -enriched hydrothermal dolomite and quartz present in the Hollinger-McIntyre-Dome mineralized domain precipitated from a relatively  $^{18}O$ -rich water component

having a  $\delta^{18}\text{O}$  of +5 to +9‰. The less  $^{18}\text{O}$ -enriched hydrothermal carbonates and quartz precipitated from water having a  $\delta^{18}\text{O}$  of +3 to +7‰. The relatively  $^{18}\text{O}$ -depleted water may have evolved from an initially miscible  $\text{H}_2\text{O}-\text{CO}_2$  fluid which underwent immiscible separation of  $\text{CO}_2$  or it may represent a separate fluid, unrelated genetically to the fluid which deposited quartz and dolomite in the " $^{18}\text{O}$ -anomalous", Hollinger-McIntyre-Dome mineralized domain.

Figure 8-10 shows that the locus of  $^{18}\text{O}$ -rich fluid incursion into the Porcupine Camp, was axially through the Hollinger-McIntyre-Dome mineralized domain. The geological features of this domain, described in Section 4.6.3.2 (Regime A and B, Fig. 4-5), strongly indicate that this regime represents a magmatic centre. It follows that the  $^{18}\text{O}$ -rich fluid, responsible for the alteration and mineralization in this domain, may have been of magmatic origin. This implication is examined in Chapter 10. It is also interesting to note that the area of the " $^{18}\text{O}$ -anomaly" falls within the large, poorly constrained limits of the  $\delta^{18}\text{O}$ -whole rock anomaly identified by Beaty (1980). Beaty (1980) concluded that the area of elevated  $\delta^{18}\text{O}$ -whole rock values represented the effect of a sea water alteration event. Could it be that this elevated  $\delta^{18}\text{O}$ -whole rock signature is really a reflection of very late hydrothermal processes and is unrelated to a sea water hydrothermal system?

#### 8.4. Enhanced Precipitation of gold

Springer (1983 and in Colvine et al. 1984, p. 48) details mechanisms by which gold could be scavenged from solution by graphite. Given the relative abundance of carbonaceous sediments in the Hollinger-McIntyre-Dome area, and the gold-rich nature of this domain, it is reasonable to suggest that gold scavenging by the carbonaceous material may have been a locally important mechanism by which gold was concentrated immediately within and adjacent to the carbonaceous units. However, one additional mechanism to induce gold precipitation involves the destruction of Au-oxidized carbon complexes.

If, in the presence of carbonaceous material, the  $fO_2$  of the hydrothermal fluid system is reduced, then the stabilization of  $CH_4$  at the expense of oxidized carbon species results in the destruction of the Au-oxidized carbon species and precipitation of gold. The presence of carbonaceous material in the Hollinger-McIntyre-Dome area, one which is richest in gold, may have contributed to the precipitation of gold by such a redox effect.

#### 8.5. Summary

1) A stratiform dolomite unit, interpreted to be a chemical precipitate of marine derivation, has  $\delta^{18}O$ - and  $\delta^{13}C$ -values of +16‰ and 0‰, equivalent to other Archean marine marbles and dolomites; its low  $\delta^{18}O$ -value with

respect to modern marine sedimentary carbonates could reflect a higher temperature of deposition ( $>150^{\circ}\text{C}$ ) or partial oxygen isotope exchange during regional metamorphism;

2) Dispersed hydrothermal calcite, interpreted to have been precipitated during a low temperature sea water alteration event, has modal  $\delta^{13}\text{C}$  and  $\delta^{18}\text{O}$  values of  $-1.7\%$  and  $11.3\%$  respectively, consistent with low temperature ( $50\text{--}150^{\circ}\text{C}$ ) precipitation from a sea water hydrothermal fluid; the variability in  $\delta^{18}\text{O}$  of the dispersed calcite ( $+8$  to  $+17\%$ ) could reflect precipitation under widely different temperatures, variable water/rock ratios during precipitation and/or post-precipitation exchange with aqueous, metamorphic fluids;

3) Two groups of hydrothermal carbonate are distinguished on the basis of their  $\delta^{13}\text{C}$  values; one group has remarkably uniform  $\delta^{13}\text{C}$  values ( $-3$  to  $-4\%$ ), regardless of stratigraphic position, size or gold tenor of the alteration zone; the second group is characterized by  $\delta^{13}\text{C}$ -values which range from  $-4$  to  $0\%$ . Both groups evolved from the same hydrothermal fluid, but the  $^{13}\text{C}$ -enriched group occur only in proximity to carbonaceous sediments where  $\text{CH}_4$  stabilization in the hydrothermal fluid generated  $^{13}\text{C}$ -enriched  $\text{CO}_2$  from which  $^{13}\text{C}$ -enriched carbonates later precipitated.

4) Replacement dolomite and magnesite in the cores

of carbonate alteration zones have identical  $\delta^{13}\text{C}$ -values of -3.5 to -5‰, where not precipitated in proximity to carbonaceous sediments, and -2 to 0‰ where precipitated in proximity to carbonaceous sediments; the lighter  $\delta^{13}\text{C}$  population (-3.5 to -5‰) has remarkably uniform  $\delta^{13}\text{C}$ -values regardless of stratigraphic setting, size or gold tenor of the alteration zone;

5) For carbonate alteration zones not proximal to carbonaceous sediments, the  $\delta^{13}\text{C}$  of the replacement carbonate is uniform (-4‰) across the dolomite or magnesite-stable zone domain but increases to 0‰ at the outer edges of the alteration zone where calcite is stable (Transitional and Hydrous Facies); this increase is attributed largely to the decrease in  $\text{CO}_2/\text{H}_2\text{O}$  molar ratio in the fluid, resulting in Rayleigh fractionation of the carbon isotopes.

6) The uniform  $\delta^{13}\text{C}$  of the unmodified hydrothermal fluid ( $\delta^{13}\text{C} = -3.7 \pm 0.6$ ) implies a carbon source reservoir which was itself large and isotopically uniform.

7) The most  $^{18}\text{O}$ -enriched vein quartz and hydrothermal dolomite lie in an area which contains the Hollinger, Dome, McIntyre, Coniaurum and Buffalo Ankerite Mines - a geographic domain from which 90% of the gold in the Porcupine Camp was extracted. The  $^{18}\text{O}$ -enrichment of the minerals may reflect precipitation from  $^{18}\text{O}$ -enriched hydrothermal water ( $\delta^{18}\text{O}_{\text{water}} = +5$  to  $+9$ ‰).

8) The " $^{18}\text{O}$ -anomaly" observed in both vein quartz and hydrothermal dolomite is coincident with the locus of greatest quartz-feldspar porphyry intrusion, and strongly suggests a magmatic origin for the  $^{18}\text{O}$ -rich, hydrothermal water.

9) Enhanced gold precipitation within the  $^{18}\text{O}$ -anomalous zone could have resulted from the collective influences of a magmatic hydrothermal system, which supplied hydrothermal constituents, and the carbonaceous sediments which induced precipitation.

## 9. Source of the Hydrothermal Constituents

Considered in this chapter are the sources of the water and  $\text{CO}_2$  which constituted the hydrothermal fluid. Each constituent is considered in terms of an isotopic tracer to help identify possible source reservoirs. The isotopic characteristics of the hydrothermal  $\text{CO}_2$  and  $\text{H}_2\text{O}$  can be estimated by direct measurement, as in the  $\delta$ D analyses of water from fluid inclusions in quartz, or indirectly if the formation temperature and the  $\delta^{13}\text{C}$  or  $\delta^{18}\text{O}$  of a precipitated mineral are known.

### 9.1. $\delta^{18}\text{O}$ of the water

Kerrick and Fryer (1979) calculated a  $\delta^{18}\text{O}$  of +10‰ for the hydrothermal fluids from which vein quartz in the Dome and Aunor Mines precipitated. They attributed this water to a metamorphic origin.

Using the  $\delta^{18}\text{O}$  values of vein quartz and dolomite from the Hollinger Mine (+15‰; Table 7-3), and precipitation temperatures of 225 to 325 °C (Table 5-1; Smith et al., 1984; Walsh et al., 1984) the  $\delta^{18}\text{O}$  of the hydrothermal water from which the quartz and dolomite precipitated (not necessarily contemporaneously) is calculated to range from +5 to +10‰.

## 9.2. $\delta D$ of the water

The  $\delta D$  of the water component in the hydrothermal fluid can be cautiously approximated using the  $\delta D$  determinations of the water from the fluid inclusions present in quartz. It was argued in Chapter 7 that the spread in  $\delta D$  values for the water in fluid inclusions could reflect the stabilization of reduced, hydrogen-bearing species in the fluid, such as methane ( $CH_4$ ). If this interpretation is correct, then the lightest  $\delta D$  should most closely represent the isotopic composition of the least modified water component in the  $CO_2$ - $H_2O$  hydrothermal fluid. This value is -40 to -60‰; Fig. 7-10).

## 9.3. $\delta^{13}C$ of the $CO_2$

The  $\delta^{13}C$  of the  $CO_2$  component in the hydrothermal fluid can be estimated indirectly from the  $\delta^{13}C$  of the precipitated carbonate. However, because  $\delta^{13}C$  of  $CO_2$  is very sensitive to changes in  $fO_2$ , pH and temperature (Ohmoto, 1972; Ohmoto and Rye, 1979; c.f. Fig. 8-8), it is necessary to constrain the pH and  $fO_2$  of the fluid to determine if the  $\delta^{13}C$  of the  $CO_2$  closely approximates that of the total dissolved carbon. For those alteration zones which did not develop under the influence of carbonaceous sediments, the  $fO_2$  and pH of the fluid during the intense carbonatization was estimated to be relatively



oxidizing and near neutral pH at 350°C (Chapter 5.1.1., 5.1.2.; Chapter 8.2.3.4., Fig. 8-8). Under these conditions, dissolved carbon in an aqueous fluid exists almost entirely as  $\text{CO}_2$  (Ohmoto, 1972; Ohmoto and Rye, 1979). Under these conditions, the  $\delta^{13}\text{C}$  of the  $\text{CO}_2$  dissolved in the aqueous fluid closely approximates the  $\delta^{13}\text{C}$  of the total dissolved carbon in the hydrothermal fluid. The  $\delta^{13}\text{C}$  of the dissolved  $\text{CO}_2$  in the hydrothermal fluid, can be estimated using the  $\delta^{13}\text{C}$  of the hydrothermal dolomite and the  $\Delta_{\text{dolomite-CO}_2}$  carbon isotope fractionation expression, derived from the  $\Delta_{\text{calcite-CO}_2}$  (Bottinga, 1969) and  $\Delta_{\text{dolomite-calcite}}$  (Sheppard and Schwarcz, 1970) carbon isotope fractionation expressions which are listed on Table 6-4. The  $\delta^{13}\text{C}$  of hydrothermal dolomite is used for this calculation because dolomite was precipitated in and adjacent to the hydrothermal conduit; therefore, its  $\delta^{13}\text{C}$  should reflect more closely that of the hydrothermal fluid because the fluid would have undergone less chemical and isotopic evolution.

Some discretion and subjectivity is involved in the selection of a representative  $\delta^{13}\text{C}$ -value for the hydrothermal dolomite to be used to calculate the  $\delta^{13}\text{C}$  of  $\text{CO}_2$ , from which the dolomite was precipitated. The  $\delta^{13}\text{C}$ -values of those hydrothermal dolomites which precipitated in proximity to carbonaceous sediments, are not considered, because the carbonaceous sediments appear to have

295

significantly influenced C-O-H fluid equilibria. The  $\delta^{13}\text{C}$  of that dolomite suite reflects the result of fluid interaction with supercrustal rocks; hence, those  $\delta^{13}\text{C}$ -values do not track very faithfully the original, least isotopically modified  $\delta^{13}\text{C}$  of the  $\text{CO}_2$  component in the hydrothermal fluid (Chapter 8.3.1.). Therefore, only the carbon isotopic values for those dolomites which did not precipitate in proximity to the carbonaceous sediments should be used to estimate the  $\delta^{13}\text{C}$  of the hydrothermal  $\text{CO}_2$ . This dolomite suite has  $\delta^{13}\text{C}$ -values which are equal to or lighter than -3‰. To select the most representative carbon isotopic value for this data suite, two approaches are possible: 1) the mean  $\delta^{13}\text{C}$  of the entire suite can be used; or 2) the lightest  $\delta^{13}\text{C}$  values can be used on the premise that they represent precipitation at the highest temperature, closest to the hydrothermal conduit, from fluids which had undergone the least interaction with the adjacent volcanic rock. The second approach is adopted for this computation.

The mean  $\delta^{13}\text{C}$  of the isotopically lightest hydrothermal dolomite population (excluding those which precipitated in proximity to carbonaceous sediments) is -4.4‰ (Table 9-1). The lightest single value for the Timmins data is -5.9‰, from the McEnaney property. Assuming that the precipitation of the hydrothermal dolomite took place between 225° and 325°C (minimum temperature

TABLE 9-1: Carbon-13 values of hydrothermal dolomites and magnesites from several properties in the Timmins area, and the Larder Lake Break.

| Property          | Property<br>Mean<br>$\delta^{13}\text{C}$ | $\sigma$ | Range        |
|-------------------|-------------------------------------------|----------|--------------|
| Aunor             | -3.7                                      | 0.3      | -4.3 to -2.5 |
| Beaumont          | -3.4                                      | 0.4      | -4.1 to -2.6 |
| Buffalo Ankerite  | -3.1                                      | 0.8      | -4.3 to -1.1 |
| Canusa            | -3.2                                      | 0.2      | -3.4 to -3.0 |
| Carshaw/ Malga    | -3.5                                      | 0.5      | -4.3 to -2.1 |
| Coniaurum         | -1.6                                      | 1.6      | -2.7 to -0.4 |
| Davidson-Tisdale  | -3.1                                      | 0.4      | -3.7 to -1.0 |
| Delnite           | -2.4                                      | 1.0      | -3.3 to -0.5 |
| Dobell            | -4.1                                      | --       | --           |
| Duval             | -4.1                                      | 0.2      | -4.6 to -3.7 |
| Faymar            | -3.4                                      | 0.1      | -3.6 to -3.2 |
| Hallnor           | -2.4                                      | 0.4      | -3.0 to -2.1 |
| Hollinger         | -0.6                                      | 0.5      | -1.5 to +0.3 |
| Kinch             | -4.0                                      | 0.3      | -4.4 to -3.6 |
| McEnaney          | -4.2                                      | 0.7      | -5.9 to -2.9 |
| McIntyre          | -1.1                                      | 1.4      | -3.7 to +0.4 |
| Pamour #1         | -1.7                                      | 0.5      | -2.6 to -1.0 |
| Porcupine Triumph | -4.4                                      | 0.4      | -4.9 to -3.4 |
| Larder Lake Break | -4.7                                      | 0.2      | -5.0 to -4.4 |

Mean of mean for entire population.....-3.1 +/- 1.2

Mean of entire population excluding  
Hollinger, McIntyre, Coniaurum,  
Hallnor and Pamour #1 data(1)..... -3.8 +/- 0.5

Mean of lightest carbon 13 values  
excluding Hollinger, McIntyre,  
Coniaurum, Hallnor and Pamour #1  
data.....-4.4 +/- 0.6

Notes:

1) Hollinger, McIntyre, Coniaurum, Hallnor and Pamour #1 suites are omitted from these calculations because carbonaceous sediments are present in the area.

constrained by fluid inclusion data; Smith et al., 1984; Table 5-1), and using the dolomite- $\text{CO}_2$  carbon isotope fractionation expression listed in Table 6-4, the  $\delta^{13}\text{C}$  of the  $\text{CO}_2$  in the hydrothermal fluid is estimated to have been:

| Calculated<br>$\delta^{13}\text{C}(\text{CO}_2)$ | Temperature | $\delta^{13}\text{C}(\text{dolomite})$ |
|--------------------------------------------------|-------------|----------------------------------------|
| -6.0                                             | 225         | -5.9                                   |
| -4.3                                             | 325         | -5.9                                   |
| -4.5                                             | 225         | -4.4                                   |
| -2.8                                             | 325         | -4.4                                   |

It must be emphasized that the dolomite- $\text{CO}_2$  carbon isotope fractionation expression is quite poorly constrained; hence, the calculated value of  $\delta^{13}\text{C}$  for the  $\text{CO}_2$  component in the hydrothermal fluid is correspondingly imprecise. Notwithstanding this cautionary note, the  $\delta^{13}\text{C}$  of the  $\text{CO}_2$  component in the hydrothermal fluid is estimated to have been in the range -3 to -6‰.

#### 9.4. Reservoirs of $\text{H}_2\text{O}$ and $\text{CO}_2$ For The Hydrothermal Fluid

Having obtained a crude estimate of the  $\delta^{13}\text{C}$ -value for the  $\text{CO}_2$  (-3 to -6‰) and  $\delta^{18}\text{O}$  (+5 to +10‰) and  $\delta\text{D}$  (-40 to -60‰) of the water components in the hydrothermal fluid, it is possible to identify reservoirs from which the hydrothermal fluid components could have been derived. Isotopic fluid classification diagrams (Fig. 9-1 and 9-3) are used to help identify the fluid source. The  $\delta^{13}\text{C}$  of

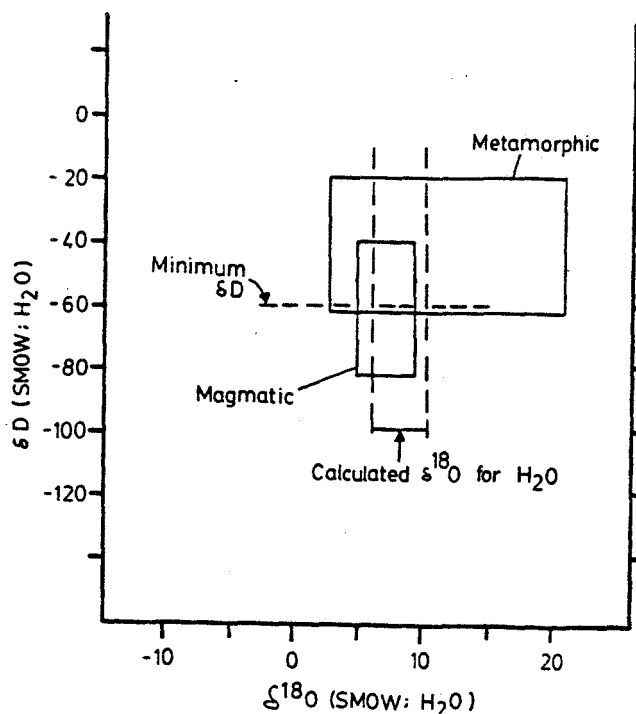


Figure 9-1:  $S_D$ - $S^{18}O$  fluid classification diagram. The metamorphic and magmatic fields are empirically deduced and cited frequently in the literature (c.f. Sheppard, 1977). The range of calculated  $S^{18}O$  for the fluid from which the hydrothermal quartz and dolomite precipitated is indicated. The minimum  $S_D$  of vein quartz-hosted fluid inclusion water is also plotted. These data plot in the overlapping part of the magmatic and metamorphic fields.

Figure 9-2: Carbon isotope compositions of terrestrial carbon-bearing phases. The horizontal bar represents the range of observed values, whereas the mean value is indicated by a vertical dash.

#### Igneous Rocks

1. Reduced carbon
2. Diamonds
3. Carbonatites
4. Carbonate in kimberlites

#### Organic Material

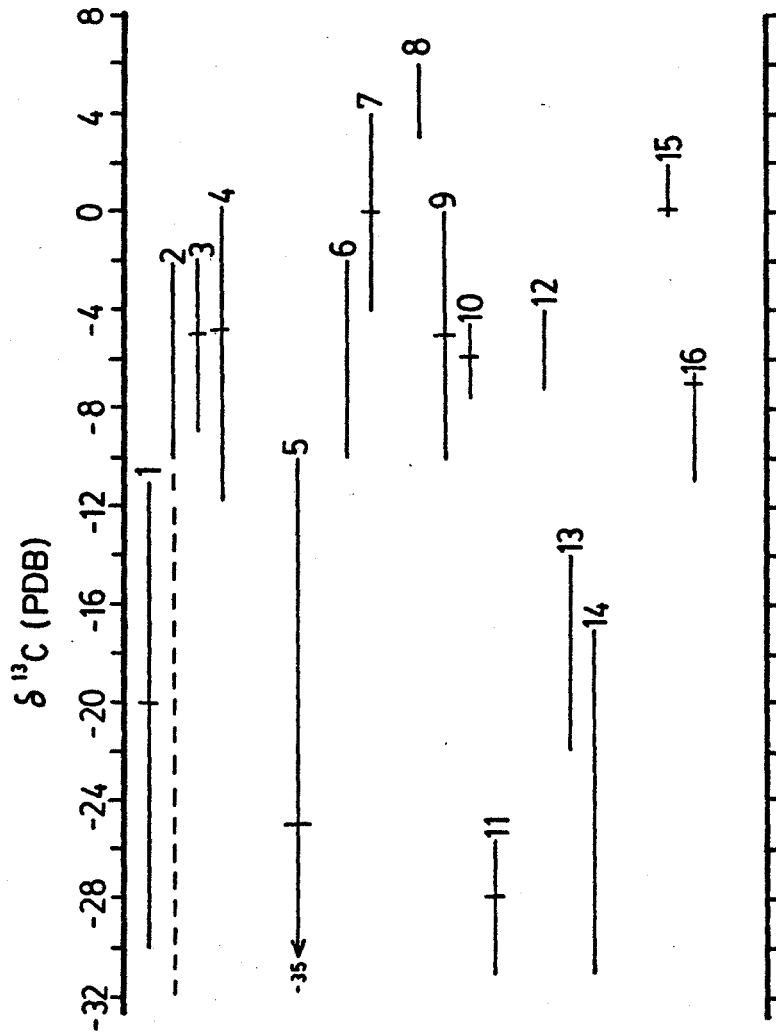
5. Reduced carbon

#### Sedimentary Carbonate

6. Freshwater
7. Marine

#### Gases

8. Metamorphic  $\text{CO}_2$  derived from decarbonatization of marine carbonate
9. Geothermal  $\text{CO}_2$
10.  $\text{CO}_2$  inclusions in mid ocean ridge basalts
11. Geothermal  $\text{CH}_4$
12.  $\text{CO}_2 + \text{H}_2\text{O}$  inclusions of variable salinity thought to have been affected by retrograde metamorphism (Hoefs, 1975): hosted in granulite rocks
13. Pure  $\text{CO}_2$  inclusions in granulite rocks (Hoefs, 1975)
14.  $\text{CO}_2$  inclusions from olivine nodules (Hoefs, 1975)
15. Modern sea water
16. Modern atmosphere



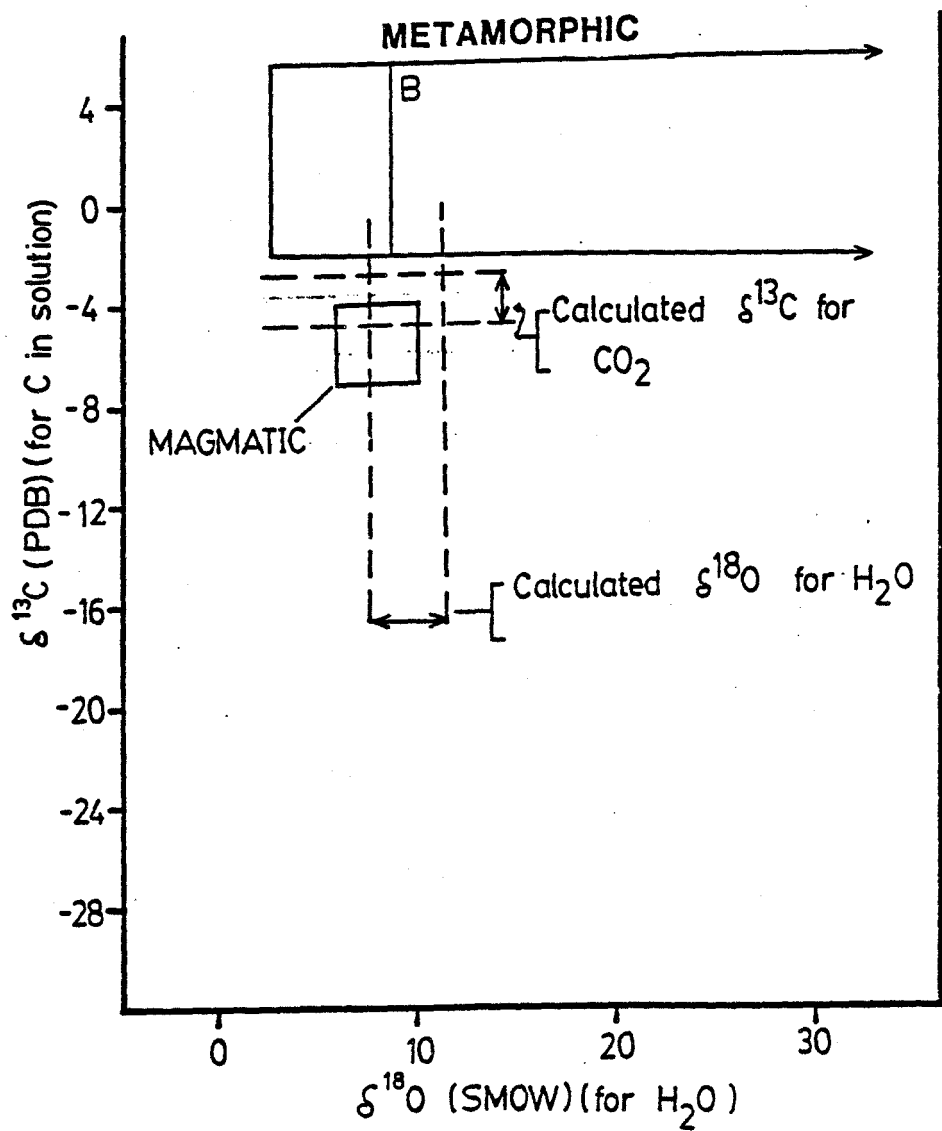
carbon derived from several possible reservoirs are summarized in Figure 9-2.

#### 9.4.1 Metamorphic H<sub>2</sub>O

The field of  $\delta^{18}\text{O}$  values for metamorphic water (Fig. 9-1) is a summary of all geological possibilities. If the geological reservoirs in the Abitibi Belt are considered, the lower  $\delta^{18}\text{O}$  limit of this field can be further constrained. Two major contributors of oxygen to a metamorphic fluid are; 1) the dispersed calcite; 2) dehydration of a sea water altered volcanic pile. The dispersed calcite constitutes only a minor portion of the rock; therefore, it is likely that the  $\delta^{18}\text{O}$  of either the  $\text{CO}_2$  or  $\text{H}_2\text{O}$  phase, released during metamorphism, will be determined by exchange with oxygen-bearing silicate minerals in the rock. Dehydration of sea water altered basalt up to and including amphibolite grade will yield an aqueous fluid having a  $\delta^{18}\text{O}$  that is essentially indistinguishable from that of the parent Rock (Garlick and Epstein, 1967; Taylor and Coleman, 1968; Shieh and Taylor, 1969). The whole rock  $\delta^{18}\text{O}$  values for volcanic rocks in the Abitibi Belt range from +6 to +12‰, with a mean of approximately +8‰ (Beaty, 1980; Kerrich and Hodder, 1982). The  $\delta^{18}\text{O}$  of water derived by metamorphic dehydration of these rocks should also lie within this range (line B, Fig. 9-3).



Figure 9-3:  $\delta^{13}\text{C}$ - $\delta^{18}\text{O}$  fluid classification diagram. The field for a  $\text{CO}_2$ -bearing aqueous fluid, derived by partial decarbonatization of either marine calcite or by the ferroan dolomite present in carbonatized igneous rock, is indicated as is the empirically deduced field for magmatic  $\text{CO}_2$ - $\text{H}_2\text{O}$  fluids. The calculated  $\delta^{18}\text{O}$ - and  $\delta^{13}\text{C}$ -values of the water and  $\text{CO}_2$  components respectively, of the carbonatizing, hydrothermal fluid, are most consistent with the derivation of that fluid from a magmatic reservoir, although a small admixture of metamorphic  $\text{CO}_2$ - $\text{H}_2\text{O}$  with the magmatic fluid is isotopically permitted by these isotopic data.



Considering both  $\delta D$  and  $\delta^{18}O$  estimates for the hydrothermal water (Fig. 9-1) yields a nonunique solution for the source of water, because the empirically deduced fields for magmatic and metamorphic fluids overlap. This information alone does not discriminate between water of metamorphic or magmatic origin because the empirically deduced isotopic fields for these fluids overlap. Thus, additional criteria are required to discriminate between possible water sources.

#### 9.4.2 Metamorphic $CO_2$

$CO_2$  gas can be produced by several processes when carbon- and carbonate-bearing rocks undergo metamorphism: 1) decarbonatization ( $3 \text{ dolomite} + 4 \text{ quartz} + H_2O = \text{talc} + 3 \text{ calcite} + 3CO_2$ ); 2) hydrolysis ( $2C + 2H_2O = CO_2 + CH_4$ ); 3) oxidation ( $C + O_2 = CO_2$ ) and 4) dissolution ( $CaCO_3 + 2H^+ = H_2CO_3 + Ca^{2+}$ ). For a typical Archean terrane, four types of material could yield  $CO_2$  gas upon burial and metamorphism: 1) sedimentary marine carbonate units; 2) dispersed calcite that is precipitated in the primary porosity of the volcanic rock during sea water alteration; 3) sedimentary carbonaceous units; 4) recycled calcite and dolomite from the intensely carbonatized rock.

When carbonate minerals undergo partial decarbonatization, the  $\text{CO}_2$  gas produced has a  $\delta^{13}\text{C}$  which is 3 to 5‰ heavier with respect to the original carbonate (Shieh and Taylor, 1969; Deines and Gold, 1969; Sheppard and Schwarcz, 1970; Schidlowski et al., 1979). In the Timmins area, marine bicarbonate was precipitated in the volcanic rock as dispersed calcite (Chapter 2.1.) which has a  $\delta^{13}\text{C}$ -value of 0 to -3‰ (Chapter 8.2.1.). In addition, one possible sedimentary marine dolomite (Chapter 1.4.1.), having a  $\delta^{13}\text{C}$  of 0‰ (Chapter 8.1) crops out on the Buffalo Ankerite Mine property (Maps 5 and 6). Thus, a carbonate reservoir having a marine  $\delta^{13}\text{C}$  signature is present in the Timmins area which could have produced  $\text{CO}_2$  gas having a  $\delta^{13}\text{C}$ -value of 0 to +5‰. This value is heavier than the  $\delta^{13}\text{C}$ -value calculated for the carbonatizing hydrothermal system and therefore decarbonatization of marine carbonate does not seem to be a reasonable process. Decarbonatization of calcite from the outer margin of the intense carbonate alteration zones is also an unlikely source of  $\text{CO}_2$ . This calcite would yield  $\text{CO}_2$  gas having a  $\delta^{13}\text{C}$ -value of 0 to +5‰, which is also too heavy. Decarbonatization of the dolomite present in the intense carbonate alteration zones is a possible mechanism by which isotopically light  $\text{CO}_2$  could be derived. However, even if the lightest  $\delta^{13}\text{C}$  values for the dolomite are used (-5‰), the liberated  $\text{CO}_2$  gas would have a  $\delta^{13}\text{C}$  of -2 to 0‰. This is somewhat

lighter than the desired value of -3 to -6.0‰, and so this process is not satisfactory.

Reduced carbon exists in Archean greenstone belts as carbonaceous sediments. All organic components in sediments, including coal, petroleum and graphite, typically have  $\delta^{13}\text{C}$ -values between -10 and -35‰ with a mean near -25‰ (Schwarcz, 1969; Ohmoto and Rye, 1979). This material may become a source of hydrothermal carbon through hydrolysis and oxidation. Both mechanisms are important at high temperature-metamorphic conditions. Although the kinetic isotope effects of the reaction and subsequent equilibration with the remaining unreacted material is complex, Ohmoto and Rye (1979) argue that the resultant  $\text{CO}_2$  will probably have  $\delta^{13}\text{C}$ -values lighter than -10‰. Thus, it is unlikely that the  $\text{CO}_2$ -bearing fluid that carbonatized the volcanic rock, contained much  $\text{CO}_2$  derived from carbonaceous sediments.

Thus, none of the carbon-bearing reservoirs present in the Abitibi greenstone belt could have served as the sole source of hydrothermal carbon having a  $\delta^{13}\text{C}$  value of -3 to -6‰.

### 9.4.3. Hydrospheric CO<sub>2</sub>

The Archean atmosphere and sea water are two carbon reservoirs which must be considered as possible sources of hydrothermal carbon. Carbon dioxide in the modern day atmosphere has a  $\delta^{13}\text{C}$  of -7‰ where respiratory CO<sub>2</sub> input from plant material is minimal (Keeling, 1958). This CO<sub>2</sub> is in equilibrium with sea water. If atmospheric CO<sub>2</sub> was also in equilibrium with sea water during the Archean, then it is possible to calculate the  $\delta^{13}\text{C}$  of the atmospheric CO<sub>2</sub> from the isotopic composition of Archean-aged marine carbonates, assuming that the Archean marine calcite precipitated in isotopic equilibrium with sea water and atmospheric CO<sub>2</sub>. Using an ambient sea water temperature of 65°C (Knauth and Epstein, 1976) and a value of 0‰ for the  $\delta^{13}\text{C}$  of Archean, sedimentary, marine calcite (Veizer and Hoefs, 1976; Schidlowski et al, 1975), the  $\delta^{13}\text{C}$  of atmospheric CO<sub>2</sub> would have been approximately -6.5‰.

Thus, on the basis of its  $\delta^{13}\text{C}$ -value, Archean atmospheric CO<sub>2</sub> is a permissive carbon reservoir. However, it is unlikely that any of this CO<sub>2</sub> could penetrate 2 to 6 kilometres into the crust where the carbonatization and quartz veining took place (see Section 5.1 for the depth estimate obtained from CO<sub>2</sub> density measurements from fluid inclusion studies). It is highly probable that CO<sub>2</sub>-buffering reactions of the type described in Chapter 5,

would remove any atmospheric  $\text{CO}_2$  present in a meteoric hydrothermal fluid during the recharge into the supercrustal package. Thus, a meteoric hydrothermal system would never evolve into the  $\text{CO}_2$ -rich hydrothermal system which affected the supercrustal rocks in the Abitibi belt.

The Archean ocean is equally unlikely to have evolved into a suitable hydrothermal fluid, because it is not  $\text{CO}_2$ -rich. Any  $\text{CO}_2$  dissolved in the sea water would be efficiently removed by  $\text{CO}_2$ -buffering reactions during the recharge into the oceanic crust. Evidence of such reactions in the Timmins area is manifest as the vesicle-filling, dispersed calcite.

Thus, hydrospheric carbon reservoirs are most unlikely to contribute carbon to the Archean  $\text{CO}_2$ -rich hydrothermal system.

#### 9.4.4. Magmatic Carbon

Igneous rocks can contain the following varieties of carbon: 1) carbonate minerals; 2)  $\text{CO}_2$  gas in fluid or gaseous inclusions; 3) elemental carbon in the form of graphite or diamonds. Isotopic characterization of these carbon varieties should provide an estimate of the carbon isotope composition of mantle derived carbon. A summary of the carbon isotopic composition of material thought to represent deep-seated carbon is given in Figure 9-2.

Hoefs (1973), Fuex and Baker (1973) Pineau et al. (1976) and Craig (1973) have demonstrated that reduced carbon in igneous rock (30-360 ppm) has  $\delta^{13}\text{C}$ -values of -11 to -28‰ with a mean approaching -20‰. Diamonds in kimberlites have  $\delta$ -values which fall within the range -2 to -8‰, although some values as light as -33‰ have been reported (Koval'skiy and Cherskiy, 1973; Kobelski et al., 1979).

Calcite and dolomite from carbonatites have  $\delta^{13}\text{C}$ -values in the range -2 to -9‰ (Sheppard and Dawson, 1973; Deines and Gold; 1973) with a mean of approximately -5‰. Carbonates from kimberlites have a somewhat greater range of  $\delta^{13}\text{C}$  from +0.2 to -11.8‰ (Kobelski et al., 1979). Although differences exist between carbonatite complexes, the variation within individual complexes is small.

$\text{CO}_2$  gas liberated from vesicles hosted in basalts from the Mid-Atlantic Ridge has  $\delta^{13}\text{C}$  compositions close to -7‰ (Pineau et al., 1976). Moore et al. (1977) found values of -4.7 to -5.8‰ for  $\text{CO}_2$  in vesicles in basalt samples from Pacific Ocean basalt.

Clearly, the  $\delta^{13}\text{C}$  for materials derived from the upper mantle is variable. Kimberlites, carbonatites and  $\text{CO}_2$  gas in vesicles from mid-ocean ridge basalts should provide one of the better indications of the carbon isotopic composition of mantle material because they are confined to cratonic



areas of continents and spreading ridges well away from any major fold belts related to subduction. Hence, it is unlikely that hydrospheric carbon, introduced into the upper mantle during subduction, has been incorporated into kimberlitic or carbonatitic mantle. Thus, the -5‰ value for carbonate in kimberlites and carbonatites is generally accepted to be representative of oxidized, mantle carbon. This value is closely matched by the -5 to -7‰ recorded for CO<sub>2</sub> from geothermal systems, corrected for a minor proportion of CH<sub>4</sub> which formed within the hydrothermal system. Thus, it is presumed that oxidized mantle carbon is most likely to have a  $\delta^{13}\text{C}$  of -5 to -7‰. This value closely matches that value of -7‰ estimated for mantle carbon from geochemical mass balance calculations (Feux and Baker, 1973). Hoefs and Touret (1975) have suggested that the  $\delta^{13}\text{C}$  of oxidized mantle carbon may actually be -17 to -29‰ on the basis of the  $\delta^{13}\text{C}$  of CO<sub>2</sub> extracted from inclusions hosted in olivine nodules of presumed mantle origin (Fig. 9-2).

The calculated range of values for the  $\delta^{13}\text{C}$  of the CO<sub>2</sub> in the Archean hydrothermal fluid is -3 to -6 ‰ and is very similar to value accepted for juvenile CO<sub>2</sub>. However, some juvenile gas systems are also characterized by isotopically heavy CO<sub>2</sub>. For example, the  $\delta^{13}\text{C}$  of CO<sub>2</sub> gas issuing from modern geothermal areas varies from about 0 to -10‰ but many values average -3‰ (data summarized by

Hoefs, 1980). The  $\delta^{13}\text{C}$  of the heavier geothermal  $\text{CO}_2$  (-3‰) could be shifted from the -5‰, thought to represent juvenile  $\text{CO}_2$ , by the formation of as little as 5 mole percent  $\text{CH}_4$  in a closed system at 200 to 300°C. This seems to have occurred in those geothermal systems which issue isotopically heavy (-3‰)  $\text{CO}_2$  gas, because in these systems, the heavy  $\text{CO}_2$  gas coexists with methane having  $\delta^{13}\text{C}$ -values of approximately -27‰.

Thus, the isotopically heavy  $\text{CO}_2$  gases issuing from some geothermal systems are almost certainly of juvenile origin and have had their  $\delta^{13}\text{C}$ -values shifted from -5 to -3‰ as a result of the stabilization of about to 5 mole percent  $\text{CH}_4$  in a closed system, within the discharge system. Such modified juvenile  $\text{CO}_2$  gas has a  $\delta^{13}\text{C}$  which lies within the deduced range of the Archean  $\text{CO}_2$ -rich hydrothermal fluid.

#### 9.4.5 Summary

Consideration of the isotopic values for possible terrestrial  $\text{CO}_2$  and water reservoirs (Figs. 9-1 and 9-3), shows that none uniquely correspond to the deduced  $\delta$ -values for the  $\text{CO}_2$  and water components in the hydrothermal fluid. Either magmatic or a mixture of magmatic and metamorphic (decarbonatization) fluids are permissive within the isotopic constraints. The stable isotopic data do indicate

that the hydrothermal fluid was not of pure metamorphic parentage.

#### 9.5. Comparison With Other Carbonatized Systems

The conclusion that the hydrothermal carbon fixed in the volcanic rocks in the Timmins area was of magmatic origin can be extended to other carbonatized rocks in different areas. Listed in Table 9-2 are the  $\delta^{13}\text{C}$ -values of hydrothermal ferroan dolomite from other areas of the Larder Lake Fault Zone also in the Abitibi belt, Archean volcanic rock from Western Australia, and the Phanerozoic-aged Motherlode Belt of California. The  $\delta^{13}\text{C}$  of ferroan dolomite and magnesite from the Larder Lake Fault Zone ( $-4.7\%$ ) is about  $1\%$  lighter than the Timmins data, but is similar to the data from Western Australia and the Motherlode. The hydrothermal ferroan dolomite from Western Australia (Donnelly et al., 1977; Golding and Wilson, 1983) and the Motherlode (Taylor, 1981) are also interpreted to have been derived from a juvenile source.

#### 9.6. Geological Constraints on Fluid Origin

It was pointed out in Chapter 8 that an area, centered on the Hollinger-McIntyre-Dome Mines, is characterized by the most  $\delta^{18}\text{O}$ -enriched vein quartz and hydrothermal dolomite. This area contains the greatest proportion of

TABLE 9-2: Carbon isotopic values of hydrothermal dolomite, magnesite and calcite from Archean gold and nickel camps and the Phanerozoic Motherlode belt in California.

| LOCATION                                                                                                    | Mean<br>C(PDB) | Range        | Reference   |
|-------------------------------------------------------------------------------------------------------------|----------------|--------------|-------------|
| =====                                                                                                       |                |              |             |
| Australia                                                                                                   |                |              |             |
| -----                                                                                                       |                |              |             |
| Kalgoorlie                                                                                                  |                |              |             |
| Golden Mile Dolerite.....                                                                                   | -5.7           |              |             |
| No. 4 Lode.....                                                                                             | -3.6 +/- 0.4   | -2.4 to -4.1 | 1           |
| Black shale.....                                                                                            | -6.5 +/- 0.8   | -5.5 to -7.5 | 2           |
| Carbonate In Altered Ultramafic Rock                                                                        |                |              |             |
| Kambalda.....                                                                                               | -6.8           |              | 1           |
| Redcross.....                                                                                               | -5.7           |              | 1           |
| Black Swan.....                                                                                             | -4.4           |              | 1           |
| Mt. Windarra.....                                                                                           | -8.7           |              | 1           |
| Mt. Keith.....                                                                                              | -5.2           |              | 1           |
| =====                                                                                                       |                |              |             |
| Timmins Camp                                                                                                |                |              |             |
| -----                                                                                                       |                |              |             |
| Dispersed Calcite Precipitated In Vesicles During Low Temperature, Sea Water Alteration<br>Of Basalt Flows. |                |              |             |
| Calcite.....                                                                                                | -1.5           | 0 to -3      |             |
| Hydrothermal Ferroan Dolomite/Magnesite Precipitated During The Intense Carbonatization.                    |                |              |             |
| Deposits proximal to carbonaceous sediments                                                                 |                |              |             |
| Coniaurum.....                                                                                              | -1.6           | -0.4 to -2.7 | 3           |
| Hallnor.....                                                                                                | -2.4           | -2.1 to -3.0 | 3           |
| Hollinger.....                                                                                              | -0.6           | +0.3 to -1.5 | 3           |
| McIntyre.....                                                                                               | -1.1           | +0.4 to -3.7 | 3           |
| Pamour #1.....                                                                                              | -1.7           | -1.0 to -2.6 | 3           |
| Deposits not proximal to carbonaceous sediments                                                             |                |              |             |
| Aunor.....                                                                                                  | -3.7           | -2.5 to -4.3 | 3           |
| Beaumont.....                                                                                               | -3.4           | -2.6 to -4.1 | 3           |
| Buffalo Ankerite.....                                                                                       | -3.1           | -1.1 to -4.3 | 3           |
| Canusa.....                                                                                                 | -3.2           | -3.0 to -3.4 | 3           |
| Carshaw/Malga.....                                                                                          | -3.5           | -2.1 to -4.3 | 3           |
| Davidson-Tisdale.....                                                                                       | -3.1           | -1.0 to -3.7 | 3           |
| Delnite.....                                                                                                | -2.4           | -0.5 to -3.3 | 3           |
| Dobell.....                                                                                                 | -4.1           | --           | 3           |
| Duval.....                                                                                                  | -4.1           | -3.7 to -4.6 | 3           |
| Faymar.....                                                                                                 | -3.4           | -3.2 to -3.7 | 3           |
| Kinch.....                                                                                                  | -4.0           | -3.6 to -4.4 | 3           |
| McEnaney.....                                                                                               | -4.2           | -2.9 to -5.9 | 3           |
| Porcupine Triump.....                                                                                       | -4.4           | -3.4 to -4.9 | 3           |
| =====                                                                                                       |                |              |             |
| Other Areas In The Abitibi Greenstone Belt.                                                                 |                |              |             |
| Larder Lake Break: Carbonatized<br>ultramafic flows from the<br>Misema River locality.....                  |                |              |             |
|                                                                                                             | -4.7 +/- 0.2   | -4.4 to -5.0 | This thesis |
| =====                                                                                                       |                |              |             |
| Phanerozoic Motherlode Belt                                                                                 |                |              |             |
| Ferroan Carbonate.....                                                                                      |                | -4.9 to -6.9 | 4           |
| =====                                                                                                       |                |              |             |

#### REFERENCES

- 1) Donnelly et al. (1977); 2) Golding and Wilson (1983); 3) Fyon et al. (1983 )
- 4) Taylor, B.E. (1981)

quartz-feldspar porphyry intrusions, and was the most auriferous domain in the Porcupine Camp. This strong spatial association between felsic intrusive activity, gold mineralization and alteration is unlikely to be coincidental and may indicate that the fluids were exsolved from the magmas which crystallized into the quartz-feldspar intrusions. Similar observations apply to virtually all the major gold camps in Ontario (Colvine et al., 1984).

Alternatively, the geological similarity between the regional structures in the Timmins area (adjacent to the Destor-Porcupine Fault), the Larder Lake Fault Zone, and the Motherlode structure, the regional extent and volume of carbonate alteration associated with these structures, and the isotopically uniform reservoir from which the  $\text{CO}_2$  was derived, suggest that the  $\text{CO}_2$ -rich fluids may have passed directly from the mantle into the supercrustal rocks along the deeply penetrating structural zones without being transported in solution within a silicate magma. This question is examined in Chapter 10. Regardless, the field and stable isotopic data strongly suggest that the  $\text{CO}_2$ -rich hydrothermal fluids were most likely of magmatic origin.

## 10. Genetic Link With Archean Granulitization

The stable isotopic evidence and the presence of abundant intrusive quartz-feldspar porphyry intrusive bodies in the heart of the Porcupine Camp, is suggestive evidence linking the origin of the CO<sub>2</sub>-rich hydrothermal fluid to exsolution from the intrusive magmas. This genetic relationship is an appealing explanation for the spatial association between gold mineralized domains, carbonate alteration and felsic magmatism which is observed on a mining camp scale (100-200 km<sup>2</sup>). In fact, all gold mining camps in the Superior Province of Ontario show this association (see discussions in Colvine et al, 1984). However, when the extent of the carbonate alteration is viewed on a greenstone belt scale, the origin of the CO<sub>2</sub>-rich fluid by exsolution from local juvenile intrusive complexes seems overly simplistic and incapable of providing the volume of CO<sub>2</sub>-bearing fluid required to alter the volume of rock adjacent to and within the regional Destor Porcupine or Larder Lake deformation zones.

Within limited portions of the regional deformation zones, intrusive centres exist, such as the Kirkland Lake alkaline intrusives, the Timmins quartz-feldspar porphyry intrusions have developed. However, carbonatization in the Abitibi Belt is extensive along the 500-600 km surface trace of these structures and is not specifically localized around

the sites of intrusive activity (Burrows, 1924; Thomson, 1924). That is, the distribution of carbonatized rock extends well beyond the intrusive centre. This suggests that the production of the CO<sub>2</sub>-rich fluids was related to a process which operated at a scale much larger than represented by the intrusive centres.

The immense volume of CO<sub>2</sub> which was fixed in the Abitibi supercrustal sequences (minimum of 490,900 moles of carbon; Chapter 3) must have been derived from a reservoir much larger than that represented by the localized sites of intrusive magmatism. The isotopic uniformity of this hydrothermal CO<sub>2</sub> ( $\delta^{13}\text{C} = -4 \pm 0.5\text{‰}$ ; Table 9-1) indicates that the carbon reservoir was not only large, but isotopically uniform.

These factors suggest that sites of localized magmatism are important controls on the development of gold mineralization processes on a camp scale (200 km<sup>2</sup>), whereas the extensive carbonatization event must be linked to processes which accessed the entire length of the major structural zones. In other words, degassing of a high level magma could not have been the sole or even the major source of the hydrothermal carbon.

The marked bimodal age of gold mineralization through geological time (Fig. 10-1) is another feature which is not adequately explained by either a purely magmatic model or the metamorphic dehydration/decarbonatization model proposed by Lumbers (1964), Henley (1973), Fyfe and Henley (1973),

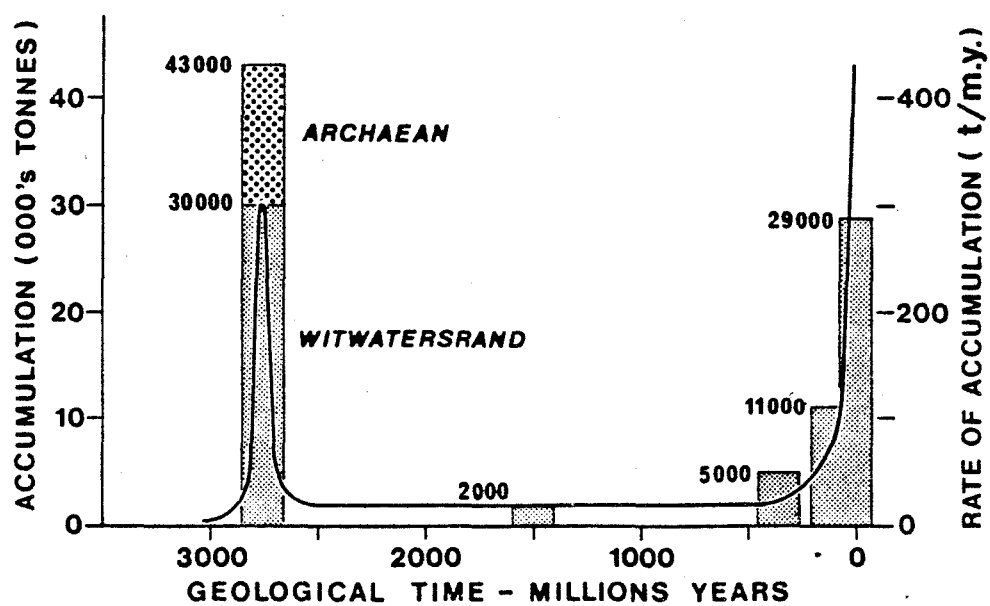


Figure 10-1: Distribution of host rock ages for lithologies which host gold mineralization (Woodall, 1979).



Kerrick and Fryer (1979) and Kerrich and Fyfe (1981). Many major orogenic events have occurred throughout the Proterozoic and Phanerozoic involving large-scale dehydration and decarbonatization, and yet relatively little gold has been won from rocks of this age until the Tertiary (<65 million year age). If the principle of Uniformitarianism is to apply, why haven't these post-Archean metamorphic events yielded significant volumes of auriferous hydrothermal fluids?

In addition, the Earth's geological history is characterized by periodic orogenic events during which magmatism was sustained. Yet, the period of maximum influx of CO<sub>2</sub>-rich hydrothermal fluids into the Earth's supercrustal sequences appears to have been during the Archean. Younger systems do occur, such as the Motherlode in California and the Bridge River area in British Columbia, but these systems have not yielded the volume of gold extracted from the Archean deposits. In fact, the bimodal age distribution of gold mineralization (Fig. 10.1) strongly indicates that the Archean gold-carbonatization event reflected the culmination of a process linked to the cratonization of the Earth. Thus, given the probability that the CO<sub>2</sub>-rich hydrothermal fluids which carbonatized the Archean supercrustal sequences were derived from a juvenile reservoir, certain speculative lineages can be drawn between this alteration event and other Archean crustal stabilization events. One feature of the cratonization

process which correlates with the observed high frequency of gold mineralization in rocks of Archean age is the granulitization of the lower crust.

Dating indicates that during the period 2.5 to 3.0 BYBP, large scale production of granulite facies rock was taking place (Moorbath, 1975). These granulite terranes are found on all continents and in all Precambrian shield areas. Granulites are present, but not abundant, in rocks younger than Proterozoic (Heier, 1973). This implies that perhaps special conditions promoted granulite formation during the Precambrian. Given the possibility that granulitization was in fact most common during the period of 2.5 to 3.0 BYBP and that the frequency of granulite ages within that range is not solely a reflection of exposed crustal level of erosion, it might be speculated that the age concurrence between peak granulite production in the lower crust and the gold-carbonatization event indicates the consanguinity of the events.

One favoured explanation for the abundance of Precambrian granulites appeals to mantle degassing (Heier, 1973; Newton et al., 1980). Mantle volatiles are inferred to have interacted with a thickened continental crust at 2.5 to 3.0 BYBP to promote amphibolite and granulite metamorphism (Moorbath, 1975). The possible genetic link between mantle degassing, lower crustal granulitization and supercrustal carbonatization is examined in more detail.

## 10.1. Characteristics of Granulite Metamorphism

### 10.1.1. Metamorphic fluid constitution

Newton et al. (1980) and Schuiling and Kreulen (1979) argue that Archean granulitization could have resulted from juvenile  $\text{CO}_2$  influx into the lower crust which depressed the ambient fugacity of  $\text{H}_2\text{O}$  (Fig. 10-2). The catalytic role of  $\text{CO}_2$ -rich fluids in granulite metamorphism has been supported by fluid inclusion studies (Touret, 1971b; 1977; Berglund and Touret, 1976; Hoefs and Touret, 1975; Hollister and Burruss, 1976). The water component of the fluids responsible for the the granulite metamorphism constitutes only 0.1 to 0.3 of the total fluid pressure, the rest being primarily composed of  $\text{CO}_2$  (Wells, 1979; Touret, 1971a; Janardhan et al., 1982). Conversely, the pore fluids in the adjacent lower grade amphibolite terranes were water-rich with water pressure approaching that of total pressure (Touret, 1971a; Wells, 1979; Madsen, 1977).

That some granulite metamorphism takes place primarily by influx of  $\text{CO}_2$ -rich fluid, rather than partial melting, follows from the patchy and vein-like appearance of charnockite, on a centimetre scale, observed in the transition zone from amphibolite to granulite facies rocks where no textural evidence of melting existed and where temperature and total pressure must have been uniform over that scale (Janardhan et al., 1982, 1979; Wells, 1979;

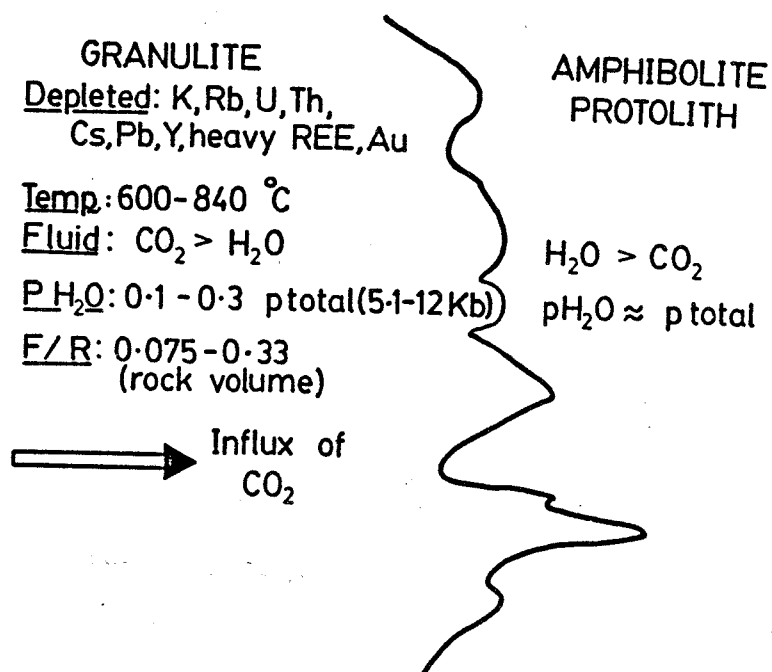


Figure 10-2: Summary of geochemical, P-T and constitutional characteristics of the fluids which are inferred to have induced granulite and amphibolite grade metamorphism. Data summarized in Newton et al. (1980).

Wilson, 1978).

This evidence strongly indicates that CO<sub>2</sub>-rich fluids did interact with the lower crust to form granulite rocks (Newton et al., 1980).

#### 10.1.1.1. Role of major, crustal structures

If some suitable conduit were available to tap the lower crust and bleed off some of this CO<sub>2</sub>-rich fluid, a mechanism would exist by which CO<sub>2</sub>-rich fluids could access and carbonatize the supercrustal volcanic sequences. In the Abitibi belt, the Destor-Porcupine-Duparquet, Kirkland Lake, and Larder Lake-Cadillac fault zones are profound crustal structures which are interpreted to have been ancestral faults that were active during the volcanological and sedimentological construction of the Abitibi belt (Dimroth and Rocheleau, 1979; Pyke, 1982). The extensive strike length of the Destor-Porcupine and Larder Lake fault zones, from the Kapuskasing Arch in Ontario east to the Grenville front in Quebec, implies that these two structures could also be deeply penetrating and may have penetrated to the lower crust. Where these regional structures are well exposed (eg. Misema River section across the Larder Lake fault zone), the Archean rocks within the fault zone are intensely carbonatized (Thomson, 1941). This and the long standing recognition that a spatial association existed between these structures and the gold deposits (Fig. 3-13)

in the Abitibi Belt support the argument that the Destor-Porcupine-Duparquet and Larder Lake-Cadillac structural zones played an important role in focussing the influx of CO<sub>2</sub>-rich fluids into the evolving volcano-sedimentary units of the Abitibi Belt.

Thus, it is apparent that regional, deeply penetrating fault zones within the Abitibi Greenstone Belt did focus the discharge of CO<sub>2</sub>-rich fluids from the lower crust into the volcano-sedimentary supercrustal rocks. Once within the supercrustal sequence, the fluids could interact with a large volume of rock by utilizing smaller subsidiary fracture systems.

#### 10.1.2. Geochemistry of granulite-grade rocks

Many low and medium pressure granulite rocks, consisting of olivine-plagioclase-cordierite-andalusite and plagioclase-hypersthene-clinopyroxene-quartz (+/-kyanite and sillimanite) respectively, are depleted in certain LIL elements (K, Rb, Cs, U, Th, Y), heavy Rare Earth Elements (HREE) and have high Ba/Rb, Ba/Sr, Ce/Yb, K/Cs and K/Rb ratios (Tarney and Windley, 1977; Lambert and Heier, 1968; Tarney et al., 1972; Sighinolfi, 1971; Heier, 1973; Heier and Thoresen, 1971; Collerson and Fryer, 1978; Cooper and Field, 1977; Drury, 1973; Rollinson and Windley, 1980; Wells, 1979). Not all granulites show these geochemical characteristics. The younger, high pressure granulites,

consisting of garnet, clinopyroxene, hypersthene and plagioclase, found in Poland and the Central European Belt, lack these elemental signatures.

#### 10.1.3. Depletion mechanism

Several mechanisms have been evoked to explain the characteristic geochemistry of the low and medium pressure granulites: 1) depletion is a primary feature of the rock (Holland and Lambert, 1973); 2) granulites represent a residuum from which a granitic melt has been removed into which all the LIL elements were partitioned (Fyfe, 1973; O'Hara and Yarwood, 1978); 3) the development of a high pressure mineral assemblage excludes LIL elements which are removed along with water (Lambert and Heier, 1968); 4) a specifically Precambrian process was effective in removing LIL elements by mantle degassing (Tarney et al., 1972; Sheraton et al., 1973); 5) LIL elements were removed by a CO<sub>2</sub>-rich fluid phase (Tarney and Windley, 1977; Rollinson and Windley, 1980; Newton et al., 1980).

Geochemical comparison between granulite rocks and protolith rocks in the adjacent amphibolite facies terrane illustrates that the K/Rb ratio of the granulites (up to 2000) is a secondary feature because the adjacent amphibolite protoliths have typical K/Rb ratios (250) and because the K/Rb ratio increases where there is a prograde transition to granulite facies (Rollinson and Windley, 1980;

Tarney and Windley, 1977).

Several field and isotopic studies suggest that there is little evidence to support anatexis and removal of LIL elements by a melt phase as a viable mechanism to produce most depleted granulite rocks (Rollinson and Windley, 1980; Janardhan et al., 1979; Hamilton et al., 1979; Newton et al., 1980). Furthermore, the existence of high pressure granulites in Poland and the Central European Belt, which have low K/Rb ratios over a range of K abundances, illustrates that the development of high pressure anhydrous assemblages does not necessarily lead to the expulsion of Rb and K from granulites.

Thus, we are left with the probability that the LIL element depletion observed in some granulites reflects the effects of a fluid-rock interaction during granulite metamorphism. Significant in this regard is the depletion of LIL elements and heavy rare earth elements (HREE) from the low and medium pressure granulites, for it has been demonstrated experimentally that, at upper mantle-lower crustal pressures, light REE are preferentially partitioned into a CO<sub>2</sub> vapour (Wendlandt and Harrison, 1978, 1979). In the presence of immiscible carbonate melts, both light, but especially heavy REE's are partitioned into the CO<sub>2</sub>-rich phase. Thus the REE distribution in these granulites is exactly what would be expected had these rocks interacted with a CO<sub>2</sub>-rich vapour.



The only study to address the distribution of gold in granulite rocks (Sighinolfi and Santos, 1976) found that granulite rocks from the Bahaia State, Brazil, contain 0.8 ppb gold (log transformed data excluding 4 "anomalous" data which exceeded 8 ppb). Inclusion of four apparently anomalous samples (8.1, 16.0, 16.2, 18.4 ppb Au) only raises the log transformed mean to 0.9 ppb gold. These data indicate that the granulite rocks from the Bahia State are depleted in gold by a factor of at least 2 with respect to either fresh crustal igneous rocks or their low grade metamorphic equivalents (Crocket, 1974; Paul et al., 1977). The 0.8 ppb gold abundance of these Brazilian granulites represents an upper limit because 27 of the 101 samples analysed by Sighinolfi and Santos (1976) contained less than the detection limit of gold (0.4 ppb). Although the gold transport capacity of CO<sub>2</sub> fluid has not been investigated experimentally, the ubiquitous presence of carbonatized wallrock in the sub-amphibolite grade, Archean gold deposits and CO<sub>2</sub>-rich nature of their fluid inclusions may indicate that gold was transported in solution by a carbonate complex. The depletion of gold in the Bahaia State granulite rocks documented by Sighinolfi and Santos (1976) is also consistent with the flushing of CO<sub>2</sub>-rich fluids through the lower crust and removal of gold during granulitization.

These geochemical observations collectively support

the premise that the granulite-grade rocks obtained their distinctive geochemistry as a result of interaction with  $\text{CO}_2$ -rich fluids. This depleted geochemical character is apparently most typical of the low and medium pressure, Precambrian and not the high pressure Phanerozoic granulite rocks (Tarney and Windley, 1977). The apparently greater abundance of granulite-grade terranes of Archean age is consistent with the premise that mantle degassing was most vigorous during the Precambrian, and that the rate of  $\text{CO}_2$  degassing from the mantle has subsequently diminished. That the low and medium pressure granulite assemblages (Low pressure: Olivine + Plagioclase + cordierite + andalusite; Medium pressure: Plagioclase + hypersthene + clinopyroxene + quartz + kyanite + sillimanite) tend to be more abundant in the Precambrian granulites with respect to the Phanerozoic-aged granulites (Tarney and Windley, 1977) could be a further consequence of vigorous mantle degassing during the Precambrian, because influx of  $\text{CO}_2$  produces a granulite from an amphibolite protolith under a P-T regime which would normally sustain amphibolite-grade mineralogy. In the absence of  $\text{CO}_2$ , higher P-T conditions would be required before amphibole or micas would undergo dehydration to produce a granulite. Therefore, higher pressure assemblages would be expected in granulites not formed by the  $\text{CO}_2$  influx model.

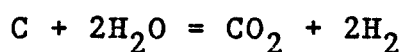
#### 10.1.4. $\delta^{13}\text{C}$ of the fluids involved in the granulite metamorphism

Few carbon isotopic studies of fluids trapped in inclusions in granulite-grade rocks have been carried out. Hoefs and Touret (1975) and Pineau et al. (1981) present data for granulite samples from South Norway which cluster into the two ranges of -14 to -24‰ and -5 to -7‰. Calcite, interpreted to have precipitated after the peak of metamorphism has a  $\delta^{13}\text{C}$  of -8.2‰ (Pineau et al., 1981). Hoefs and Touret (1975) considered the lighter values (-15 to -20‰) to represent juvenile compositions, while the heavier values (-5 to -7‰) were interpreted as fractionated retrograde fluids. Interpretation of these carbon isotopic data is not unambiguous. It is reasonable that the  $\text{CO}_2$  fluid phase which equilibrated with the calcite (-8‰) in the Norwegian granulite terrane was of juvenile origin. The textural characteristics of this calcite and its oxygen isotope composition suggests that it was a late synmetamorphic phase and hence that juvenile  $\text{CO}_2$ -rich fluids were dominant at that stage (Pineau et al., 1981). Further, Pineau et al. (1981) interpreted the light  $\delta^{13}\text{C}$  values (-14 to -21‰) from the  $\text{CO}_2$ -rich fluid inclusions to represent a mixture of  $\text{CO}_2$  derived by oxidation of reduced carbon in the lower crustal rocks and  $\text{CO}_2$  derived by decarbonatization of marine carbonates.

An alternative explanation for the presence of  $^{12}\text{C}$ -enriched  $\text{CO}_2$  is that a primary, nearly pure  $\text{CO}_2$  fluid could

have equilibrated with a graphite-bearing rock at differing P, T and  $fO_2$  to yield variable amounts of methane ( $CH_4$ ). The mole fraction of  $CH_4$  in the resultant fluid could exceed 0.25 depending on the initial activity of  $H_2O$  and the system (Hollister and Burruss, 1976). In this regard,  $CH_4$ -rich fluid inclusions are present in the Khtada Lake granulite complex in samples that contain graphite (Hollister and Burruss, 1976). Also, graphite is present in the Norwegian granulite complexes (Andreae, 1974; Pineau et al., 1981).

None of the explanations of the very light  $\delta^{13}C$  values (-14 to -25‰) for the early  $CO_2$ -rich fluid are entirely satisfactory. Reactions producing  $CH_4$  leave heavier  $CO_2$ , not lighter, unless reduced carbon is oxidized to  $CO_2$  in a closed system. However, oxidation of crustal graphite poses some problems if a mass balance is considered. Consider the formation of  $CO_2$  by oxidation of graphite:



Assume the initial concentration of carbon in the granulite protolith is 4000 ppm, the upper limit reported for typical sedimentary sequences. A cubic kilometre of such rock having a density of 2.8 g/cc weighs  $2.8 \times 10^{15}$  grams and contains about  $1 \times 10^{13}$  grams of reduced carbon. If all this reduced carbon is oxidized, it would produce  $9 \times 10^{11}$  mole  $CO_2$ . Rollinson and Windley (1980) and Newton et al.

(1980) estimate that the volume of fluid required to form a granulite is 0.3 of the rock volume, assuming that the partial pressure of  $H_2O$  in the fluid was 0.3 total pressure. To granulitize a cubic kilometre of rock,  $3 \times 10^{14}$  cubic centimetres of fluid would be required. Of this, 70% or  $2 \times 10^{14}$  cubic centimetres is  $CO_2$ . Assuming ideal gas laws apply at the P-T regime of granulite metamorphism (600 to 800°C; 7 to 9 Kb) approximately  $3 \times 10^{13}$  moles of  $CO_2$  are required to affect the granulitization of this volume of rock. However, only  $9.3 \times 10^{11}$  moles of  $CO_2$  can be produced by oxidation of the 4000 ppm carbon in the rock, or only 3% of the amount required can be achieved by this process. To derive all the  $CO_2$  by oxidation of indigenous, reduced carbon, the rock would have to contain approximately 85700 ppm carbon or 8.5 wt.%. This abundance is clearly unreasonably large for typical supercrustal rock sequences. Thus, it appears that large volumes of isotopically light  $CO_2$  cannot be derived by oxidation of reduced carbon in typical crustal rock sequences.

Thus, the interpretation of the very light  $\delta^{13}C$  values of the early  $CO_2$ -rich fluid inclusions hosted in granulite terranes is problematical and may reflect complex kinetic reactions between  $CO_2$ ,  $H_2O$ ,  $CH_4$  and  $H_2$  induced by the influx of  $CO_2$  into an amphibolitic terrane where  $p_{H_2O}$  approximated total pressure. In addition, low temperature isotope exchange reactions between  $H_2O$ - $CH_4$ - $CO_2$ - $H_2$  within the

inclusions could have taken place long after the peak metamorphism and would yield complex isotopic data.

Until more detailed studies on the chemical and isotopic evolution of fluids effecting granulitization of the lower crust become available, it must be supposed that the most probable source of the  $\text{CO}_2$ -rich fluids was the mantle and that the  $\delta^{13}\text{C}$  of that fluid inclusion population (-5 to -7‰) is typical of the mantle-derived  $\text{CO}_2$ .

## 10.2. Model

The relevance of these observations regarding granulite geochemistry to the carbonatization system which operated in the Timmins mining camp and other areas is the notable depletion of LIL (eg.  $\text{K}_2\text{O}$ , Rb, Li, Cs, U, Th),  $\text{SiO}_2$ , heavy REE's and gold from the granulite protoliths. Although the geochemical characterization of the carbonatized rock in the Timmins area is far from being exhaustive, certain general features are recognized which appear to link the  $\text{CO}_2$ -induced granulitization process with the intense carbonatization of the Abitibi Belt supercrustal rocks. These features include the large volume of hydrothermal  $\text{CO}_2$  of probable juvenile origin fixed in the rocks, and the enrichment of certain LIL elements such as K, Rb, Li, and B (Whitehead et al., 1979; Fyon and Crocket, 1982) in the carbonatized rock. That element suite which has been depleted from the granulite rocks appears to have been

enriched in the carbonatized rock of the Timmins area. Partitioning of this trace element suite into a juvenile  $\text{CO}_2$ -rich fluid during granulitization of the lower crust, is a mechanism by which chemical mass transfer could take place from the upper mantle (source of  $\text{CO}_2$ ) and lower crust (source of trace elements) to the upper crust, where carbonatization induced mass precipitation in suitable permeable rock structures (Fig. 10-3). Such a mechanism is favoured over the dehydration of greenschist or amphibolite source areas because dehydration reactions would produce fluids which would be dominantly  $\text{H}_2\text{O}$ -rich (Touret, 1971a; Wells, 1979).

#### 10.2.1. Extension of the model

A model involving the pervasion of a mantle-derived  $\text{CO}_2$ -rich fluid into the lower crust and ultimately into the volcano-sedimentary supercrustal rocks is consistent with other aspects of the carbonatization-mineralization history of the gold deposits and the volcanic evolution of the Abitibi Belt.

##### 10.2.1.1 Fluid evolution with progressive $\text{CO}_2$ influx

Guha et al. (1982) documented the fluid evolution in the Doyon Mine, Bousquet area, Quebec. They illustrated that the first fluid to evolve was a water-rich mixture with  $\text{CO}_2$ . The fluid system evolved to become progressively

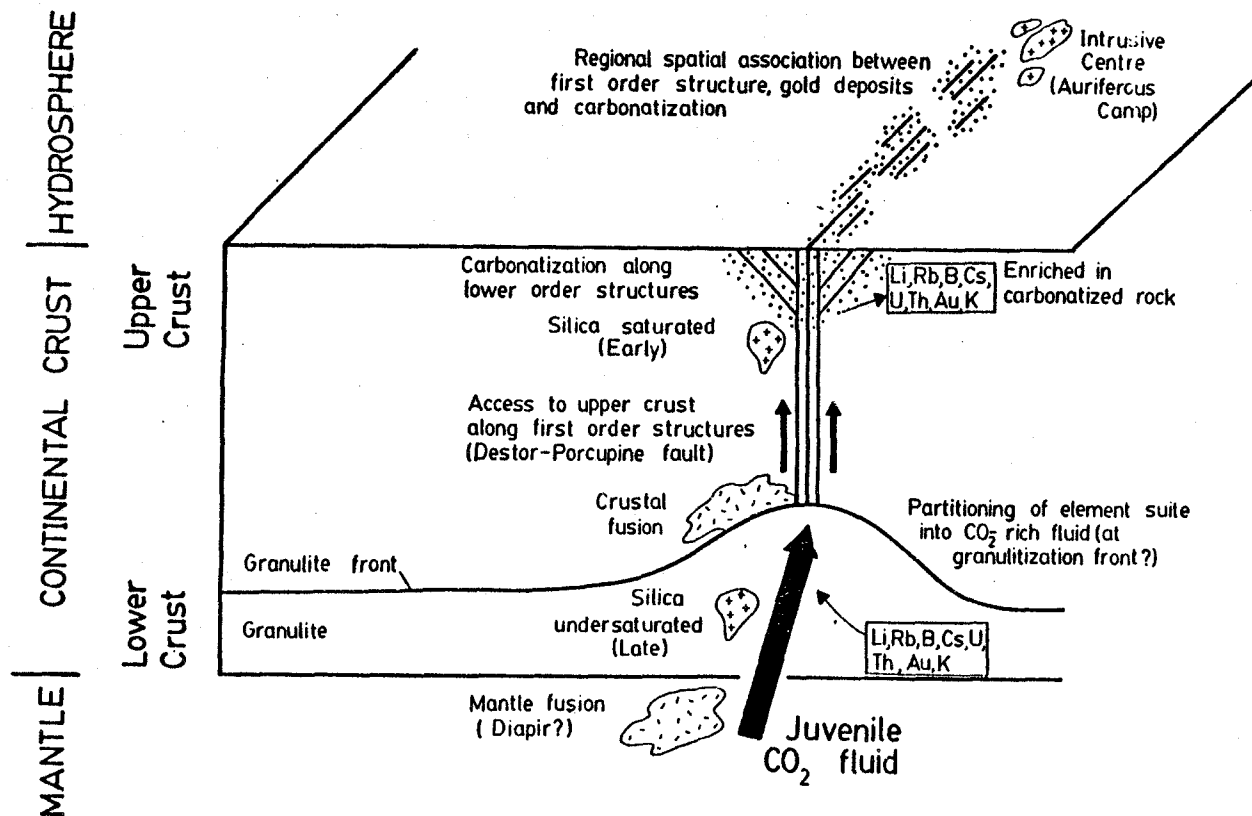


Figure 10-3: Schematic representation of events leading to lower crustal granulitization.  $\text{CO}_2$  fluids, evolved from the upper mantle either by mantle degassing or prolonged mantle fusion, flux into the lower crust, promote granulitization and escape to the upper crust along deeply penetrating fracture systems. This  $\text{CO}_2$ -rich fluid is responsible for the carbonatization of the supracrustal rocks.



richer in  $\text{CO}_2$ . The gold mineralization is associated with a  $\text{CO}_2$ -dominant fluid. Such an evolution is consistent with the expected evolution of fluids as a result of influx of mantle  $\text{CO}_2$  into the lower crust. Initial fluids, liberated by dehydration of the granulite-protolith (ie. lower crustal amphibolitic rocks) as a result of juvenile  $\text{CO}_2$  influx, would be  $\text{H}_2\text{O}$ -rich. As the fluid and conduit system evolved, subsequent fluids should show more influence of the influxing mantle-derived  $\text{CO}_2$  and hence, should become correspondingly richer in  $\text{CO}_2$ . Such an hypothetical evolution in the composition of the fluid leaving the lower crustal regime is consistent with the observed fluid inclusion evolution documented in the Mine Doyon (Guha et al., 1982).

#### 10.2.1.2 Associated igneous K- and Na-rich intrusive suite

Alkaline and sodium-rich intrusive and extrusive igneous rocks are often proximal or intimately associated with some gold producing areas in the Abitibi belt. Alkaline igneous rocks are prominent in the Kirkland Lake area (Cooke and Moorhouse, 1969) and the eastern extent of the Destor-Porcupine fault zone, east of Matheson. This igneous association is also consistent with the presence of a  $\text{CO}_2$ -rich fluid in the upper mantle. Mysen and Boettcher (1975) demonstrated that, during the melting of hydrous peridotite in the presence of  $\text{CO}_2$ - $\text{H}_2\text{O}$  vapour,  $\text{H}_2\text{O}$  is

strongly partitioned into the melt fraction with respect to  $\text{CO}_2$ . Consequently, if the vapour persists in the zone of melting, it becomes richer in  $\text{CO}_2$  as the melting progresses. Melts in equilibrium with  $\text{H}_2\text{O}$ -rich vapour ( $X_{\text{H}_2\text{O}} > 0.6$ ) are silica saturated and can be andesitic in composition, whereas melts in equilibrium with a  $\text{CO}_2$ -rich vapour are less silica saturated and can become silica undersaturated if  $X_{\text{H}_2\text{O}} < 0.5$  (Mysen and Boettcher, 1975). Successive melting in the presence of  $\text{H}_2\text{O}$ - $\text{CO}_2$  vapour, should produce a spectrum of melt compositions, initially having silica saturated, andesitic compositions, and eventually becoming quite alkaline (olivine nephelinite) in composition. Hence, the presence of alkaline igneous rocks in some gold mining camps, could be ascribed to melting of an hydrous mantle in the presence of a vapour rich in  $\text{CO}_2$ . The appearance of these alkaline igneous rocks late in the volcanological evolution of an area is consistent with experimental evolution of partial melts produced in the presence of a fluid which becomes progressively  $\text{CO}_2$ -rich as melting proceeds. The spatial and temporal association of carbonatites and alkaline-igneous rocks in zones of rifting (deeply penetrating structures) is well known in the Proterozoic and Phanerozoic rock record and adds additional evidence that the regionally continuous Destor-Porcupine and Larder Lake deformation zones were also deeply penetrating structures.

Similarly, the presence of sodium-rich, intrusive rocks in the gold camps (quartz feldspar porphyry intrusives) may also be a consequence of mantle-derived,  $\text{CO}_2$ -catalyzed, lower crustal granulitization. Incongruent dissolution of feldspars, under conditions appropriate for granulite metamorphism, is strongly enhanced in the presence of a fluid having high  $\text{CO}_2/\text{H}_2\text{O}$  ratios, with the ion solubilities being sodium (Na) > potassium (K) >> calcium (Ca) (Glassley, 1983). The process of mantle-derived  $\text{CO}_2$  influx into the lower crust, should produce Ca- and Al-enriched, Na-, K-, and Si-depleted residues in the deep crust, consistent with the known geochemistry of granulite terranes. Some, if not all of the Na and K released during the granulitization of the lower crust, may become incorporated into siliceous, partial melts, generated at a higher crustal level. In this way, sodic (Albite dykes) and potassic magmas could be generated which may then be intruded into the supercrustal rocks along those zones of crustal weakness being utilized by the mantle-derived,  $\text{CO}_2$ -rich fluids.

#### 10.2.1.3 Sodic and potassic alteration

Sodic and potassic wallrock alteration are not uncommon characteristics of Archean gold mineralization. Albite is a common accessory mineral in and immediately adjacent to many Archean, gold-quartz vein systems. K-rich

feldspar is a known to occur in wallrock alteration assemblages which have developed adjacent to higher temperature, Archean gold mineralization (c.f. the Hemlo mineralization; Colvine et al., 1983). Some of the sodium and potassium that is liberated from the lower crust during its granulitization, may alternatively become incorporated into feldspar structures which crystallize in quartz vein systems or adjacent to the quartz veins as a wallrock alteration assemblage.

#### 10.2.2 Summary

Thus the spatial association of carbonate alteration, alkaline and sodium-rich igneous rocks and gold mineralization along major crustal structures is coherent expression of a process where mantle-derived,  $\text{CO}_2$ -rich fluids interact with the lower crust to induce granulitization by depressing the ambient partial pressure of  $\text{H}_2\text{O}$ , thus effectively dehydrating the lower crustal rocks. The expelled  $\text{H}_2\text{O}$  is then capable of interacting with other Archean lower crustal rock above the  $\text{CO}_2$  front to produce partial melts of andesitic or basaltic composition. The granulitization process yields a chemically modified  $\text{CO}_2$ -rich fluid bearing certain LIL and heavy REE elements and certain transition group elements such as gold and tungsten. Influx of this modified  $\text{CO}_2$ -rich fluid along major crustal structures into the volcano-sedimentary

supercrustal rocks culminates with the intense carbonatization of susceptible lithologies adjacent to the main and parallel deformation zones. These carbonatized rocks are enriched with certain incompatible elements. Melting in the lower crust or upper mantle in the presence of a  $\text{CO}_2\text{-H}_2\text{O}$  fluid produces a continuum of igneous rock types becoming silica undersaturated as the fluid evolves and becomes richer in  $\text{CO}_2$ . The marked peak in gold enrichment in the supercrustal rocks during the Archean (Fig. 10-1) is also consistent with this model in so far as a large source of gold (lower crustal rocks) is accessible by mantle-derived  $\text{CO}_2$ -rich fluids.

Incidentally, it is now acknowledged that the primitive Earth's mantle underwent a significant differentiation which culminated at 2.5 to 2.8 BYBP with the isolation of continental crust and an underplated mantle residue (Bell et al., 1982). The growth of this underplated mantle material beneath the continents is proposed to have accumulated by thermal freezing of asthenosphere and diapiric rise of mesospheric material (Brooks et al., 1976). The age concurrence of this major mantle differentiation event with the Superior Province magmatism, carbonatization and gold mineralization events suggests that the underplating process may have triggered the mantle  $\text{CO}_2$  degassing and the Superior Province magmatism. Juxtaposition of hot, diapiric mesospheric material against

a cooler, "frozen" underplate of mantle material would enhance devolatilization of the lower crustal block and could initiate partial melting. This early crustal magmatism would be silica-saturated and the dissolved vapour in the silicate magma would be  $H_2O$ -rich. As melting progressed, the residual vapour would become  $CO_2$ -rich and ultimately silicate magmas would become silica-undersaturated. During the final stages of the supercrustal sequence stabilization, following most if not all of the magmatism, the residual vapour would have evolved into its most  $CO_2$ -rich state and granulitization rate would become highest. Maximum flux of the residual  $CO_2$ -rich, mantle-derived fluid along the major fault systems into the supercrustal sequence would have taken place late in the evolution of the volcano-sedimentary sequence (at least post volcanism). This chronology is consistent with the chronology deduced from the field characteristics of the carbonate alteration zones. Thus, the observed magmatic/gold metallogenic evolution of the Abitibi belt can be modelled closely by a sequence of subcrustal/upper mantle events which culminated at 2.5 to 2.8 BYBP.

## References

- Andreae, M.O. (1974): Chemical and stable isotope composition of the high grade metamorphic rocks from the Arendal Area, southern Norway; *Contrib. Mineral. Petrol.*, v.47, pp. 299-316.
- Andrews, A.J. (1977): Low temperature fluid alteration of oceanic layer 2 basalts; DSDP Leg 37, *Can. Jour. Earth Sci.*, v.14, pp. 911-926.
- Anon. (1944): Malga Porcupine Gold Mines Limited; Information bulletin published by Malga Porcupine Gold Mines Limited, 19 p.
- Arndt, N.T. and Nisbet, E.G. (1982): What is a komatiite?; pp. 19-27 in *Komatiites*, ed. by N.T. Arndt and E.G. Nisbet; George Allen and Unwin, London, 526 p.
- Aumento, F., Mitchell, W.S. and Fratta, M. (1976): Interaction between sea water and oceanic layer two as a function of time and depth - 1. Field evidence; *Can. Min.*, v. 14, pp. 269-290.
- Bain, G.W. (1933): Wall-rock mineralization along Ontario gold deposits; *Econ. Geol.*, v. 28, no. 8, Dec. 1933, pp. 705-743.
- Beaty, D.W. (1980): The oxygen isotope geochemistry of the Abitibi Greenstone Belt; unpubl. Ph.D. Thesis, California Inst. Technology, Part 1, pp. 209-463.
- Beaty, D.W., and Taylor, H.P. Jr. (1979): Oxygen isotope geochemistry of the Abitibi greenstone belt, Ontario: Evidence for seawater/rock interaction and implications regarding the isotopic composition and evolution of ocean and oceanic crust; Abstract, p. 386 in *Abstracts with programs*, *Geol. Soc. Amer.*, 1979, v. 11, no. 7, 559 p.
- (1982): Some petrologic and oxygen isotopic relationships in the Amulet Mine, Noranda, Quebec, and their bearing on the origin of Archean massive sulfide deposits; *Econ. Geol.*, v. 77, pp. 95-108.
- Becker, R. H. (1971): Carbon and oxygen isotope ratios in iron-formation and associated rocks from the Hammersley

- Range of Western Australia and their implications:  
Unpub. Ph.D. thesis, Univ. Chicago, 138p..
- Bell, K., Blenkinsop, J., Cole, T.J.S., and Menagh, D.P. (1982): Evidence from Sr-isotopes for long-lived heterogeneities in the upper mantle; *Nature*, v. 298, pp. 251-253.
- Berglund, L., Touret, J. (1976): Garnet-biotite gneiss in "Système du Graphite" (Madagascar): Petrology and Fluid Inclusions. *Lithos*, v. 9, pp 139-148.
- Bevington, P.R. (1969): Data Reduction and Error Analysis for the Physical Sciences, McGraw-Hill, New York, 336p.
- Blattner, P. and Hulston, J.R. (1978): Proportional variations of geochemical  $^{18}\text{O}$  scales - an interlaboratory comparison; *Geochim. Cosmochim. Acta*, v. 42, pp. 59-62.
- Bottinga, Y. (1968): Calculation of fractionation factors for carbon and oxygen exchange in the system calcite-carbon dioxide-water; *Jour. Phys. Chem.*, v. 72, pp. 800-808.
- Bottinga, Y. (1969): Calculated fractionation factors for carbon and hydrogen isotope exchange in the system calcite- $\text{CO}_2$ -graphite-methane-hydrogen and water vapour; *Geochim. Cosmochim. Acta*, v. 33, pp. 49-64.
- Bowers, T.S., and Helgeson, H.C. (1983): Calculation of the thermodynamic and geochemical consequences of nonideal mixing in the system  $\text{H}_2\text{O}-\text{CO}_2-\text{NaCl}$  on phase relations in geologic systems : Equation of state for  $\text{H}_2\text{O}-\text{CO}_2-\text{NaCl}$  fluids at high pressures and temperatures; *Geochim. Cosmochim. Acta*, v. 47, pp 1247-1275.
- Boyle, R.W. (1979): The Geochemistry of Gold and its Deposits; *Can. Geol. Sur. Bull.* 280, 584 p.
- Brooks, C., James, D. E. and Hart, S. R. (1976): Ancient lithosphere: Its role in young continental volcanism; *Science*, v. 193, pp. 1086-1094.
- Buffam, B.S.W. (1948): Moneta Porcupine Mine, pp. 457-464 in Structural Geology of Canadian Ore Deposits; Canadian Inst. Min. Met., Jubilee Volume, 948 p.
- Burrows, A.G. (1912): The Porcupine Gold Area; Ontario Bureau of Mines, Vol. 20, Part 2, 1912: The Porcupine Gold Area, Second Report; Ontario Bureau of Mines, Vol. 21, Part 1, pp. 205-249. Accompanied by Map 21a, scale



1 inch to 1 mile.

- (1924): The Porcupine gold area; accompanied by Map 33a; Ontario Dept. Mines, v. 33, pt. 2, pp. 1-84 (Published 1925).
- Cameron, E.M. (1975): Geochemical methods of exploration for massive sulfide mineralization in the Canadian Shield; pp. 21-49, in Geochemical Exploration 1974, ed. I.L. Elliott and W.K. Fletcher, Elsevier, New York, 720 p.
- and Baumann, A. (1972): Carbonate sedimentation during the Archean; Chem. Geol., v. 10, pp. 17-30.
- Carlson, H.D. (1967): The geology of Ogden, Deloro and Shaw Townships, District of Cochrane, Ontario; Ontario Dept. Mines, OFR 5012, 117 p., accompanied by Maps P. 341, P. 342, P. 343, scale 1 inch to 1/4 mile.
- Clayton, R.N. (1981): Isotopic thermometry; pp. 85-109 in Thermodynamics of Minerals and Metals, eds. R.C. Newton, A. Navrotsky, and B.J. Wood, Springer-Verlag, New York, 304 p.
- and Epstein, S. (1961): The use of oxygen isotopes in high-temperature geological thermometry; Jour. Geol., v. 69, pp. 447-452.
- Clayton, R.N. and Mayeda, T.K. (1963): The use of bromine pentafluoride in the extraction of oxygen from oxides and silicates for isotopic analysis; Geochim. Cosmochim. Acta, v. 27, pp. 43-52.
- , O'Neil, J.R., and Mayeda, T.K. (1972): Oxygen isotope exchange between quartz and water: Jour. Geophys. Res., v. 77, pp. 3057-3067.
- Collerson, K.D. and Fryer, B.J. (1978): The role of fluids in the formation and subsequent development of early continental crust; Contrib. Mineral. Petrol., v. 67, pp. 151-167.
- Colvine, A.C., Andrews, A.J., Cherry, M.E., Durocher, M.E., Fyon, A.J., Lavigne, Jr.M.J., Macdonald, A.J., Marmont, S., Poulsen, K.H., Springer, J.S., and Troop, D.G. (1984): An integrated model for the origin of Archean Lode Gold deposits; Ontario Geol. Surv., OFR 5524, 98p.
- Cooke, D.L. and Moorhouse, W.W. (1969): Timiskaming volcanism in the Kirkland Lake area, Canada; Can. Jour.

Earth Sci., v. 6, pp. 117-132.

- Cooper, D.C. and Field, D. (1977): The chemistry and origins of Proterozoic low-potash, high-iron, charnockitic gneisses from Tromoy, south Norway; Earth Planet. Sci. Lett., v. 35, pp. 105-115.
- Craig, H. (1957): Isotopic standards for carbon and oxygen and correction factors for mass spectrometric analysis of carbon dioxide; Geochim. Cosmochim. Acta, v. 12, pp. 133-149.
- (1961): Standard for reporting concentrations of deuterium and oxygen-18 in natural waters; Science, v. 133, pp. 1833-1834.
- (1973): The geochemistry of the stable carbon isotopes; Geochim. Cosmochim. Acta, v. 12, pp. 133-149.
- Craig, J. R. and Vaughn, D. J. (1981): Ore Microscopy and Ore Petrography; J. Wiley and Sons, Toronto, 406p.
- Crocket, J.H. (1974): Gold; pp. 79-B-1 to 79-O-1 in v. 11-5, Handbook of Geochemistry, ed. K.H. Wedepohl, Springer-Verlag, New York.
- Davies, J.F. (1977): Structural interpretation of the Timmins mining area, Ontario; Can. Jour. Earth Sci., v. 14, pp. 1046-1053.
- Davies, J. F. and Luhta, L. (1978): An Archean "Porphyry-type" disseminated copper deposit, Timmins, Ontario; Econ. Geol., v. 73, pp. 383-396.
- , Whitehead, R.E.S., Cameron, R.A., and Duff, D. (1980): Regional and local patterns of CO<sub>2</sub>-K-Rb-As alteration: A guide to gold mineralization in the Timmins area, abstract, Can. Inst. Min. Met. Bull., v. 73, pp. 63-64.
- (1982): Regional and local patterns of CO<sub>2</sub>-K-Rb-As alteration: A guide to gold in the Timmins area; pp. 130-143 in Geology of Canadian Gold Deposits; Can. Inst. Min. Met., Special Volume 24, 286 p.
- Dawson, J.B. (1980): Kimberlites and Their Xenoliths; Springer-Verlag, New York, 252 p.
- Deines, P. (1977): On the oxygen isotope distribution among mineral triplets in igneous and metamorphic rocks;

- Geochim. Cosmochim. Acta, v. 41, pp 1709-1730.
- and Gold, D.P. (1969): The change in carbon and oxygen isotopic composition during contact metamorphism of Trenton limestone by the Mt. Royal pluton; Geochim. Cosmochim. Acta, v. 33, pp. 421-424.
- (1973): The isotopic composition of carbonatite and kimberlite carbonates and their bearing on the isotopic composition of deep-seated carbon; Geochim. Cosmochim. Acta, v. 37, pp. 1709-1733.
- DePado, D.J., Manton, W.I., Grew, E.S. and Halpern, M. (1982): Sm-Nd, Rb-Sr and U-Th-Pb systematics of granulite facies rocks from Fyfe Hills, Enderby Land Antarctica; Nature, v. 298, pp. 614-618.
- Dimroth, E. and Lichtblau, .P. (1979): Metamorphic evolution of Archean hyaloclastites, Noranda Area, Quebec, Canada. Part 1: Comparison of Archean and Cenozoic sea-floor metamorphism; Can. Jour. Earth Sci., v. 16, pp 1315-1340.
- and Rocheleau, M. (1979): Volcanology and sedimentology of Rouyn-Noranda area, Quebec, GAC-MAC field trip guide A-1, 199 p.
- , Imreh, L., Rocheleau, M. and Goulet, N. (1982): Evolution of the south-central part of the Archean Abitibi Belt, Quebec. Part 1: Stratigraphy and paleogeographic model, Canadian Jour. Earth Sci., v. 19, pp. 1729-1758.
- Donnelly, T. H., Lambert, I., Oehler, D. Z., Hallberg, J., Hudson, D. R., Smith, J. W., Bavinton, O. A. and Golding, L. (1977): A reconnaissance study of stable isotope ratios in Archean rocks from the Yilgarn Block, Western Australia; Jour. Geol. Soc. Austr., v. 24, pp. 409-420.
- Downes, M.J. (1979): Kirkland Lake area, stratigraphic mapping, district of Timiskaming, pp. 121-125 in Summary of Field Work, 1979, by the Ontario Geol. Surv., ed. V.G. Milne, O.L. White, R.B. Barlow, and C.R. Kustra, Ontario Geol. Surv., MP 90, 245 p.
- Drury, S.A. (1973): The geochemistry of Precambrian granulite facies rocks from the Lewisian complex of Tiree, Inner Hebrides; Chem. Geol., v. 11, pp 167-188.
- Dunbar, R. (1948): Structural relations of the Porcupine ore deposits; pp. 442-456 in Structural Geology of

Canadian Ore Deposits, CIM Jubilee Volume, 948p.

- Ebbutt, F. (1948): Relationships of minor structures to gold deposition in Canada; pp. 64-77 in Structural Geology of Canadian Ore Deposits, CIM Jubilee Volume, 948p.
- Eckstrand, O.R. (1975): The Dumont serpentinite: A model for control of nickeliferous opaque mineral assemblages by alteration reactions in ultramafic rocks; Econ. Geol., v. 70, pp. 183-201.
- Ellis, A.J. (1959): The solubility of calcite in carbon dioxide solutions; Amer. Jour. Sci., v. 257, pp. 354-365.
- (1963): The solubility of calcite in sodium chloride solutions at high temperatures; Amer. Jour. Sci., v. 261, pp. 259-267.
- Eugster, H.P. (1981): Compositions and thermodynamics of metamorphic solutions, pp. 183-202 in Thermodynamics in Geology, ed. D.G. Fraser
- Ferguson, S.A., Buffam, B.S.W., Carter, O.F., Griffis, A.T., Holmes, T.C., Hurst, M.E., Jones, W.A., Lane, H.C. and Longley, C.S. (1968): Geology and ore deposits of Tisdale Township, District of Cochrane; Ontario Dept. Mines, GR 58, 177 p., Accompanied by Map 2075, scale 1 inch to 1,000 feet.
- Ferry, J.M. and Burt, D.M. (1982): Characterization of metamorphic fluid composition through mineral equilibria, pp. 207-262 in Characterization of Metamorphism Through Mineral Equilibria, ed. J.M. Ferry, Mineralogical Soc. Amer.; Revs. Mineralogy, v. 10, 397 p.
- Forsythe, D. L. (1971): Vertical zonation of gold-silver tellurides in the Emperor Gold Mine, Fiji; Proc. Australas. Inst. Min. Metall., No. 240, pp. 25-31.
- Foster, R.P. (1980): The controls of gold precipitation in Archean gold deposits; Mining and Engineering (Zimbabwe), June 1980, pp. 21-23, 25 and August 1980, p. 31.
- Friedman, I. and Gleason, J.D. (1973): A new silicate inter-comparison standard for  $^{18}\text{O}$  analysis; Earth Planet. Sci. Lett., v. 18, 124p.
- and O'Neil, J.R. (1977): Compilation of stable

isotope fractionation factors of geochemical interest, Chapter KK, Data of Geochemistry; U.S. Geol. Surv., Professional Paper 440-KK.

Fryer, B.J. and Hutchinson, R.W. (1976): Generation of metal deposits on the sea floor; Can. Jour. Earth Sci., v. 13, pp. 126-135.

-----, Kerrich, R., Hutchinson, R.W., Peirce, M.G. and Rogers, D.S. (1979): Archean precious-metal hydrothermal systems, Dome Mine, Abitibi Greenstone Belt, 1, Patterns of alteration and metal distribution; Can. Jour. Earth Sci., v. 16, pp. 421-439.

Fuex, .N. and Baker, D.R. (1973): Stable carbon isotopes in selected granitic, mafic and ultramafic rocks; Geochim. Cosmochim. Acta, v. 37, pp 2509-2521.

Furse, G.D. (1948): McIntyre Mine, pp. 482-496 in Structural Geology of Canadian Ore Deposits, CIM Jubilee Volume, 948 p.

Fyfe, W.S. (1973): The granulite facies, partial melting and the Archean crust; Phil. Trans. R. Soc. London, v. A273, pp. 457-461.

----- and Henley, R.W. (1973): Some thoughts on chemical transport processes with particular reference to gold; Miner. Sci. Engng., v. 5, no. 4, pp 295-303.

-----, Kerrich, R., Gorman, B. E., and Studemeister, P. A. (1982): Geochemistry and field relations of lode gold deposits in felsic igneous intrusions, Ontario Geoscience Research Grant Program, Grant 56, Ontario Geological Survey, OFR , p..

Fyon, J.A. (1980): Seawater alteration of Early Precambrian (Archean) volcanic rock and exploration criteria for stratiform gold deposits, Porcupine camp, Abitibi greenstone belt, northeastern Ontario, unpublished M.Sc. thesis, McMaster University, 238 p.

----- and Crocket, J.H. (1981a): Volcanic environment of carbonate alteration and stratiform gold mineralization, Timmins area; pp. 47-58 in Genesis of Archean, Volcanic-Hosted Gold Deposits, Symposium held at the University of Waterloo, March 7, 1980, Ontario Geological Survey, MP 97, 175 p.

----- (1982): Gold exploration in the Timmins district using field and lithogeochemical characteristics of carbonate alteration zones; pp. 113-

129 in Geology of Canadian Gold Deposits, Canadian Institute of Mining and Metallurgy, Special Volume 24, 286 p.

Fyon, J. A. and Karvinen, W.O. (1978): Volcanic environment of gold mineralization in the Timmins area; pp. 202-205, in Summary of Field Work, 1978, by the Ontario Geological Survey, ed. V.G. Milne, O.L. White, R.B. Barlow, and J.A. Robertson, Ontario Geological Survey, MP 82, 235 p.

----- Crocket, J.C. and Schwarcz, H.P. (1983a): Timmins gold deposit types: characteristics and exploration criteria; McGill University-Ecole Polytechnique de Montreal Mineral Exploration Research Institute, Paper 83-1, 66 p.

----- (1983b): Magnesite abundance as a guide to gold mineralization associated with ultramafic flows, Timmins Area; Jour. Geochemical Exploration, v. 18, pp. 245-266.

----- (1983c): The Carshaw and Malga iron-formation hosted gold deposits of the Timmins area, pp. 98-110 in The Geology of Gold in Ontario, ed. J.C. Colvine, Ontario Geological Survey, MP 110.

----- (1983d): Application of stable isotope studies to gold metallogeny in the Timmins-Porcupine camp; Ontario Geoscience Research Grant Program, Grant No. 49, Ontario Geological Survey, OFR 5464, 182 p.

-----, Schwarcz, H.P. and Crocket, J.H. (1980): Carbon and oxygen isotope geochemistry of replacement carbonates from the Timmins-Porcupine gold camps; Grant 49, pp. 72-82, in Geoscience Research Grant Program, Summary of Research, 1979-1980, ed. E.G. Pye, Ontario Geological Survey, MP 93, 262 p.

----- and Knyf, M. (1982): Gold exploration potential using oxygen, carbon, and hydrogen stable isotope systematics of carbonatized rock and quartz veins, Timmins area; Grant 49, pp 59-64, in Geoscience Research Grant Program, Summary of Research 1981-1982, ed. E.G. Pye, Ontario Geological Survey, MP 103, 219 p.

-----, Kabir, A., and Knyf, M. (1981): Trace element and stable isotope geochemistry of auriferous iron formations in the

- Timmins area; Grant 49, pp. 90-107 in Geoscience Research Grant Program, Summary of Research 1980-1981, ed. E.G. Pye, Ontario Geological Survey, MP 98, 340 p.
- Garlick, G.D. and Dymond, J.R. (1970): Oxygen isotope exchange between volcanic materials and ocean water; Geol. Soc. Amer. Bull., v. 81, pp 2137-2142.
- and Epstein, S. (1967): Oxygen isotope ratios in co-existing minerals of regionally metamorphosed rocks; Geochim. Cosmochim. Acta, v. 31, pp 181-214.
- Gascoyne, M. (1979): Isotope and geochronologic studies of speleothem; Unpubl. Ph.D. Thesis, McMaster University.
- Gelinas, L., Brooks, C., Perrault, G., Carignan, J., Trudel, P. and Grasso, F. (1977): Chemo-stratigraphic divisions within the Abitibi volcanic belt, Rouyn-Noranda District, Quebec; pp. 265-295 in Geol. Assoc. Canada, Special Paper 16.
- Golding, S. D. and Wilson, A. F. (1983): Geochemical and stable isotope studies of the No. 4 lode, Kalgoorlie, Western Australia; Econ. Geol., v. 78, pp. 438-450.
- Gordon, J.B. (1977): Gold deposits of Ontario, east central sheet, districts of Thunder Bay, Algoma, Cochrane, Sudbury, Timiskaming and Nipissing: Ontario Geol. Surv., Prelim. Map P.1228, Mineral Deposits Serial Scale 1:1013760 or 1 inch to 16 miles. Compilation 1974, 1975, 1976.
- , Lovell, H. L., de Grijjs, J. and Davie, R. F. (1978): Gold Deposits of Ontario, Part 2: Part of District of Cochrane, Districts of Muskoka, Nipissing, Parry Sound, Sudbury, Temiskaming, and Counties of Southern Ontario; Ontario Geological Survey, Mineral Deposits Circular 18, 253p.
- Graton, L.C., McKinstry, H.E. and others (1933): Outstanding features of Hollinger geology; Canadian Inst. Min. Met., Trans., v. 36, pp. 1-20.
- Griffis, R. (1972): Genesis of a magnesite deposit, Deloro Township, Ontario; Econ. Geol., v. 67, pp. 63-71.
- Groves, P.I., Phillips, G.N., Ho, S.E., Henderson, C.A., Clark, M.E. and Wood, G.M. (1984): Controls on distribution of Archean hydrothermal gold deposits in Western Australia; in Proc. Symp. Gold 82, Geol. Soc. Zimbabwe Spec. Pub. 1, A.A. Balkema, Rotterdam, Netherlands.

- Grunsky, E.C. (1980): Abitibi alteration study, pp. 74-78 in Summary of Field Work, 1980, Ontario Geological Survey, ed. V.G. Milne, O.L. White, R.B. Barlow, J.A. Robertson and A.C. Colvine, Ontario Geological Survey, MP 96, 201 p.
- Guha, J., Gauthier, A., Vallee, M., Descarreaux, J., and Lange-Brard, F. (1982): Gold mineralization patterns at the Doyon Mine (Silverstack), Bousquet, Quebec; pp. 50-57 in Geology of Canadian Gold Deposits, Canadian Inst. Min. Met., Special Volume 24, 286 p.
- Haas, J.L., Jr. (1971): The effect of salinity on the maximum thermal gradient of a hydrothermal system at hydrostatic pressure; Econ. Geol., v. 66, pp 940-946.
- Hamilton, P.J., Evensen, N.M., O'Nions, R.K., and Tarney, J. (1979): Sm-Nd systematics of Lewisian gneisses: implications for the origin of granulites; Nature, v. 277, pp. 25-28.
- Hangari, K. M., Ahmad, S. N., and Perry, E. C., Jr. (1980): Carbon and oxygen isotope ratios in diagenetic siderite and magnetite from Upper Devonian ironstone, Wadi Shatti District, Libya; Econ. Geol., v. 75, pp. 538-545.
- Heier, K.S. (1973): Geochemistry of granulite facies rocks and problems of their origin; Phil. Trans. Roy. Soc. London A., v. 273, pp. 429-442.
- and Thoresen, K. (1971): Geochemistry of high grade metamorphic rocks, Lofoten-Vesteralen, North Norway; Geochim. Cosmochim. Acta, v. 35, pp 89-99.
- Hemley, J.J. and Jones, W.R. (1964): Chemical aspects of hydrothermal alteration with emphasis on hydrogen metasomatism; Econ. Geol., v. 59., pp. 538-569.
- Hendel, E.M. and Hollister, L.S. (1981): An empirical solvus for  $\text{CO}_2$ - $\text{H}_2\text{O}$ -2.6 wt.% salt; Geochim. Cosmochim. Acta, v. 45, pp. 225-228.
- Henley, R.W. (1973): Solubility of gold in hydrothermal chloride solutions; Chem. Geol., v. 11, pp. 73-87.
- Higgins, N.C. and Kerrich, R. (1982): Progressive  $^{18}\text{O}$  depletion during  $\text{CO}_2$  separation from a carbon-dioxide-rich hydrothermal fluid: evidence from the Grey River tungsten deposit, Newfoundland; Can. Jour. Earth Sci., v. 19, pp 2247-2257.



- Hobbs, B.E. (1968): Recrystallization of single crystals of quartz; Tectonophysics, vol. 6, pp. 353-401.
- Hodgson, C. J. (1983): Preliminary report on the Timmins-Kirkland Lake area gold deposits file, Ontario Geological Survey, OFR 5467, 434 p., 17 tables, 40 figures, 9 appendices and 11 maps.
- Hodgson, C.J. (1983): The structure and geological development of the Porcupine Camp - A re-evaluation; pp. 211-225 in The Geology of Gold in Ontario; ed. A.C. Colvine, Ontario Geological Survey, MP 110, 278 p.
- Hoefs, J. (1973): Ein Beitrag zur isotopen-geochemie des kohlenstuffs in magmatischen gest einen; Contrib. Mineral. Petrol., v. 41, pp. 277-300. (not read).
- (1975): The carbon isotopic composition of CO<sub>2</sub> from fluid inclusions; Fortschr. Miner., v. 52, Spec. Issue IMA meeting Berlin-Regensburg 1974, pp. 475.
- (1980): Stable isotope geochemistry; Springer-Verlag, New York, 208 p.
- and Touret, J. (1975): Fluid inclusion and carbon isotope study from Bamble Granulites (south Norway); Contrib. Mineral. Petrol., v. 52, pp 165-174.
- Holland, J.G. and Lambert, R.St.J. (1973): Comparative major element geochemistry of the Lewisian rocks of the mainland of Scotland, pp. 51-62 in The Related Precambrian Rocks of Scotland and Related Rocks of Greenland, ed. R.G. Park and J. Tarney, Univ. Keele, 200 p.
- Hollister, L.S. and Burruss, R.C. (1976): Phase equilibria in fluid inclusions from the Khtada Lake metamorphic complex; Geochim. Cosmochim. Acta, v. 40, pp. 163-175.
- Holloway, J.R. (1981): Compositions and volumes of supercritical fluids in the Earth's crust, pp. 13-38, in Fluid Inclusions: Applications to Petrology; MAC short course, v. 6, May, 1981, 304p.
- Honnorez, J. (1978): Generation of phillipsites by plagonitization of basaltic glass in seawater and the origin of potassium-rich, deep-sea sediments; pp. 245-258 in Natural Zeolites, ed. L.B. Sand and F.A. Mumpton, Int. Conference on the occurrence, properties and utilization of natural zeolites, Tucson, June, 1976, Pergamon Press, New York, 546 p.

- Hurst, M.E. (1935): Vein formation at Porcupine, Ontario; Econ. Geol., v. 30, pp 103-127.
- Janardhan, A.S., Newton, R.C. and Smith, J.V. (1979): Ancient crustal metamorphism at low  $pH_2O$ : charnockite formation at Kabbaldurga, South India; <sup>2</sup>Nature, v. 278, pp 511-514.
- and Hansen, E.C. (1982): The transformation of amphibolite facies gneiss to Charnockite in southern Karnataka and northern Tamil Nadu, India; Contrib. Mineral. Petrol., v. 79, pp 130-149.
- Jensen, L.S. (1976): A new cation plot for classifying subalkalic volcanic rocks; Ontario Div. Mines, MP66, 22p.
- Johannes, W. (1969): An experimental investigation of the system  $MgO-SiO_2-H_2O-CO_2$ ; American J. Sci., v. 267, pp.1083-1104.
- Jolly, W.T. (1978): Metamorphic history of the Archean Abitibi Belt; Geological Survey of Canada Paper 78-10, pp.63-77.
- (1980): Development and degradation of Archean lavas, Abitibi Area, Canada, in light of major element geochemistry; Jour. Petrol., v. 21, pp. 323-363.
- Jones, W.H. (1948): Hollinger Mine, pp. 464-481, in Structural Geology of Canadian Ore Deposits, CIM Jubilee Volume, 948p.
- Karvinen, W.O. (1976): Distribution of carbonate-rich rocks, porphyries and gold deposits, Timmins area; pp. 182-183 in Summary of Field Work, 1976, by the Geological Branch, ed. V.G. Milne, W.R. Cowan, K.D. Card, and J.A. Robertson, Ontario Div. Mines, MP67, 183p.
- (1978): The Porcupine camp - A model for gold exploration in the Archean; Canadian Mining Journal, Sept., pp. 48-53.

- (1981): Geology and evolution of gold deposits, Timmins area, Ontario; pp.29-46 in Genesis of Archean, volcanic-hosted gold deposits, Symposium held at the University of Waterloo, March 7, 1980, Ontario Geological Survey, MP97, 175p.
- Kavanagh, P. M. (1979): Precambrian gold deposits;pp. 47-62 in Proceedings of the gold Workshop, Yellowknife, Northwest Territories, December 3-7, 1979; ed. by R. D. Morton, 354p..
- Keeling, C.D. (1958): The concentration and isotopic abundance of carbon dioxide in rural areas; Geochim. Cosmochim. Acta, v. 13, pp. 322-334.
- Keith, M. L. and Weber, J. N. (1964): Isotopic composition and environmental classification of selected limestones and fossils; Geochim. Cosmochim. Acta, v. 28, pp. 1787.
- Kerrich, R. (1981): Archean gold bearing chemical sediments and veins: a synthesis of stable isotope and geochemical relations, pp. 144-167 in Genesis of Archean, volcanic-hosted gold deposits, Symposium held at University of Waterloo, March 7, 1980, Ontario Geological Survey, MP97, 175p.
- and Fryer, B.J. (1979): Archean precious metal hydrothermal systems, Dome Mine, Abitibi Greenstone Belt. II REE and oxygen isotope relations, Canadian Jour. Earth Sci., v. 16, pp. 440-458.
- and Fyfe, W.S. (1981): The gold carbonate association: source of CO<sub>2</sub> fixation reactions in Archean lode deposits; Chemical Geology, v. 33, pp. 265-294.
- and Hodder, R.W. (1982): Archean lode gold and base metal deposits: evidence for metal separation into independent hydrothermal systems, pp. 144-160 in Geology of Canadian Gold Deposits, CIM Special Volume 24, 286p.
- , Beckinsale, R.D. and Durham, J.J. (1977): The Transition between deformation regimes dominated by intercrystalline diffusion and intracrystalline creep evaluated by oxygen isotope thermometry; Tectonophysics, v. 38, pp. 241-257.

- , Kishida, A., and Willmore, L. M. (1984): Timing of Abitibi Belt lode gold deposits: Evidence from  $^{39}\text{Ar}/^{40}\text{Ar}$  and  $^{87}\text{Rb}-^{87}\text{Sr}$ ; pp. 78 in Program with Abstracts, Joint Annual Meeting Geological Assoc. Canada and Min. Assoc. Canada, London, Ontario, May 14-16, 1984, 128p..
- Knauth, L.P. and Epstein, S. (1976): Hydrogen and oxygen isotope ratios in nodular and bedded cherts; *Geochim. Cosmochim. Acta*, v. 40, pp. 1095-1108.
- and Lowe, D.R. (1978): Oxygen isotope geochemistry of cherts from the Onverwacht Group (3.4 Billion years), Transvaal, South Africa, with implications for secular variations in the isotopic composition of cherts; *Earth. Planet. Sci. Lett.*, v. 41, pp. 209-222.
- Kobelski, B.J., Gold, D.P. and Deines, P. (1979): Variations in stable isotope compositions for carbon and oxygen in some South African and Lesothan Kimberlites; pp. 252-271 in *Kimberlites, Diatremes, and Diamonds: Their Geology, Petrology and Geochemistry*, Boyd, F.R. and H.O.A. Meyer eds., Proc. 2nd Int'l Kimberlite Conf., v. 1, Amer. Geophys. Union, 400 p.
- Koval'skiy, V.V. and Cherskiy, N.V. (1973): Possible sources and isotopic composition of carbon in diamonds; *Int. Geol. Rev.*, v. 15, pp. 1224-1228.
- Krupka, K.M., Ohmoto, H. and Wickman, F.E. (1977): A new technique in neutron activation analysis of Na/K ratios of fluid inclusions and its application to the gold-quartz veins at the O'Brien Mine, Quebec, Canada. *Canadian Jour. Earth Sci.*, v. 14, pp. 2760-2770.
- Lakind, J.S. (1984): Geochemical study of gold-quartz veins, Red Lake Gold Camp, Northwest Ontario; M.Sc. Thesis (Unpubl.), University of Wisconsin-Madison, 56p.
- Lambert, I.B. and Heier, K.S. (1968): Chemical investigations of deep-seated rocks in the Australian Shield; *Lithos*, v. 1, pp. 30-53.
- Langford, G.B. (1941): Geology of the McIntyre Mine; Amer. Inst. Min. Met. Engineers, Trans., v. 144, pp. 151-169.
- Longstaffe, F.J. (1977): The oxygen isotope and elemental geochemistry of Archean rocks from northern Ontario; unpubl. Ph.D. Thesis, McMaster University, 564p.

- Lorsong, J. (1975): Stratigraphy and sedimentology of the Porcupine Group (Early Precambrian), northeastern Ontario. Unpublished B. Sc. thesis, Univ. of Toronto, Ontario.
- Lumbers, S.B. (1964): Preliminary report on the relationship of mineral deposits to intrusive rocks and metamorphism in part of the Grenville Province of Southern Ontario, Ontario Dept. Mines, PR1964-4, 37p.
- Macdonald, A.J. (1983): The iron formation-gold association evidence from Geraldton area, pp. 75-83 in The Geology of Gold in Ontario, ed. A.C. Colvine, Ontario Geological Survey, MP 110, 278p.
- Madsen, J.K. (1977): Composition and microthermometry of fluid inclusions in the Kleivan Granite, south Norway; Amer. Jour. Sci., v. 277, pp. 673-696.
- Matsuhisa, Y. (1974):  $^{18}\text{O}/^{16}\text{O}$  ratios of NBS-28 and some silicate reference samples; Geochem. Jour., v. 8, pp.103-107.
- , Goldsmith, J.R. and Clayton, R.N. (1979): Oxygen isotopic fractionation in the system quartz-albite-anorthite-water; Geochim. Cosmochim. Acta, v. 43, pp. 1131-1140.
- Matthews, A. and Katz, A. (1977): Oxygen isotope fractionation during the dolomitization of calcium carbonate; Geochim. Cosmochim Acta; v. 41, pp. 1431-1438.
- and Beckinsale, R.D. (1979): Oxygen isotope equilibration systematics between quartz and water; Amer. Mineralogist, v. 64, pp. 232-240
- , Goldsmith, J.R., and Clayton, R.N. (1983a): On the mechanisms and kinetics of oxygen isotope exchange in quartz and feldspars at elevated temperatures and pressures; Geol. Soc. Amer. Bull., v. 94, pp. 396-412.
- Metz, P. and Trommsdorff, V. (1968): On phase equilibria in metamorphosed siliceous dolomites; Contrib. Mineral. Petrol., v. 18, pp. 305-309.
- Milne, V. G. (1972): Geology of the Kukatush-Sewell Lake Area, District of Sudbury; Ontario Div. Mines, GR 97. Accompanied by Maps 2230 and 2231, scale 1 inch to 1/2 mile.
- Moorbath, S. (1975): The geological significance of Early

- Precambrian rocks; Geol. Assoc. London, Proc., v. 86, pp. 259-274.
- Moore, J.G., Bachelder, J.N. and Cunningham, C.G. (1977): CO<sub>2</sub>-filled vesicles in mid-ocean basalt; Jour. Volcanol. Geotherm. Res., v. 2, pp. 309-327.
- Muehlenbachs, K. (1977): Oxygen isotope geochemistry of rocks from DSDP Leg 37, Canadian Jour. Earth Sci., v. 14, pp. 771-776.
- and Clayton, R.N. (1977): Oxygen isotope studies of fresh and weathered submarine basalts; Canadian Jour. Earth Sci., v. 9, pp. 172-176.
- Muir, T.L. (1979): Discrimination between extrusive and intrusive Archean ultramafic rocks in the Shaw Dome area using selected major and trace elements; Canadian Jour. Earth Sci., v. 16, pp. 80-90.
- Mysen, B.O. and Boettcher, A.L. (1975): Melting of a hydrous mantle: II Geochemistry of crystals and liquids formed by anatexis of mantle peridotite at high pressure and temperature as a function of controlled activities of water, hydrogen and CO<sub>2</sub>; Jour. Petrol., v. 16, pp. 549-593.
- McCrea, J.M. (1950): On the isotope chemistry of carbonates and a paleotemperature scale; Jour. Chem. Phys., v. 18, pp. 849-857.
- Newton, R.C., Smith, J.V. and Windley, B.F. (1980): Carbonic metamorphism, granulites and crustal growth; Nature, v. 288, pp. 45-50.
- Northrop, D.A. and Clayton, R.N. (1966): Oxygen-isotope fractionations in systems containing dolomite; Jour. Geology, v. 74, pp. 174-196.
- Nunes, P. D. and Pyke, D. R. (1980): Geochronology of the Abitibi Metavolcanic Belt, Timmins-Matachewan Area-Progress Report, pp34-39 in Summary of Geochronology Studies 1977-1979, ed. by E. G. Pye, Ontario Geological Survey, MP 92, 45p..
- O'Hara, M.J. and Yarwood, G. (1978): High pressure-temperature point on an Archean geotherm, implied magma genesis by crustal anatexis and consequences for garnet pyroxene thermometry and barometry; Phil. Trans. Royal Soc. London, v. A288, pp. 441-456.
- Ohmoto, H. (1972): Systematics of sulfur and carbon

- isotopes in hydrothermal ore deposits; Econ. Geol., v. 72, pp. 551-578.
- and Kerrick, D. (1977): Devolatilization equilibria in graphitic systems; Amer. Jour. Sci., v. 277, pp. 1013-1044.
- and Rye, R.O. (1979): Isotopes of sulphur and carbon; pp. 509-567 in Geochemistry of hydrothermal ore deposits, H.L. Barnes, ed., J. Wiley and Sons, New York, 798p.
- O'Neil, J.R., and Taylor, H.P., Jr. (1969): Oxygen isotope equilibrium between muscovite and water; Jour. of Geophys. Res., v. 74, pp. 6012-6022.
- , Clayton, R.N. and Mayeda, T.K. (1969): Oxygen isotope fractionation in divalent metal carbonates; Jour. Chem. Phys., v. 51, pp. 5547-5558.
- Paul, D.K., Crocket, J.H. and Nixon, P.H. (1977): Abundances of palladium, iridium and gold in kimberlites and associated nodules, pp. 272-279 in Kimberlites, Diatremes and Diamonds: Their Geology, Petrology and Geochemistry, ed. F.R. Boyd and H.O.A. Meyer, v. 1, Amer. Geophys. Union, 400 p.
- Phillips, G. N., Groves, D. I., and Martyn, J. E. (1984): An epigenetic origin for Archean banded iron-formation-hosted gold deposits; Econ. Geol., v. 79, pp. 162-171.
- Phinney, W.C. (1963): Phase equilibria in the metamorphic rocks of St. Paul Island and Cape North, Nova Scotia; Jour. Petrol., v. 4, pp. 90-130.
- Pineau, F., Javoy, M. and Bottinga, Y. (1976):  $^{13}\text{C}/^{12}\text{C}$  ratios of rocks and inclusions in popping rocks of the Mid-Atlantic Ridge and their bearing on the problem of isotopic composition of deep-seated carbon; Earth Planet. Sci. Lett., v. 29, pp. 413-
- , Behar, F., and Touret, J. (1981): La géochimie isotopique du faciès granulite du Bamble (Norvège) et l'origine des fluides carbonés dans la croûte profonde; Bull. Mineral., v. 104, pp. 630-641.
- Price, P. and Bray, R.C.E. (1948): Pamour Mine, pp. 558-565 in Structural Geology of Canadian Ore Deposits, CIM Jubilee Volume, 948p.
- Pyke, D.R. (1975): On the relationship of gold mineralization and ultramafic volcanic rocks in the

Timmins area; Ontario Div. Mines, MP62, 23p.

----- (1978a): Geology of the Redstone River area, District of Temiskaming. Ontario Div. Mines, GR 161, 75p. Accompanied by Maps 2362 and 2364, scale 1:31,680.

----- (1978b): Regional geology of the Timmins-Matachewan area, Districts of Cochrane and Timiskaming: pp. 73-77 in Summary of Field Work, 1978, by the Ontario Geological Survey, ed. by V. G. Milne, O. L. White, R. B. Barlow and J. A. Robertson, Ontario Geol. Survey, MP 82, 235p..

----- (1981): Relationship of gold mineralization to stratigraphy and structure in Timmins and surrounding area; pp. 1-15 in Genesis of Archean, Volcanic-Hosted Gold Deposits, Symposium held at University of Waterloo, March 7, 1980, Ontario Geological Survey, MP97, 175p.

----- (1982): Geology of the Timmins area, District of Cochrane; Ontario Geological Survey Report 219, 141p. Accompanied by Map 2455, Scale 1:50,000, 3 charts, and 1 sheet microfiche.

Roberts, R.G. (1981): The volcanic-tectonic setting of gold deposits in the Timmins area, Ontario; pp. 16-28 in Genesis of Archean, volcanic-hosted gold deposits, Symposium held at the University of Waterloo, March 7, 1980, Ontario Geological Survey, MP97, 175 p.

----- and Reading, D.J. (1981): The volcanic-tectonic setting of gold deposits in the Timmins district-carbonate-bearing rocks at Dome Mine; Grant 32, pp. 222-232 in Geoscience Research Grant Program, Summary of Research 1980-1981, ed. E.G. Pye, Ontario Geological Survey, MP98, 340 p.

----- and Spiteri, J.C. (1979): Volcanic-tectonic setting of gold deposits in the Timmins District; Grant 32, pp. 37-41 in Geoscience Research Grant Program, Summary of Research, 1978-1979, ed. E.G. Pye, Ontario Geological Survey, MP87, 152 p.

-----, Carnevali, J., and Harris, J.D. (1978): The volcanic-tectonic setting of gold-quartz vein systems in the Timmins District, Ontario; pp. 187-190 in Current Research, Part B; Geological Survey of Canada, Paper 78-1b.

Roedder, E. (1984): Fluid inclusion evidence on the environments of gold deposition; in Proc. Symp. Gold



- 82, Geol. Soc. Zimbabwe, Spec. Pub. 1, H.A. Balkema, Rotterdam, Netherlands.
- Rollinson, H.R. and Windley, B.F. (1980): Selective elemental depletion during metamorphism of Archean granulites, Scourie, N.W. Scotland; Contrib. Mineral. Petrol., v. 72, pp. 257-263.
- Rye, R.O., Schuiling, R.D., Rye, D.M., and Jansen, J.B.H. (1976): Carbon, hydrogen and oxygen isotope studies of the regional metamorphic complex at Naxos, Greece; Geochim. Cosmochim. Acta, v. 40, pp. 1031-1049.
- Safonov, Yu.G., Radhakrishna, B.P., Krishna Rao, B., Vasudev, V.N., Krishnam Raju, K., Nosik, L.P., and Pashkov, Y.N. (1980): Mineralogical and geochemical features of endogene gold and copper deposits of South India; Jour. Geol. Soc. India, v. 21, pp. 365-378.
- Sakai, H. (1968): Isotopic properties of sulfur compounds in nature; Geochim. Cosmochim. Acta, v. 32, pp. 150-169.
- Satterly, J. and Armstrong, H.S. (1947): Geology of Beatty Township; Ontario Dept. Mines, v. 56, part 7, 34p.
- Scarfe, C.M. and Smith, D.G.W. (1977): Secondary minerals in some basaltic rocks from DSDP Leg 37; Canadian Jour. Earth Sci., v. 14, pp. 903-910.
- Schidlowski, M., Eichmann, R. and Junge, C.E. (1975): Precambrian sedimentary carbonates: C + O isotope geochemistry and implications for the terrestrial oxygen budget; Precambrian Res., v. 2, pp. 1-69.
- , Appel, P.W.U., Eichmann, R., and Junge, C.E. (1979): Carbon isotope geochemistry of the 3.7 x 10<sup>9</sup> yr-old Isua sediments, West Greenland: implications for the Archean carbon and oxygen cycles; Geochim. Cosmochim. Acta, v. 43, pp. 189-199.
- Schuiling, R.D. and Kreulen, R. (1979): Are thermal domes heated by CO<sub>2</sub>-rich fluids from the mantle? Earth. Planet. Sci. Lett., v. 43, pp. 198-302.
- and Vink, B.W. (1967): Stability relations of some titanium-minerals (sphene, perovskite, rutile, anatase); Geochim. Cosmochim. Acta, v. 31, pp. 2399-2411.
- Schwarcz, H.P. (1969): The stable isotopes of carbon, pp. 6-B-1 to 6-B-16 in Handbook of Geochemistry, ed. K.H.

Wedepohl, Springer-Verlag, New York.

- , Clayton, R.N., and Mayeda, T. (1970): Oxygen isotopic studies of calcareous and pelitic metamorphic rocks, New England; Geological Survey of America Bull., v. 81, pp. 2299-2316.
- Seward, T.M. (1973): Thio complexes of gold and the transport of gold in hydrothermal ore solutions; Geochim. Cosmochim. Acta, v. 37, pp. 379-399.
- (1979): Modern hydrothermal systems in New Zealand and their relation to gold mineralization processes; pp. 56-64 in Gold Mineralization, J.E. Glover and D.I. Groves, ed., Geology Department and Extension Service of the University of Western Australia, Pub. #3, 106p.
- Sharma, T. and Clayton, R.N. (1965): Measurement of  $O^{18}/O^{16}$  ratios of total oxygen of carbonates; Geochim. Cosmochim. Acta, v. 29, pp. 1347-1354.
- Sheppard, S.M.F. (1977): Identification of the origin of ore-forming solutions by the use of stable isotopes, pp. 25-41 in Geol. Soc. London, Special Publ. #7, 188p.
- and Dawson, J.B. (1973):  $^{13}C/^{12}C$  and D/H isotope variations in "primary" igneous carbonates; Fortschr. Mineral., v. 50, pp. 128-129.
- and Schwarcz, H.P. (1970): Fractionation of carbon and oxygen isotopes and magnesium between coexisting metamorphic calcite and dolomite; Contrib. Mineral. Petrol., v. 26, pp. 161-198.
- , Nielsen, R.L. and Taylor, H.P. Jr. (1969): Oxygen and hydrogen isotope ratios of clay minerals from porphyry copper deposits; Econ. Geol., v. 64, pp. 755-777.
- Sheraton, J.W., Skinner, A.C., and Tarney, J. (1973): The geochemistry of the Scourian gneisses of the Assynt district, pp. 13-30 in The Early Precambrian Rocks of Scotland and Related Rocks of Greenland, ed. R.G. Park and J. Tarney, Univ. Keele, 200 p.
- Shieh, Y.N. and Taylor, H.P. (1969): Oxygen and carbon isotope studies of contact metamorphism of carbonate rocks; Jour. Petrol., v. 10, pp. 307-331.
- Sighinolfi, G.P. (1971): Investigations into deep crustal

- levels: Fractionating effects and geochemical trends related to high-grade metamorphism; *Geochim. Cosmochim. Acta*, v. 35, pp. 1005-1021.
- and Santos, A.M. (1976): Geochemistry of gold in Archean granulite facies terrains; *Chem. Geol.*, v. 17, pp. 113-123.
- Smith, T.J. and Kesler, S.E. (1985): Relation of fluid inclusion geochemistry to wallrock alteration and lithogeochemical zonation at the Hollinger-McIntyre gold deposit, Timmins, Ontario, Canada; *Canadian Inst. Min. Met. Bull.*, v. 78, pp. 35-46.
- Smith, T.J., Cloke, P.L. and Kesler, S.E. (1984): Geochemistry of fluid inclusions from the McIntyre-Hollinger gold deposit, Timmins, Ontario, Canada; *Econ. Geol.*, v. 79, pp. 1265-1285.
- Spooner, E.T.C. and Fyfe, W.S. (1973): Sub-sea floor metamorphism, heat and mass transfer; *Contrib. Mineral. Petrol.*, v. 42, pp. 287-304.
- Springer, J.S. (1983): Invisible gold; pp. 240-250 in *The Geology of Gold in Ontario*, ed. A.C. Colvine, Ontario Geol. Surv., MP110, 278p.
- Takenouchi, S. and Kennedy, G.C. (1964): The binary system  $H_2O-CO_2$  at high temperatures and pressures; *Amer. Jour. Sci.*, v. 262, pp. 1055-1074.
- Takenouchi, S. and Kennedy, G.C. (1965): The solubility of carbon dioxide in NaCl solutions at high temperatures and pressures; *Amer. Jour. Sci.*, v. 263, pp. 445-454.
- Tarney, J. and Windley, B.F. (1977): Chemistry, thermal gradients and evolution of the lower continental crust; *Jour. Geol. Soc. London*, v. 134, pp. 153-172.
- , Skinner, A.C. and Sheraton, J.W. (1972): A geochemical comparison of major Archean gneiss units from Northwest Scotland and East Greenland, pp. 162-174 in *Sect. 1, 24th Int. Geol. Congr. Montreal*, 379 p.
- Taylor, B.E. (1981): Hydrothermal fluids in the Motherlode gold deposits of California; pp 1059 In *Abstracts, EOS*, v. 62, number 45.
- Taylor, H.P. (1968): The oxygen isotope geochemistry of igneous rocks; *Contrib. Mineral. Petrol.*, v. 19, pp. 1-71.

- and Coleman, R.G. (1968):  $^{18}\text{O}/^{16}\text{O}$  ratios of coexisting minerals in glaucophane-bearing metamorphic rocks; Geol. Soc. Amer. Bull., v. 79, pp. 1727-1756.
- , Albee, A.L. and Epstein, S. (1963):  $^{18}\text{O}/^{16}\text{O}$  ratios of coexisting minerals in three assemblages of kyanite-zone pelitic schists; Jour. Geol., v. 71, pp. 513-522.
- Thayer, T. (1966): Serpentinization considered as a constant volume metasomatic process; Amer. Mineral, v. 51, pp. 685-710.
- Thomson, J.E. (1941): Geology of McGarry and McVittie Townships, Larder Lake Area; Ontario Department of Mines, v. 50, pt. 7, pp. 1-99. Accompanied by Maps 50a,b scale 1 inch to 1000 feet; 50d, scale 1 inch to 400 feet.
- Thompson, A.B. (1971):  $\text{PCO}_2$  in low-grade metamorphism: zeolite, carbonate, clay mineral, prehnite relations in the system  $\text{CaO-Al}_2\text{O}_3\text{-SiO}_2\text{-CO}_2\text{-H}_2\text{O}$ ; Contrib. Mineral. Petrol., v. 33, pp. 145-161.
- Todheide, K. and Franck, E.V. (1963): Das zweiphasengebiet und die kritische kurve im kohlendioxid-wasser bis zu drucken von 3500 bar; Z. Phys. Chem. N.F., v. 37, pp. 387-401 (Not read).
- Touret, J. (1971a): Le facies granulite en Norvege Meridionale; 1. Les associations mineralogiques; Lithos, v. 4, pp. 239-249.
- (1971b): Le facies granulite en Norvege Meridionale; 2. Les inclusions fluides; Lithos, v. 4, pp. 423-436.
- (1977): The significance of fluid inclusions in metamorphic rocks, pp. 203-227 in Thermodynamics in Geology, ed. D.G. Fraser, Dordrecht-Holland, D. Reindell Publishing Co.
- Truesdell, A.H. (1974): Oxygen isotope activities and concentrations in aqueous salt solutions at elevated temperatures - Consequences for isotope geochemistry; Earth Planet. Sci. Lett., v. 23, pp. 387-396.
- Urey, H.C. (1947): The thermodynamic properties of isotopic substances; Jour. Chem. Soc., pp. 562-581.

- Veizer, J. and Hoefs, J. (1976): The nature of  $^{18}\text{O}/^{16}\text{O}$  and  $^{13}\text{C}/^{12}\text{C}$  secular trends in sedimentary carbonate rocks; *Geochim. Cosmochim. Acta*, v. 40, pp. 1387-1395.
- Walsh, J.F., Haynes, F.M., and Kesler, S.E. (1984): Fluid inclusion analyses of auriferous vein quartz from the Porcupine District, Ontario; in Program with Abstracts, GAC/MAC, London, May 14-16, 1984.
- Wendlandt, R.F. and Harrison, W.J. (1978): Phase equilibria and rare earth element partitioning between coexisting immiscible carbonate and silicate liquids and  $\text{CO}_2$  vapour in the system  $\text{K}_2\text{O}-\text{Al}_2\text{O}_3-\text{SiO}_2-\text{CO}_2$ ; *Carnegie Inst. Wash. Year Book* 77, Annual Report 1977-1978, pp 695-703.
- Wenner, D.B., and Taylor, H.P., Jr. (1971): Temperatures of serpentinization of ultramafic rocks based on  $^{18}\text{O}/^{16}\text{O}$  fractionation between coexisting serpentine and magnetite; *Contrib. Mineral. Petrol.*, v. 32, pp. 165-185.
- Wells, P.R.A. (1979): Chemical and thermal evolution of Archean Sialic crust, Southern West Greenland; *Jour. Petrol.*, v. 20, pp. 187-226.
- Whitehead, R.E.S., Cameron, R.A., and Davies, J.F. (1979): The relation of gold deposits to concentrations of  $\text{CO}_2$  in volcanic rocks; Grant 30, pp. 108-116, in *Geoscience Research Grant Program, Summary of Research, 1978-1979*, ed. E.G. Pye, OGS, MP87, 152p.
- Willars, J.G. (1982): Report on Gowganda Resources Inc. Carshaw Gold Property, Timmins area, Ontario; unpublished company report, 12p.
- Wilson, A.F. (1964): The petrological features and structural setting of Australian granulites and charnockites; *Int. Geol. Cong.*, v. 22 (13), pp. 21-44.
- Wood, P.C., Thomas, I.V., Burrows, D.R., Macdonald, A.J., Noble, S.R. and Spooner, E.T.C. (1984):  $\text{CO}_2$ -bearing low-moderate salinity fluids in Archean gold-quartz-carbonate- (W-Mo) vein deposits and magmatically derived Mo, W, Ta, and Sn mineralization; G.S.A. abs. with Program, Reno, November 4-7, 1984.
- Woodall, R. (1979): Gold - Australia and the world, pp. 1-34 in *Gold Mineralization*, ed. J.E. Glover and D.I. Groves, Geology Department and Extension Service of the University of Western Australia, Publ. #3, 106p.

- Yonge, C.J. (1982): Stable isotope studies of water extracted from speleothems; Unpubl. Ph.D. Thesis, McMaster University, 298p.
- York, D. (1969): Least squares fitting of a straight line with correlated errors; Earth Planet. Sci. Lett., v. 5, pp 320-324.
- York, D., Masliwec, A., McMaster, N. S., and Kuybida, P. (1985): Dating of Ontario's gold deposits, pp.4 in Geoscience Research Seminar and Open House '85, December 4-5, 1985, Abstracts, Ontario Geological Survey, 20p.

Appendix-1  
Geochemical Data Base And Some  
Property Maps

- Part A: List of field maps on micro-fiche.
- Part B: List of field maps which accompany the  
geochemical data base in Part C.
- Part C: Key to abbreviations used in the geochemical  
data base, contained on micro-fiche.
- Part D: Geochemical data base and accompanying  
field maps, contained on micro-fiche.

Part A: List Of Maps Which Appear On  
Micro-fiche.

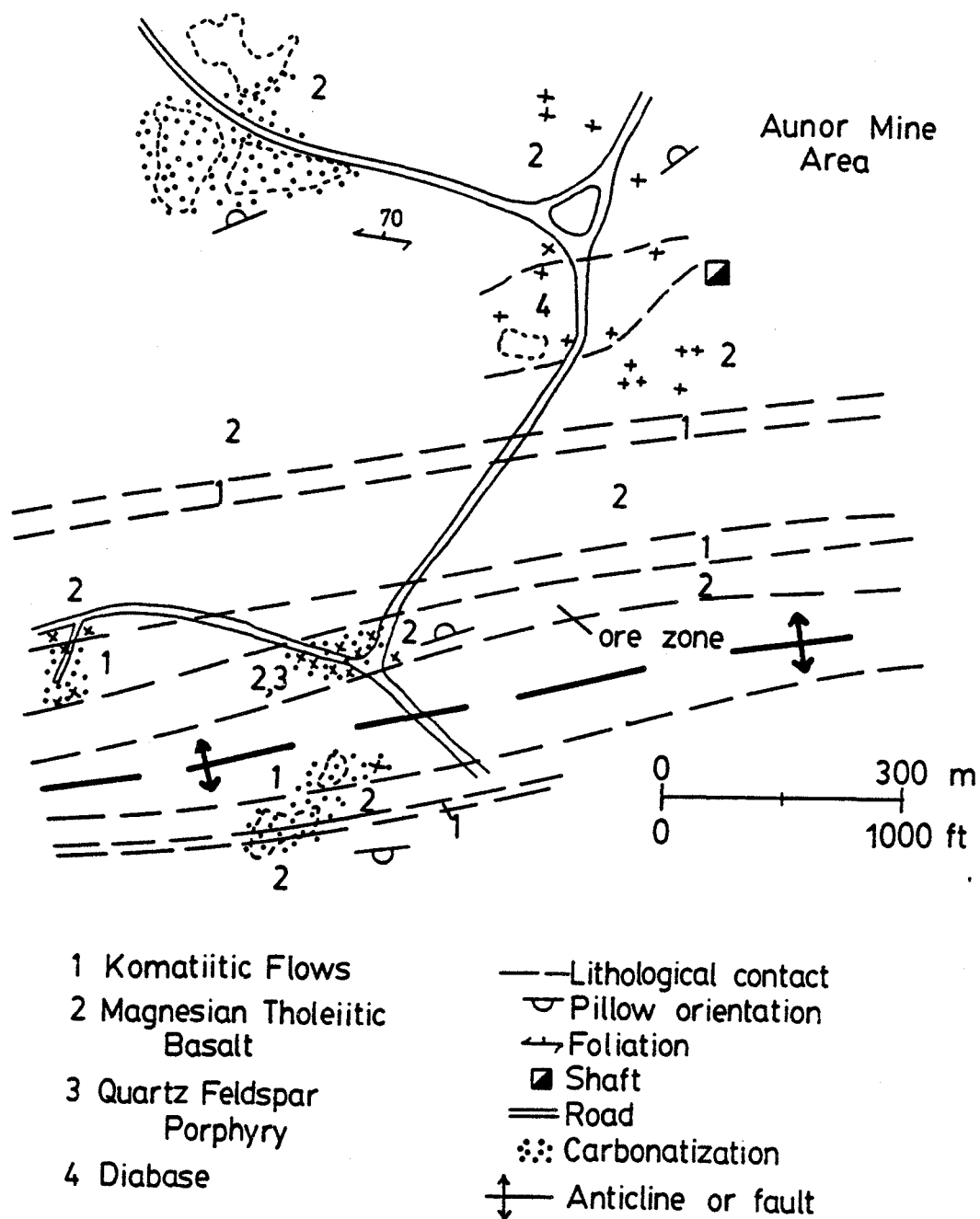
Map No. Property/Area

- 3. Beaumont
- 5. Buffalo Ankerite
- 7. Canusa
- 9a. Carshaw
- 9b. Malga
- 10a. Davidson-Tisdale
- 12. Armstrong-McGibbon/Crown Chartered
- 13. Delnite
- 14. Dobell
- 21. Northern Whitney Township
- 24. Kinch
- 25b. McEnaney, detail trench area
- 27. Russel
- 28. Stewart Abate
- 30. Tisdale Township, Northeast Area
- 31. Whitney Township, Northwest area
- 32. Whitney Township, Northeast area
- 33. Deloro Township, Northwest area



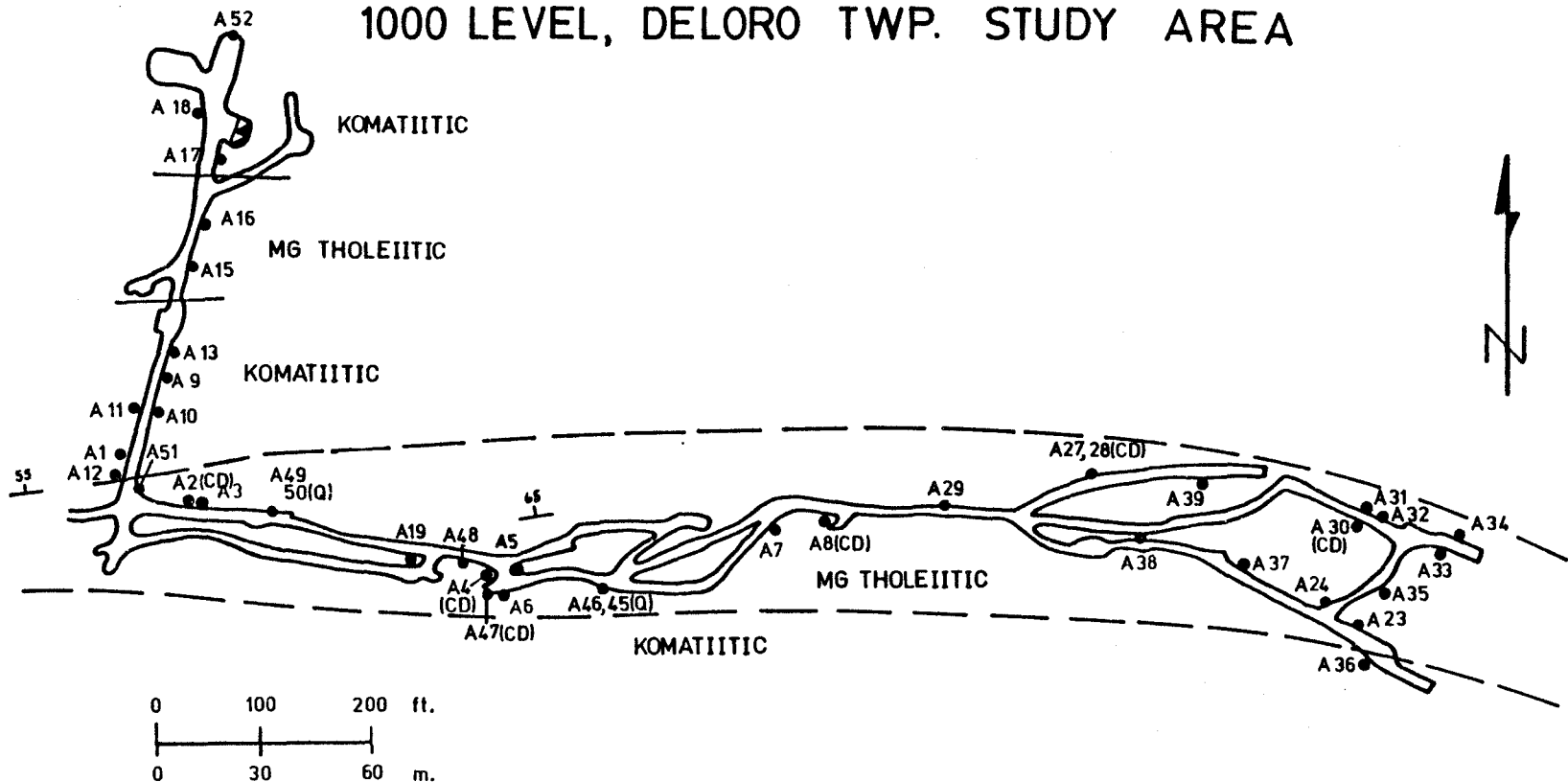
Part B: List Of Field Maps Which Appear With The  
Geochemical Data, on micro-fiche.

| Map Property/Area<br>No.                                        | File              |
|-----------------------------------------------------------------|-------------------|
| 1. Aunor Surface                                                | Aunor             |
| 2. Aunor, 1000 foot level                                       | Aunor             |
| 4. Broulan Reef                                                 | Broulan Reef      |
| 6. Buffalo Ankerite, northwest                                  | Buffalo Ankerite  |
| 8. Canusa                                                       | Canusa            |
| 10. Davidson-Tisdale,<br>Armstrong-McGibbon,<br>Crown Chartered | Davidson-Tisdale  |
| 11. Davidson-Tisdale glory hole                                 | Davidson-Tisdale  |
| 15. Duval area                                                  | Duval             |
| 16. Duval glory hole                                            | Duval             |
| 17. Duval south vein                                            | Duval             |
| 18. Faymar                                                      | Faymar            |
| 19. Hugh Pam                                                    | Hugh Pam          |
| 22. North Whitney                                               | North Whitney     |
| 23. Hollinger                                                   | Hollinger         |
| 26. Porcupine Triumph                                           | Porcupine Triumph |
| 25. McEnaney                                                    | McEnaney          |



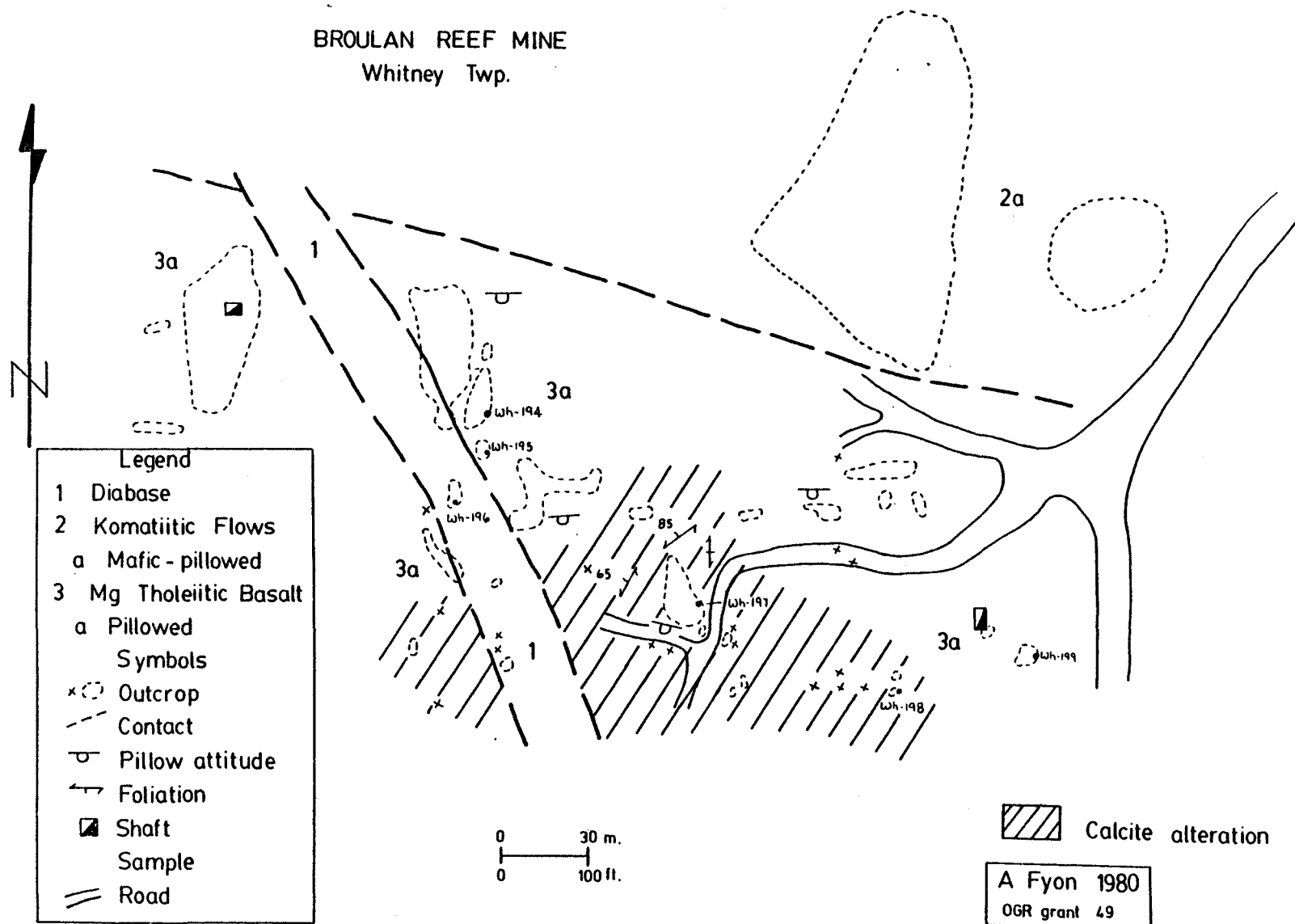
MAP 1: Aunor Mine area, surface geological plan.

# GEOLOGICAL PLAN OF AUNOR MINE, 1000 LEVEL, DELORO TWP. STUDY AREA

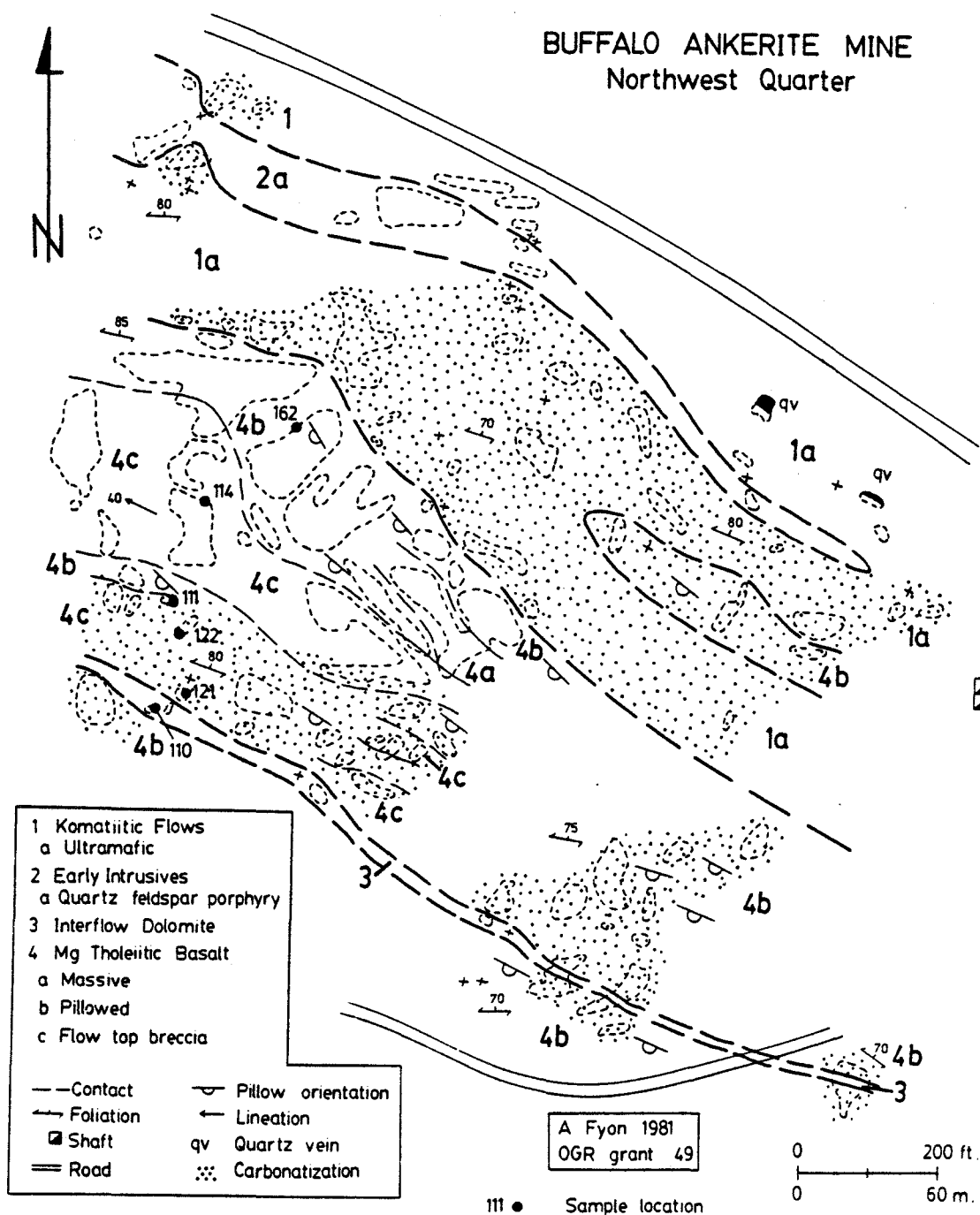


MAP 2: Aunor Mine, 1000 foot level, simplified geology

BROULAN REEF MINE  
Whitney Twp.

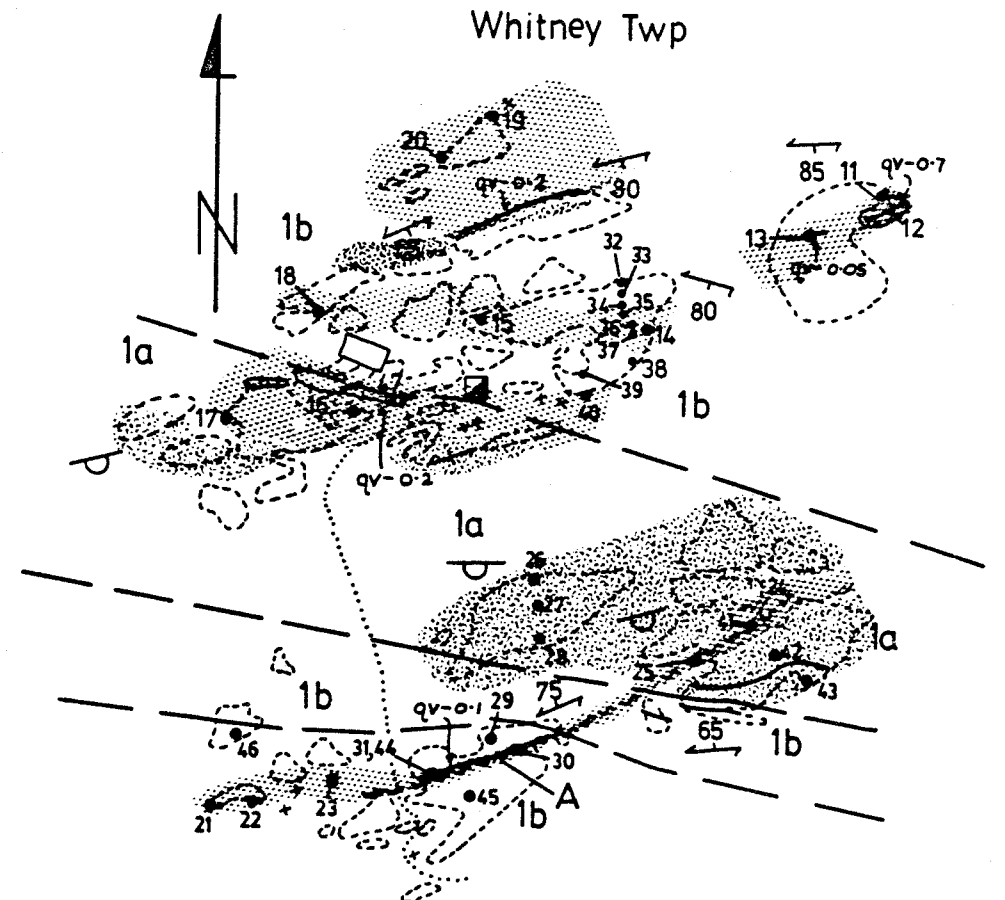


MAP 4: Broulan Reef Mine, surface geological plan



Map 6: Detailed geology of the northwest quarter of the Buffalo Ankerite Mine property, Deloro Township.

# CANUSA MINE Whitney Twp



## LEGEND - SYMBOLS

1 Magnesium Tholeiitic Basalt

a Pillowed

b Massive

○ × Outcrop

--- Contact

~~~~~ Shear

→ Foliation

⊖ Pillow top

⊖ Pit

■ Shaft

⤴ Dump

□ Building

qv--2 Quartz vein-width(m)

..... Road

Can-1 • Sample

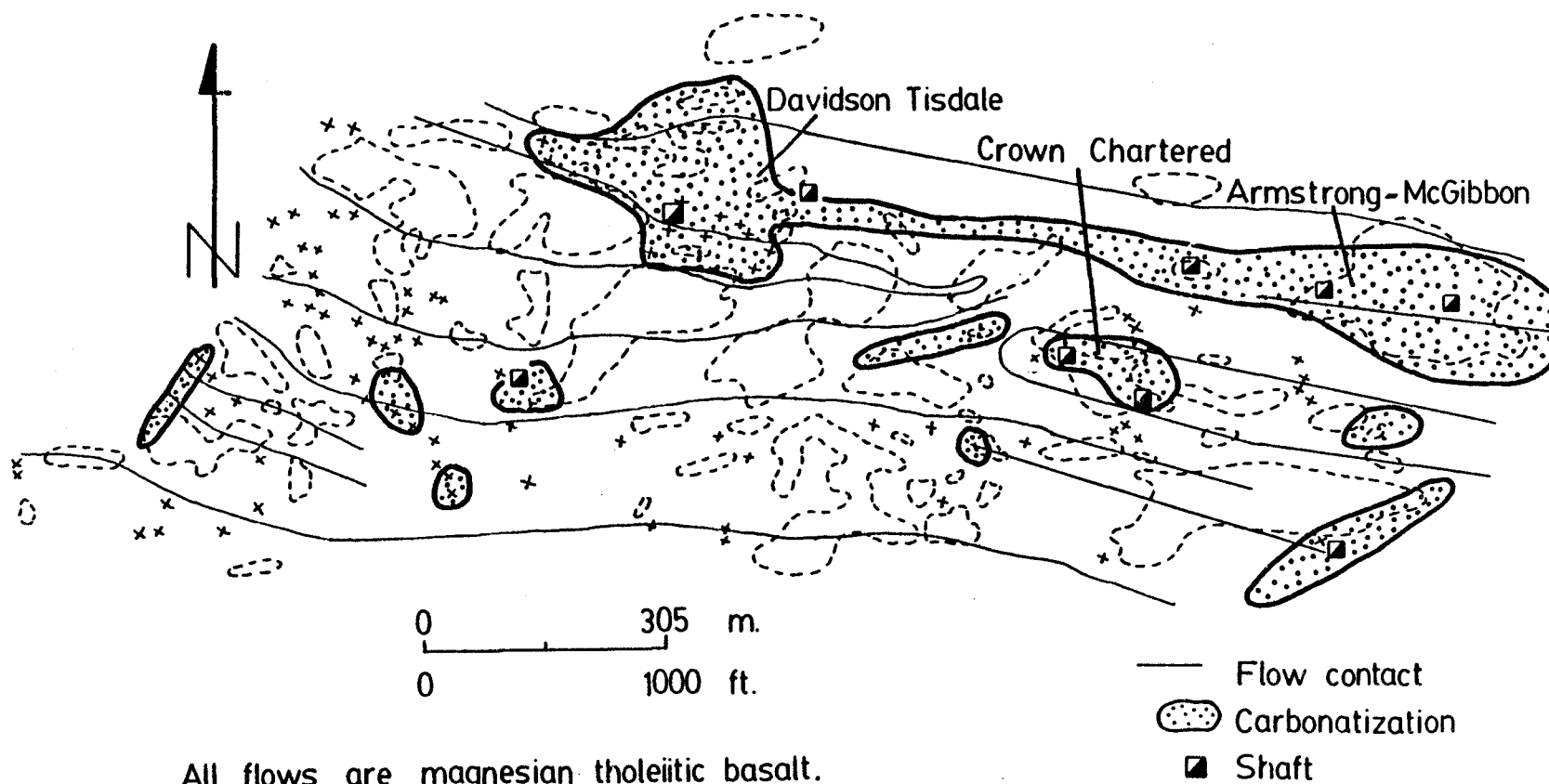
Carbonatization

▨ Dolomite zone

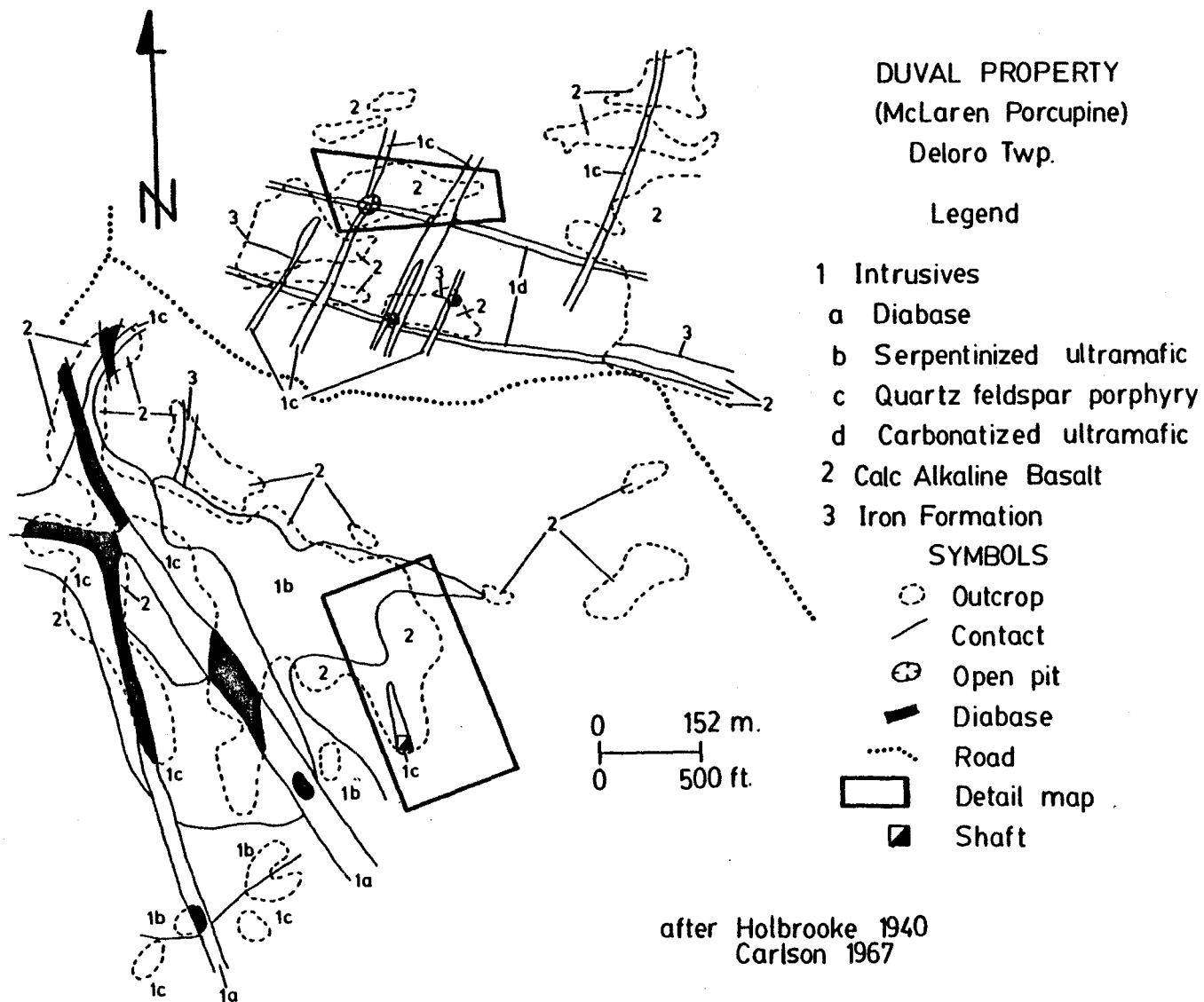
▨ Calcite zone

Geology: A Fyon-1977
OGS project 76-37

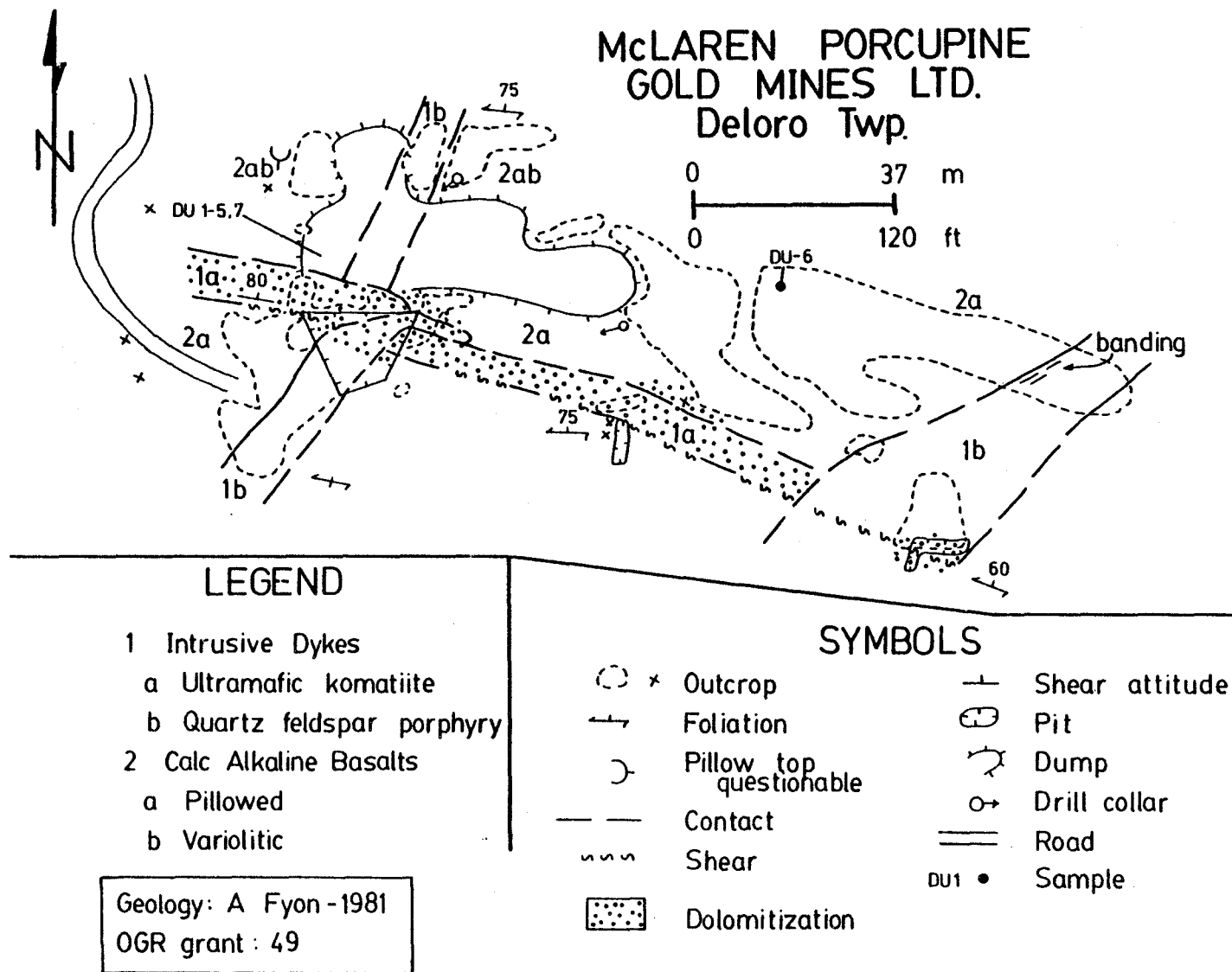
MAP 8: Canusa Mine, surface geology of glory hole area.
Zone A is a carbonatized shear zone.



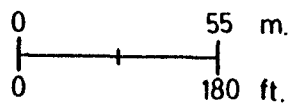
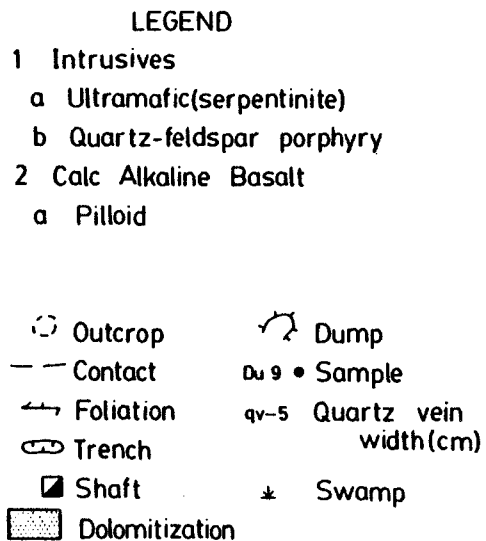
MAP 10: Simplified surface geology of the Davidson-Tisdale, Armstrong-McGibbon and Crown Chartered Properties, Tisdale Township.



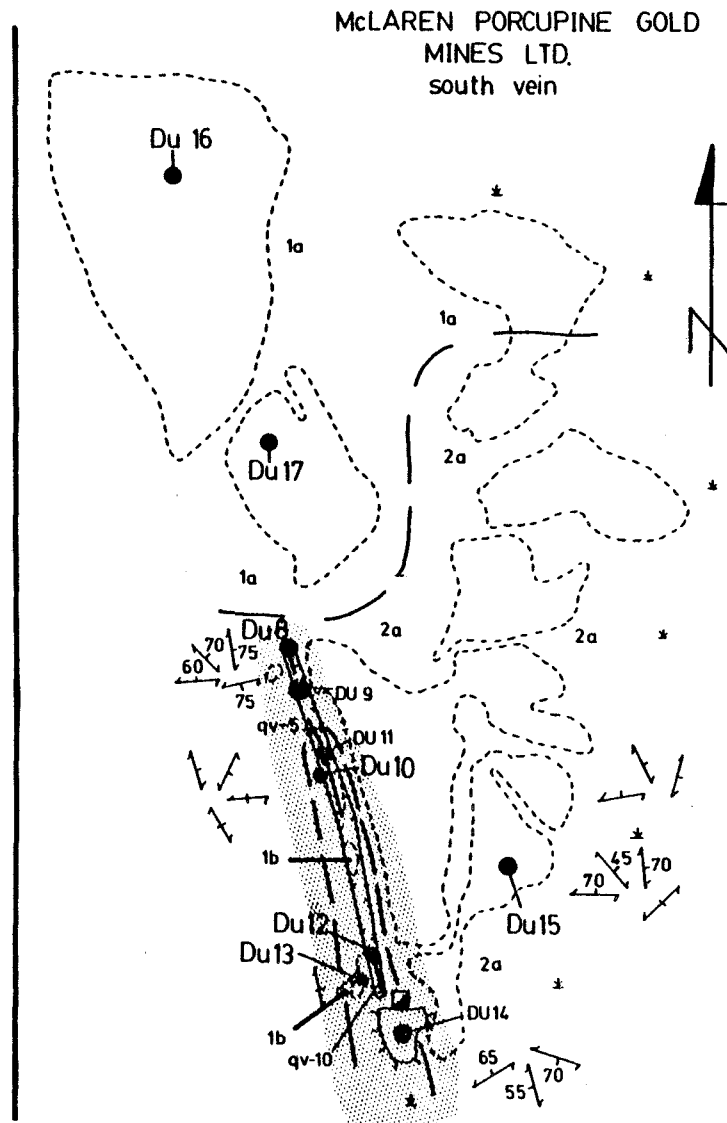
MAP 15: Duval property, generalized surface geology.



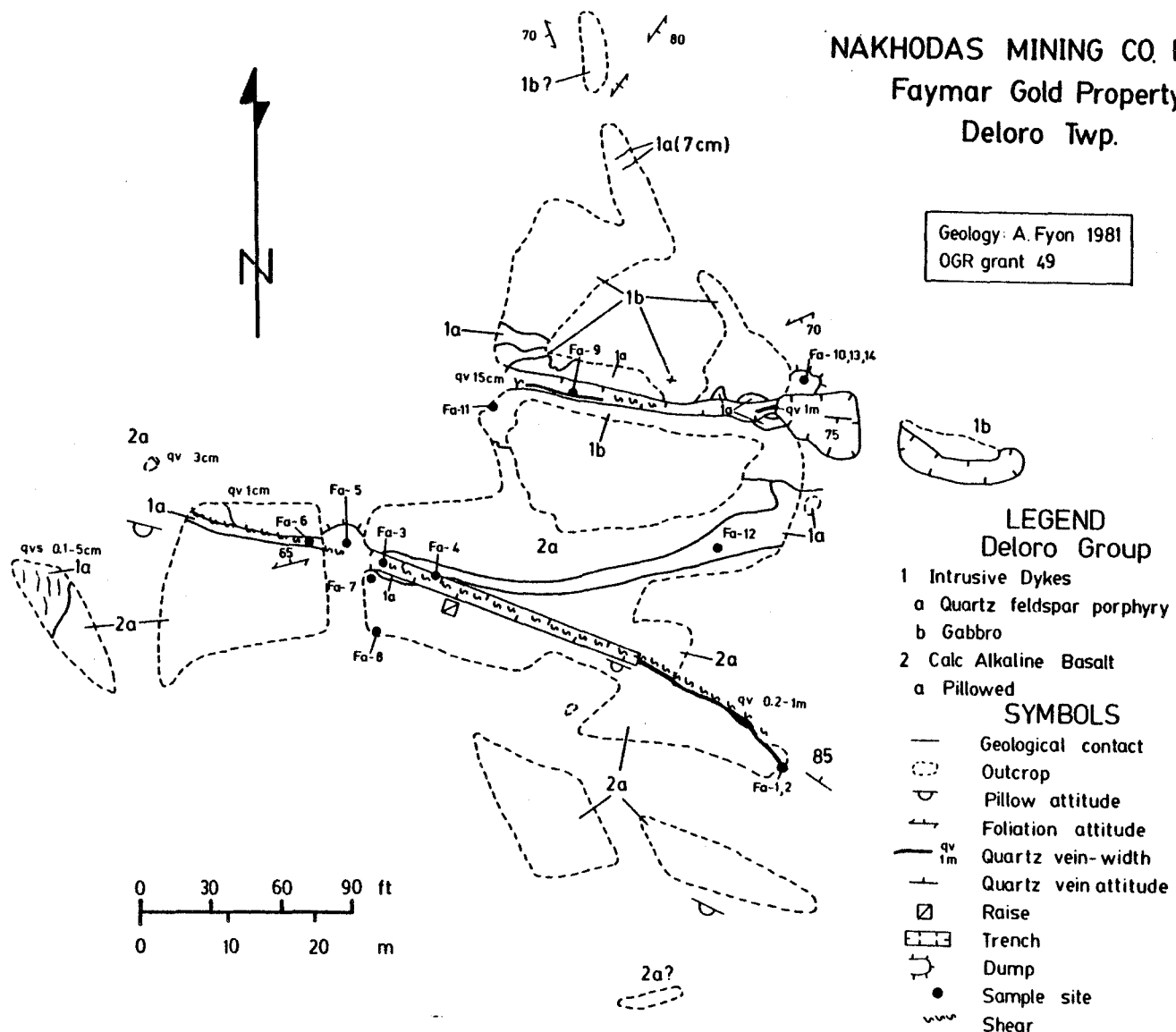
MAP 16: Duval property, glory hole area surface geology.



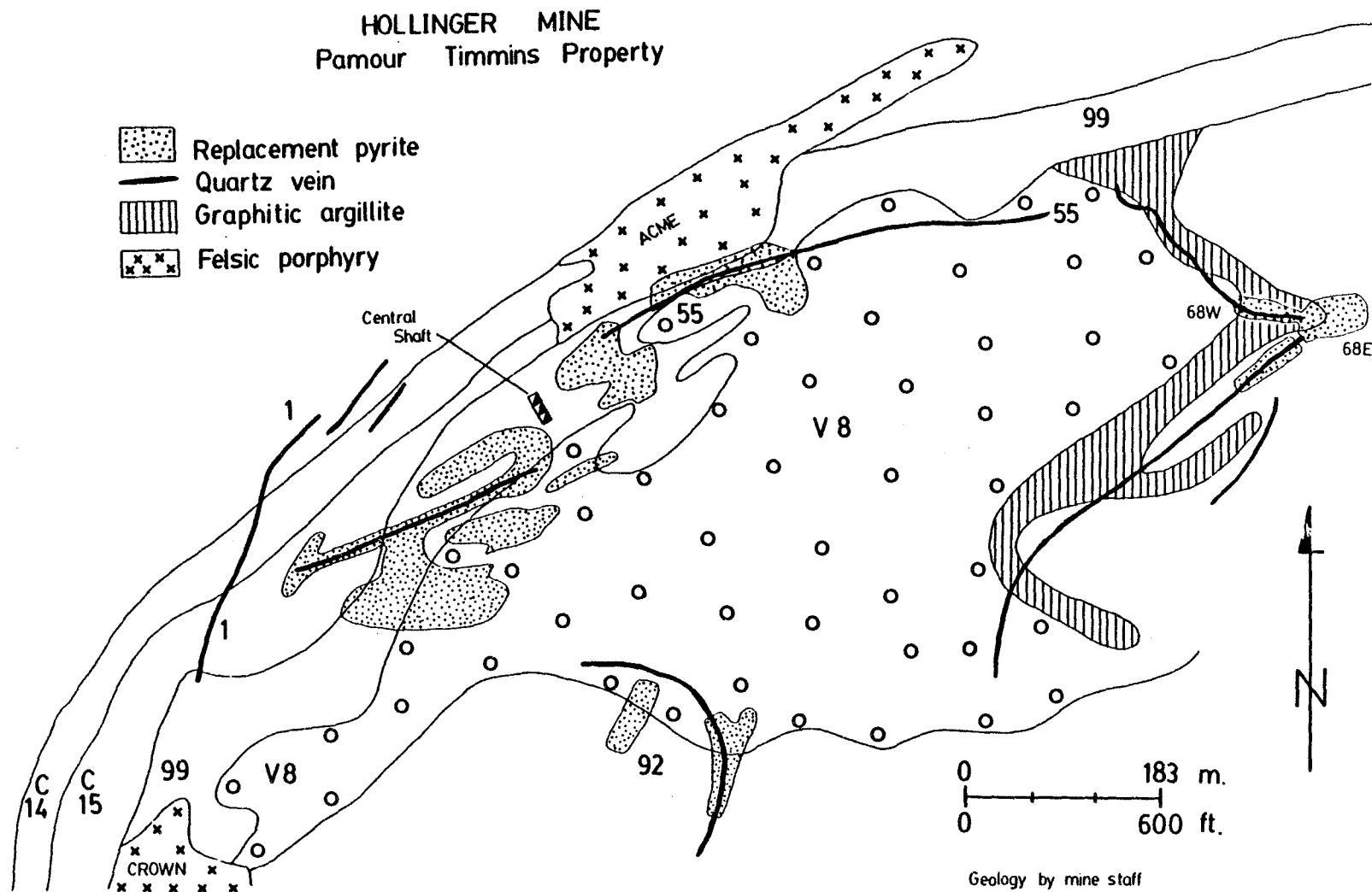
Geology: A. Fyon 1981
 OGR grant: 49



MAP 17: Duval property, south vein showing surface geology.

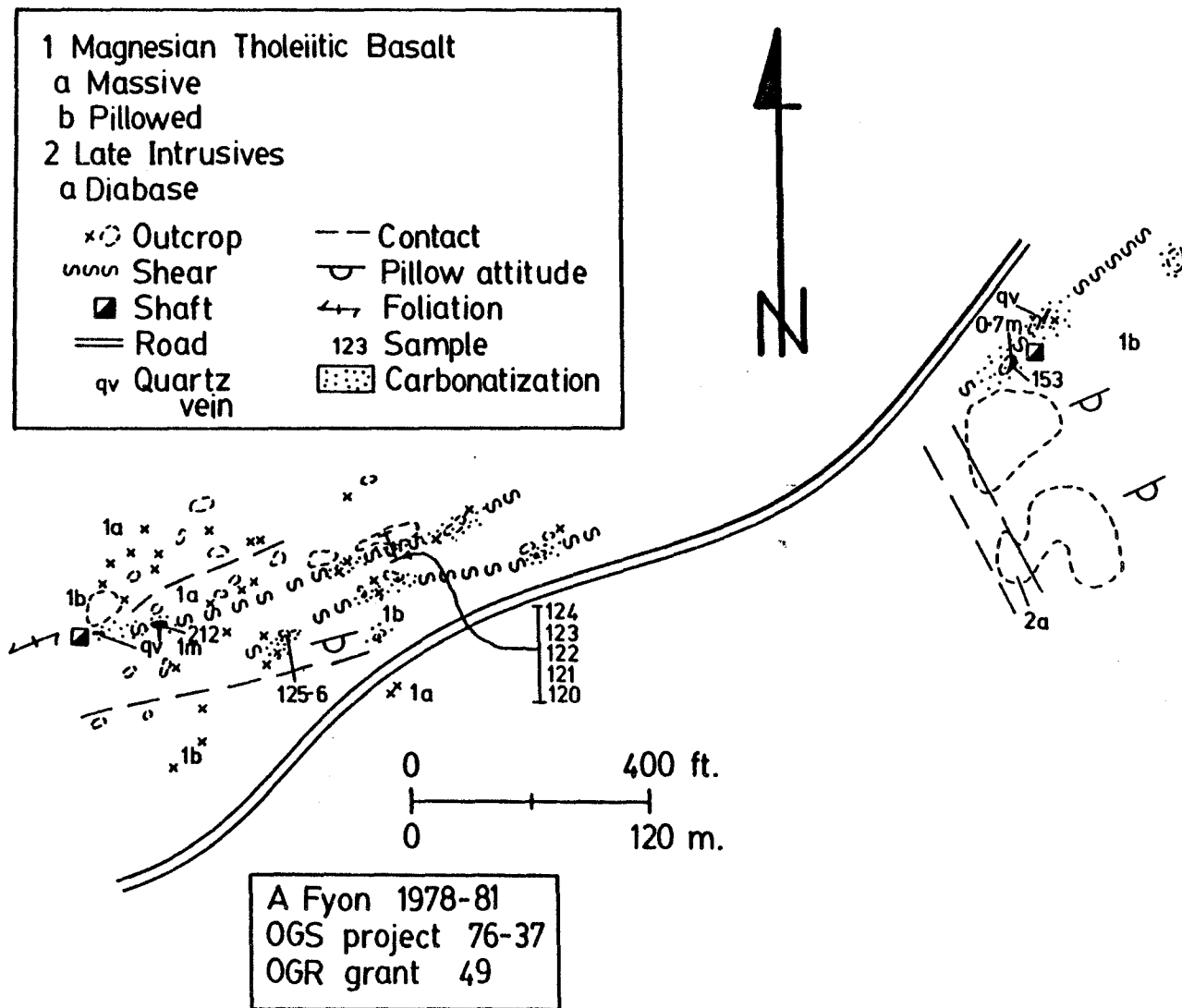


MAP 18: Faymar Mine, surface geology of the crown pillar area.

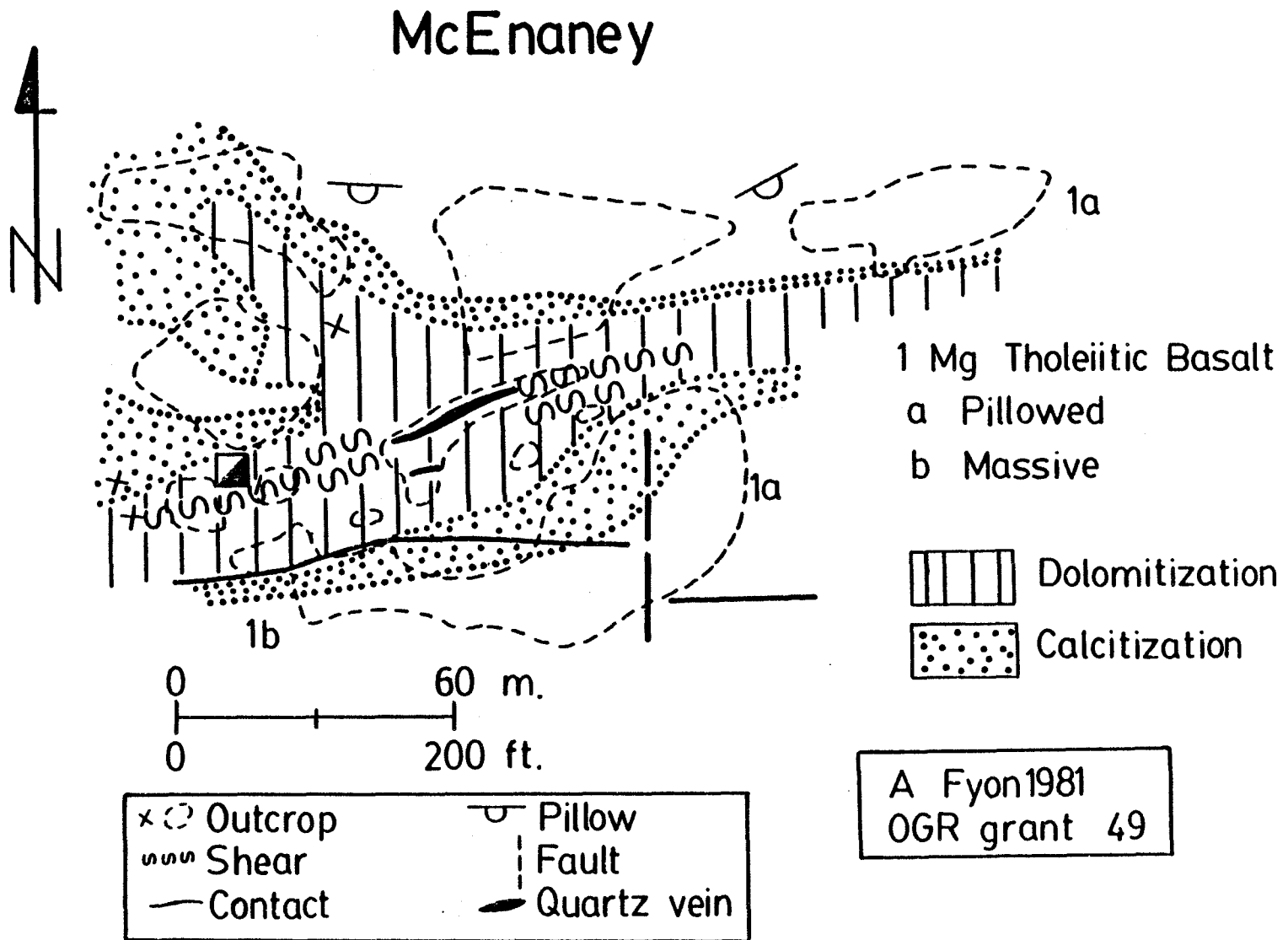


Map 23:
Simplified surface geology of the former Hollinger Mine, Tisdale Township,
Prepared by the Mine Staff.

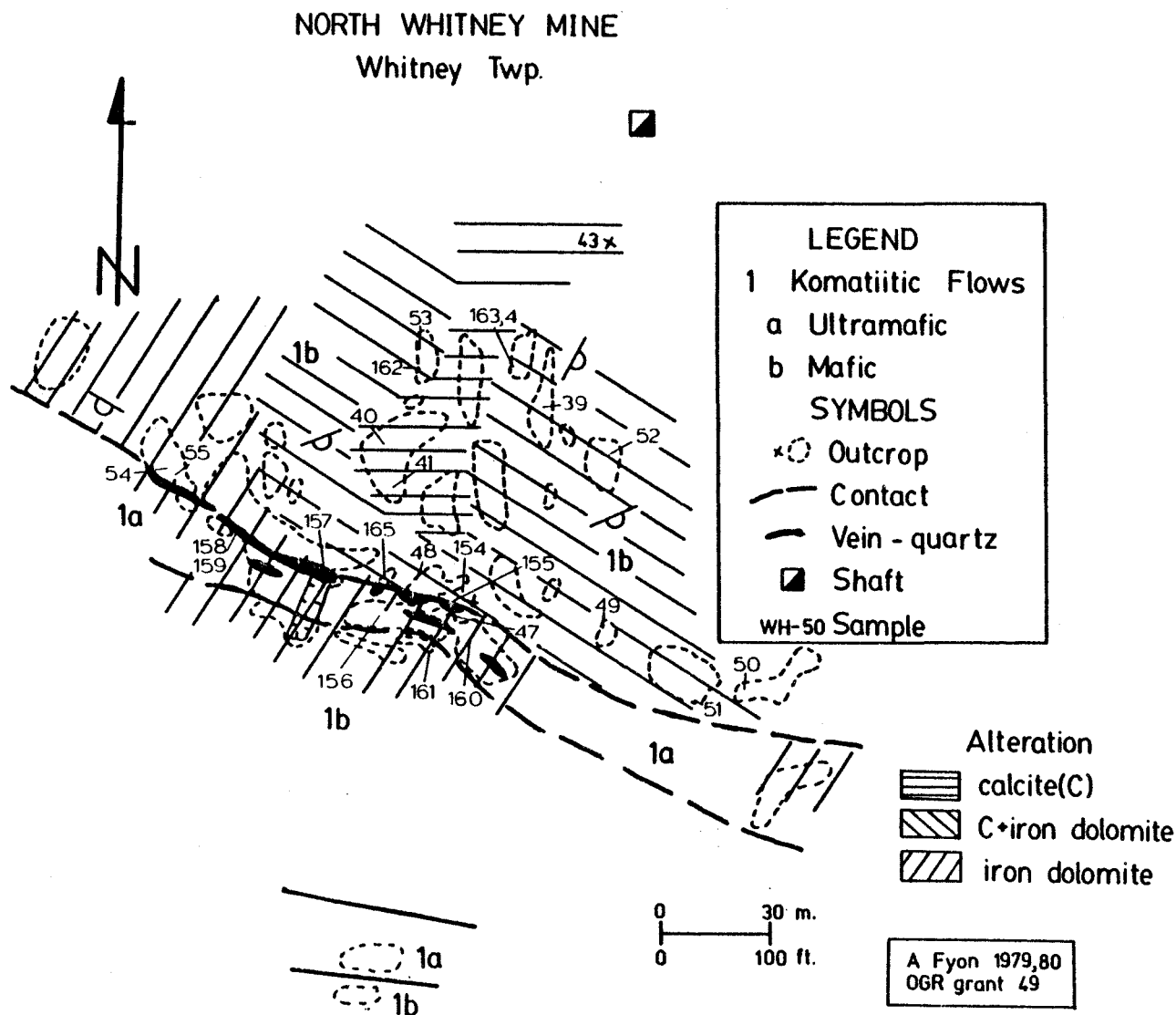
HUGH PAM PROPERTY



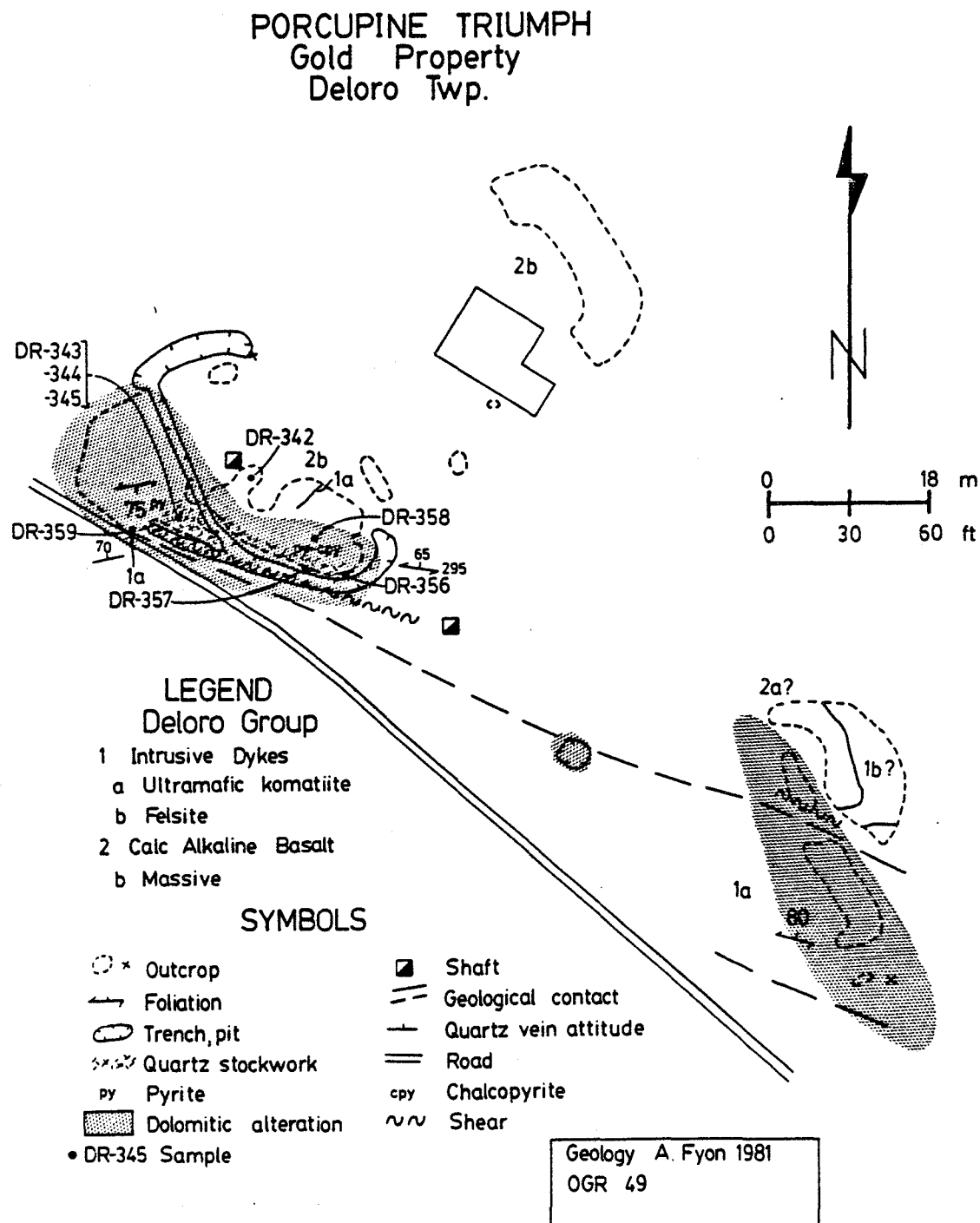
Map 19: Generalized surface geology of the Hugh Pam Property, Whitney Township.



Map25: Surface Geology of the McEnaney property, Ogden Township.



Map 22: Surface geology of the North Whitney property, Whitney Township.



Map 26: Surface geology of the Porcupine Triumph property, Deloro Township.

STEWART ABATE GOLD PROPERTY

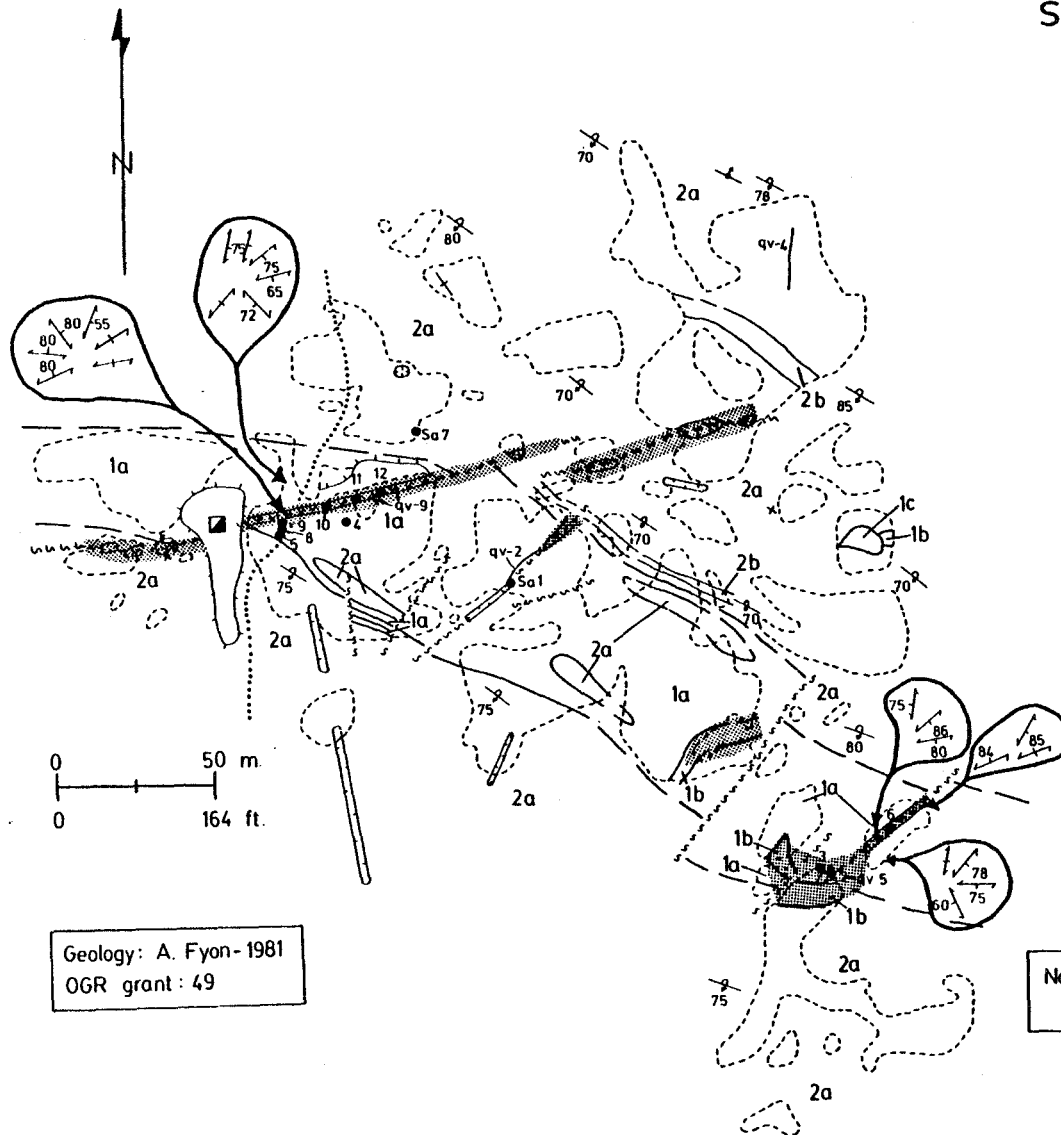
Beatty Twp.

LEGEND

1. Intrusive Dykes
 - a Gabbro
 - b Syenite
 - c Lamprophyre
2. Turbidite Metasediments
 - a Greywacke-siltstone
 - b Sericite schist

SYMBOLS

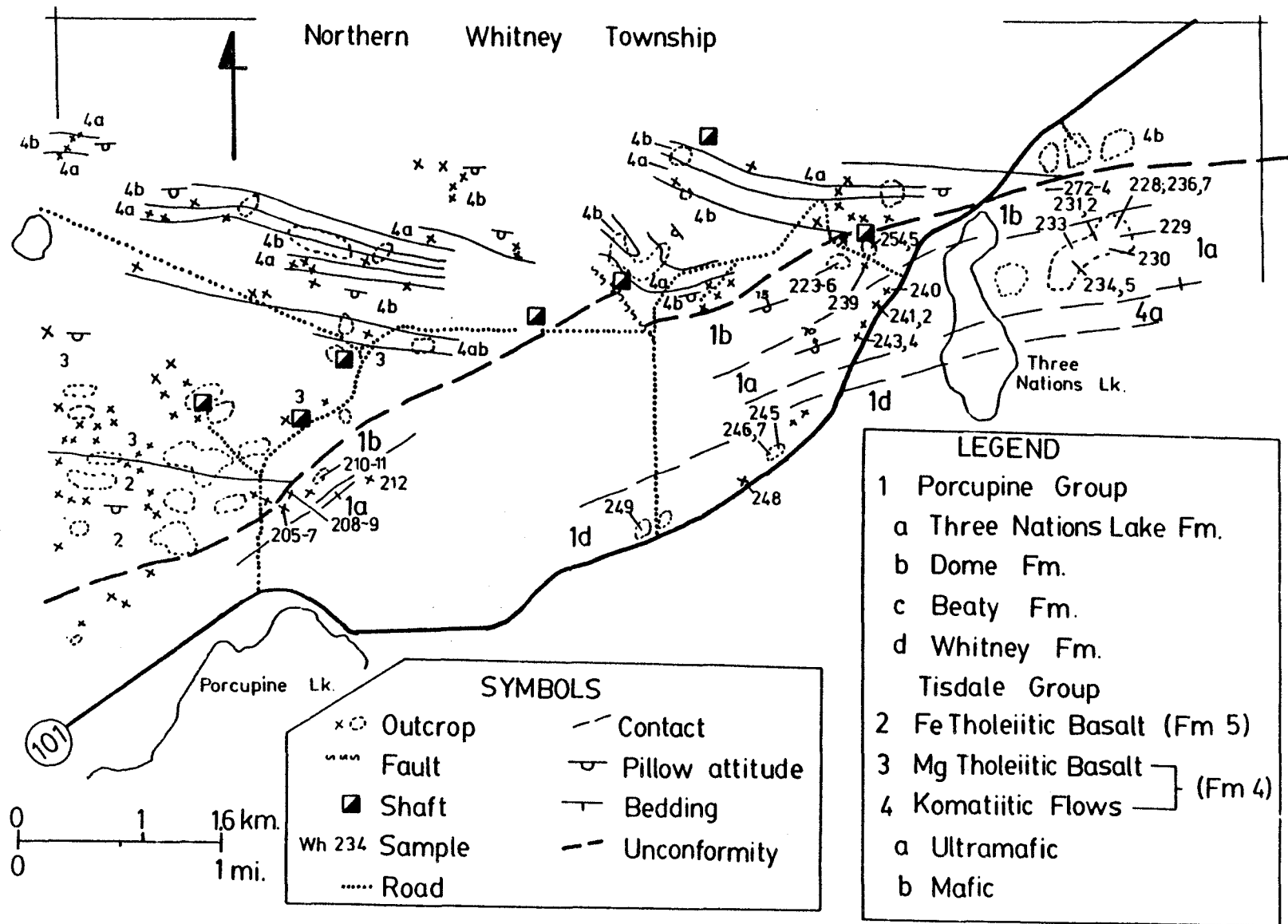
- x Outcrop
- Geological contact
- + Bedding attitude, overturned
- + Graded bedding
- + Foliation attitude
- Fault
- Trench-pit
- Shaft
- ⌵ Dump
- Road
- ▨ Dolomite carbonate alteration
- qv-5 Quartz vein-width(cm)
- Sa-1 • Sample



Geology: A. Fyon-1981
OGR grant : 49

Note: Carbonate is present in virtually
metasedimentary outcrops

Map 28: Detailed geology of the shaft area, Stewart Abate property.



Map 21: Simplified geology of northern Whitney Township.

APPENDIX-2

Textural Relationships Between and Paragenesis Of Carbonate and Silicate Phases In Quartz Veins

A2.1. Introduction

Quartz veins from the following properties (number of thin sections) have been studied: Aunor, 1000 level (1); Canusa (3); Carshaw (4); Dobell (2); Hollinger (6); Hugh Pam (2); Porcupine Triumph (1); Faymar (5). Admittedly, from such a small base a definitive statement regarding textural relationships cannot be made; however, certain general paragenetic relationships are recognized. The consistency of these relationships, both within and between deposits, is perhaps the best measure of their uniformity and credibility. A brief textural description follows for each vein system or deposit.

A2.1.1 Aunor, 1000 level

This sample (A-33) was collected from the eastern extent of the workings. Quartz demonstrates variable grain size from 1 centimetre (cm.) to 0.05 millimetres (mm.). The large grains have sutured grain boundaries and undulatory extinction. Many fluid inclusion trains define healed fractures. The small quartz grains appear to constitute crushed domains of quartz, which are now largely strain free and polygonalized. The distribution of the fine grained quartz domains on the thin section scale is irregular. Dolomite occurs as small grains (0.1 mm.) and veinlets which cut, raft and resorb quartz fragments. Generally dolomite is restricted to crushed quartz grain arrays. Tourmaline

cross cuts and replaces quartz and dolomite. This tourmaline generally occurs as euhedral crystals (0.1 mm.) and is restricted to the crushed quartz array. Traces of chlorite appear to resorb dolomite, but the temporal relationship between the chlorite and tourmaline is uncertain because the two phases do not touch.

A2.1.2. Canusa

Three separate veins were studied from the Canusa property: Can-44, quartz-dolomite vein in the south shear zone; Can-47, glory hole quartz vein; Can-49, quartz vein in west showing. Only granular quartz was observed in the glory hole sample. In Can-44, south shear zone, coarse grained quartz (1-2 cm.) having undulatory extinction, is replaced and cut by dolomite. Similar textural relationships between quartz and dolomite are developed in Can-49. In addition, traces of white mica lie along the same quartz grain boundaries where dolomite occurs. However, the dolomite and mica do not touch and hence their temporal relationship is uncertain.

A2.1.3. Carshaw

Quartz veins cutting the iron formation and the basaltic country rock generally show the same textural relationships. Quartz occurs as large (1-2 cm.) anhedral to euhedral grains which are cross cut and resorbed by

dolomite. All quartz shows strained extinction and sutured grain boundaries. Where found, chlorite either replaces quartz or fills vugs and coats euhedral quartz crystals. No chlorite and dolomite were observed in the same section and hence, their temporal relationship is uncertain.

A2.1.4 Dobell

Two quartz veins were examined from the Dobell property. Both veins contain only traces of dolomite and white mica. Both replace and cross cut quartz. Dolomite and mica were not observed in contact, although both occupied the fracture system. Hence the temporal relationship between mica and dolomite is uncertain.

A2.1.5. Hollinger

The following quartz vein systems from the Hollinger surface were examined: 68 East Zone; west end of 400 pit; #1 vein; 65E vein and 55 vein system. The following general paragenetic succession is recognized. When present albite is embayed or replaced by quartz. Pyrite tends to be resorbed when hosted in quartz which suggests a pre-quartz formation age of pyrite. The temporal relationship between pyrite and albite is unknown. Dolomite always replaces albite, quartz and pyrite. White mica, either sericite or talc, also replaces albite and quartz, but its relationship with dolomite is unclear. In general, domains rich with

white mica are devoid of dolomite, suggesting the mica has replaced dolomite. Minor amounts of scheelite are present in the #1 and 68E vein zones. This scheelite is intimately associated spatially with the white mica and hence is possibly late in the paragenetic sequence.

Gold occurs as inclusions in pyrite as does chalcopyrite and galena. The paragenetic position of these minor phases is uncertain, although it is suggested that all may have been roughly contemporaneous.

A2.1.6. Hugh Pam

Samples taken from both the west and east shaft areas were examined. A variety of laminated quartz is seen to consist of very small (0.05 mm.), polygonalized quartz which probably represents crushed zones. Mixed in, and subparallel to the micro-grain array, are domains of larger (1-2 cm.) quartz showing undulatory extinction and sutured grain boundaries. Both tourmaline and dolomite are restricted to the crushed quartz zone and occur as veinlets. Dolomite replaces quartz, whereas tourmaline resorbs both dolomite and quartz.

A2.1.7. Porcupine Triumph

Veins of quartz, dolomite and chlorite are hosted in a pyritized, locally sheared carbonatized basalt. Chlorite replaces both quartz and dolomite. This chlorite occurs as

mats of micro-booklets (0.2 mm.). Dolomite resorbs quartz, suggesting quartz was the earliest phase. Quartz is coarse (1 cm.), shows undulatory extinction and has sutured boundaries against an adjacent quartz grain. Many fluid inclusion trains are contained in the quartz, implying healed fractures.

A2.1.8. Faymar

Unlike the previously described veins, calcite is the accessory carbonate in the quartz veins. This calcite appears to fill vugs and to occupy fractures which cross cut euhedral quartz grains. The quartz displays euhedral terminations in vugs and is coarse grained (1 cm.), or quartz can exist as fine grained (0.1 mm.) polygonalized arrays which probably developed by crushing or shearing of the vein. In the crushed quartz zones, pyrite exhibits cataclastic textures and white mica occurs as veinlet masses which resorb quartz. Chlorite always occurs as fibro-radial mats of micro-booklets (0.1 mm.) and replaces quartz and calcite.

Pyrite (1-5 mm.) is generally anhedral, even in unsheared domains, and is enclosed by quartz. This pyrite contains inclusions of gold and chalcopyrite which average 0.05 millimetre. Chalcopyrite also occurs as discrete, anhedral grains (0.5 mm.) which cut, raft and resorb quartz suggesting a post quartz introduction age.

APPENDIX-3

Sample preparation, analytical techniques and
model calculations for oxygen and carbon
isotopic measurements

A3.1. Preparation of Quartz Vein Material

From the quartz veins, the following minerals were analyzed isotopically; quartz, dolomite, calcite, and chlorite. All minerals were hand picked from single handsamples in which the minerals occurred within several centimetres of each other. Ideally, mutually adjacent minerals should be sampled, but in these vein systems, it is rarely possible to find three different minerals in mutual contact. Because of the relatively coarse grain size of quartz, such material free from other mineral impurities, could be acquired. The chlorite sampled occurred as clots in vugs or as coarse aggregates in the quartz; hence, pure chlorite specimens also could be hand picked from the veins. Most carbonate samples contained an admixture of quartz; however, because of the carbonate isotope preparation method, the presence of quartz presented no problem as it does not react with phosphoric acid. All minerals were ground to -200 mesh in preparation for the isotopic analysis.

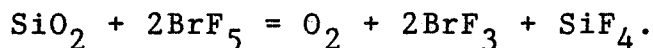
A3.2. Preparation of Rock Samples for Carbonate Analysis

To measure the carbon and oxygen isotope composition of the replacement carbonates in altered igneous rock, whole rock samples were crushed to -200 mesh. No mineral separation was attempted because the intensely carbonatized samples consist essentially of quartz and carbonate (plus albite if rock is basaltic) with traces of white mica and

chlorite. Sample weight varied depending on the degree of carbonatization; however, sufficient rock sample was reacted to yield approximately 0.02 mole CO_2 (approximately 0.03 gram if pure CaCO_3 is used).

A3.3. Silicate Fluorination

The silicate samples were reacted with BrF_5 in nickel tubes at approximately 600°C to produce oxygen and waste gases:



The oxygen diffuses through liquid nitrogen traps and is converted to CO_2 by reaction with a carbon rod at approximately 550°C (carbon rod is orange-red colour). Approximately 20 mg of silicate material was reacted. The procedure followed is that outlined by Longstaffe (1974) which was modified after Clayton and Mayeda (1963). The resultant CO_2 gas was then analysed mass spectrometrically using a Micromas 602 C.

A3.3.1. Conversion of Raw δ -Results to SMOW

Listed in table A3-1 are symbols used for this derivation. The conversion outlined is basically that used by Gascoyne (1979) and Schwarcz (1971). The conversion is treated as a three part process:

- 1) to correct isotopic analyses for machine characteristics

Table A3-1: Symbols used to convert raw δ -value to SMOW.

$$R_X^{18} = (^{18}\text{O} / ^{16}\text{O})_X$$

$$R_{\text{SMOW}}^{18} = (^{18}\text{O} / ^{16}\text{O})_{\text{SMOW}} \quad (\text{total oxygen})$$

$$\delta_{\text{SMOW}}^{18}(\text{X}) = [(R_X^{18} / R_{\text{SMOW}}^{18}) - 1](1000)$$

GCS-CO₂ = CO₂ liberated from GCS calcite by reaction with 100% phosphoric acid at 25°C.

GCS-ΣO = Total oxygen from GCS calcite as determined by fluorination.

SMOW-ΣO = Total oxygen from SMOW as determined by fluorination.

The acid fractionation factor for calcite is:

$$\frac{R_{\text{GCS-CO}_2}}{R_{\text{GCS-O}}} = 1.01025\% \quad (\text{Sharma and Clayton, 1965})$$

$$\delta_{\text{PDB}}^{18}(\text{X}) = [(R_X^{18} / R_{\text{PDB}}^{18}) - 1] 10^3 \quad ; \text{X may be GCS, NBS-20}$$

Now, the $\delta^{18}\text{O}$ -value of CO₂ produced by reaction of PDB calcite with 100% phosphoric acid at 25°C is +0.22 per mil relative to CO₂ equilibrated with SMOW water (Friedman and O'Neil, 1977). That is:

$$\frac{R_{\text{PDB-CO}_2}}{R_{\text{CO}_2\text{-SMOW}}} = 1.00022$$

Now;

$$R_{\text{CO}_2\text{-SMOW}} = 1.0412 \quad (\text{Friedman and O'Neil, 1977})$$

$$\delta_{\text{GCS-CO}_2}^{18\text{O}(\text{NBS-20})} = 7.66\% \quad (\text{Gascoyne, 1979})$$

$$\delta_{\text{PDB-CO}_2}^{18\text{O}(\text{NBS-20})} = -4.18\% \quad (\text{Blattner and Hulston, 1978})$$

$$\delta^{13}\text{C}_{\text{GCS-CO}_2}(\text{NBS-20}) = -1.747\text{‰} \text{ (Gascoyne, 1979)}$$

$$\delta^{13}\text{C}_{\text{PDB-CO}_2}(\text{NBS-20}) = -1.06\text{‰} \text{ (Blattner and Huiston, 1978)}$$

the difference between sequential correction values ($\delta^{18}\text{O}$

and $\delta^{13}\text{C}$) is less than 0.001‰.

and isotope abundances and so obtain $\delta^{18}\text{O}_{\text{NBS-GCS}}$ and $\delta^{13}\text{C}_{\text{NBS-GCS}}$;

- 2) to use these values and known relationships of NBS-20 to PDB to determine $\delta^{18}\text{O}_{\text{NBS-GCS}}$ and $\delta^{13}\text{C}_{\text{NBS-GCS}}$;
- 3) to correct raw sample δ -values for machine characteristics and isotope abundances, as in 1) above and then to use the relevant $\delta_{\text{GCS-PDB}}$ relationships to determine $\delta^{18}_{\text{X-PDB}}$, $\delta^{18}\text{O}_{\text{X-SMOW}}$ and $\delta^{13}\text{C}_{\text{PDB}}$, where X = sample.

A3.3.1.1. Oxygen

A3.3.1.1.1. Tail correction

No correction for value mixing and tail contribution is required for the micromass 602D (M.Knyf, pers. comm., 1980).

A3.3.1.1.2. Correction for contribution of ^{17}O , ^{13}C etc.

Correction for the contribution of isobaric species such as C^{17}O_2 , $^{13}\text{C}^{16}\text{O}^{17}\text{O}$, etc. was carried out using relationships derived by Craig (1957):

$$\delta^{18}\text{O}(\text{X}) = (1.0014)(\delta^{46}) + (0.0091)[\delta^{13}(\text{X})]$$

$$\delta^{13}\text{C}(\text{X}) = (1.0677)(\delta^{45}) - (0.0338)[\delta^{18}(\text{X})]$$

As outlined by Gascoyne (1979), these equations are solved by successive approximation, initially substituting δ^{46} for δ^{18} and δ^{45} for δ^{13} . The approximation is iterated until

the difference between sequential correction values ($\delta^{18}\text{O}$ and $\delta^{13}\text{C}$) is less than 0.001 per mil.

A3.3.1.1.3. Conversion of data to SMOW-total oxygen

The mass spectrometric operating standard is GCS. Its $\delta^{18}\text{O}$ -value with respect to NBS-20 ($\delta_{\text{GCS-NBS-20}}$) is calculated from the known $\delta^{18}\text{O}$ -value of NBS-20 (7.66‰; Gascoyne, 1979) using the following conversion:

$$\delta_{\text{A-B}} = [\delta_{\text{B-A}} (1000)] / [(1000) + (\delta_{\text{B-A}})]$$

Therefore:

$$\delta^{18}\text{O}_{\text{NBS-20-CO}_2}(\text{GCS}) = \frac{-(7.66)(1000)}{(1000) + 7.66} = -7.602 \text{‰}.$$

Now:

$$\delta^{18}\text{O}_{\text{PDB-CO}_2}(\text{NBS-20}) = -4.18 \text{‰} (\text{Blattner and Hulstron, 1978}).$$

Since:

$$\delta_{\text{A-C}} = \delta_{\text{A-B}} + \delta_{\text{B-C}} + (\delta_{\text{A-B}})(\delta_{\text{B-C}})(10^{-3})$$

where, A = GCS, B = NBS-20, C = PDB.

Therefore:

$$\begin{aligned} \delta^{18}\text{O}_{\text{PDB}}(\text{GCS}) &= -7.602 + (-4.18) + (-7.602)(-4.18)(10^{-3}) \\ &= -11.75 \text{‰} . \end{aligned}$$

That is:

$$\frac{R_{\text{GCS-CO}_2}}{R_{\text{PDB-CO}_2}} = 0.98832$$

Now:

$$\begin{aligned} \frac{R_{\text{GCS-}\Sigma\text{O}}}{R_{\text{SMOW-}\Sigma\text{O}}} &= \frac{R_{\text{GCS-}\Sigma\text{O}}}{R_{\text{GCS-CO}_2}} \cdot \frac{R_{\text{GCS-CO}_2}}{R_{\text{SMOW-}\Sigma\text{O}}} \\ &= \frac{1}{1.01025} \cdot \frac{R_{\text{GCS-CO}_2}}{R_{\text{SMOW-}\Sigma\text{O}}} \end{aligned}$$

$$\begin{aligned}
&= (0.98985) \cdot \frac{R_{\text{GCS-CO}_2}}{R_{\text{PDB-CO}_2}} \cdot \frac{R_{\text{PDB-CO}_2}}{R_{\text{SMOW-O}}} \\
&= (0.98985) \cdot \frac{R_{\text{GCS-CO}_2}}{R_{\text{PDB-CO}_2}} \cdot \frac{R_{\text{PDB-CO}_2}}{R_{\text{CO}_2\text{-SMOW}}} \cdot \frac{R_{\text{CO}_2\text{SMOW}}}{R_{\text{SMOW-O}}} \\
&= (0.98985)(0.98832)(1.00022)(1.0412) \\
&= 1.01882
\end{aligned}$$

Now:

$$\begin{aligned}
\delta^{18}\text{O}_{\text{SMOW-}\Sigma\text{O}}(\text{X}) &= \frac{R_{\text{X}} - 1}{R_{\text{SMOW}}} (1000) \\
1 + [10^3 \delta^{18}\text{O}(\text{X})] &= \frac{R_{\text{X}}}{R_{\text{SMOW-}\Sigma\text{O}}} \\
&= \frac{R_{\text{X}}}{R_{\text{GCS-CO}_2}} \cdot \frac{R_{\text{GCS-CO}_2}}{R_{\text{GCS-}\Sigma\text{O}}} \cdot \frac{R_{\text{GCS-}\Sigma\text{O}}}{R_{\text{SMOW-}\Sigma\text{O}}} \\
&= \frac{R_{\text{X}}}{R_{\text{GCS-CO}_2}} \cdot (1.01025)(1.01882) \\
&= [1 + (10^3) \delta^{18}\text{O}_{\text{GCS-CO}_2}(\text{X})] (1.02926) \\
&= 1.02926 + (1.02926)(10^3) \delta^{18}\text{O}_{\text{GCS-CO}_2}(\text{X}) \\
(10^3) \delta^{18}\text{O}_{\text{SMOW-}\Sigma\text{O}}(\text{X}) &= 0.02926 + (1.02926)(10^3) (\delta^{18}\text{O}_{\text{GCS-CO}_2}(\text{X})) \\
\delta^{18}\text{O}_{\text{SMOW-}\Sigma\text{O}}(\text{X}) &= 29.26 + (1.02926) [\delta^{18}\text{O}_{\text{GCS-CO}_2}(\text{X})]
\end{aligned}$$

A3.2.2.1.1 Carbon

A similar approach is followed to express raw carbon δ -values with respect to the PDB calcite standard. To

determine the $\delta^{13}\text{C}_{\text{GCS-PDB}}$ values:

$$\delta^{13}\text{C}_{\text{GCS-CO}_2}(\text{NBS-20}) = -1.747\text{‰}(\text{Gascoyne, 1979})$$

and

$$\delta_{\text{A-B}} = \frac{\delta_{\text{B-A}} \cdot (1000)}{(1000) + \delta_{\text{B-A}}}$$

Therefore:

$$\delta^{13}\text{C}_{\text{GCS-NBS-20}} = 1.750\text{‰}$$

Now, since:

$$\delta_{\text{A-C}} = \delta_{\text{A-B}} + \delta_{\text{B-C}} + (\delta_{\text{A-B}})(\delta_{\text{B-C}})(10^{-3})$$

where A = GCS, B = NBS-20, C = PDB.

$$\begin{aligned}\delta^{13}\text{C}_{\text{PDB-CO}_2}(\text{GCS}) &= 1.75 - 1.06 + (1.75)(-1.06)(10^{-3}) \\ &= 0.688\text{‰}\end{aligned}$$

A3.2.2.1.1.1 Determination of $\delta^{13}\text{C}_{\text{X-PDB}}$

Raw sample results:

$$\delta^{46} = 1.00$$

$$\delta^{45} = -4.00$$

- 1) No correction is required for machine characteristics.
- 2) Correction for isotopic abundance:

$$\delta^{18}\text{O}_{\text{X-GCS}} = 1.0014 \delta^{46}_{\text{Corr}} + 0.0091 \delta^{13}\text{C}_{\text{X-GCS}}$$

$$\delta^{13}\text{C}_{\text{X-GCS}} = 1.0677 \delta^{45}_{\text{Corr}} - 0.0338 \delta^{18}\text{O}_{\text{X-GCS}}$$

$$\delta^{18}\text{O}_{\text{X-GCS}} = 0.965$$

$$\delta^{13}\text{C}_{\text{X-GCS}} = -4.305$$

Now, to convert to PDB scale:

$$\delta_{\text{PDB-CO}_2}^{13}(\text{GCS}) = 0.688 \text{ ‰}$$

$$\text{for } {}^{13}\text{R} = {}^{13}\text{C} / {}^{12}\text{C}$$

$$\frac{{}^{13}\text{R}}{{}^{13}\text{R}_{\text{PDB}}} = 1.00069$$

$$\begin{aligned} 1 + (10^{-3}) \delta_{\text{PDB}}^{13}(\text{X}) &= \frac{{}^{13}\text{R}_{\text{X}}}{{}^{13}\text{R}_{\text{PDB}}} \\ &= \frac{{}^{13}\text{R}_{\text{X}}}{{}^{13}\text{R}_{\text{GCS}}} \cdot \frac{{}^{13}\text{R}_{\text{GCS}}}{{}^{13}\text{R}_{\text{PDB}}} \\ &= \frac{{}^{13}\text{R}_{\text{X}}}{{}^{13}\text{R}_{\text{GCS}}} \cdot 1.00069 \\ &= (1.00069) [1 + (10^{-3}) \delta_{\text{GCS}}^{13}(\text{X})] \end{aligned}$$

$$\delta_{\text{PDB}}^{13}(\text{X}) = 0.688 + (1.00069) \delta_{\text{GCS}}^{13}(\text{X}) \dots \dots (1)$$

Alternatively, we may use:

$$\delta_{\text{A-C}} = \delta_{\text{A-B}} + \delta_{\text{B-C}} + (\delta_{\text{A-B}})(\delta_{\text{B-C}})(10^{-3})$$

$$\delta_{\text{GCS-PDB}}^{13}\text{C} = \delta_{\text{Corr}}^{13}(\text{X}) + (0.688) + (0.688)[\delta_{\text{Corr}}^{13}(\text{X})](10^{-3}) \dots 2$$

For the data given, using equation "1":

$$\begin{aligned}\delta_{\text{PDB}}^{13}(\text{X}) &= 0.688 + (1.00069)(-4.305) \\ &= -3.62 \text{ ‰}\end{aligned}$$

Using equation "2":

$$\begin{aligned}\delta_{\text{PDB}}^{13}(\text{X}) &= (-4.305) + (0.688) + (0.688)(-4.305)(10^{-3}) \\ &= -3.62 \text{ ‰}\end{aligned}$$

A3.3.2. Conversion Of Raw D/H Data

A program (DDELD), listed in the thesis by Young (1982), was used to convert the raw hydrogen isotope ratios to δ_{D} . The δ_{D} of the working "in-house" water standard was 123 ‰ (SMOW), not 110 ‰ as listed in DDELD. Because the D/H ratios for the sample waters were measured relative to DTAP (distilled tap water), the following conversion was applied to transform $\delta_{\text{X-SMOW}}$ to $\delta_{\text{X-SMOW}}$:

$$\delta_{\text{X-SMOW}} = \delta_{\text{X-DTAP}} + \delta_{\text{DTAP-SMOW}} + (10^{-3})(\delta_{\text{X-DTAP}})(\delta_{\text{DTAP-SMOW}})$$

For example, $\delta_{\text{D-X-DTAP}} = 100 \text{ ‰}$

$$\delta_{\text{D-DTAP-SMOW}} = -123 \text{ ‰}$$

$$\begin{aligned}\delta_{\text{X-SMOW}} &= (100) + (-123) + (10^{-3})(100)(-123) \\ &= -35.3 \text{ ‰}\end{aligned}$$

A3.4 Thermal Decrepitation Of Fluid Inclusions Contained In Vein Quartz

Thermal decrepitation was chosen over grinding in vacuum to release fluids from inclusions in quartz to avoid the adsorption of CO_2 onto the surfaces of the ground material. However, thermal decrepitation can induce isotope exchange between species if the decrepitation temperature is too low; hence, decrepitation was effected at approximately 1000°C (Hoefs, 1975).

A3.4.1 Sample preparation

Vein quartz was crushed and sized to fall between 0.5 and 1.5 mm.. This material was acid washed at room temperature with aqua regia for 24 hours and rinsed with distilled water.

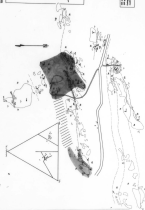
3.4.2 Extraction technique

Gases were recovered from vein quartz using a vacuum line design modified after Ohmoto (1968). Between 1.0 and 7.0 grams of prepared quartz was heated to 1000°C for approximately 30 minutes. Decrepitated gases were collected using iso-propyl alcohol/ dry ice and liquid nitrogen traps, under static vacuum. Noncondensable gas volume was measured on a McLeod gauge and pumped away. The liquid N_2 fraction (CO_2 predominantly) was expanded into the glass line system, its volume measured and then frozen into a removable, glass cold finger and stored for future isotope analysis. This procedure was then followed for the alcohol-dry ice condensable, gas fraction (H_2O predominantly).

| Item | Quantity | Unit | Price | Total |
|---|----------|------|---------|---------|
| 1. The first step is to identify the problem. | 1 | hr | \$10.00 | \$10.00 |
| 2. The second step is to define the problem. | 1 | hr | \$10.00 | \$10.00 |
| 3. The third step is to analyze the problem. | 1 | hr | \$10.00 | \$10.00 |
| 4. The fourth step is to develop a solution. | 1 | hr | \$10.00 | \$10.00 |
| 5. The fifth step is to implement the solution. | 1 | hr | \$10.00 | \$10.00 |
| 6. The sixth step is to evaluate the solution. | 1 | hr | \$10.00 | \$10.00 |
| 7. The seventh step is to monitor the solution. | 1 | hr | \$10.00 | \$10.00 |
| 8. The eighth step is to maintain the solution. | 1 | hr | \$10.00 | \$10.00 |
| 9. The ninth step is to improve the solution. | 1 | hr | \$10.00 | \$10.00 |
| 10. The tenth step is to document the solution. | 1 | hr | \$10.00 | \$10.00 |

| Item | Quantity | Unit | Price | Total |
|---|----------|------|---------|---------|
| 1. The first step is to identify the problem. | 1 | hr | \$10.00 | \$10.00 |
| 2. The second step is to define the problem. | 1 | hr | \$10.00 | \$10.00 |
| 3. The third step is to analyze the problem. | 1 | hr | \$10.00 | \$10.00 |
| 4. The fourth step is to develop a solution. | 1 | hr | \$10.00 | \$10.00 |
| 5. The fifth step is to implement the solution. | 1 | hr | \$10.00 | \$10.00 |
| 6. The sixth step is to evaluate the solution. | 1 | hr | \$10.00 | \$10.00 |
| 7. The seventh step is to monitor the solution. | 1 | hr | \$10.00 | \$10.00 |
| 8. The eighth step is to maintain the solution. | 1 | hr | \$10.00 | \$10.00 |
| 9. The ninth step is to improve the solution. | 1 | hr | \$10.00 | \$10.00 |
| 10. The tenth step is to document the solution. | 1 | hr | \$10.00 | \$10.00 |

1. The first step is to identify the problem.
 2. The second step is to define the problem.
 3. The third step is to analyze the problem.
 4. The fourth step is to develop a solution.
 5. The fifth step is to implement the solution.
 6. The sixth step is to evaluate the solution.
 7. The seventh step is to monitor the solution.
 8. The eighth step is to maintain the solution.
 9. The ninth step is to improve the solution.
 10. The tenth step is to document the solution.





LEGEND

| | |
|-----------------|-------------|
| 1. Study Area | 10. Road |
| 2. Control Area | 11. River |
| 3. Urban Area | 12. Lake |
| 4. Rural Area | 13. Forest |
| 5. Water | 14. Wetland |
| 6. Agriculture | 15. Pasture |
| 7. Forest | 16. Field |
| 8. Wetland | 17. Meadow |
| 9. Pasture | 18. Field |

MAP 1.1
 STUDY AREA LOCATION
 (NORTH TEXAS)

1. 1000' 2. 2000' 3. 3000' 4. 4000' 5. 5000' 6. 6000' 7. 7000' 8. 8000' 9. 9000' 10. 10000' 11. 11000' 12. 12000' 13. 13000' 14. 14000' 15. 15000' 16. 16000' 17. 17000' 18. 18000' 19. 19000' 20. 20000' 21. 21000' 22. 22000' 23. 23000' 24. 24000' 25. 25000' 26. 26000' 27. 27000' 28. 28000' 29. 29000' 30. 30000' 31. 31000' 32. 32000' 33. 33000' 34. 34000' 35. 35000' 36. 36000' 37. 37000' 38. 38000' 39. 39000' 40. 40000' 41. 41000' 42. 42000' 43. 43000' 44. 44000' 45. 45000' 46. 46000' 47. 47000' 48. 48000' 49. 49000' 50. 50000' 51. 51000' 52. 52000' 53. 53000' 54. 54000' 55. 55000' 56. 56000' 57. 57000' 58. 58000' 59. 59000' 60. 60000' 61. 61000' 62. 62000' 63. 63000' 64. 64000' 65. 65000' 66. 66000' 67. 67000' 68. 68000' 69. 69000' 70. 70000' 71. 71000' 72. 72000' 73. 73000' 74. 74000' 75. 75000' 76. 76000' 77. 77000' 78. 78000' 79. 79000' 80. 80000' 81. 81000' 82. 82000' 83. 83000' 84. 84000' 85. 85000' 86. 86000' 87. 87000' 88. 88000' 89. 89000' 90. 90000' 91. 91000' 92. 92000' 93. 93000' 94. 94000' 95. 95000' 96. 96000' 97. 97000' 98. 98000' 99. 99000' 100. 100000'



MAP 2B STEWART AGATE GOLD PROPERTY

Locality Map

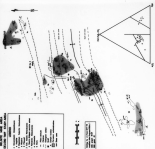


| LEGEND | |
|--------|-------------|
| 1 | Survey Area |
| 2 | Section |
| 3 | Section |
| 4 | Section |
| 5 | Section |
| 6 | Section |
| 7 | Section |
| 8 | Section |
| 9 | Section |
| 10 | Section |
| 11 | Section |
| 12 | Section |
| 13 | Section |
| 14 | Section |
| 15 | Section |
| 16 | Section |
| 17 | Section |
| 18 | Section |
| 19 | Section |
| 20 | Section |
| 21 | Section |
| 22 | Section |
| 23 | Section |
| 24 | Section |
| 25 | Section |
| 26 | Section |
| 27 | Section |
| 28 | Section |
| 29 | Section |
| 30 | Section |
| 31 | Section |
| 32 | Section |
| 33 | Section |
| 34 | Section |
| 35 | Section |
| 36 | Section |
| 37 | Section |
| 38 | Section |
| 39 | Section |
| 40 | Section |
| 41 | Section |
| 42 | Section |
| 43 | Section |
| 44 | Section |
| 45 | Section |
| 46 | Section |
| 47 | Section |
| 48 | Section |
| 49 | Section |
| 50 | Section |
| 51 | Section |
| 52 | Section |
| 53 | Section |
| 54 | Section |
| 55 | Section |
| 56 | Section |
| 57 | Section |
| 58 | Section |
| 59 | Section |
| 60 | Section |
| 61 | Section |
| 62 | Section |
| 63 | Section |
| 64 | Section |
| 65 | Section |
| 66 | Section |
| 67 | Section |
| 68 | Section |
| 69 | Section |
| 70 | Section |
| 71 | Section |
| 72 | Section |
| 73 | Section |
| 74 | Section |
| 75 | Section |
| 76 | Section |
| 77 | Section |
| 78 | Section |
| 79 | Section |
| 80 | Section |
| 81 | Section |
| 82 | Section |
| 83 | Section |
| 84 | Section |
| 85 | Section |
| 86 | Section |
| 87 | Section |
| 88 | Section |
| 89 | Section |
| 90 | Section |
| 91 | Section |
| 92 | Section |
| 93 | Section |
| 94 | Section |
| 95 | Section |
| 96 | Section |
| 97 | Section |
| 98 | Section |
| 99 | Section |
| 100 | Section |

Note: Contours are present in vicinity of all subsidiary claims.

Stewart Agate Gold
Gold Mine

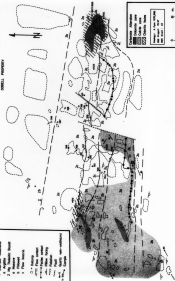
1. The first part of the map shows the location of the station relative to the surrounding area. The station is located on the left side of the map, near the top. The surrounding area is shown with a grid of lines.



LEGEND - SYMBOLS

- 1. Boundary Subunits
- 2. Apple
- 3. Big
- 4. Medium
- 5. Small
- 6. Pine
- 7. Pine
- 8. Pine
- 9. Pine
- 10. Pine
- 11. Pine
- 12. Pine
- 13. Pine
- 14. Pine
- 15. Pine
- 16. Pine
- 17. Pine
- 18. Pine
- 19. Pine
- 20. Pine
- 21. Pine
- 22. Pine
- 23. Pine
- 24. Pine
- 25. Pine
- 26. Pine
- 27. Pine
- 28. Pine
- 29. Pine
- 30. Pine
- 31. Pine
- 32. Pine
- 33. Pine
- 34. Pine
- 35. Pine
- 36. Pine
- 37. Pine
- 38. Pine
- 39. Pine
- 40. Pine
- 41. Pine
- 42. Pine
- 43. Pine
- 44. Pine
- 45. Pine
- 46. Pine
- 47. Pine
- 48. Pine
- 49. Pine
- 50. Pine
- 51. Pine
- 52. Pine
- 53. Pine
- 54. Pine
- 55. Pine
- 56. Pine
- 57. Pine
- 58. Pine
- 59. Pine
- 60. Pine
- 61. Pine
- 62. Pine
- 63. Pine
- 64. Pine
- 65. Pine
- 66. Pine
- 67. Pine
- 68. Pine
- 69. Pine
- 70. Pine
- 71. Pine
- 72. Pine
- 73. Pine
- 74. Pine
- 75. Pine
- 76. Pine
- 77. Pine
- 78. Pine
- 79. Pine
- 80. Pine
- 81. Pine
- 82. Pine
- 83. Pine
- 84. Pine
- 85. Pine
- 86. Pine
- 87. Pine
- 88. Pine
- 89. Pine
- 90. Pine
- 91. Pine
- 92. Pine
- 93. Pine
- 94. Pine
- 95. Pine
- 96. Pine
- 97. Pine
- 98. Pine
- 99. Pine
- 100. Pine

ROAD N
DIRECTION



LEGEND - SYMBOLS

1. Boundary Subunits

2. Apple

3. Big

4. Medium

5. Small

6. Pine

7. Pine

8. Pine

9. Pine

10. Pine

11. Pine

12. Pine

13. Pine

14. Pine

15. Pine

16. Pine

17. Pine

18. Pine

19. Pine

20. Pine

21. Pine

22. Pine

23. Pine

24. Pine

25. Pine

26. Pine

27. Pine

28. Pine

29. Pine

30. Pine

31. Pine

32. Pine

33. Pine

34. Pine

35. Pine

36. Pine

37. Pine

38. Pine

39. Pine

40. Pine

41. Pine

42. Pine

43. Pine

44. Pine

45. Pine

46. Pine

47. Pine

48. Pine

49. Pine

50. Pine

51. Pine

52. Pine

53. Pine

54. Pine

55. Pine

56. Pine

57. Pine

58. Pine

59. Pine

60. Pine

61. Pine

62. Pine

63. Pine

64. Pine

65. Pine

66. Pine

67. Pine

68. Pine

69. Pine

70. Pine

71. Pine

72. Pine

73. Pine

74. Pine

75. Pine

76. Pine

77. Pine

78. Pine

79. Pine

80. Pine

81. Pine

82. Pine

83. Pine

84. Pine

85. Pine

86. Pine

87. Pine

88. Pine

89. Pine

90. Pine

91. Pine

92. Pine

93. Pine

94. Pine

95. Pine

96. Pine

97. Pine

98. Pine

99. Pine

100. Pine

Hand-drawn map showing a road network and various land parcels. The map includes a north arrow pointing upwards. The road network is shown with solid and dashed lines. Land parcels are outlined and some are shaded. The map is labeled with various numbers and letters, corresponding to the legend symbols. The map is oriented with the road running horizontally across the middle.

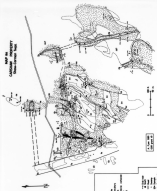
Map of the ... of the ...

Scale: 1:100,000
 Date: 1950
 Author: ...

- Legend
- 1. ...
- 2. ...
- 3. ...
- 4. ...
- 5. ...
- 6. ...
- 7. ...
- 8. ...
- 9. ...
- 10. ...
- 11. ...
- 12. ...
- 13. ...
- 14. ...
- 15. ...
- 16. ...
- 17. ...
- 18. ...
- 19. ...
- 20. ...
- 21. ...
- 22. ...
- 23. ...
- 24. ...
- 25. ...
- 26. ...
- 27. ...
- 28. ...
- 29. ...
- 30. ...
- 31. ...
- 32. ...
- 33. ...
- 34. ...
- 35. ...
- 36. ...
- 37. ...
- 38. ...
- 39. ...
- 40. ...
- 41. ...
- 42. ...
- 43. ...
- 44. ...
- 45. ...
- 46. ...
- 47. ...
- 48. ...
- 49. ...
- 50. ...
- 51. ...
- 52. ...
- 53. ...
- 54. ...
- 55. ...
- 56. ...
- 57. ...
- 58. ...
- 59. ...
- 60. ...
- 61. ...
- 62. ...
- 63. ...
- 64. ...
- 65. ...
- 66. ...
- 67. ...
- 68. ...
- 69. ...
- 70. ...
- 71. ...
- 72. ...
- 73. ...
- 74. ...
- 75. ...
- 76. ...
- 77. ...
- 78. ...
- 79. ...
- 80. ...
- 81. ...
- 82. ...
- 83. ...
- 84. ...
- 85. ...
- 86. ...
- 87. ...
- 88. ...
- 89. ...
- 90. ...
- 91. ...
- 92. ...
- 93. ...
- 94. ...
- 95. ...
- 96. ...
- 97. ...
- 98. ...
- 99. ...
- 100. ...



Scale: 1:100,000
 Date: 1950
 Author: ...



| Symbol | Description |
|----------|-------------|
| [Symbol] | Temple |
| [Symbol] | Field |
| [Symbol] | River |
| [Symbol] | Path |
| [Symbol] | Wall |
| [Symbol] | Gate |
| [Symbol] | Well |
| [Symbol] | Tree |
| [Symbol] | Shrine |
| [Symbol] | Stupa |
| [Symbol] | Monument |
| [Symbol] | Archway |
| [Symbol] | Platform |
| [Symbol] | Roof |
| [Symbol] | Door |
| [Symbol] | Window |
| [Symbol] | Staircase |
| [Symbol] | Chimney |
| [Symbol] | Flagpole |
| [Symbol] | Well |
| [Symbol] | Tree |
| [Symbol] | Shrine |
| [Symbol] | Stupa |
| [Symbol] | Monument |
| [Symbol] | Archway |
| [Symbol] | Platform |
| [Symbol] | Roof |
| [Symbol] | Door |
| [Symbol] | Window |
| [Symbol] | Staircase |
| [Symbol] | Chimney |
| [Symbol] | Flagpole |

Scale: 1 inch = 100 feet

North Arrow

2. The second part of the map shows the location of the study area in the state of Texas. The map is oriented with North at the top. The study area is located in the central part of the state, between the cities of Austin and San Antonio. The map shows the major highways and the location of the study area.

3. The third part of the map shows the location of the study area in the state of Texas. The map is oriented with North at the top. The study area is located in the central part of the state, between the cities of Austin and San Antonio. The map shows the major highways and the location of the study area.



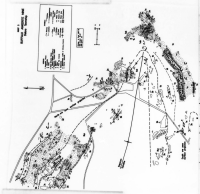
4. The fourth part of the map shows the location of the study area in the state of Texas. The map is oriented with North at the top. The study area is located in the central part of the state, between the cities of Austin and San Antonio. The map shows the major highways and the location of the study area.

1. The first part of the map shows the location of the station relative to the coast. The station is located on the coast of the Gulf of Mexico, about 10 miles from the mouth of the river.



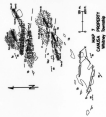
The map shows the location of the station relative to the coast and the river. The station is located on the coast of the Gulf of Mexico, about 10 miles from the mouth of the river.



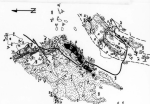


Geological Map of the State of New York, showing the distribution of the various geological formations, and the location of the principal cities and towns.

1. The first map shows the distribution of the species in the study area. The second map shows the distribution of the species in the study area. The third map shows the distribution of the species in the study area.

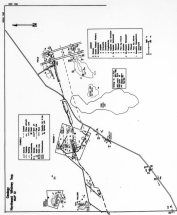


1. 1000' 2. 2000' 3. 3000' 4. 4000' 5. 5000' 6. 6000' 7. 7000' 8. 8000' 9. 9000' 10. 10000' 11. 11000' 12. 12000' 13. 13000' 14. 14000' 15. 15000' 16. 16000' 17. 17000' 18. 18000' 19. 19000' 20. 20000' 21. 21000' 22. 22000' 23. 23000' 24. 24000' 25. 25000' 26. 26000' 27. 27000' 28. 28000' 29. 29000' 30. 30000' 31. 31000' 32. 32000' 33. 33000' 34. 34000' 35. 35000' 36. 36000' 37. 37000' 38. 38000' 39. 39000' 40. 40000' 41. 41000' 42. 42000' 43. 43000' 44. 44000' 45. 45000' 46. 46000' 47. 47000' 48. 48000' 49. 49000' 50. 50000' 51. 51000' 52. 52000' 53. 53000' 54. 54000' 55. 55000' 56. 56000' 57. 57000' 58. 58000' 59. 59000' 60. 60000' 61. 61000' 62. 62000' 63. 63000' 64. 64000' 65. 65000' 66. 66000' 67. 67000' 68. 68000' 69. 69000' 70. 70000' 71. 71000' 72. 72000' 73. 73000' 74. 74000' 75. 75000' 76. 76000' 77. 77000' 78. 78000' 79. 79000' 80. 80000' 81. 81000' 82. 82000' 83. 83000' 84. 84000' 85. 85000' 86. 86000' 87. 87000' 88. 88000' 89. 89000' 90. 90000' 91. 91000' 92. 92000' 93. 93000' 94. 94000' 95. 95000' 96. 96000' 97. 97000' 98. 98000' 99. 99000' 100. 100000'

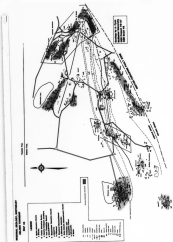


| Peak | Elevation |
|----------------------|-----------|
| 1. Mount [illegible] | 10,000' |
| 2. [illegible] | 9,500' |
| 3. [illegible] | 9,000' |
| 4. [illegible] | 8,500' |
| 5. [illegible] | 8,000' |
| 6. [illegible] | 7,500' |
| 7. [illegible] | 7,000' |
| 8. [illegible] | 6,500' |
| 9. [illegible] | 6,000' |
| 10. [illegible] | 5,500' |
| 11. [illegible] | 5,000' |
| 12. [illegible] | 4,500' |
| 13. [illegible] | 4,000' |
| 14. [illegible] | 3,500' |
| 15. [illegible] | 3,000' |
| 16. [illegible] | 2,500' |
| 17. [illegible] | 2,000' |
| 18. [illegible] | 1,500' |
| 19. [illegible] | 1,000' |
| 20. [illegible] | 500' |

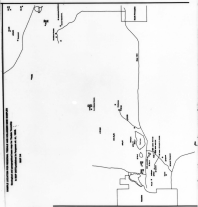
1. 1000' 2. 2000' 3. 3000' 4. 4000' 5. 5000' 6. 6000' 7. 7000' 8. 8000' 9. 9000' 10. 10000' 11. 11000' 12. 12000' 13. 13000' 14. 14000' 15. 15000' 16. 16000' 17. 17000' 18. 18000' 19. 19000' 20. 20000' 21. 21000' 22. 22000' 23. 23000' 24. 24000' 25. 25000' 26. 26000' 27. 27000' 28. 28000' 29. 29000' 30. 30000' 31. 31000' 32. 32000' 33. 33000' 34. 34000' 35. 35000' 36. 36000' 37. 37000' 38. 38000' 39. 39000' 40. 40000' 41. 41000' 42. 42000' 43. 43000' 44. 44000' 45. 45000' 46. 46000' 47. 47000' 48. 48000' 49. 49000' 50. 50000' 51. 51000' 52. 52000' 53. 53000' 54. 54000' 55. 55000' 56. 56000' 57. 57000' 58. 58000' 59. 59000' 60. 60000' 61. 61000' 62. 62000' 63. 63000' 64. 64000' 65. 65000' 66. 66000' 67. 67000' 68. 68000' 69. 69000' 70. 70000' 71. 71000' 72. 72000' 73. 73000' 74. 74000' 75. 75000' 76. 76000' 77. 77000' 78. 78000' 79. 79000' 80. 80000' 81. 81000' 82. 82000' 83. 83000' 84. 84000' 85. 85000' 86. 86000' 87. 87000' 88. 88000' 89. 89000' 90. 90000' 91. 91000' 92. 92000' 93. 93000' 94. 94000' 95. 95000' 96. 96000' 97. 97000' 98. 98000' 99. 99000' 100. 100000'



Hand-drawn map of the coastal area of the island of Sumatra, showing the location of the study area. The map includes a scale bar (1:100,000) and a north arrow. The study area is indicated by a dashed line.

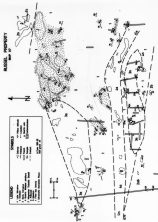


1. The first part of the map shows the location of the station relative to the coast. The station is located on the coast of the Gulf of Mexico, near the mouth of the Mississippi River. The map shows the coastline of the Gulf of Mexico, the Mississippi River, and the location of the station.

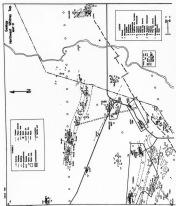


This map was prepared by the U.S. Navy Hydrographic Office, and is based on the latest available information. It is not intended to be used for navigation, and is not a substitute for a nautical chart.

1. *Phragmites australis* (Cav.) Trin. ex Steud.
 2. *Spartina patens* (L.) Muhl.
 3. *Scirpus americanus* (L.) Pers.
 4. *Cyperus tenuifolius* (L.) Presl.
 5. *Cyperus tenuifolius* (L.) Presl.
 6. *Cyperus tenuifolius* (L.) Presl.
 7. *Cyperus tenuifolius* (L.) Presl.
 8. *Cyperus tenuifolius* (L.) Presl.
 9. *Cyperus tenuifolius* (L.) Presl.
 10. *Cyperus tenuifolius* (L.) Presl.







Map showing a coastal area with a river and various land parcels. The map includes a north arrow, a scale bar, and two inset maps. The main map shows a river flowing from the top left towards the bottom right, with several land parcels marked with numbers and letters. A north arrow is located in the upper left quadrant. A scale bar is in the upper right quadrant. Two inset maps are present: one in the top left showing a larger area with a river and a north arrow, and another in the bottom right showing a detailed view of a specific area. The map is oriented with North at the top.